



# **Reconstruction of depositional and post-depositional processes at Obishirian sites (Central Asia – Kyrgyzstan)**

Greta Brancaleoni, MSc

Supervisor:

Dr. hab. Maciej T. Krajcarz, prof. ING PAN

PhD thesis in Earth and Environmental Sciences

This research was funded by the National Science Centre of Poland

grant number 2018/29/B/ST10/00906

Institute of Geological Sciences of the Polish Academy of Sciences

29/11/2023



*Site formation processes are “the factors that create the historic and archaeological records”  
(Schiffer, 1987, 7)*

# ***Acknowledges***

This research was funded by the National Science Centre of Poland, grant number 2018/29/B/ST10/00906. I acknowledge my supervisor, Dr. hab. Maciej T. Krajcarz, Prof. INGPAN, who introduced me to the fine field of micromorphology and guided me throughout this Ph.D. journey. I express gratitude to Dr. Magdalena Krajcarz for consistently providing the most insightful ideas and advice. Special thanks are extended to Dr. Svetlana Shnaider and her international research teams for organizing remarkable fieldwork experiences filled with fun, discoveries, and even the occasional mishap that turned into an exciting adventure. Dr. Claudio Berto deserves acknowledgment for his unwavering support. I want to give a special mention to Prof. Aida Abdykanova, Dr. Saltanat Alysher kyzy, Dr. Małgorzata Kot, Dr. Temerlan Tima Charynov, Dr. Gayrathon Muhtarov, and all the individuals I had the pleasure of working with during these years. I appreciate Ewa Deput for producing beautiful thin sections and her patience with my Polish, as well as the same patience shown by my colleagues and the administrative staff at the Institute of Geological Sciences. I want to remember Bartek, who is no longer with us. Special thanks go to Dr. Beata Gebus-Czupyt for her guidance during these years and support during my ankle injury. The same gratitude extends to Nikos, Elena, Nadav, and Asia, who treated me like family.

Embarking on a Ph.D. study is challenging, especially during these difficult times; a pandemic occurred, and two wars in the heart of Europe have begun. I could not have made it without the lifelong support from my family (Nonno, Nonna, Stevfanina, Andrea, Marco, Suz, Cecca, and Maria Pia), my distant good old friends Andrea and Francesca. Among good old friends, special thanks go to Dr. Carlotta Leoncini for her invaluable comments on a previous version of this thesis. Last but not least, my partner, Dr. Wojtek Wegner, for our long and constructive, not always peaceful, discussions about the world around us, his academic life-coaching suggestions, and his final remarks on this piece of work. I also want to acknowledge the people I had the pleasure of meeting during my fieldworks in Central Asia, especially the host families who showed kindness and hospitality always. Their beautiful lands are plenty of (pre)history. Rakhmat!

Ultimately, thanks to Alexandra Elbakyan and Sci-Hub!

# **Certification**

22/11/2023

I, Greta Brancaleoni, fully aware of my legal responsibility, declare that this doctoral dissertation is my own work unless otherwise referenced or acknowledged, and does not contain any content obtained in a non-conforming manner with applicable regulations. I also declare that the presented thesis has not been previously submitted for obtaining a doctoral degree at any other academic institution. In conclusions, I declare that the printed and electronic versions of this doctoral work are identical except for layout adjustments made for printing purposes.

## ***Oświadczenie***

Świadomy odpowiedzialności prawnej oświadczam, że niniejsza rozprawa doktorska została napisana przeze mnie samodzielnie i nie zawiera treści uzyskanych w sposób niezgodny z obowiązującymi przepisami.

Oświadczam również, że przedstawiona rozprawa nie była wcześniej przedmiotem procedur związanych z uzyskaniem stopnia doktora w wyższej uczelni lub innej jednostce naukowej.

W zakończeniu oświadczam, że drukowana i elektroniczna wersja niniejszej pracy doktorskiej są identyczne, z wyjątkiem dostosowań układu dokonanych w celu drukowania.



Greta Brancaleoni

## ***Thesis-related publications***

1. **Brancaleoni, G.**, Shnaider, S., Osipova, E., Danukalova, G., Kurbanov, R., Deput, E., Alisher kyzy, S., Abdykanova, A., Krajcarz, M. T. (2022). Depositional history of a talus cone in an arid intermontane basin in Central Asia: An interdisciplinary study at the Late Pleistocene–Late Holocene Obishir-I site, Kyrgyzstan. *Geoarchaeology*, 37, 350–73. <https://doi.org/10.1002/gea.2189>
2. **Brancaleoni, G.**, Kot, M., Shnaider, S., Mroczek, P., Kurbanov, R., Abdykanova, A., Alisher kyzy, S., Khudjanazarov, M., Pavlenok, K., Krajcarz, M. T. (2023). A closer look at clasts and groundmass: Micromorphological features in sediments with archaeological significance in Obishir and Katta Sai complexes (Central Asia), *Journal of Archaeological Science: Reports*, 51, 104118, <https://doi.org/10.1016/j.jasrep.2023.104118>.
3. **Brancaleoni, G.**, Shnaider, S., Lempart-Drozd, G., Deput, E., Abdykanova, A., Krajcarz, M. T. Geoarchaeological approach for tackling the function and preservation state of the Obishir-5 site, the earliest Neolithic site in the Fergana Valley, submitted on 23<sup>rd</sup> October 2023 at *Journal of Archaeological and Anthropological Sciences*

# ***Abstract***

The research is dedicated to investigating the reconstruction of depositional and post-depositional processes at Obishirian archaeological sites in Kyrgyzstan, Central Asia. These sites are situated along the Silk Road, one of the most important and ancient trade routes in the region. The Obishirian represent an early Neolithic cultural unit, characterized mainly by the use of microlithics. This culture extends from the Western Tian Shan to the Pamirs, and is estimated to have existed between 9500 and 6500 years before present (BP), standing as the earliest Neolithic cultural unit in the interior mountains of Central Asia. Obishirian artifacts have been retrieved from various sites, with Obishir-5 being the most significant site. Other important sites include Obishir-1, Istikskaya Cave, Kurteke rockshelter, and Oshkhona.

This dissertation mainly focuses on two sites—Obishir-1 and Obishir-5—located on a slope in SW Kyrgyzstan in a small, arid intermontane basin. Obishir-1 and Obishir-5 are re-studied sites, which means that previous investigations were researched to acquire preliminary material. Additionally, a geoarchaeological investigation was designed for a detailed and state-of-the-art study of site formation. The investigation focused on two scales: the site scale and the microscopic scale. During fieldworks, detailed descriptions of site stratigraphy was carried out. Strategic bulk and micromorphological sampling was performed. Micromorphological studies were accompanied by complementary analysis such as grain size analysis, basic geochemical and mineralogical analyses. Furthermore, the designed approach, together with faunal assemblage analyses, allowed to reconstruct the paleoenvironment characterizing the research area. Moreover, archaeological artifact spatial distribution was analyzed. To determine the age of sediments, chronometric dating (radiocarbon and luminescence) was also considered. Altogether, the mentioned analyses provide useful information on the main sedimentological processes involved at the sites. What is also important is that the methodology allows a better understanding of the anthropogenic impact at the sites and the post-depositional disturbances due to anthropogenic, pedogenic, or geogenic factors.

The sites share similar geological and geomorphological settings, i.e., they are located at the base of a steep carbonate cliff in front of one or more rockshelters, and the archaeological and zoological material is generally embedded in talus deposits. The Quaternary sediments are an unsorted, mainly angular-shaped mixture of coarse and fine material. Being on a slope, the main processes involved in the site formation are colluvial; however, another important process responsible for the accumulation of fine materials is aeolian. At Obishir-5, anthropogenic and human-related activity inputs are also consistent especially in the Obishirian cultural unit, such as bones, charcoals and herbivore dung. The sites are affected by a wide range of post-depositional

processes, such as later translocation of material down the slope at Obishir-1, later vertical translocation of fine material by gravity and bioturbation, anthropogenic disturbances, especially in the cultural units, as well as weak soil formation. At Obishir-5, the presence of herbivore dung within the microstratigraphy of the Obishirian cultural unit supported the evidence of the use of livestock purported by the study on faunal remains. These pieces of evidence were dated around 8000 BP, providing the earliest use of livestock in the interior corridors of Central Asia.

Especially with the help of micromorphology, this study has brought to light important aspects of the animal husbandry process during the Neolithic turnover in Central Asia. Another compelling aspect is that the region is poorly studied, especially colluvial deposits. This research will supposedly contribute to the analysis of colluvial sequences and their micromorphological aspects in the region, and therefore to a better recognition of similar deposits and the depositional processes involved in similar environmental settings.

**Keywords:** geoarchaeology, site formation, micromorphology, Neolithic, Pleistocene/Holocene transition, Obishirian, Central Asia

# ***Abbreviations***

CA – Central Asia

BP – Before Present

Myr – Million years

asl – above sea level

BCE – Before Common Era

MP – Middle Paleolithic

UP – Upper Paleolithic

EPP – Epipaleolithic

SU – Stratigraphic Unit

DEM – Digital Elevation Model

SEM-EDS – Scanning Electron Microscope coupled with Energy Dispersive Spectroscopy

CHNS - carbon (C), hydrogen (H), nitrogen (N), and sulfur (S)

ICP-MS – Inductively coupled plasma mass spectrometry

PXRD - Powder X-ray diffraction

FTIR – Fourier Transform Infra-Red spectroscopy

C-14 – Radiogenic carbon

OSL - Optically stimulated luminescence dating

SAR – Stratigraphic Accumulation Rate

LGM – Last Glacial Maximum



# Contents

<i>Acknowledges</i> .....	i
<i>Certification</i> .....	ii
<i>Thesis-related publications</i> .....	iii
<i>Abstract</i> .....	iv
<i>Abbreviations</i> .....	vi
<i>List of figures</i> .....	x
<i>List of tables</i> .....	xiv
1 Introduction .....	1
1.1 Background .....	1
1.2 Research objectives .....	4
1.3 Thesis significance and structure .....	5
2 Macro-regional contexts and archaeological background .....	7
2.1 Geographic context .....	7
2.2 Geologic context .....	8
2.3 Regional climate and paleoclimate .....	10
2.4 Archaeological background .....	11
2.4.1 Paleolithic .....	11
2.4.2 Epipaleolithic .....	12
2.4.3 Neolithic and Neolithization .....	12
3 The sites .....	15
3.1 Geological and geomorphological setting .....	16
3.2 Soviet scholar research .....	18
3.3 New studies .....	20
3.4 Faunal remain studies .....	20
3.5 Archaeological assemblages .....	20
4 The rationale .....	22
4.1 Introduction .....	22
4.2 Building blocks of site formation studies .....	23
4.2.1 Types of sediments at archaeological sites .....	23
4.2.2 The concept of stratigraphy at archaeological sites .....	24
4.3 Site formation .....	26
4.4 Sediments in arid and semi-arid settings .....	27
4.5 Colluvial deposits .....	29
4.5.1 Rockshelter deposits .....	30
4.6 Sedimentary clues for human and human-related activities .....	31
5 The methods applied .....	34

5.1	Introduction .....	34
5.2	Field observation and stratigraphy .....	34
5.3	Sampling .....	35
5.4	Micromorphology .....	37
5.4.1	SEM-EDS.....	39
5.4.2	Epifluorescent microscopy .....	40
5.5	Grain size analysis.....	42
5.6	Geochemistry and mineralogy .....	42
5.6.1	Basic geochemistry .....	42
5.6.2	Powder X-ray diffraction (PXRD) and Infra-Red spectroscopy (FTIR).....	44
5.7	Faunal assemblage .....	45
5.8	Dating methods .....	46
5.8.1	Radiocarbon dating .....	46
5.8.2	Optically stimulated luminescence dating (OSL) .....	47
5.9	Distribution of artifacts .....	48
6	Results .....	49
6.1	Introduction.....	49
6.2	Depositional history of a talus cone in an arid intermontane basin in Central Asia: An interdisciplinary study at the Late Pleistocene–Late Holocene Obishir-I site, Kyrgyzstan....	49
6.2.1	Summary .....	50
6.3	A closer look at clasts and groundmass: Micromorphological features in sediments with archaeological significance in Obishir and Katta Sai complexes (Central Asia).....	54
6.3.1	Summary .....	54
6.4	Geoarchaeological approach for tackling the function and preservation state of the Obishir-5 site, the earliest Neolithic site in the Fergana Valley .....	57
6.4.1	Summary .....	57
6.5	Synopsis .....	59
7	Discussions and conclusions .....	61
7.1	Introduction.....	61
7.2	Case studies at comparison .....	62
7.2.1	The Obishirian sites at comparison .....	62
7.2.2	Local paleoenvironmental conditions .....	66
7.3	Implication and significance of this thesis .....	67
7.4	Future work .....	69
7.4.1	Other Obishirian sites.....	69
7.4.2	Central Asian fumiers .....	70
	<i>Bibliography</i> .....	72
	<i>Appendix A - Scientific paper 1</i>	

*Appendix B – Scientific paper 2*

*Appendix C – Scientific paper 3*

*Appendix D – Author contribution statement*

# List of figures

<b>Figure 1-1</b> Hunting scene in Shakhty Cave archaeological site in the Pamirs (Tajikistan, CA), the paintings are attributed to the Mesolithic era. ....	2
<b>Figure 2-1</b> Location of the study area. The countries that are encompassed by the two geographic terms ‘Middle Asia’ and ‘Central Asia’ are illustrated according to Cowan (2007)..	8
<b>Figure 2-2</b> Most important geographic elements of CA. Mean annual precipitation (MAP) isohyets are also shown, taken from Song et al. (2021). ....	8
<b>Figure 2-3</b> Location map showing the major tectonic structures of the western Tian Shan and regional subdivisions from Brunet, Sobel and Mccann (2017). The red circle indicates the location of Obishirian sites.....	9
<b>Figure 2-4</b> Modeled dispersal of domestic animals into CA proposed by Taylor et al. (2021).....	13
<b>Figure 2-5</b> Spatial distribution of Obishirian and Pre-Obishirian sites. GTOPO30 base map (DEM-Digital Elevation Model; gt30e060n90 and n40; source USGS EROS Archive from <a href="https://www.usgs.gov">https://www.usgs.gov</a> ) and cultural vector map data from ( <a href="http://www.naturalearthdata.com">www.naturalearthdata.com</a> ).....	14
<b>Figure 3-1</b> Localization and schematic tectonic setting <b>a)</b> Location of the site together with the other archeological sites excavated in the area; <b>b)</b> Tectonic scheme of the studied area after Hnylko et al. (2019). Key: <b>1</b> – (Par)autochthon Alay structural unit made of Devonian-Carboniferous Alay carbonate platform succession and Upper Carboniferous synorogenic flysch/olistostrome deposits. <b>2</b> – Lower nappes built in Silurian–Carboniferous terrigenous, pelagic and carbonate platform formations. <b>3</b> – Upper nappes represented by the ocean-derived formations with the Silurian to Devonian ophiolitic fragments. In the area, these nappes form a synformal structure. <b>4</b> – Neogene formations and <b>5</b> - Quaternary deposits. ....	15
<b>Figure 3-2</b> Location of the Obishirian sites along the Eshme ridge with section profiles. <b>a)</b> Drone imagery comprising the southern slope of the Eshme ridge where Obishir archaeological sites were discovered; <b>b)</b> schematic sections AA’ and BB’.....	18
<b>Figure 3-3</b> Excavation area at the Obishir-1 location .....	19
<b>Figure 3-4</b> Excavation plan at the Obishir-5 site. Key: <b>1</b> – 1966 probe trench; <b>2</b> – 1967 excavation; <b>3</b> – 1968-1969 excavation; <b>4</b> – 1970 excavation; <b>5</b> – 1971 excavation; <b>6</b> – 1973 trench; <b>7</b> – 2015-2016 excavation; <b>8</b> – rock-shelter after Taylor et al. (2021).....	19
<b>Figure 4-1</b> Different types of stratigraphy applied to the same profile. The stratigraphy from an archaeological site can represent the combined effects of depositional (lithostratigraphy) and post-depositional processes (soil stratigraphy), coupled with human activities (archeostratigraphy or cultural stratigraphy) taken from Goldberg and Macphail (2006) figure 2.1, modified from Courty, Goldberg and Macphail (1989), figure 3.3. ....	25

<b>Figure 4-2</b> Basic stratigraphic principles. <b>1)</b> This panel illustrates that the unit deposited at time t1 is older than time t2, that is older than t3, older units are found at the bottom and younger ones are found at the top; units tend to be laid down horizontally with lateral continuity; <b>2)</b> this panel illustrates how a feature (pit) that is cutting through unit-t3 and unit-t2 is younger than both units; <b>3)</b> slope deposits can be responsible for an inverted stratigraphy as at time t3; <b>4)</b> in situ units are those that have not been moved from their original place of deposition. In archeology, an in situ object is also the object found in its original place of deposition.....	25
<b>Figure 4-3</b> Workflow in site formation studies taken from Shahack-Gross (2017).....	27
<b>Figure 4-4</b> Suite of post-depositional processes affecting dung taken from Shahack-Gross (2011).....	33
<b>Figure 5-1</b> Sampling location at Obishir-1. Sampling took place during the campaigns between 2016 and 2021, taken from Brancaleoni et al. (2022).....	36
<b>Figure 5-2</b> Sampling location at Obishir-5. Sampling was conducted over various campaigns from 2016 to 2021.....	37
<b>Figure 5-3</b> Examples of fabric, fabric unit and partial fabric and different magnitudes of observations modified after (Stoops, 2003); <b>a)</b> the yellow matrix (partial fabric) looks homogeneous and mottled by Fe oxides nodules; <b>b)</b> looking at higher magnification, the partial fabric matrix is not homogenous but made of other fabric units, such as clay coatings (co) completely filling voids, pores (p) and nodules (n); <b>c)</b> increasing the magnification the clay matrix is made of quartz (q) grains.....	39
<b>Figure 5-4</b> Dung pellet found at Obihshir-5 under lighting microscopy (a, b) and SEM (c, d), worth noting is that the internal structure of the specimen under lighting microscopy is hidden, but becomes accessible under SEM. <b>a)</b> dung pellet under ppl; <b>b)</b> same specimen under xpl; <b>c)</b> same specimen (rotated) under SEM; <b>d)</b> under SEM at increased magnification .....	40
<b>Figure 5-5</b> Different lighting conditions of two specimens found in the sedimentary record at Obishir-5. <b>a)</b> Bone specimen showing yellow coloration in ppl; <b>b)</b> bone specimen showing reddened coloration in ppl; <b>c)</b> same specimen showed in a) but under epifluorescent light showing the typical green fluorescence; <b>d)</b> same specimen in b) not showing fluorescence, due to possibly heating transformations.....	41
<b>Figure 6-1</b> Depositional history of Obishir-1 after Brancaleoni et al. (2022). <b>a)</b> Last Glacial Maximum (LGM). Accumulation of the bottom part of Unit 6 under cold and periglacial conditions where aeolian processes were dominant. <b>b)</b> Late Glacial. Accumulation of the top part of SU6. Shifting to more humid conditions with a weakly formed soil, more efficient frost cracking and the first human occupation horizon (unknown Paleolithic). <b>c)</b> Late Glacial. Accumulation of SU5 possibly due to an erosional event after fire-related events. <b>d)</b> Early – Middle Holocene. Accumulation of SU4. Onset of the Holocene. Second cultural occupation	

horizon (Obishirian). **e**) Middle – Late Holocene. Soil formation and consequently cease of accumulation (SU3). ..... 51

**Figure 6-2** Schematic stratigraphic profiles at the studied locations after Brancaleoni et al. (2023) with location of micromorphology sampling. .... 52

**Figure 6-3 a–b)** Siltic-textured soil characterizing the central part of SU6, vughy and blocky alternating massive microstructure, vertical planes, clay capping (arrow) and vertical oriented clasts (b) were interpreted as frost action microfeatures (thin section: MM1A II). **c**) Yellowish more loamy soil with fine granular microstructure with low degree of separation of aggregates and angular charcoal fragments (arrows) represents the not in situ soil noticed in the upper part of SU6, just below the scour structure (Unit 5 lower boundary – MM1B II). **d**) Early and Mid-Holocene soil is more brownish with loamic texture characterized by large soil mesofauna structures in which coarse pedons (to notice is the different internal fabric) are surrounded by finer organo-mineral excrements (MM3 I). **e**) Boundary (dashed line) between SU4 and SU3 (dark paleosol below Islamov’s dump), the microstructure of SU3 is complex whereas SU4 shows mainly a massive structure (MM4 I). **f**) Coarse granular microstructure with a high degree of separation as an effect of soil fauna activity characterizes the top of SU3 (MM4 II). The micro photos are in plane polarized light after Brancaleoni et al. (2022). ..... 52

**Figure 6-4** Artefact distribution within the profile at Obishir-1. **a**) Projected lithic artifacts from 0–1.5 m distance from the E wall of the 2016–2018 excavation. **b) – c**) Scatter plots of all recorded lithic artifacts. From Brancaleoni et al. (2022). .... 53

**Figure 6-5** A summary of observed features in sediments at the Obishir and Katta Sai complexes from Brancaleoni et al. (2023) ..... 56

**Figure 6-6** Microphotographs illustrating occupational facies; **a c**) Bronze and Middle Ages (SU1) facies is characterized by an horizon with (ab) micro laminated structure with differing b-fabric, white arrow is indicating a whitish gray crystallitic b-fabric due to sorted mineral grains (mainly quartz and calcite), red arrow is indicating steeple speckled due to loamy brown material; and (c) broken elongated phytolith, evidence of post-depositional modifications due to trampling; **d-f**) Obishirian (SU2 and SU3), total reworking reflects the chaotic arrangement and typical granular microstructure of the fabric, (de) groundmass made of biological droppings, black and white arrows point a dung aggregate in ppl and xpl respectively, fecal spherulites occur within the aggregate and in the surrounding groundmass, (e) b-fabric is dotted due to fecal spherulites, except for voids which are partially filled by micritic calcite; (f) this facies is featured by typical association of components, that are dung aggregates (red arrow), bone (white arrow) and charcoal fragments, note that the bone is in situ cracked (a close-up on the cracks is given in Fig. 5f) **g h**) Paleolithic’s typical compacted micro-granular structure (SU4 and SU5) and rare amount of archaeological components and the presence of phosphatic features led to a suspected

decomposition of elements, as shown in h the white arrow points a phosphatic rim characterizing a sub-rounded limestone pebble. From Brancaleoni et al. (submitted).....	59
<b>Figure 7-1</b> Ternary plot after grain size analysis for the fine fraction < 2 mm from Obishir-1 and Obishir-5.....	63
<b>Figure 7-2</b> Phosphorus profiles at the selected locations. <b>a)</b> Phosphorous profiles at Obishir-1 (in yellow) and Obishir-5 (in black); <b>b)</b> Boxplot showing the P mean values for Obishir-1 and Obishir-5.....	64
<b>Figure 7-3</b> Example of micromorphological thin sections from the two locations. <b>a)</b> Obishir-1, thin section MM3.1, SU4, the thin section is almost sterile, high amount of coarse limestone fragments and coarse burrows (example in dash line); <b>b)</b> Obishir-5, thin section MM3.1, SU2.2, the coloration is much darker, and there is the presence of coarse bone and charcoal fragments (black and red arrows), as well as the presence of dung pellets (pink arrow). .....	66
<b>Figure 7-4</b> Archaeological sites with stabling facies, DEM depths are in m asl.....	71

# ***List of tables***

<b>Table 1</b> The three scientific publications related to this thesis and their main results are summarized .....	4
<b>Table 2</b> Types of sediments modified after Goldberg and Macphail (2006), Karkanas and Goldberg (2018), between brackets are indicated the lithified equivalents .....	24
<b>Table 3</b> Different types of stratigraphy that can be utilized in an archaeological context after Goldberg and Macphail (2006), Morrissey, Mentzer and Wurz (2022) .....	26
<b>Table 4</b> Characteristics of non-laminated loess-derived colluvial sediments from Mûcher, Steijn and Kwaad (2010).....	29
<b>Table 5</b> Few rules for recognizing in situ from not in situ features during micromorphological analysis (Mûcher, Steijn and Kwaad, 2010; Stoops, Marcellino and Mees, 2010) .....	30



*To my beloved ones*  
*And to peoples of Central Asia*

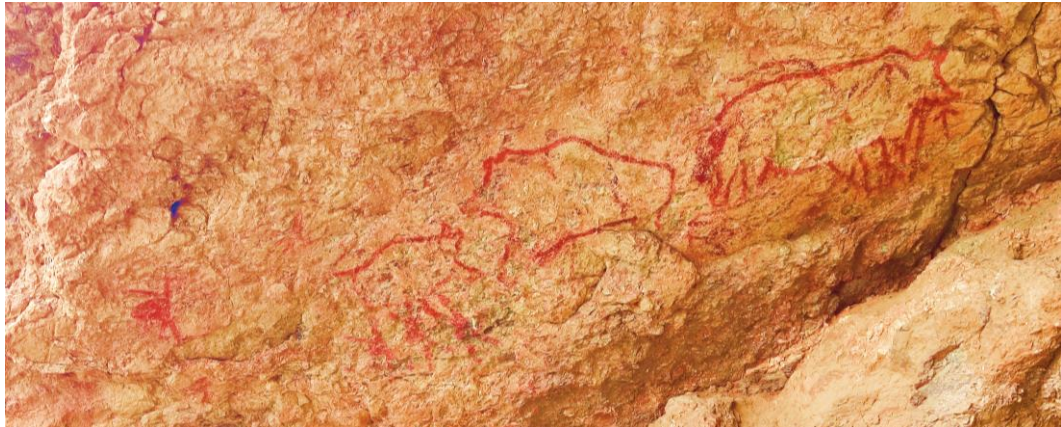
# 1 Introduction

## 1.1 Background

Central Asia (CA) is a cross-road for human migrations and cultural exchange thanks to its central position in the Asian continent. Since prehistory, it has acted as a bridge between the West and the East, and vice versa (Iovita *et al.*, 2020; Finestone *et al.*, 2022). Its territories have witnessed the dispersals of hominins, cultures and animals (e.g., Zwyns *et al.*, 2019; Shnaider *et al.*, 2020; Taylor *et al.*, 2021; Ghasidianid *et al.*, 2023). It is a region of diverse landscapes, ranging from deserts to alpine forests in mountain regions, characterized by continentality and progressive aridification. Different landscapes have provided the groundwork for the evolution of differing sustainable strategies and practices (Spengler, 2014; Shnaider *et al.*, 2023). The arid climate has also offered examples of adaptation under extreme conditions and has likely supported migration strategies within the region (Comas *et al.*, 1998; Spengler, 2014; Prudnikova, 2017). A crucial moment in the development of human cultures, globally and also in CA, was the Neolithization process. The Neolithization process stands as a pivotal event in cultural and economic development. It marks the introduction of food production practices and often coincides with the emergence of sedentary lifestyles, cultivation, and/or animal husbandry activities (Vigne, 2015).

In the last decades, Neolithic archaeological research has been increasingly focusing on CA (Taylor *et al.*, 2020, 2021; Brunet, 2021; Nishiaki *et al.*, 2022; Spate, Leipe and Motuzaite Matuzeviciute, 2022; Suska-Malawska *et al.*, 2022; Shnaider *et al.*, 2023). And the Neolithization process in the region is believed to have occurred mainly because of dispersal and/or interaction with the farming societies of Southwest Asia (Nishiaki *et al.*, 2022). Little is known about the phenomenon of Neolithization in the interior mountains of CA, and the associated dispersal of animals and cultures from the Levant to Asia (Taylor *et al.*, 2021). What is known so far is that this process was a long one, with its roots from the Mesolithic to the Chalcolithic (Brunet, 2021). There is a lack of general trends in the adoption of different economic strategies (Brunet, 2021), and local conditions may have favored various strategies, such as an economy based on hunting and herding, but also fishing, as seen in the Keltaminar culture (Brunet, 2021). Nevertheless, climate and local environment are not to be considered as driving factors in explaining the emergence of new lifestyles and economic strategies (Brunet, 2021). According to the same author, more relevant elements include art (an example is given in **Figure 1-1**), high-value items, architecture, burial practices and animal domestication (Brunet, 2021). Similar conclusions based

on relatively minor changes in the malacological record in the Fergana valley at Obishir-5 location were drawn by one of my coauthored papers (Osipova *et al.*, 2021).



**Figure 1-1** *Hunting scene in Shakhty Cave archaeological site in the Pamirs (Tajikistan, CA), the paintings are attributed to the Mesolithic era.*

The Obishirian culture might have played a pivotal role in the development of early forms of Neolithization in the interior mountains of CA. The culture was firstly discovered by Soviet scholars in the mid-20<sup>th</sup> century (Islamov, 1972, 1980) and initially attributed to the Epipaleolithic (Mesolithic), i.e., it was regarded as a Holocene continuation of the Paleolithic hunter-gatherer lifestyle inherited from the Pleistocene. More recent studies, however, unveiled the presence of domestic animals in the Obishirian sedimentary record, raising evidence of its link with the Neolithization process. For instance, a pivotal study presented in one of my coauthored papers (Taylor *et al.*, 2021), assessed the presence of domestic sheep and goat at one of the Obishirian locations—Obishir-5. This evidence is very strong, supported by proteomic identification of taxonomy, the mitochondrial DNA identification of domestic sheep haplogroup from Southwest Asia, and radiocarbon dating. These finds make the Obishirian a key archaeological unit in mountainous CA, directly connected with the introduction and spread of Neolithic traits.

The challenge with Obishirian sites lies in the scarcity, fragmentation, and poor preservation of bone remains (Taylor *et al.*, 2021; Serdyuk *et al.*, 2023). This limitation constrains the analytical applications in zooarchaeology, thereby restricting interpretational possibilities and hindering our comprehensive understanding of the Obishirian role in the Neolithization network. An unresolved question pertains to how the culture adopted herding strategies, and whether it adopted them at all. For instance, the presence of domestic animals does not necessarily imply pastoralism. It could also indicate hunting for feralized animals, or access to imported meat from neighboring Neolithic communities, as seen in some European Mesolithic hunter-gatherer societies (Rowley-Conwy, 2011; Krause-Kyora *et al.*, 2013). Even if the assumption of local herding is accepted at Obishirian sites (Taylor *et al.*, 2021), questions arise about the quality and stability of these herding practices. These questions encompass various aspects, such as the

sharing of herding activities (foraging, stabling, butchering, foddering) among specific sites, the use of adopted spaces for activities like stabling animals overnight, during winter, or for processing (shearing, butchering, breeding, etc.), and the management of such adopted spaces (e.g., cleansing to remove accumulated excrements). While zooarchaeological methods are constrained by the preservation state of bones, geoarchaeological approaches offer avenues to explore answers to these crucial questions.

Another challenge concerning Obishirian sites is the presence of colluvial facies. Colluvial facies are poorly understood, and their complex structure and history may involve syn- and post-depositional processes that could impact or completely obliterate the archaeological record. Colluvial facies are also affected by the issue of equifinality, where different processes may result in similar sedimentological characteristics (Bertran and Texier, 1999). Therefore, the application of geoarchaeological approaches becomes an effective strategy in the study of Obishirian sites, their formation history, and the evaluation of the integrity of their archaeological record. The geoarchaeological approach proves particularly effective in unveiling unresolved issues, such as the herding problem observed in Obishirian sites, and brings to light stratigraphic aspects that other techniques may overlook (Goldberg and Aldeias, 2018).

Moreover, geoarchaeological studies are poorly carried out in CA. This thesis stands out as one of the few endeavors that apply a geoarchaeological approach to investigate and address specific issues related to the formation history of the selected locations. Specifically, this thesis centers on two adjacent Obishirian sites—Obishir-1 and Obishir-5. My efforts have been directed towards establishing a geoarchaeological context for these locations, and the outcomes are documented in three papers, as outlined in **Table 1**.

**Table 1** The three scientific publications related to this thesis and their main results are summarized

Paper	Main results
Brancaleoni, G., Shnaider, S., Osipova, E., Danukalova, G., Kurbanov, R., Deput, E., Alisher kyzy, S., Abdykanova, A., Krajcarz, M. T. (2022). Depositional history of a talus cone in an arid intermontane basin in Central Asia: An interdisciplinary study at the Late Pleistocene–Late Holocene Obishir-I site, Kyrgyzstan. <i>Geoarchaeology</i> , 37, 350–73. <a href="https://doi.org/10.1002/gea.2189">https://doi.org/10.1002/gea.2189</a>	This paper explores the site formation history at one of the Obishir locations, in particular the Obishir-1 site
Brancaleoni, G., Kot, M., Shnaider, S., Mroczek, P., Kurbanov, R., Abdykanova, A., Alisher kyzy, S., Khudjanazarov, M., Pavlenok, K., Krajcarz, M. T. (2023). A closer look at clasts and groundmass: Micromorphological features in sediments with archaeological significance in Obishir and Katta Sai complexes (Central Asia), <i>Journal of Archaeological Science: Reports</i> , 51, 104118, <a href="https://doi.org/10.1016/j.jasrep.2023.104118">https://doi.org/10.1016/j.jasrep.2023.104118</a>	This paper explores one of the sedimentological aspects encountered at the Obishirian sites, which is the mutual presence of gravel and silt sedimentary materials, and aims at drawing parallels concerning post-depositional disturbances of archaeological artifacts.
Brancaleoni, G., Shnaider, S., Lempart-Drozd, G., Deput, E., Abdykanova, A., & Krajcarz, M. T. (in press). Geoarchaeological approach for tackling the function and preservation state of the Obishir-5 site, the earliest Neolithic site in the Fergana Valley, submitted on 23 <sup>rd</sup> October 2023 at <i>Journal of Archaeological and Anthropological Sciences</i>	This paper explores the site formation of the Obishir-5 site and tackles the issue of herding practices at this location

## 1.2 Research objectives

This thesis was conceived as part of a broader geoarchaeological investigation comprising multiple sites in CA (National Science Center of Poland, grant number 2018/29/B/ST10/00906). Specifically, the focus of this thesis is on two Obishirian sites, with the following objectives:

1. Defining the site formation processes at these sites, which involves comprehending the natural and anthropogenic factors contributing to the accumulation of materials and potential disturbances at the selected locations, with a specific focus on colluvial deposits. This geoarchaeological investigation aims to provide context to the archaeological record and offer insights into the human-environment relationship in the interior corridors of CA.
2. Addressing site-specific issues, such as the challenge of understanding herding practices at Obishir-5. Although the faunal assemblage suggests the use of domestic animals, it does not conclusively determine whether the

livestock was present at the site while alive. The application of a micro-stratigraphic approach is intended to shed light on this matter.

3. Assessing the integrity of the Obishirian assemblages at the selected locations, as a correct interpretation of the archaeological record relies on understanding the processes responsible for potential disturbances affecting both the deposit and the archaeological record.

To achieve the aforementioned objectives, a comprehensive and multifaceted approach was employed in the study of site formation. This approach encompassed various techniques at both macroscopic and microscopic scales, beginning with accurate field recording and strategic sampling, which served as the foundation for subsequent analyses. The primary technique employed was micromorphology, recognized as one of the most effective tools in site formation studies, providing a basis for contextualizing other analyses (McAdams, 2020). Consequently, grain size analysis, geochemical characterization, and mineralogical assessment of the sedimentary record were also integrated into the methodology. The study also exploited the results of faunal remains, particularly mollusk assemblages, offering insights into the palaeoecological and paleoenvironmental conditions of deposition. Additionally, artifact distribution was examined to explore the spatial arrangement of artifacts at the locations and potential disturbances. Ultimately, radiocarbon measurements and luminescence dating were incorporated to confirm the chronology of the studied units.

## 1.3 Thesis significance and structure

The significance of the thesis lies in shedding light on both physical and anthropogenic processes occurring at the selected sites, and the development of a methodological approach to tackle specific aspects of colluvial facies, such as the matrix-clast relationship within those sediments. The thesis also aims at gaining insights into essential aspects of the Neolithization process in the interior mountains of CA and a better understanding of sedimentary facies, particularly colluvial deposits, which are poorly studied, especially in arid settings. The thesis is divided into seven chapters:

- **Chapter 1 Introduction** provides an overview on the general topic, where the thesis objectives and significance are defined
- **Chapter 2 Macro-regional contexts and archaeological background** provides a regional context for the study area, offering descriptions of the geographical, geological, and climatic conditions, as well as the archaeological background of the macro region

- **Chapter 3 The sites** delves into the description of the sites, detailing their local settings, prior research conducted during the second half of the last century, recent studies, and characteristics of the archaeological assemblages
- **Chapter 4 The rationale** outlines the theoretical framework of the geoarchaeological approach, with a particular focus on the types of sediment expected to be found at the selected locations
- **Chapter 5 The methods applied** provides an overview of the methodologies employed for studying the archaeological sites, and a critical discussion of each methodology
- **Chapter 6 Results** summarizes the obtained results enclosed in the three scientific papers
- **Chapter 7 Discussions and conclusions** draws conclusions comparing the case studies, emphasizes the significance of the dissertation, and also outlines potential future directions.

## 2 Macro-regional contexts and archaeological background

### 2.1 Geographic context

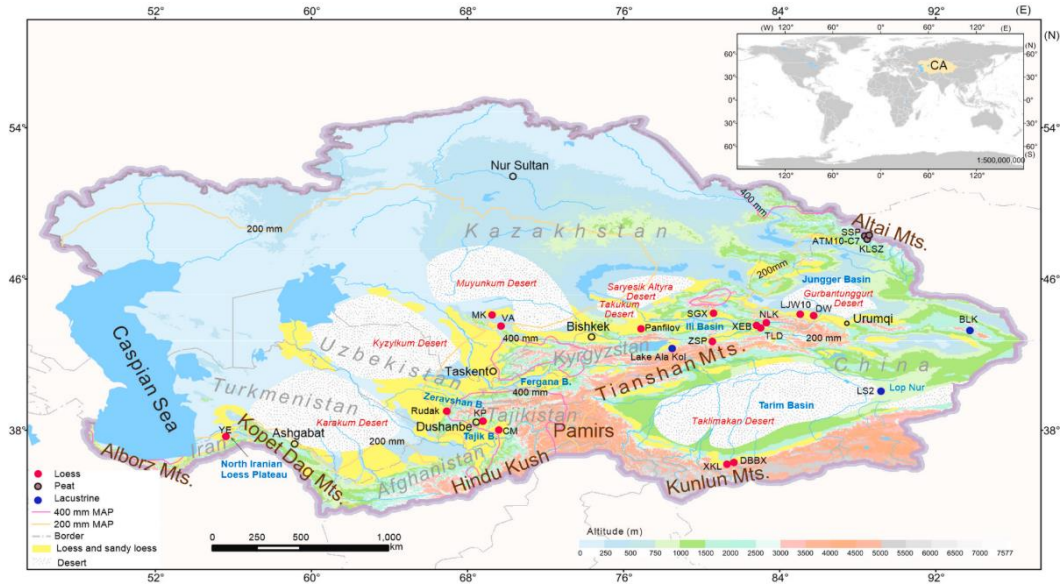
The Obishirian archaeological complex is located in southwestern Kyrgyzstan, within CA (**Figure 2-1**). There are several geographic terms to refer to the central area of Asia, among others, that is ‘Middle Asia’ and ‘Central Asia’ (Cowan, 2007) (**Figure 2-1**). The broader term ‘Central Asia’ (CA) is adopted in this study and encompasses Xinjiang, Kazakhstan, Kyrgyzstan, Uzbekistan, Tajikistan, Afghanistan, Pakistan, Kashmir, Tibet, Qinghai, Gansu, Inner Mongolia, Mongolia and the Russian Federation (Cowan, 2007). The term ‘Middle Asia’ used in Soviet Union refers to Kazakhstan, Turkmenistan, Uzbekistan, Tajikistan and Kyrgyzstan (Cowan, 2007). Most of these countries are landlocked, meaning they lack access to the sea, which is located at a considerable distance. CA geographic position works as a corridor connecting the West with the East. Its mountain corridors have been used since ancient times, with the establishment of a proper road—the Silk road—connecting western and eastern territories of Asia.

CA sits at mid- and low-altitudes (**Figure 2-1** and **Figure 2-2**) and is characterized by aridity, tectonic activity, continentality, high elevations (the highest peak—Victory peak—reaches 7439 m above sea level—asl) and depressions (with the lowest elevation being 154 m below sea level in the Turfan depression). These geographical features result in a wide variety of landscapes, including the Kara Kum, TaklaMakan and KyzylKum deserts (**Figure 2-2**), and highlands with steppe vegetation, which are distinctive features of the Tian Shan and the Pamirs mountains (**Figure 2-2**). This geographic context is a direct expression of the complex geological history of CA.





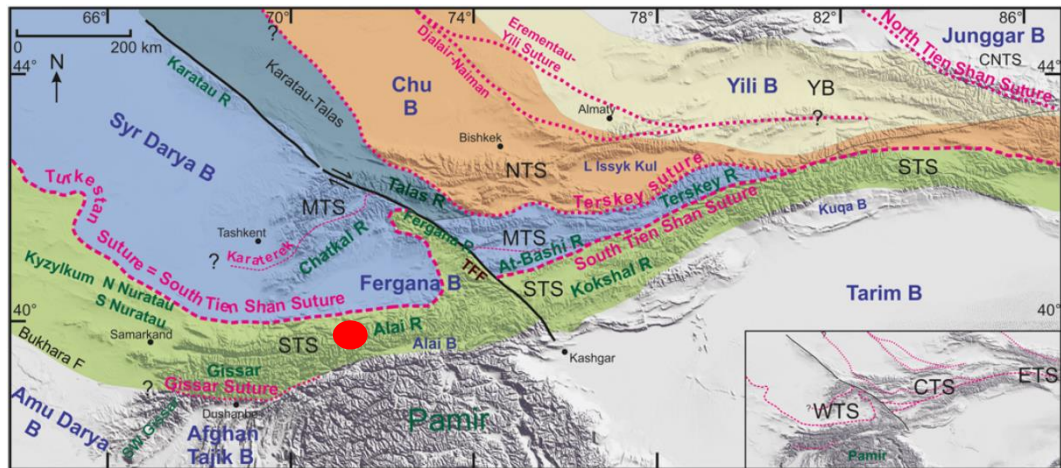
**Figure 2-1** Location of the study area. The countries that are encompassed by the two geographic terms ‘Middle Asia’ and ‘Central Asia’ are illustrated according to Cowan (2007).



**Figure 2-2** Most important geographic elements of CA. Mean annual precipitation (MAP) isohyets are also shown, taken from Song *et al.* (2021).

## 2.2 Geologic context

The geologic context of CA is complex and poorly studied (Brunet, Sobel and Mccann, 2017). To date, the only comprehensive geological cartography is the Soviet one at a scale of 1:100k. Bigger scales are rare, scattered, fragmented and are carried out to fulfill specific purposes (e.g., Hnylko *et al.*, 2019; Cuthbertson *et al.*, 2021).



**Figure 2-3** Location map showing the major tectonic structures of the western Tian Shan and regional subdivisions from Brunet, Sobel and Mccann (2017). The red circle indicates the location of Obishirian sites

The geological history that shaped CA saw three main geotectonic events that are: 1) the Precambrian-Paleozoic orogenesis; 2) Mesozoic accretion of Cimmerian blocks (Triassic-Early Jurassic) and consequent sedimentary basin formations; and the Indian-Eurasian collision (Early-Middle Eocene); and 3) Arabia-Eurasia (Late Eocene-Early Oligocene) collision during the Cenozoic. These events also shaped the elongated belt—Tian Shan—stretching along an E-W axis (**Figure 2-3**) from Xinjiang in NW China to the Aral Sea in Uzbekistan. Importantly, the aforementioned geological history triggered a gradual continentality and therefore aridification of CA.

Quaternary deposits across CA remain inadequately studied and are only fragmentally mapped. The predominant focus in previous research has been on aeolian, glacial, and lacustrine deposits due to their significance as valuable regional and global paleoenvironmental records, coupled with their relative ease of dating. However, this thesis uniquely centers its attention on slope deposits, particularly those found in taluses containing loess-like sediments, such as those observed at Obishirian sites (Brancaleoni *et al.*, 2022, 2023). Previous studies indicate that slope deposits are ubiquitous in mountainous regions of CA. Solifluction deposits, for instance, are prevalent at altitudes between 900 and 1400 m asl in the Tian Shan and Pamir mountains (Gorbunov and Seversky, 1999). Debris flow deposits were recognized in valleys of the Pamirs at an altitude between 1800 and 4000 m asl (Stübner *et al.*, 2021). In addition, various slope-related landforms associated with glaciation and deglaciation have been identified within river systems (Hewitt, 2002; Stübner *et al.*, 2021).

Concerning talus deposits in CA, which are found at Obishir-1 and Obishir-5, they have been mentioned in studies related to earthquake-induced instability (Strom and Wang, 2022). In particular, the term “talus” or “scree” generally refers to coarse-grained deposits situated along

and at the base of a slope resulting from processes like rockfall and other gravity-related phenomena. Taluses tend to be associated with steep cliffs and directly onlap the bedrock (Turner, 1996; Ventra, Diaz and De boer, 2013; Brancaleoni *et al.*, 2022).

Shifting the focus to aeolian deposits, the study centers on loess and loess-like deposits. Loess deposits are well-sorted, quartz-rich terrestrial clastic sediments composed predominantly of silt-sized particles formed essentially by the accumulation of wind-blown dust (Pye, 1987, 1995; Pécsi, 1990; Dlussky, 2009; Lancaster, 2020). Field investigation and previous studies suggest that loess sediments are predominantly distributed on river terraces and windward piedmonts of Central Asian high mountains since the Upper Pliocene (mainly Upper Pleistocene) (Song *et al.*, 2021) (**Figure 2-2**). Additionally, loess-like deposits can be found incorporated into slope deposits such as taluses (Brancaleoni *et al.*, 2022, 2023).

## 2.3 Regional climate and paleoclimate

As a result of geographic position and geological history, CA has a continental arid and semi-arid climate (Lioubimtseva and Henebry, 2009). This means low precipitation rate, with mean annual precipitation rate between 200 and 400 mm/yr (**Figure 2-2**) and daily and annual high temperature amplitudes. This results in the development of weak and sparse surface vegetation, and therefore to the development of bare landscapes prone to incision and erosion (French, 2019).

Climate in CA is mainly driven by the interaction among Westerlies, Asia monsoons and Siberian Highs (Shi *et al.*, 2020; Song *et al.*, 2021). The complex orography and geographic position of CA also contribute to the establishment of micro-climates within the entire region especially in the mountainous areas which possibly constituted refugia for hominids, animals and flora during coldest and driest phases since the Late Pleistocene (Beeton *et al.*, 2014; Spate, Leipe and Motuzaitė Matuzeviciute, 2022). Therefore, in study archaeological sites in the region is of the utmost importance the understanding of local conditions rather than regional where long-term trends are poorly understood (Iovita *et al.*, 2020; Spate, Leipe and Motuzaitė Matuzeviciute, 2022).

Nevertheless, studies on loess and fluvial deposits within CA reveal that the paleoclimate and paleoenvironment manifest a long-term stepwise drying or desertification trend of CA over the past 1 Million years (Myr), with at least one major drying event occurring at about ~0.5–0.6 Myr (Song *et al.*, 2021). One of the consequences of this is the development of modern deserts (e.g., Kara Kum, KyzylKum). Despite the overall drying trend since the last interglacial period, the Holocene is characterized by a persistent wetting trend with millennial-scale oscillation (Song

*et al.*, 2021). Overall, climate has also a strong impact on human behavioral patterns. Successful exploitation of these marginal areas require economy diversification, high mobility or food storage strategies together with exchange systems (French, 2019).

## 2.4 Archaeological background

CA occupies a strategic position as a crossroads linking East and North Asia to Europe and the Levant. It has played a pivotal role in the West-East transfer route since ancient times, dating back to the Palaeolithic (Iovita *et al.*, 2020; Finestone *et al.*, 2022). Some scholar suggested the existence of a “paleo-Silk road” since the Palaeolithic era (Nasab, Clark and Torkamandi, 2013; Frachetti *et al.*, 2017; Iovita *et al.*, 2020). Consequently, much archaeological research in CA focuses on determining the timing and routes of dispersal concerning mainly hominids (e.g., Zwyns *et al.*, 2019; Ghasidianid *et al.*, 2023) but also cultures and animals (e.g., Shnaider *et al.*, 2020; Taylor *et al.*, 2021).

However, it is important to note that the archaeological record in CA is relatively sparse, fragmented and dating is challenging. Scholars have argued that the reason of the scarcity of the archaeological record and its challenges is rather a matter of site preservation, disturbances and/or archaeological survey logistics rather than infrequent human occupation (Beeton *et al.*, 2014; Iovita *et al.*, 2020; Varis *et al.*, 2022). Moreover, many archaeological sites lack geoarchaeological investigation and the understanding of site formation in the region (Varis *et al.*, 2022). This limitation hinders our understanding of hominin and cultural dispersal over time (Taylor *et al.*, 2021; Finestone *et al.*, 2022; Nishiaki *et al.*, 2022; Varis *et al.*, 2022).

This section provides an introductory overview of the Paleolithic era and primarily focuses on the Epipaleolithic (also known as Mesolithic or Pleistocene-Holocene transition) and the Neolithic periods (Early Holocene-Middle Holocene) across a broader geographical region. At Obishir-1 and Obishir-5, the earliest archaeological record dates back to Epipaleolithic, however in the micro-region Sel’Ungur Cave holds evidence of human presence since the late Middle Paleolithic (MP) (Krivoshapkin *et al.*, 2020).

### 2.4.1 Paleolithic

Archaeological evidence traces hominin dispersals back to the Lower Paleolithic (approximately 3.3 Myr to 300.000 years ago) in CA, with the Kul’dara cultural unit in the Tajik depression as the earliest example (Dodonov, 1991). In the MP (about 300.000 years ago to 30.000 years ago), DNA evidence supports presence of various hominin species, including Neanderthals and Denisovans, indicating Neanderthal dispersal into CA (Andreeva *et al.*, 1990;

Krause *et al.*, 2007; Slon *et al.*, 2018). Significant MP discoveries have been made in cave sites in mountainous regions, such as Teshik Tash Cave, Obi-Rakhmat Cave, Sel'Ungur Cave, Denisova Cave and Chagyrskaya Cave. During the Upper Paleolithic (UP; from roughly 50.000 to 10.000 years ago), *H. sapiens* from western and eastern Europe emigrated through CA (Fu *et al.*, 2014; Zavala *et al.*, 2021). Overall, the UP is poorly represented in CA (Ranov and Davis, 1979; Davis and Ranov, 1999; Kolobova *et al.*, 2013a). Some cave sites, including Denisova Cave and Obi-Rakhmat Cave, feature UP assemblages.

## 2.4.2 Epipaleolithic

In the context of Near East and CA, the term 'Epipaleolithic' (EPP) is preferred over 'Mesolithic'. This period, particularly in CA, has received limited scholarly attention, and at times, overlaps with the UP. A.P. Okladnikov first introduced the concept of Late Pleistocene-Early Holocene archaeological sites in CA, Siberia and Far East (Shnaider *et al.*, 2020). He categorized geometric microlithic industries as "Mesolithic" based on the European paradigm (Shnaider *et al.*, 2020). However, the term "Epipaleolithic" is now used to encompass all assemblages from western CA in the timeframe between the Last Glacial Maximum (roughly 18000 BCE) and the onset of the Neolithic (8000 BCE). This term emphasizes cultural similarities between CA and the Levant/Zagros (Shnaider *et al.*, 2020). Emblematic EPP sites are: Tutkaul, Obi-Kiik and Kulbulak. S. Shnaider, as mentioned in Shanaider *et al.* (2020), suggests a roughly synchronous distribution of similar types of geometric microlithics between the Levant and Zagros with sites from western CA (i.e., Tutkaul and Obi-Kiik). This suggests a similar cultural trajectory of Epipaleolithic complexes on a macro-regional scale. Along with that, other authors (e.g. Richter, 2009; Olszewski, 2012) suggest antiquity of cultural contacts and dispersal of tool techniques between these regions (Shnaider *et al.*, 2020).

## 2.4.3 Neolithic and Neolithization

The Neolithic period, spanning roughly from 10000 to 3000 years ago, is characterized by significant cultural evolution and technological advancements. The Neolithization process stands as a pivotal event in cultural and economic development, marking the introduction of food production practices and often coinciding with the emergence of sedentary lifestyles, cultivation, and/or animal husbandry activities (Vigne, 2015). The earliest manifestations of sedentism and food production can be traced back to the Levant at the close of the 9th millennium BCE (**Figure 2-4**). From there, the process of Neolithization gradually extended its influence. In western Europe, evidence of this transition dates to the 6th millennium BCE (Hamon and Manen, 2021). Simultaneously, it spread eastward to the Iranian plateau (Brunet, 2021), and further into CA (**Figure 2-4**) (Taylor *et al.*, 2021).



**Figure 2-4** Modeled dispersal of domestic animals into CA proposed by Taylor *et al.* (2021)

In CA, the Neolithization process was marked by the emergence of sites characterized by mixed steppe and oasis cultural assemblages (Brunet, 2021). The Neolithic is traditionally associated with the establishment of the Jeitun culture during the 7<sup>th</sup> to 6<sup>th</sup> millennium BCE in South Turkmenistan and with tribes of Iran (Sarianidi, 1992; Nishiaki *et al.*, 2022).

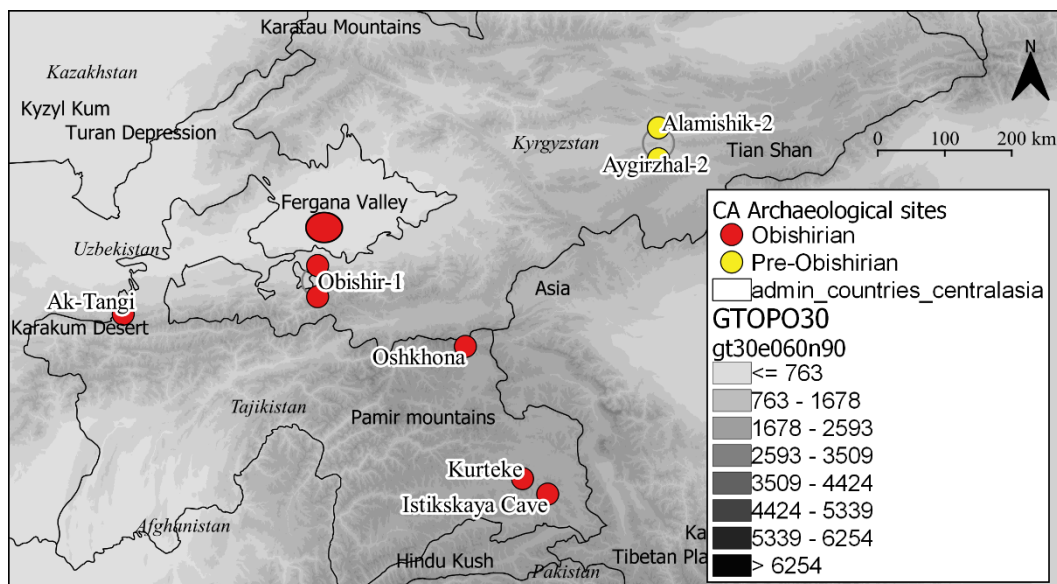
In the south-eastern region of the KyzylKum desert in Uzbekistan, the Keltaminar culture represented a nomadic population engaged in animal herding, along with hunting, gathering and fishing (Brunet, 2021; Nishiaki *et al.*, 2022; Suska-Malawska *et al.*, 2022). Earliest dates are from the stratified site of Ajakagytm, attesting to an occupation as early as 7300 BP (Brunet, 2012, 2021), at the same site there is evidence of camel husbandry dated between 5000-4000 BP (Suska-Malawska *et al.*, 2022). On top of that, the Neolithization process in CA was influenced by cultures such as the Hissar (in the mountain areas of South Tajikistan; **Figure 2-4**) and Central Fergana. On the easternmost fringe of CA, in southern and northern Xinjiang which includes the Tarim basin, animal husbandry and hunting were primary economic activities limited to oasis regions (Zhimin, 1992).

However, the Neolithization process in the mountainous regions of CA remains less understood (Nishiaki *et al.*, 2022). Here, rockshelter sites play a crucial role in shedding light on the Neolithization process (Taylor *et al.*, 2021; Nishiaki *et al.*, 2022). And, Obishir-5 provides some of the earliest evidence for the use of livestock (Taylor *et al.*, 2021). This discovery contributes significantly to our understanding of the development and spread of agro-pastoralism in a region where there is limited knowledge about when and how this transformation first occurred (Taylor *et al.*, 2021).

### 2.4.3.1 The Obishirian

The Obishirian is an archaeological cultural unit closely associated with the increasing number of archaeological sites in the Fergana Valley and its surrounding territories during the Early Holocene (**Figure 2-5**). The term "Obishirian" was first introduced by a Soviet scholar U. I. Islamov in 1980 (Islamov, 1980). Initially, the Obishirian culture was attributed to a group of Epipaleolithic sites in the Sokh River valley, believed to be at the origin of the Neolithic culture in the Fergana Valley (Sayfullaev, 2017). Renewed interest in this culture emerged through recent scholarly expeditions, commencing in 2015 led by S. Shnaider. Initially categorized as an Epipaleolithic unit (Shnaider *et al.*, 2017), recent discoveries related to the faunal assemblage have confirmed that it represents the early Neolithic. The Obishirian culture is widespread, extending from the Pamir mountains in the south to the Tian Shan in the north and east, with sites depicted in **Figure 2-5**.

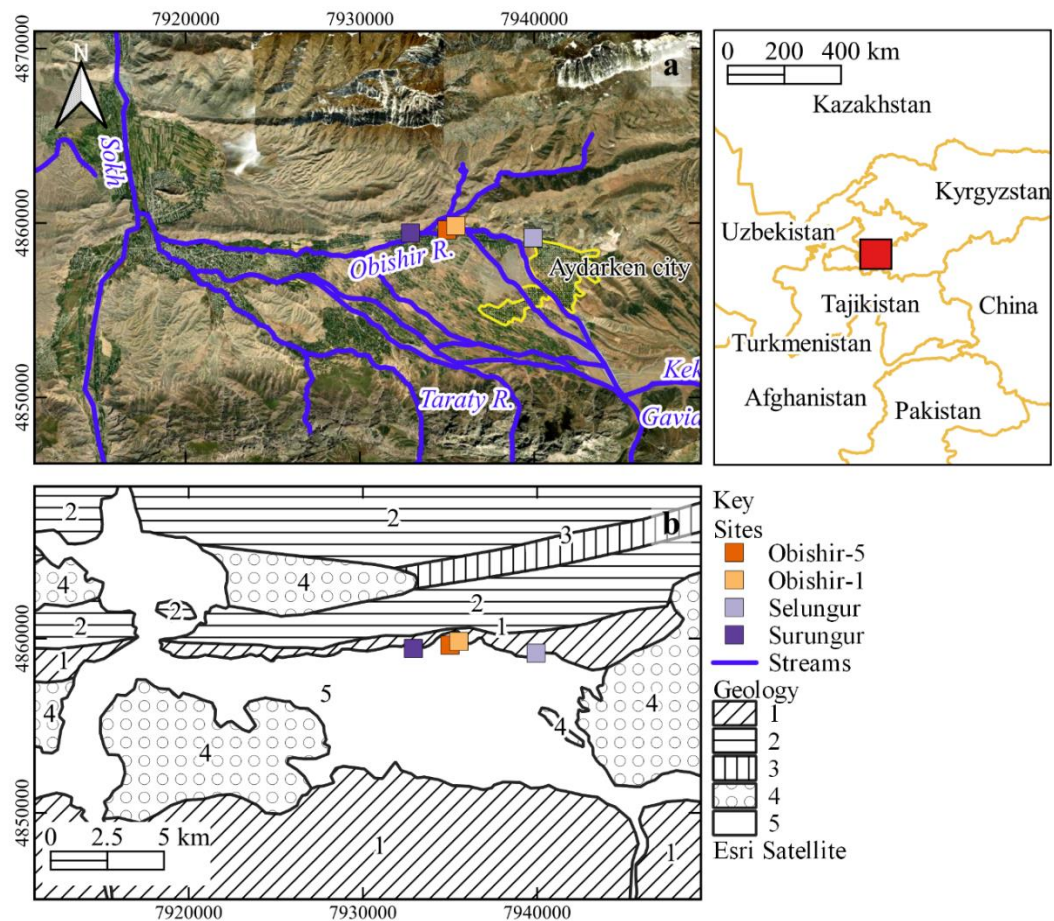
The Obishirian culture is characterized by its distinctive microlithic technology, boasting an industry primarily dominated by microblade pressure knapping, bladelets and microblades featuring alternating and ventral retouch, unitary segments, choppers, and chopping-tools (Fedorchenko *et al.*, 2018). The unit is closely dated between 9500 and 6500 BP (Taylor *et al.*, 2021; Brancaleoni *et al.*, 2022). Archaeological sites bearing Obishirian material are: Obishir-1, Ak-Tangi, Central Fergana complexes, Istykskaya Cave, Oshkhona, and Kurteke rockshelter (Shnaider, pers. comm.)(**Figure 2-5**).



**Figure 2-5** Spatial distribution of Obishirian and Pre-Obishirian sites. GTOPO30 base map (DEM-Digital Elevation Model; *gt30e060n90* and *n40*; source USGS EROS Archive from <https://www.usgs.gov>) and cultural vector map data from ([www.naturalearthdata.com](http://www.naturalearthdata.com)).

### 3 The sites

The Obishir-1 (39°57'28.6" N, 71°17'08.9" E; 1,731 m asl) and the Obishir-5 (39°57'23.3" N, 71°16'52.4" E; 1710 m asl) sites are located at the foothills of an ENE-WSW-oriented Eshme ridge (indicated as Eshme Too in Soviet topographic maps, 1:100k). Toward the south, the ridge faces the Aydarken Basin drained by several streams, including the Obishir (**Figure 3-1a**).



**Figure 3-1** Localization and schematic tectonic setting **a)** Location of the site together with the other archeological sites excavated in the area; **b)** Tectonic scheme of the studied area after Hnylko et al. (2019). Key: **1** – (Par)autochthon Alay structural unit made of Devonian-Carboniferous Alay carbonate platform succession and Upper Carboniferous synorogenic flysch/olistostrome deposits. **2** – Lower nappes built in Silurian–Carboniferous terrigenous, pelagic and carbonate platform formations. **3** – Upper nappes represented by the ocean-derived formations with the Silurian to Devonian ophiolitic fragments. In the area, these nappes form a synformal structure. **4** – Neogene formations and **5** - Quaternary deposits.

These streams are small, braided, and temporarily recharged by meltwaters from winter snow and mountain glaciers of the South Tian Shan mountains (towards S), thus restricting the outflow mainly to the winter and spring seasons. The drainage is ESE-WNW diverting within the valley (**Figure 3-1a**) where artificial drainage is also present. The basin stretches for ca. 18 km



from E to W and is *ca.* 6 km wide. The surrounding landscape is mainly mountainous and dissected with the Aydarken Basin, which is a small intermountain basin surrounded by E-W oriented ridges to the north and the south and filled with Quaternary deposits (mostly of alluvial, aeolian, and colluvial origin). The valley closes to the west, where the streams converge into the Sokh (**Figure 3-1a**).

Several urban areas are located in the basin. Aydarken (Rus. Khaydarkan) is one of the largest and most urbanized towns, second only to Sokh. Excluding these, standalone rural houses and farming structures are spread within the basin. Agriculture and pastoralism comprise the most common land use types, and fruit orchards are generally grown for local commercial production. It is worth mentioning that the Eshme ridge has been extensively exploited for its mineral resources since the 1940s (UNEP, UNITAR, and Zoï E. Network, 2009). Therefore, the landscape is dominated by tailings piles, mines, and shafts.

### 3.1 Geological and geomorphological setting

In particular, the studied Obishirian sites are located at the foothills of the Alay range in the South Tian Shan orogen (**Figure 2-3**). The latter is a Late Paleozoic-aged, fold-and-thrust belt formed during the Precambrian-Paleozoic orogenesis. As a result of this collision and consequent sedimentary basin formations, the Aydarken basin was structured (**Figure 3-1a**).

Specifically, the Obishirian sites are located on the foothills of a south-directed nappe belt (Eshme ridge, in the Soviet Topographic map 1:100k). The ridge is made of a) upper ocean-derived thrust sheets (**Figure 3-1b** key 3); b) lower thrust sheets including carbonate platform formations, basin sediments between them (**Figure 3-1b** key 2); and c) (para)autochthon unit filled with carbonate platform formations (**Figure 3-1b** key 1). The cliff that houses Obishirian rockshelters is built of the c) type. The central portion of the Aydarken basin is filled with Quaternary deposits (**Figure 3-1b** key 5) mainly of fluvial, colluvial and aeolian origins. Neogene conglomeratic deposits form minor hills scattered within the basin, and a large paleo fan to the East valley (**Figure 3-1b** key 4). The paleo fan is topped irregularly by loess-like deposits (Late Pleistocene?), and remodeled by weathering processes and, only partially vegetated.

The southern margin of Eshme ridge is more exposed than the northern one. Thus resulting in a more dynamic slope characterized by ubiquitous talus deposits both apron and cones (**Figure 3-2a**). Moreover, the two main lithologies occurring in this portion of the ridge make the slope steeper where the limestone outcrops, whereas gentle where the shales do (**Figure 3-2a**). Several grottos of differing size characterize the ridge, as a consequence of karstic processes. The grottos mainly occur at the lithological contact between the limestone and the shale. The karstic landforms are expressions of late stage of karst and are in most of the cases tectonically aided.

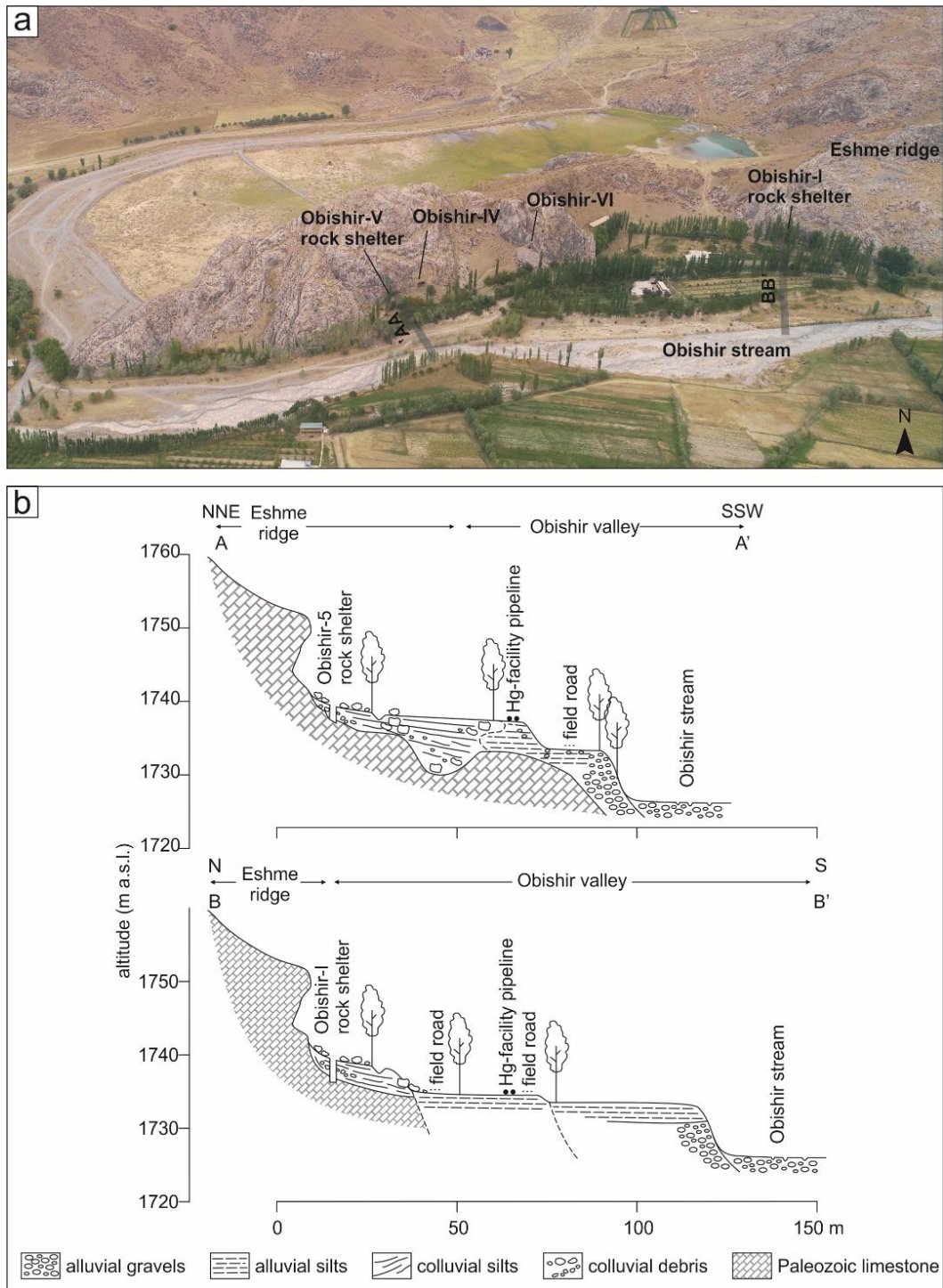
The archaeological sites are characterized by rockshelters, and not well-developed caves such as Sel'Ungur cave. In the hills above Obishirian sites, cataclastic deformation bands can be observed and accumulation of debris deposits on the slope is ubiquitous (**Figure 3-2a**).

According to the present-day Köppen-Geiger map (Beck et al., 2018), the climate affecting the study area is arid (B), steppe (S), and cold (k), with a mean annual air temperature (MAT) below 18 °C and mean annual precipitation (MAP) estimated to be below 250 mm a<sup>-1</sup>. Being arid, the terrain is subjected to the development of weak and sparse surface vegetation (Cooke, Warren and Goudie, 1993) and prone to mobilization downslope in mass movement erosive episodes (French, 2019). Moreover, in arid and semi-arid environments, rock outcrops and superficial debris are commonly affected by flaking, spalling, splitting, and granular disintegration (Cooke, Warren and Goudie, 1993).

Several archaeological sites (e.g., Obishir-1, Sel'Ungur Cave, Surungur rockshelter) are on the southern flank of the Eshme ridge (**Figure 3-2a**), and they have a geomorphological setting similar to that characterizing Obishir-5 (**Figure 3-2b**). They are located at the foot of a steep cliff, in front of a rockshelter niche or a cave entrance, where associated talus deposits overlay the bedrock or a flat alluvial terrace. The steep cliffs face mainly the south, and their heights range 20–30 m. The Obishir stream flows just in front of the Obishirian sites, approximately 100-150 m away toward the south (**Figure 3-2a**). Its flat terraces are used for agriculture and pastoralism.

At Obishir-1, the talus cone is approximately 60 m wide and spans the circa 30 m downslope from the cliff toe toward the south, where greater boulders overlap a flat alluvial terrace (**Figure 3-2b**). Its total thickness is up to circa 4 m. After comparing our data with the literature, we found that the Obishir-1 talus is immature, as the relationship between the slope height (15–25 m) and the average talus height (*ca.* 4 m) does not satisfy the equation proposed by Sanders, Ostermann and Kramers (2009). It is also possible that the cone originally had a greater length, which was reduced by later fluvial erosion, but no evidence supporting this was possibly observed in the field.

At Obishir-5, the talus cone is approximately 60 m wide and spans the circa 50 m downslope from the cliff toe toward the south, where is interfingering with the alluvial terrace (**Figure 3-2b**). The bedrock surface at Obishir-5 is not even (**Figure 3-2b**), as revealed by geophysical surveys carried out at the site (Olenchenko *et al.*, 2017), there are bumps approximately 10 m deep filled with soft sediments. The uneven bedrock surface is likely due to karstic processes. The talus' maximum thickness therefore up to circa 10 m (**Figure 3-2b**). It is also possible that the cone originally had a greater length and height, which was reduced by later erosional processes.

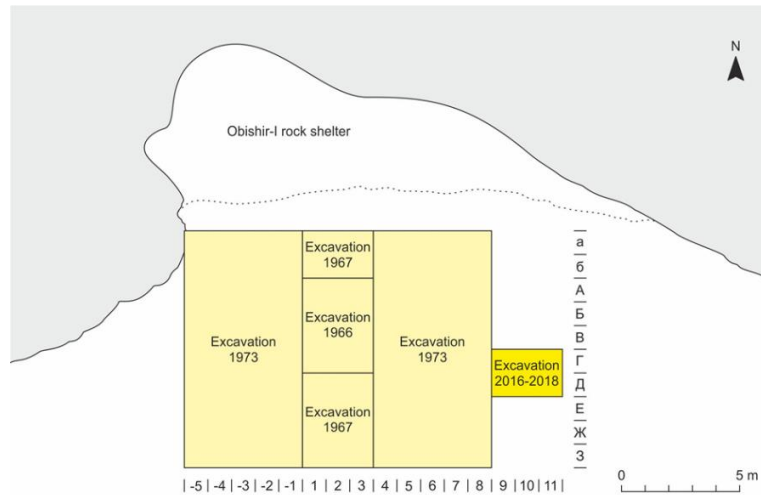


**Figure 3-2** Location of the Obishirian sites along the Eshme ridge with section profiles. *a)* Drone imagery comprising the southern slope of the Eshme ridge where Obishir archaeological sites were discovered; *b)* schematic sections AA' and BB'.

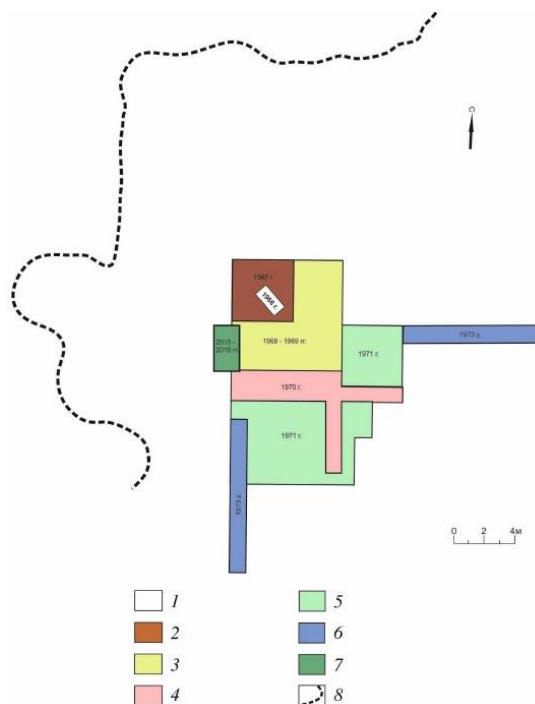
### 3.2 Soviet scholar research

The sites were first discovered in the mid-20<sup>th</sup> century by U. I. Islamov (Islamov, 1972), who subsequently also studied the sites during three archaeological excavation seasons between 1966 and 1973 (Islamov, 1980; **Figure 3-3** and **Figure 3-4**). The investigations yielded a

substantial collection of lithic finds (2511 artifacts) and provided preliminary geological and archaeological interpretations (Islamov, 1980). In the aftermath, the stratigraphic units were described in their original position (*in situ*), and the archaeological assemblage was attributed to the Epipaleolithic (Mesolithic) tradition based on technical and typological comparisons with other sites in the vicinity. Furthermore, lithic assemblage similarities were recognized between Obishir-1 and Obishir-5, attributed both to a unique cultural unit, named Obishirian.



**Figure 3-3** Excavation area at the Obishir-1 location



**Figure 3-4** Excavation plan at the Obishir-5 site. Key: **1** – 1966 probe trench; **2** – 1967 excavation; **3** – 1968-1969 excavation; **4** – 1970 excavation; **5** – 1971 excavation; **6** – 1973 trench; **7** – 2015-2016 excavation; **8** – rock-shelter after Taylor et al. (2021)

### 3.3 New studies

A new joint Russian-Kyrgyz archaeological expedition, led by S. Shnaider and A. Abdykanova, was carried out during 2015–2018. At Obishir-1, this new research involved an excavation area of 6 m<sup>2</sup>. At Obishir-5, new campaigns involved an excavation area at today of approximately 16 m<sup>2</sup>. During the excavations, modern excavation and documentation techniques were applied. This provided access to the internal part of the talus cones and allowed to study their sedimentological and geological structure and geometry, sampling for various purposes (such as chronology, micromorphology and bulk samples), and provided material for the analysis of fossil faunal remains.

### 3.4 Faunal remain studies

New studies focused on faunal remains. At Obishir-5, archaeological and biomolecular evidence established the presence of domesticated sheep by *ca* 8000 BP in the stratigraphic units (SU) 2 and 3 (Taylor *et al.*, 2021). Zooarchaeological and collagen peptide mass fingerprinting show exploitation of *Ovis* and *Capra*, while cementum analysis of intact teeth implicates possible pastoral slaughter during the fall season (Taylor *et al.*, 2021). Most significantly, ancient DNA revealed these directly dated specimens as the domestic *O. aries*, within the genetic diversity of domesticated sheep lineages (Taylor *et al.*, 2021). Together, these results provide the earliest evidence for the use of livestock in the mountains of the Fergana Valley, predating previous evidence by 3000 years and suggesting that domestic animal economies reached the mountains of interior CA far earlier than previously recognized (Taylor *et al.*, 2021).

Local paleoenvironmental conditions at the sites were inferred from fossil mollusks and small mammal assemblages (Osipova *et al.*, 2021; Brancaloni *et al.*, 2022; Serdyuk *et al.*, 2023). From the analyses of taxonomic composition of mollusks, it resulted that the paleo landscapes and vegetation during the accumulation of the studied deposits remained almost unchanged (Osipova *et al.*, 2021). This was also purported by the study of small vertebrate assemblage (Serdyuk *et al.*, 2023). Both studies pointed toward constant dry and warm climatic conditions during the Holocene. The landscape was dominated by steppe or desert-steppe with shrubs or sparse forests and temporary water bodies (Osipova *et al.*, 2021; Brancaloni *et al.*, 2022; Serdyuk *et al.*, 2023).

### 3.5 Archaeological assemblages

At both sites, two archaeological horizons were distinguished, the Obishirian and the EPP. At Obishir-5, a Bronze Age, Early Iron Age and Middle Ages assemblages were also found

(Shnaider *et al.*, 2019). The EPP at Obishir-1 and Obishir-5 is fragmented and scarce and clustered around 15000 BP to 11000 BP. The types of identified artifacts, such as core flakes, bladelets, microbladelets, end-scrapers, backed microblades, and notched pieces, are common in the wide spectrum of late UP and up to early Neolithic complexes of CA (Brancaleoni *et al.*, 2022). Together with assemblages found in Istyskaya Cave and the Alai site, these have been recently classified as Alayan complexes (Shnaider, pers. comm.). Analogies could be found, for example, within EPP assemblages of the late Kulbulakian, and Tutkaulian (Kolobova *et al.*, 2013b; Shnaider *et al.*, 2020; Brancaleoni *et al.*, 2022).

The Obishirian assemblages at the sites are dated between 9500-6500 BP. At Obishir-5, a total of 428 lithic tools were classified as Obishirian and they are mainly composed of microblades with ventral retouch, end-scrapers, retouched flakes and micro-scrapers. Stone ornaments and bone items comprise a small portion of the total assemblage (Fedorchenko *et al.*, 2018). At Obishir-1, the Obishirian lithic collection consists of 289 artifacts, including 181 shatter and debris pieces (Brancaleoni *et al.*, 2022). Amongst the cores are a prismatic core and two core's shatters (Brancaleoni *et al.*, 2022). According to the morphology of available cores and the composition of the blank collection, the reduction sequence was mainly performed for microbladelet production (Brancaleoni *et al.*, 2022). The industry is characterized by pressure knapping aimed on bladelets produced from volumetric and narrow-faced cores with a tool kit dominated by retouched microbladelets (Shnaider *et al.*, 2017; Brancaleoni *et al.*, 2022).

At Obishir-5, the study carried out on pottery remains allowed the identification of late Bronze Age until Middle Ages assemblages in the stratigraphic unit 1 (Shnaider *et al.*, 2019; Selin *et al.*, 2023) The discovery of pottery sherds typical of the Chust cultures indicates that the area was also inhabited during the Late Bronze Age (Shnaider *et al.*, 2019; Selin *et al.*, 2023).

# 4 The rationale

## 4.1 Introduction

Geoarchaeology is a multi-disciplinary field concerned with the Quaternary landscape and stratigraphic formations and their modification processes (Dincauze, 2000; Branch, 2015). This also includes the understanding of the relationship of landscape and stratigraphy with humans and human-related activities. Geoarchaeological investigation primarily draws on Earth science techniques to investigate the archaeological record (Canti and Huisman, 2015; Karkanis and Goldberg, 2018; McAdams, 2020).

Most commonly, geoarchaeologists investigate archaeological sites and their surroundings. The majority of archaeological sites is found in sedimentary contexts (Goldberg and Macphail, 2006). Therefore, in the understanding of the relationship between the sedimentary record and past human activity is of utmost importance to recognize how sediments have been deposited at the site, and eventually disturbed by syn- and post-depositional processes, and how archaeological objects came to be included within them (Schiffer, 1987; Shahack-Gross, 2017; McAdams, 2020). The understanding and accounting of depositional and post-depositional processes acting at archaeological sites goes under the name of site formation.

Concerning geoarchaeology in CA, there are several problems that hinder a comprehensive understanding of human-environment interactions. Firstly, data on archaeological sites is limited in CA, hence connections between occupation timing, living area setting, and paleoenvironmental conditions are inconclusive (Finestone *et al.*, 2022). Secondly, except for very few contexts (Mallol, Mentzer and Wrinn, 2009; Krajcarz *et al.*, 2016; Morley *et al.*, 2019; Égüez *et al.*, 2020; Varis *et al.*, 2022), most archaeological sites in CA have not been investigated with a geoarchaeological approach aimed at the understanding of site formation of a site (Iovita *et al.*, 2020; Varis *et al.*, 2022). Thirdly, sedimentary sequences in CA showed features connected with erosive episodes and complex formation history (Mallol, Mentzer and Wrinn, 2009; Krajcarz *et al.*, 2016; Varis *et al.*, 2022), disrupting the integrity of the archaeological assemblages (Krajcarz *et al.*, 2016; Brancaloni *et al.*, 2022).

This chapter aims to lay the foundation for this thesis research workflow. In Chapter 4.2, general concepts, such as types of sediments that can be found at archaeological sites (Chapter 4.2.1), and the concept of stratigraphy at archaeological sites (Chapter 4.2.2) are described. In Chapter 4.3, the formation theory is outlined. This is followed by types of deposits encountered at Obishirian sites (Chapters 4.5, 4.6 and 4.7); and Chapter 4.8 discusses how sediments in archaeological sites can contain records for human-related activities.

## 4.2 Building blocks of site formation studies

### 4.2.1 Types of sediments at archaeological sites

The majority of archaeological sites is found in sedimentary contexts (Goldberg and Macphail, 2006). Sediments are broadly categorized into three fundamental types: 1) clastic, 2) chemical, and 3) biological (refer to **Table 2**). Clastic sediments are the most commonly encountered at archaeological sites, typically transported and deposited by water, air, ice and gravity-induced processes. Archaeological objects adhere to the same principles as geological clasts during transportation. Distinct sedimentary structures, such as grading, laminations, ripples, and cross-bedding, are produced by different types of sediments and modes of transportation. These structures serve as diagnostic indicators for identifying the deposition processes involved.

Gravity-induced processes are confined to slope settings and can be indirectly triggered by water or ice, which reduce the strength of the slope material and act as a lubricant (Karkanas and Goldberg, 2018). The overarching term for describing slope waste material is “colluvium” (Miller and Juilleret, 2020), extensively explored in Chapter 4.5.

Biogenic sediments result from biological activity. In cave and rockshelter environments, among various biogenic sediments, the most prevalent include excreta from bats, birds, and other inhabitants, including large mammals. These specific biogenic sediments, along with archaeological material arising from firing activities, were identified at Obishir-5, and are comprehensively discussed in Chapter 4.6. For a comprehensive description of sediments and related processes in various environments the reader is referred to Hassan (1974), Goldberg and Macphail (2006), Karkanas and Goldberg (2018), among others.



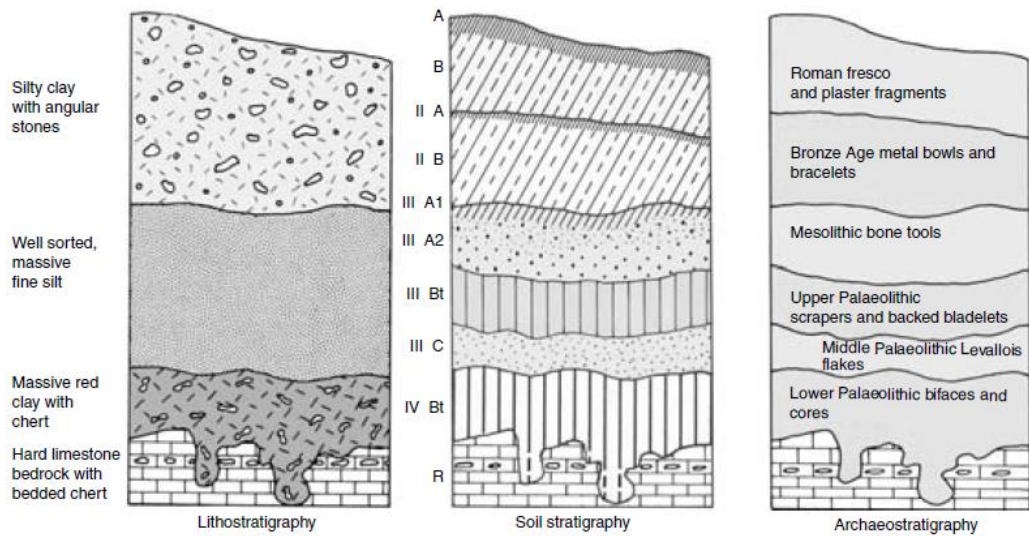
**Table 2** Types of sediments modified after Goldberg and Macphail (2006), Karkanas and Goldberg (2018), between brackets are indicated the lithified equivalents

Clastic and bioclastic		Non clastic	
Volcaniclastic	Terrigenous and marine	Chemical	Biological
Lapilli, blocks, bombs;	Cobbles, boulder, gravel (conglomerate);	Carbonates: <ul style="list-style-type: none"> <li>■ Typically marine (limestone);</li> <li>■ Terrestrial: Travertines, flowstones (cave and karst settings);</li> </ul>	Plant fragments: peat (lignite, coal);
Volcanic ash	Silt (siltstone), Clay (shale);  Bioclastic: <ul style="list-style-type: none"> <li>■ coarse (e.g., coquina);</li> <li>■ fine (chalk);</li> </ul>	Chlorides, sulphates (evaporites), Silicates (chert), Phosphates (phosphorite)	Algae, bacteria (stromatolite), diatoms (diatomite), ostracods, foraminifera;  Excrements: bat and/or bird guano; Mammal feces (cave and karst settings and human-controlled gathering places)
	Ash (from wildfires)		
	Human-related material: Pottery, bone, lithic, mortar and other construction material, fire by-products (ash, charcoal and char)		

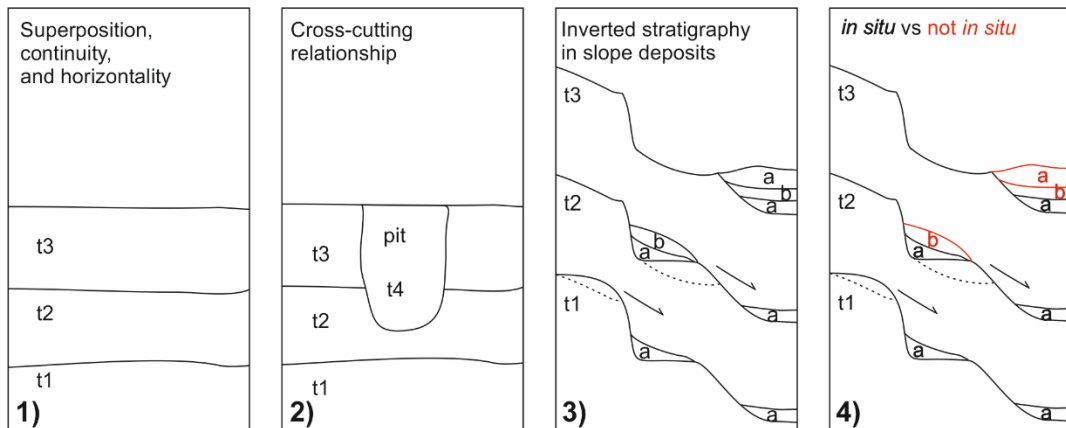
## 4.2.2 The concept of stratigraphy at archaeological sites

It is a common practice in geological sciences to classify deposits by defining their stratigraphy. Stratigraphy is the three-dimensional organization in space and time of either geological layers, or soils, or archaeological features and artifacts (Goldberg and Macphail, 2006) (**Figure 4-1**). Stratigraphy stands on basic principles that can also be applied to archaeological sites, as illustrated in **Figure 4-2**. The concepts of superposition, continuity, and horizontality tell us that younger units are deposited on top of older units, and they tend to be laterally continuous and laid down horizontally thanks to gravity (**Figure 4-2** panel 1). This is also valid for archaeological material. Dipping beds can be either a result of specific processes such as those forming talus cones, or a result of post-depositional processes (such as slumping, subsidence, faulting) (Karkanas and Goldberg, 2018). The concept of cross-cutting tells us that when a feature cuts through others, it is younger than the features it cuts (**Figure 4-2** panel 2). In slope deposits a common feature is the inverted stratigraphy as illustrated in **Figure 4-2** panel 3. Moreover, the concept of *in situ* refers to the condition where the unit or the archaeological object were not moved from its original place of deposition, such as unit ‘a’ at the time t1 and t2 in **Figure 4-2** panel 4. Defining the stratigraphic units of a site provides a chronological framework for the

findings and serves as a foundational element in the analysis of site formation. In **Table 3**, different types of stratigraphy that can be employed in archaeological sites are summarized.



**Figure 4-1** Different types of stratigraphy applied to the same profile. The stratigraphy from an archaeological site can represent the combined effects of depositional (lithostratigraphy) and post-depositional processes (soil stratigraphy), coupled with human activities (archeostratigraphy or cultural stratigraphy) taken from Goldberg and Macphail (2006) figure 2.1, modified from Courty, Goldberg and Macphail (1989), figure 3.3.



**Figure 4-2** Basic stratigraphic principles. **1)** This panel illustrates that the unit deposited at time t1 is older than time t2, that is older than t3, older units are found at the bottom and younger ones are found at the top; units tend to be laid down horizontally with lateral continuity; **2)** this panel illustrates how a feature (pit) that is cutting through unit-t3 and unit-t2 is younger than both units; **3)** slope deposits can be responsible for an inverted stratigraphy as at time t3; **4)** in situ units are those that have not been moved from their original place of deposition. In archeology, an in situ object is also the object found in its original place of deposition.

**Table 3** Different types of stratigraphy that can be utilized in an archaeological context after Goldberg and Macphail (2006), Morrissey, Mentzer and Wurz (2022)

Type	Description	Examples	Notes
Lithostratigraphy	Lithostratigraphic units are defined on the base of physical properties (texture, color, composition, thickness, upper and lower boundary)	In a cave, a layer of rock fall mixed with clay	It can be applied to the majority of geoarchaeological situation
Allostratigraphy	Allostratigraphic units are constrained between erosional surfaces (disconformity or unconformity)	Stream terrace deposits produced by successive episodes of alluvial deposition and erosion	It is convenient to use in fluvial deposits or cave deposits
Soil stratigraphy	Soil stratigraphic units are identified as one or more horizons of a buried soil	The interglacial Sangamon Geosol (US)	Units represent relatively short periods of geological time
Biostratigraphy	Biostratigraphic units are based on the remains of particular faunal or flora species assemblage	Younger Drias (pollen zone)	In Osipova <i>et al.</i> (2021) the concept of malacozones was applied
Chronostratigraphic	Chronostratigraphic units are defined by their absolute dates	Quaternary period, ca 2.8 to 0 Ma	They relate to divisions of time
Cultural stratigraphy	Stratigraphic units are defined based on significant changes in the artifact assemblages excavated from a site	Bronze Age horizon in an archaeological profile	Largely applied in archaeology
Arbitrary stratigraphy	Spits are arbitrary units excavated based on depth below a defined point	Interval of 10 cm during archaeological excavations	Largely applied during archaeological excavations

## 4.3 Site formation

Site formation processes are a collective set of processes operating within and around an archaeological site that contribute to its creation and eventual disturbance. The study of site formation processes, also known as Formation theory, helps archaeologists better understand and interpret the archaeological record (Shahack-Gross, 2017). “Formation Processes of the Archaeological Record,” by M.B. Schiffer (Schiffer, 1987), laid the foundation for Formation theory. In this seminal book, Schiffer categorized formation processes into two groups: environmental and cultural. The former are related to natural environmental factors, the latter are human-induced (**Figure 4-3**). Schiffer’s initial unit of analysis was the archaeological assemblage (e.g., artifacts). Over time, as geoarchaeology advanced (Rapp and Hill, 2006), the unit of analysis shifted from the artefact to the deposit, which refers to the actual sediments where the

archaeological assemblage is found (Shahack-Gross, 2017). Another significant development in Formation theory occurred when the sediments in archaeological sites began to be considered as artifacts themselves, reflecting human activity (Shahack-Gross, 2017). This shift became more clear, especially with the application of micromorphology (Goldberg and Macphail, 2006).

In addition to distinguishing natural and cultural processes, it is common practice to differentiate between depositional (primary) and post-depositional (secondary) processes. This distinction aims to recognize the original causes and processes responsible for the deposition of the sedimentary and archaeological record, and their subsequent transformations (syn- or post-depositional). Understanding these secondary processes is of particular importance in assessing the integrity of the archaeological record in order to properly interpret past human behavior (Figure 4-3).

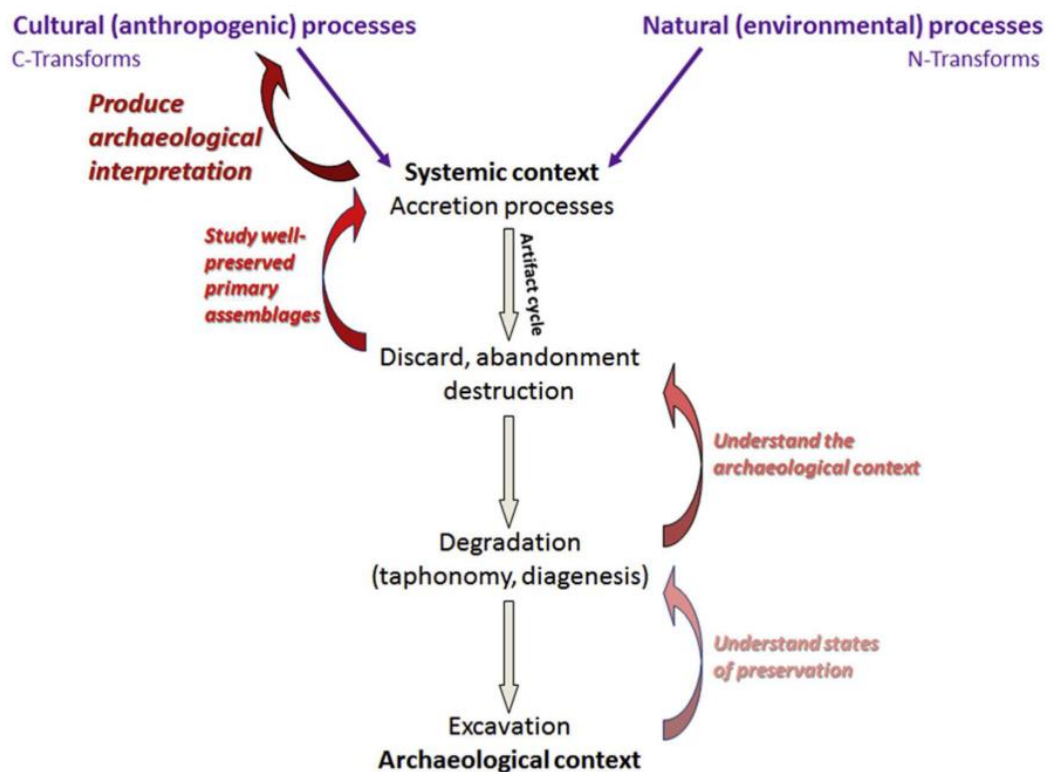


Figure 4-3 Workflow in site formation studies taken from Shahack-Gross (2017)

## 4.4 Sediments in arid and semi-arid settings

In arid settings such as CA, climatic factors play a crucial role in landscape and sediment development (French, 2019). Sediments are more susceptible to soil erosion due to low precipitation rate and daily and annual high temperatures. In CA, precipitation typically ranges from 200-400 mm/yr (Figure 2-2, Chapter 2.1), which hinders surface vegetation development. Vegetation plays a key role in promoting water percolation and stabilizing soil and sediments.

Therefore, in areas with sparse and weak vegetation, the terrain becomes more vulnerable to erosion. In addition, high evapotranspiration rates and low humidity reduce vegetative cover, leaving landscapes bare and susceptible to soil erosion (French, 2019). Moreover, in arid conditions, common physical weathering processes include rock shattering and debris fall.

Erosion can be easily triggered by rainfall in such terrains, resulting in increased runoff (Cooke, Warren and Goudie, 1993). This, in turn, contributes to downslope mass movement erosive episodes (French, 2019). Identifying erosional features, as observed at the Obishir-1 site (Brancaleoni *et al.*, 2022), has been instrumental in formulating the formation history of the archaeological site and gaining a better understanding of the site preservation and its assemblage. Other examples of erosional processes acting at archaeological sites can be found in Uzbekistan, like Katta Sai and Ertash Sai, where archaeological assemblages were eroded by water flow and re-deposited in secondary position as documented in (Krajcarz *et al.*, 2016) and in one of my forthcoming work included in (Kot *et al.*, in press). Erosional processes were recorded also across several caves in Kazakhstan (Varis *et al.*, 2022).

Moreover, the elevated soil temperatures in arid conditions intensify insect activity, which enhances sediment bioturbation (French, 2019). Bioturbation, one of the most common secondary processes affecting archaeological sites, is particularly prominent in open-air and rockshelter sites in arid and semi-arid settings (Mallol and Goldberg, 2017; Fitzsimmons *et al.*, 2020). Examples from the region include Katta Sai and the Obishir complex (Krajcarz *et al.*, 2016; Brancaleoni *et al.*, 2022, 2023). Bioturbation can significantly impact the recognition of original depositional processes because it tends to mix, rework, homogenize and rearrange sedimentary material (Goldberg *et al.*, 2009; Goldberg, Miller and Mentzer, 2017; Miller and Juilleret, 2020). Additionally, bioturbation can interfere with chronometric dating, hindering the collection of chronometric samples and producing unreliable results (Fitzsimmons *et al.*, 2020). Archaeological sediments are often affected by post-depositional processes related to bioturbation (Karkanas and Goldberg, 2018), and sedimentary materials rich in organic matter, such as dung and charcoal fragments, like those found at Obishir-5 (Brancaleoni *et al.*, submitted), are perfect candidates for soil fauna activity. Micromorphology can be a reliable tool for the recognition and of bioturbation processes in the sedimentary record (Karkanas and Goldberg, 2018; Kielhofer *et al.*, 2020; Stoops, 2021). Among other post-depositional processes, physical and chemical weathering processes are accelerated in these environments, leading to the formation of secondary calcium accumulations (Khormali, Abtahi and Stoops, 2006; Brancaleoni *et al.*, 2023) and iron minerals (French, 2019).

## 4.5 Colluvial deposits

Obishir-1 and Obishir-5 are sites on a slope located at the toe of a carbonate cliff embedded in talus deposits. A more general term for slope deposits is the term “colluvium”, which refers to transported regolith formed by the accumulation of clastic sediments through mass-gravity movement, where water can act as a lubricant (Miller and Juilleret, 2020). These deposits typically exhibit heterogeneous particle sizes, frequently including angular rock fragments, poor sorting, and minimal to no stratification. They are usually found on slopes and at their bases, often resulting from processes like mass movement, creep, and solifluction (Miller and Juilleret, 2020).

Colluvial deposits, along with landslides, are classified based on their type of movement (e.g., fall, topple, sliding, spreading, flow and complex) and the type of material involved (such as rock, debris and earth) (Varnes, 1978; Bertran and Texier, 1999). Depending on their type of movement and the material involved, sedimentological features may vary (Bertran *et al.*, 1997; Bertran and Texier, 1999; Sanders, 2010). Although, debris flows, rock avalanches, earth flows, and to a certain extent, dry grain flows may be characterized by similar microscopic facies (Bertran and Texier, 1999). For instance, laminated colluvium may suggest overland water erosion of cohesive material (Bertran and Texier, 1999; Mücher, Steijn and Kwaad, 2010), whereas non-laminated colluvium might indicate rockfall talus (Bertran and Texier, 1999)(**Table 4**).

Micromorphology allow the understanding of colluvial processes in sediments through the determination of: 1) *in situ* features, 2) features inherited from the parent material, 3) not *in situ* features. Micromorphological features used for distinguishing whether a deposit is *in situ* or translocated down the slope are listed in **Table 5**. However, the presence of only one of the features in **Table 5** is often not enough to indicate translocation (Mücher, Steijn and Kwaad, 2010). For instance, fragments of clay coatings incorporated in the groundmass can also arise from biological activity and frost action.

**Table 4** Characteristics of non-laminated loess-derived colluvial sediments from Mücher, Steijn and Kwaad (2010)

In the field	In thin section
A silty loam texture;	Silt-sized mineral grains;
Mainly massive but sometimes have a weakly developed angular blocky structure;	Small amount of clay;
Medium and fine pores.	Pedofeatures (anorthic iron oxide nodules);
	Fragments of clay coatings from Bt horizon;
	Fragments of chert and other rock types not occurring in the area;
	Coal and brick fragments.

**Table 5** Few rules for recognizing *in situ* from not *in situ* features during micromorphological analysis (Mücher, Steijn and Kwaad, 2010; Stoops, Marcellino and Mees, 2010)

<i>In situ</i> features	Inherited/Not <i>in situ</i> features	Not <i>in situ</i>
Impregnative features (nodules, hypocoatings) with diffuse boundaries and composition		Fragment of pedofeatures (clay coating, crusts)
Fabric of the coarse material similar to the surrounding groundmasses	Nodules and coarse material fabric are different from those in the surrounding groundmasses	Typic ferruginous nodules with sharp boundaries
Surface or void features, coatings associated with the surface of voids	Coherent coatings covering the surface of grains (iron oxide coating on transported sand grains or pebbles)	Horizontally oriented root fragments
Infillings post-date void formation, passage features		Rounded aggregates composed of material derived from other soil horizons
Intercalations		Relicts of paleosol intervals
Euhedral crystals of minerals known to form in soil environments (more soluble ones)		Anthropogenic materials
		Sharply bounded and mostly (sub)rounded rock fragments
		Fresh rock fragments practically free of weathering rims and/or unknown in the area.

#### 4.5.1 Rockshelter deposits

The Obishirian sites are archaeological sites in front of rockshelters. A rockshelter is a natural cavity enclosed by one or more rock walls and an overhang that provides protection from wind, precipitation, sun, or a combination thereof (Mentzer, 2017). While rockshelters can be found in differing types of landscapes and lithologies (Mentzer, 2017), they are typically situated along carbonate cliffs and in karstic environments, as seen at the Obishirian sites. A comprehensive classification of rockshelter settings is provided by Mentzer (2017).

Due to their morphology, rockshelters offer shelter to both animals and humans. Evidence of human activity in rockshelters dates back to the Paleolithic era (Mallol and Goldberg, 2017). In addition, by providing protection from weathering agents, to some extent rockshelters contribute to the preservation and protection of archaeological records (Mentzer, 2017). Rockshelter deposits are usually located at the base of an overhanging wall. They generally resemble colluvial deposits, consisting of a mixture of coarse and fine-grain sediments. The coarse material is typically autochthonous, resulting from processes such as roof spall and debris falls (also known as *éboulis*); whereas the fine material can be both autochthonous and allochthonous. Allochthonous fine material may have aeolian origin or be transported by runoff. Autochthonous fine material results from physical and chemical weathering. In addition to geogenic sediments, rockshelter sites may contain biogenic (dung, bird and bat guan) and anthropogenic materials

(artifacts, bones, charcoals, ash). Eventually, karst settings, including rockshelter and caves, have been linked with herding activities especially in the Mediterranean area (Boschian and Montagnari-Kokelj, 2000; Angelucci *et al.*, 2009; Fernández-Palacios *et al.*, 2023) but also around the globe (Abell *et al.*, 2019; Dedov *et al.*, 2021; Shnaider *et al.*, 2023). Common post-depositional processes in these settings include erosion caused by wind, water, and/or mass-wasting. Biological activity, especially soil mesofauna activity in arid settings, can also be prominent. Mineral precipitation (e.g., sulfates, carbonates, and phosphates) and dissolution are common occurrences.

## **4.6 Sedimentary clues for human and human-related activities**

At Neolithic sites, various geoarchaeological microscopic indicators of human activities are anticipated, including living floors, plant residues (such as cultivated plant or plant used for grazing and foddering), pottery sherds, remains of combustion features, and residues of domestic animals. Microscopic indicators related to living floors may include trampling and compaction of the sedimentary record (Friesem, 2016), along with the horizontal alignment of sedimentary components. It is worth noting that these features may be erased by later bioturbation (Macphail and Goldberg, 2017; French, 2019). Regarding plants, indicators such as pollen and phytoliths within the sedimentary record are crucial (Matthews *et al.*, 1997; Shillito, Bull, *et al.*, 2011). Phytoliths have been identified in the Obishir-5 record (Brancaleoni *et al.*, submitted), but further specialized studies are needed to fully understand their significance. In the case of pottery sherds, the sedimentary record may contain microscopic fragments. During investigations at Obishir locations, efforts were made to search for micro pottery fragments, but only a few suspected fragments were found in the Obishir 5 record. Additionally, macro pottery is scarce at these locations (Shnaider *et al.*, 2019; Selin *et al.*, 2023).

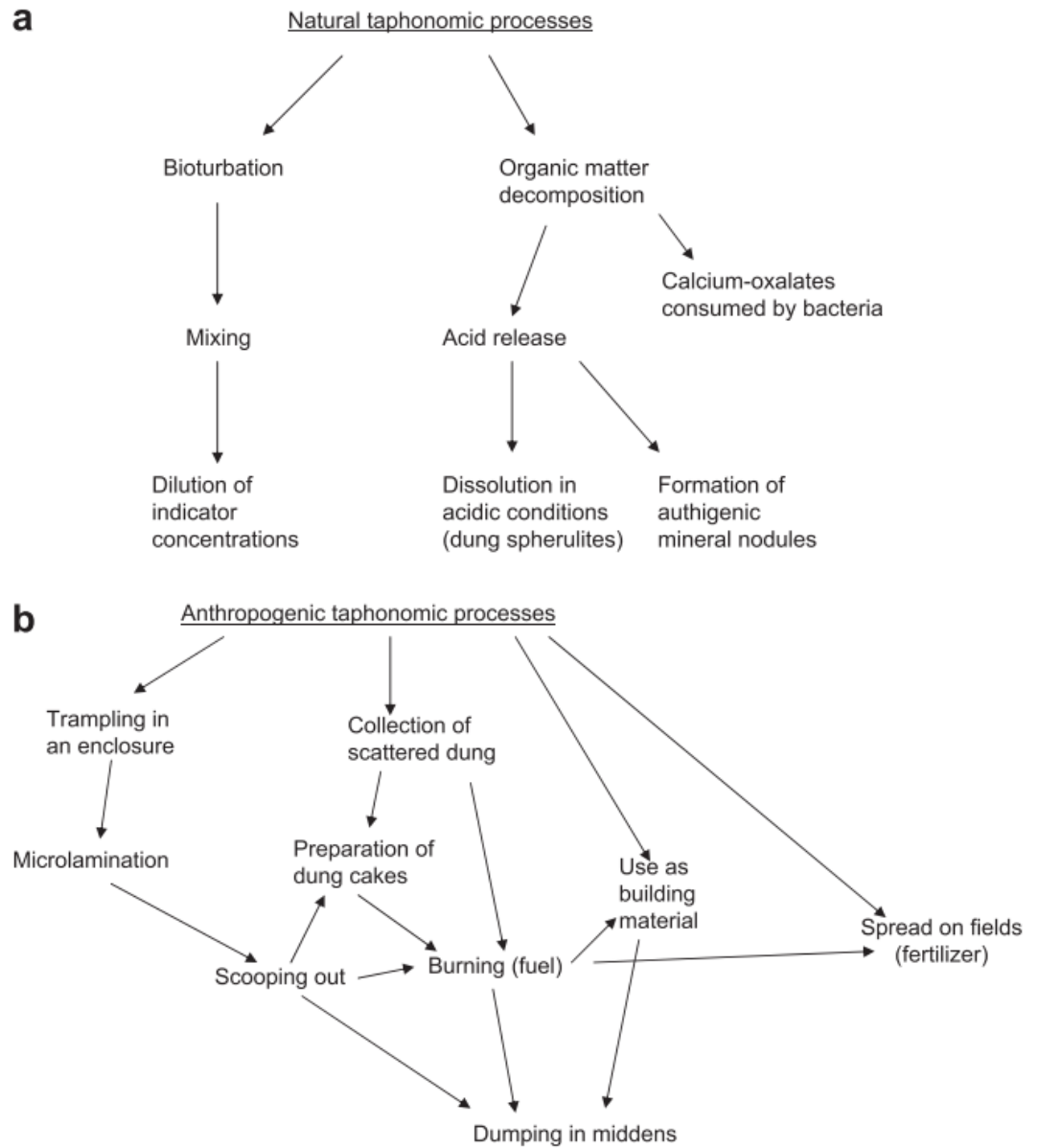
Combustion features are the result of firing activities. Firing involves exposing materials like wood, bone, dung, clay, and sediments to high temperatures. Fire has served various purposes throughout history, including providing a source of light, cooking, heating, and protection (March *et al.*, 2014; Mentzer, 2014). Therefore, the recognition of firing activity at the site enables the understanding of its function and the identification of the cultural activities that took place there (Mentzer, 2014). Furthermore, studying firing processes can provide insights into past environmental conditions, such as the availability of fuel resources (e.g., wood, dung), which may have influenced the firing methods (Mentzer, 2014). An interesting example is given by the study at Kurteke rockshelter site (Pamirs, Tajikistan) where by-products of firing within the sediments



were examined and enabled to infer the use of dung as fuel as a result of high-elevation adaptation (Shnaider *et al.*, 2023). In summary, identifying fire by-products, such as charcoals and ash, can help distinguish between a cultural and natural deposit. For example, the presence of charcoals within the micro-stratigraphic record enabled to infer the presence of a paleo surface at the Obishir-1 site (Brancaleoni *et al.*, 2022). Moreover, the appearance of charcoal and dung in the micro-sedimentary record of Obishir-5 enabled archaeologists to better distinguish the Obishirian cultural horizon and led to the interpretation of a culture that relied on herding practices (Brancaleoni *et al.*, submitted).

Sedimentary deposits may record evidence of herding practices. When a site is frequented by animals, they may leave evidence of their presence within sediments. For instance, animals produce excreta, especially feces and urine that tend to accumulate on the surface at the site. Once deposited, dung enters the sedimentary record and it can be studied through the micro-stratigraphic approach. A seminal example is the geoarchaeological investigation carried out with a micro-stratigraphic approach at Arene Candide Cave (Macphail *et al.*, 1997) where herbivore dung, ash and plant pseudomorphs were identified within the laminated sediments at the site (Macphail *et al.*, 1997). Studies on faunal remains can provide evidence of the use of feralized and/or domesticated animals in a location. For instance, at Obishir-5, the presence of *Ovis* and *Capra* remains were found (Taylor *et al.*, 2021). However, as discussed in the Introduction (Chapter 1), faunal studies cannot solve most of the questions around herding practices as they are limited to the bone assemblage. A micro-stratigraphic approach instead may actually answer the question whether the animals were kept at the site.

While it is ideal for fecal material to undergo effective preservation for proper identification, modern approaches, such as assessing taphonomic processes, enable the identification of dung even if it has experienced various post-depositional processes (Shahack-Gross, 2011)(**Figure 4-4**). Studying dung in the sediments can help identify which animals frequented the site (Shillito, Bull, *et al.*, 2011), and shed light on the site's function during occupation (Shillito, Matthews, *et al.*, 2011), as also as demonstrated in (Brancaleoni *et al.*, submitted). At Obishir-5, the recognition of herbivore dung material within the sedimentary record attested the presence of the livestock alive on site. This contributed to the understanding of economic strategies based on the use of domestic animals adopted by the Obishirian culture (Brancaleoni *et al.*, submitted).



**Figure 4-4** Suite of post-depositional processes affecting dung taken from Shahack-Gross (2011)

# 5 The methods applied

## 5.1 Introduction

The approach adopted draws on multiple methodologies, with an important focus on two scales: the site scale and the microscopic scale. At the site scale, the concept of stratigraphy is of paramount importance in archaeological excavation and interpretation (Morrissey, Mentzer and Wurz, 2022). I utilized a hybrid lithostratigraphic and allostratigraphic approach to describe units, enabling the physical characterization of deposits and the potential identification of macro sedimentary structures, especially erosional surfaces (to recognize possible erosion and re-deposition events and sources of material, as well as to indicate hiatuses).

The stratigraphic description of units in the field was further complemented by bulk analyses, including grain size, geochemical and mineralogical analysis. Grain size analysis serves as a tool for classifying sedimentary environments (Blott and Pye, 2001). In this context, our grain size analyses were undertaken with the aim of characterizing sediment texture and sorting, in order to find differences or similarities with other deposit types or akin sediments intra sequence and inter sites. Geochemistry was employed to identify geogenic and anthropogenic inputs, pedogenic or weathering horizons and to indirectly detect any temporary cessation of sedimentary processes. To gain a comprehensive understanding of the mineral phases within the Obishir-5 deposit, I utilized both Powder X-ray diffraction (PXRD) and Fourier-Transform infrared spectroscopy (FTIR).

For the microscopic description of sedimentary deposits, micromorphology was applied. Micromorphology is an effective tool for studying site formation, and the analysis of microstratigraphy can provide useful insights in the final formulation of site formation, and archaeological interpretation. In conjunction with this, chronometric dating was used to get the age of the deposits. Faunal assemblages were also examined by our colleagues (Dr. Evgenia Osipova and Prof. Guzel Danukalova) to provide information about the paleoenvironmental conditions during the deposition of stratigraphic units. The spatial distribution of artifacts was also investigated. This chapter is structured into subsections corresponding to the various methods applied and a discussion is given on the limitations and advantages of those.

## 5.2 Field observation and stratigraphy

The investigation of the sites employed a conventional geological approach, drawing from methodologies outlined in Goldberg and Macphail (2006), Macphail and Goldberg (2017);

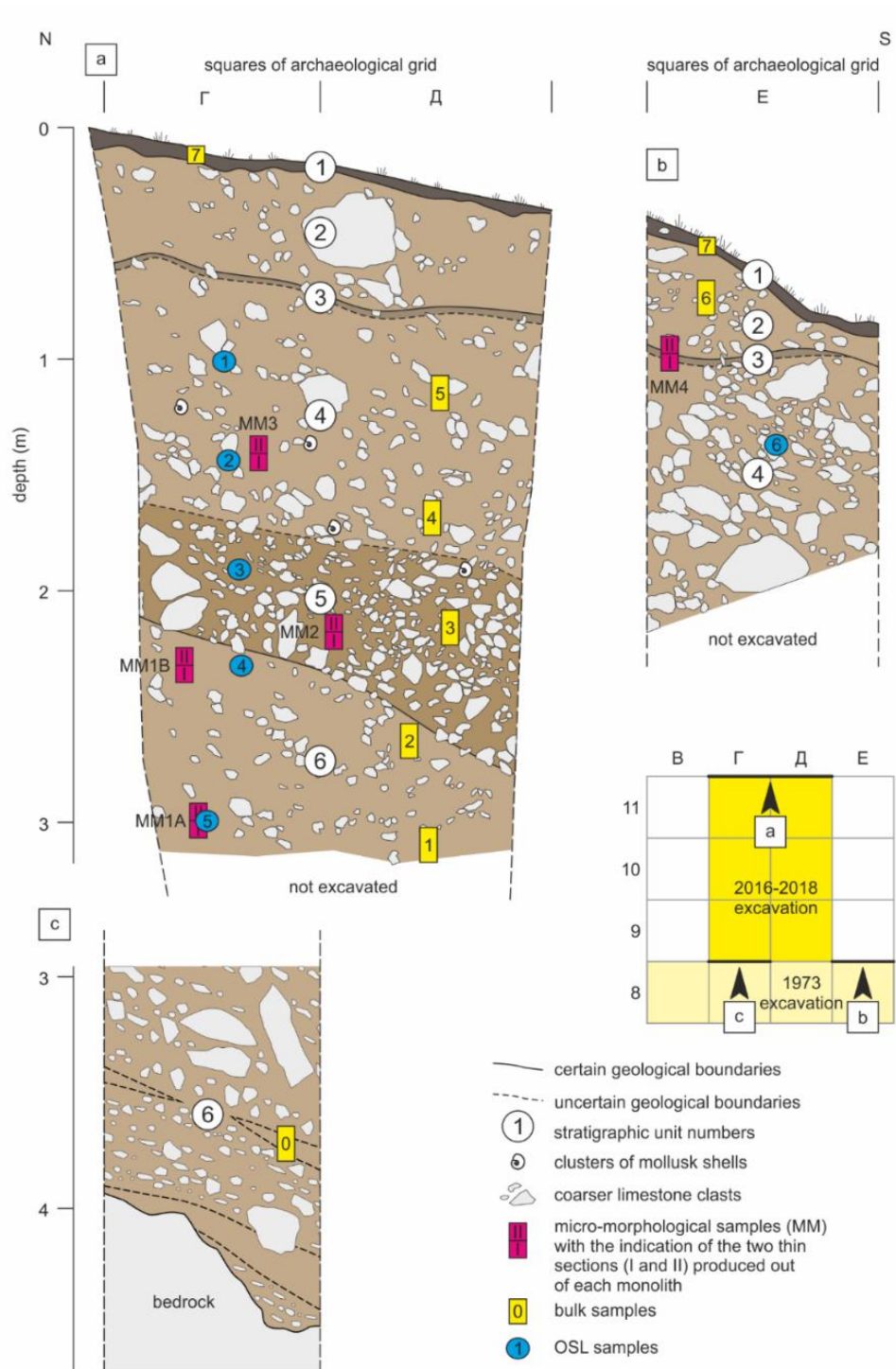
Karkanis and Goldberg (2018), Krajcarz *et al.* (2020), and Brancaleoni *et al.* (2022). Together with stratigraphic description, main elements of the landscape, characteristics of the bedrock (such as inclination of bedding), surface morphologies, ground surface description were noted in the field book and documented using a photographic camera. To identify the stratigraphic units at the Obishirian sites, a combination of lithostratigraphic characteristics (including distinctions in texture, color, and subtle sedimentary structures) and an allostratigraphic approach (recognizing the presence of unconformities) was used. For details the reader is referred to Brancaleoni *et al.* (2022).

Detailed descriptions of site stratigraphy and its correct interpretation are paramount for the effectiveness of subsequent methodological steps, such as sampling for micromorphology (French, 2019), grain size analysis, geochemical and mineralogical analysis. Moreover, a correct description and interpretation of site stratigraphy can effectively constrain micromorphological observation and interpretations. Archaeological sites are typically subjected to the equifinality effect (Kielhofer *et al.*, 2020; Brancaleoni *et al.*, 2023), meaning that different processes may lead to similar effects. For example, various slope processes often result in similar facies and microfacies (Bertran and Texier, 1999). Therefore, a correct understanding and interpretation of macro-features at archaeological sites and their surroundings can aid in distinguishing the correct process. Moreover, stratigraphic descriptions are susceptible to subjectivity (Goldberg and Macphail, 2006). For instance, when describing the color of a matrix, even with the support of the Munsell chart, different operators may perceive and evaluate the color differently. To mitigate biases, more quantitative tests should be performed. For instance, for the color determination, a possible solution is the application of colorimetry where a variety of instruments, for instance spectrophotometers, are used.

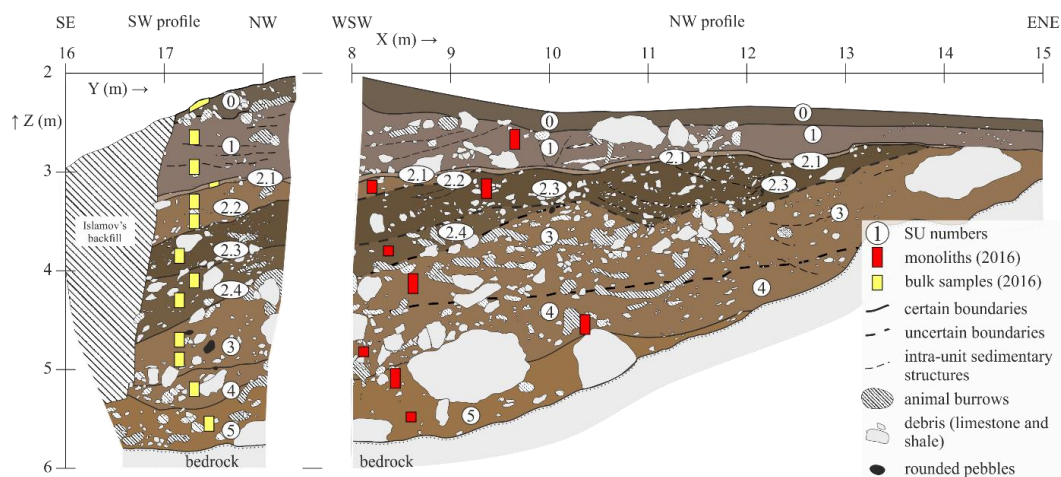
## 5.3 Sampling

A strategic sampling is crucial for the effectiveness of various techniques applied to the directed samples. For example, at Obishir-1 (**Figure 5-1**), I aimed to cover the entire profile during sampling for micromorphology and bulk analysis. This approach enables a more comprehensive characterization of the site's deposits, covering a larger surface area. Typically, bulk samples are taken along a vertical profile at specified intervals, ensuring coverage from top to bottom of the profile. The shorter the interval, the better the resolution of the results. Sampling at the Obishirian sites was conducted in multiple campaigns, with personal involvement in sampling the Obishir-1 sequence and collecting a few micromorphology samples from the Obishir-5 profile. Most Obishir-5 samples were collected before the start of the PhD study. Unfortunately, further sampling of Obishir-5 was hindered by the COVID pandemic restrictions on travels. Sampling strategies should also account for the complexity of the stratigraphy and be

somewhat strategic based on the available time and funds. For instance, Obishir-5 stratigraphy (**Figure 5-2**) is more complex than that of Obishir-1, which, in contrast, is more homogeneous. Therefore, bulk sampling at Obishir-5 involved shorter intervals (15 cm) to accommodate its greater complexity.



**Figure 5-1** Sampling location at Obishir-1. Sampling took place during the campaigns between 2016 and 2021, taken from Brancaleoni et al. (2022)



**Figure 5-2** Sampling location at Obishir-5. Sampling was conducted over various campaigns from 2016 to 2021

## 5.4 Micromorphology

Ewa Deput, a technician at the Institute of Geological Sciences of the Polish Academy of Sciences in Warsaw, produced thin sections following the procedure described in Brancaloni *et al.* (2022)(*Appendix A - Scientific paper 1*). These thin sections underwent analysis under various lighting conditions best described in the Supplementary material of Brancaloni *et al.* (submitted) (*Appendix C – Scientific paper 3*), including plane-polarized light (ppl), cross-polarized light (xpl), oblique incident light (oil), and epifluorescence. Additionally, I utilized a Scanning Electron Microscope (SEM) in conjunction with Energy Dispersive Spectroscopy (EDS) for elemental and morphological analyses of selected components (for example dung pellet and authigenic minerals) within specific thin sections. In compliance with guidelines set forth by Stoops (2021), the thin sections were described, and further details can be found in Brancaloni *et al.* (2022).

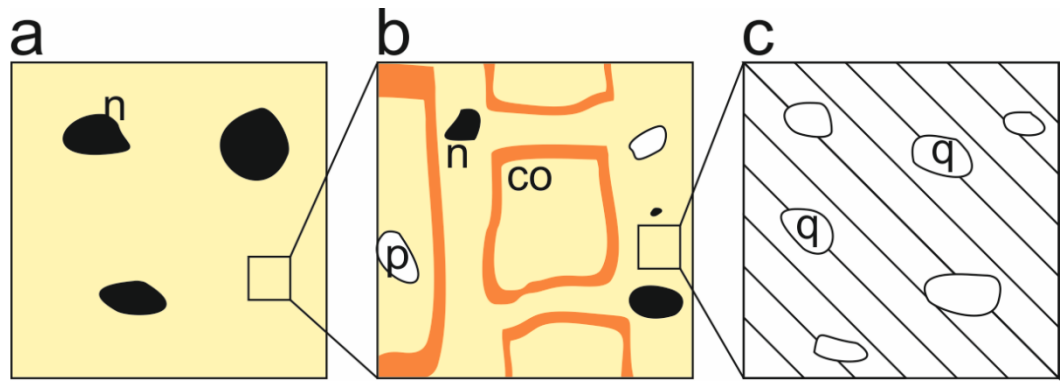
Micromorphological studies represent a common approach for the evaluation of site formation history. Micromorphology is based on the analysis of sediment thin sections, where thin slices of sediment samples are examined under a microscope. Thin sections are produced from undisturbed blocks of sediment carved out from a sedimentary profile on site. This provides the ability to observe the original spatial arrangement of soil components and their interrelationships at the microscopic scale (Miller, 2015). Its effectiveness relies on accurate field recording of site stratigraphy and strategic sampling (French, 2019; McAdams, 2020).

The method was first introduced to the scientific world in 1938 by Walter L.K.R. von Kubiena (1897-1970), considered the father of soil micromorphology (Verrecchia and Trombino, 2021). Other important contributors to this discipline were Ewart A. FitzPatrick and George Stoops, both involved in the promotion of micromorphology thanks to their clear and well-illustrated guidelines (e.g., Stoops, 2003, 2021). This method is also mainly applied to

archaeological studies for the understanding of site formation history and geoethnoarchaeological studies. Pioneers in this field are Marie Courty, Paul Goldberg, and Richard I. Macphail, known for their book “Soil and Micromorphology in Archaeology” (1989).

Micromorphology is based on the concept of **fabric**. *Soil Fabric* is expressed by the spatial arrangements and organization of the soil/sediment constituents (solid, liquid and gaseous), in terms of their shape, size and frequency, and from a configurational, functional and genetic viewpoint (Bullock *et al.*, 1985; Stoops, 2003). The fabric can consist of different components, such as mineral, organic, biogenic resulting from soil formation and other processes. The fabric can be very complex and change depending on different light, magnification, and scale of observation (Verrecchia and Trombino, 2021). The fabric can be characterized by descriptive elements and concepts provided by guidelines, such as those proposed by Stoops (2003, 2021). A *Fabric unit*, on the other hand, is a finite, three-dimensional unit within the soil fabric that is identifiable, statistically homogeneous, and distinct from other units at the examined scale (Bullock *et al.*, 1985; Stoops, 2003). Concurrently, the concept of *partial fabric*, applied in Brancaloni *et al.* (2023), is used to study the relationship among groups of materials in a more abstract, interpretative manner (Stoops, 2021). This approach is exemplified in the study of distinctions between coarse and fine sedimentary particles, as demonstrated in Brancaloni *et al.* (2023). An example of fabric and partial fabric is given in **Figure 5-3**.

Micromorphology has the limitation of studying a very small portion of the profile, which, without contextualization (macroscopic information) and complementary analysis can lead to incorrect interpretation (Goldberg and Berna, 2010; Goldberg and Aldeias, 2018). Integrating micromorphology with other methodologies, such as SEM-EDS, bulk soil chemistry, micro- and macro-fossils, allows for a better and more accurate interpretation of the archaeological sites (Goldberg and Berna, 2010; Macphail and Goldberg, 2017). For instance, observing thin sections only under the petrographic microscope is insufficient for a comprehensive recognition of components in the sediments. The internal structure of components is hidden under the optical microscope, and different minerals can have similar optical properties, especially authigenic minerals in the form of spherulites. A holistic observation of thin sections under different lighting conditions is recommended, preferably under a SEM coupled with EDS, to explore *in situ* the internal structure and the chemical and mineralogical composition of different components.



**Figure 5-3** Examples of fabric, fabric unit and partial fabric and different magnitudes of observations modified after (Stoops, 2003); **a**) the yellow matrix (partial fabric) looks homogeneous and mottled by Fe oxides nodules; **b**) looking at higher magnification, the partial fabric matrix is not homogenous but made of other fabric units, such as clay coatings (co) completely filling voids, pores (p) and nodules (n); **c**) increasing the magnification the clay matrix is made of quartz (q) grains.

#### 5.4.1 SEM-EDS

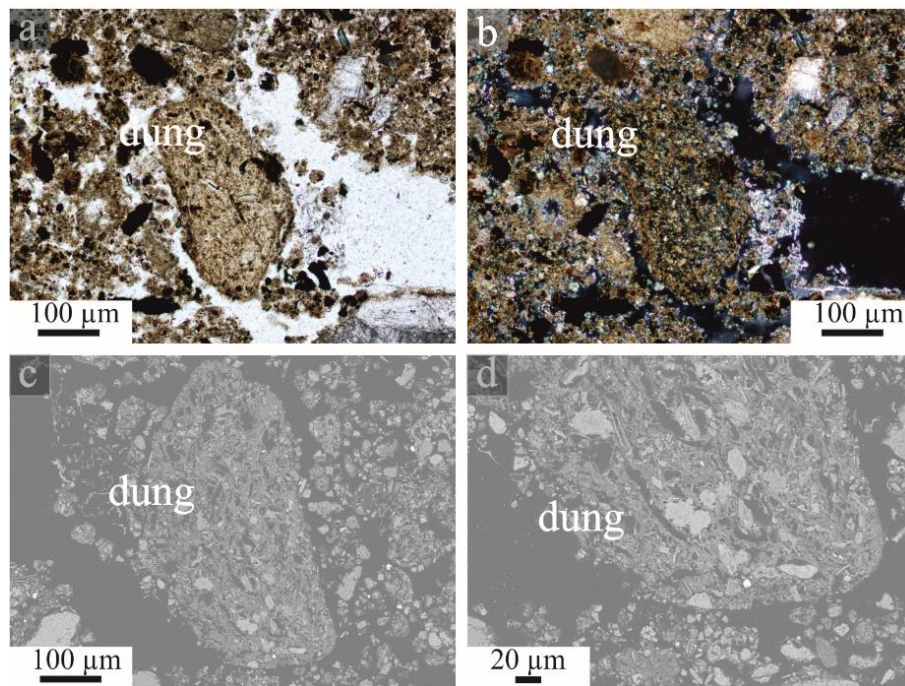
Observations and analysis were conducted at the Faculty of Geology of the University of Warsaw with initial assistance from the laboratory technician Marcin Lacki and Stefano Giunti, MSc. Technical specifics are detailed in the Supplementary material for Brancaloni *et al.* (submitted)(*Appendix C – Scientific paper 3*) SEM allows the observation of thin sections at much higher spatial resolutions than petrographic microscopes. SEM utilizes electrons to gather images rather than light, enabling the observation of the internal structure of many components. In **Figure 5-4**, the example of a dung specimen is presented, highlighting the higher resolution obtained with the SEM imagery products (**Figure 5-4** panels **c**, **d**) compared to lighting microscopy (**Figure 5-4** **a**, **b**).

In SEM, the images are formed by detecting secondary electrons and backscattered electrons from the sample surface when bombarded by a focused electron beam (Goldstein *et al.*, 2017). Backscattered electrons create shinier or brighter portions in the image, reflecting mineralogical changes inside the sample. This contrast is often related to differences in atomic number and density of the sample materials (Goldstein *et al.*, 2017). Heavier elements (higher atomic numbers) tend to generate more backscattered electrons and, therefore, higher signal intensity compared to lighter elements (Goldstein *et al.*, 2017). Secondary electrons, on the other hand, provide information about the topography and composition of the sample surface (Goldberg and Macphail, 2006; Goldstein *et al.*, 2017).

When high-energy electrons from the beam strike the sample, they can create electron vacancies in the inner shell of the atoms. To fill the vacancies, outer shell electrons may transition to lower energy levels, releasing energy in the form of X-rays (Goldstein *et al.*, 2017). The emitted X-rays are characteristics of the elements in the sample. These X-rays are detected by the EDS



system, resulting in an energy spectrum that represents the distribution of X-ray energies emitted by the sample. This allows the study of chemical and mineralogical composition of the sample. The technique not only allows for the study of *in situ* components, but also enables the employment of different sample types, such as bulk samples. The limitations of the technique are connected with the equipment used and strong X-ray background intensity affecting detectability for low concentrations.



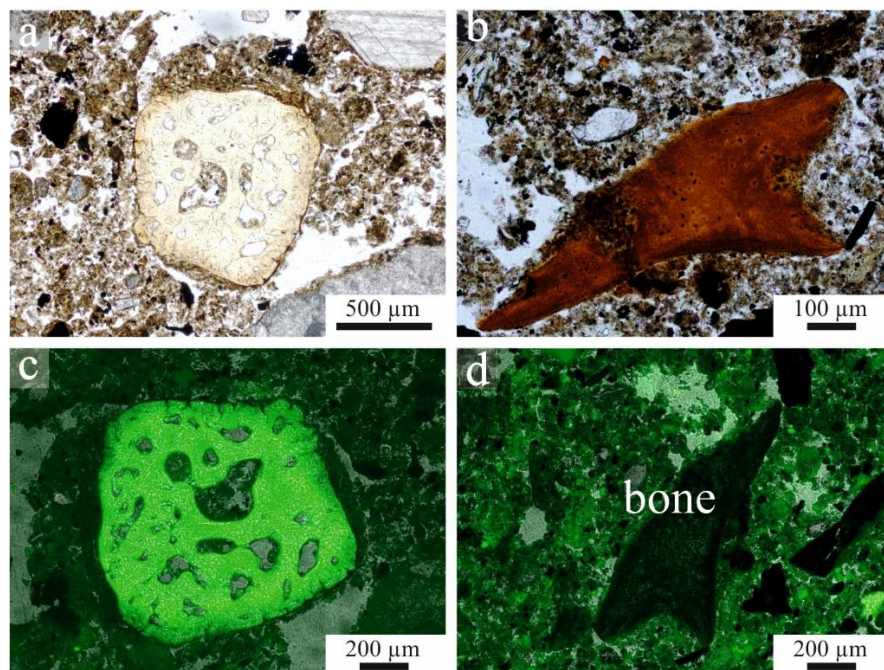
**Figure 5-4** Dung pellet found at Obihsir-5 under lighting microscopy (a, b) and SEM (c, d), worth noting is that the internal structure of the specimen under lighting microscopy is hidden, but becomes accessible under SEM. **a)** dung pellet under ppl; **b)** same specimen under xpl; **c)** same specimen (rotated) under SEM; **d)** under SEM at increased magnification

## 5.4.2 Epifluorescent microscopy

Epifluorescent microscopy was conducted at the Institute of Geological Sciences of The Polish Academy of Sciences in Cracow with the assistance of Jan Goleń, MSc. Technical specifics of the instrumentation used are provided in the Supplementary Material for Brancaloni *et al.* (submitted)(Appendix C – Scientific paper 3).

The technique operates based on the fluorescence phenomenon, wherein an object absorbs radiation and emits light with longer wavelengths (Stoops, 2017). Epifluorescence involves oblique incident radiation of short wavelengths, used with a set of excitation and suppression filters to isolate wavelengths and observe fluorescence (Stoops, 2017). In archaeological micromorphology, this technique is employed to detect phosphatic components, such as bone fragments, excrements and authigenic minerals (Brönnimann *et al.*, 2017; Stoops, 2017; Villagran

*et al.*, 2017), as well as calcium carbonates, organics, and phytoliths (Stoops, 2017). Epifluorescence can also be applied to assess if sedimentary components (like bones) underwent taphonomic processes, such as burning (Villagran *et al.*, 2017), thereby aiding in the reconstructing of site formation processes (Villagran *et al.*, 2017). Notably, bones are autofluorescent and emit green fluorescence upon excitation with UV-blue light (Stoops, 2017; Villagran *et al.*, 2017; Lambrecht and Mallol, 2020). Heated bones undergo transformations in the organic (proteins and lipids) and mineral parts (hydroxyapatite), gradually hindering their capacity to be autofluorescent and resulting in a change in fluorescence color (Villagran *et al.*, 2017; Lambrecht and Mallol, 2020). An example from Obishir-5 is provided in **Figure 5-5**. This phenomenon potentially allows the identification of burning processes in the past (Villagran *et al.*, 2017). In Brancaleoni *et al.* (submitted) (*Appendix C – Scientific paper 3*), I compared my observations under epifluorescent light with previously published experimental results (Villagran *et al.*, 2017) to infer the degree of burning of my specimens and interpret the site formation processes at the site. Although many experiments have confirmed bone color changes through heating (Krap *et al.*, 2017; Villagran *et al.*, 2017; Lambrecht and Mallol, 2020), optical properties alone are not sufficient to establish burned bones (Villagran *et al.*, 2017). Other processes may cause color transformations, such as humification. This issue of equifinality may require the application of microanalytical techniques (such as micro-FTIR) to determine if the bones found in thin sections have been heated (Villagran *et al.*, 2017).



**Figure 5-5** Different lighting conditions of two specimens found in the sedimentary record at Obishir-5. **a)** Bone specimen showing yellow coloration in ppl; **b)** bone specimen showing reddened coloration in ppl; **c)** same specimen showed in a) but under epifluorescent light showing the typical green fluorescence; **d)** same specimen in b) not showing fluorescence, due to possibly heating transformations

## 5.5 Grain size analysis

Grain size was employed to characterize the sediments, aiming to understand material sorting due to sedimentary processes and the coexistence of different deposition modes, such as allochthonous and autochthonous material (Brancaleoni *et al.*, 2022), or geogenic and anthropogenic inputs, as discussed in Brancaleoni *et al.* (submitted). Technical specifics are detailed in Brancaleoni *et al.* (2022, 2023). In general, grain size analysis is utilized to obtain the particle size distribution of a sediment sample (Konert and Vandenberghe, 1997), providing important insights into sediment provenance, transport history, and depositional conditions (e.g., Folk and Ward, 1957; Friedman, 1979). For instance, the uniformity of grain size (sorting) may provide information on the type of sediment source (Goldberg and Macphail, 2006).

Traditionally, grain size is determined using the sieve method for coarse fractions (> 2 mm), and the pipette method, based on the ‘Stokes’ sedimentation rates, for the fine fractions (< 2 mm) (Konert and Vandenberghe, 1997). Other techniques for the analysis of the fine fraction include measurement by laser diffraction size analysis, X-ray sedigraph and Coulter counter (Blott and Pye, 2001). The results are typically subjected to statistical analysis, followed by the classification of sediment using descriptive terms.

Grain size analysis has its limitations. For instance, if the sediment contains aggregates, disaggregation of the clasts may not reflect depositional energies (Goldberg and Macphail, 2006). Moreover, anthropogenic deposits may limit the method’s applicability, as sedimentary dynamics cannot be determined as in the case of geogenic sediments (Goldberg and Macphail, 2006). More generally, grain size analysis faces challenges in obtaining representative samples. To obtain information about the cobbles and boulders greater than 50 mm, the maximum diameter of the clasts was annotated during the field survey (Brancaleoni *et al.*, 2022). Moreover, non-standard sieves were used for the coarse fractions at Obishirian sites (Brancaleoni *et al.*, 2022, 2023), and the material was dry sieved on-site. This complicates correlation with other sites where samples were sieved with standard sieves and, the dry sieving contributes to a loss of very fine particles, which are more likely to be volatile. Considering transportation costs, efforts in future should be made in using standard sieves and wet sieving, perhaps by utilizing local laboratories.

## 5.6 Geochemistry and mineralogy

### 5.6.1 Basic geochemistry

The chemical and mineralogical composition of sediments were applied to identify geogenic, anthropogenic, pedogenic, or weathering horizons, as well as any temporary cessation of sedimentary action at the Obishirian locations (Brancaleoni *et al.*, 2022, submitted). For

instance, phosphorous (P) present in soil is an archaeologically significant indicator of human activity (Holliday and Gartner, 2007) and it may infer the prehistoric anthropogenic land use of an area (Weihrauch, Söder and Stoddart, 2022). Personally, I was involved in the Carbonate content and Organic matter content determination, and preparation of samples for carbon (C), hydrogen (H), nitrogen (N), and sulfur (S) (CHNS) elemental analysis, Inductively Coupled plasma Mass Spectrometry (ICP-MS) and mineralogical analysis. Anna Mulczyk, MSc, a technician at the Institute of Geological Sciences of the Polish Academy of Sciences in Warsaw, performed CHNS elemental analysis (using a Vario MicroCUBE CHNS analyzer). ICP-MS was subcontracted to the Bureau Veritas Minerals Laboratory in Vancouver, Canada. Technical specifics are described in Brancaleoni *et al.* (2022).

The treatment of sediment samples with various reagents to remove carbonate or organic matter content is a routine part of the preparation of samples for further mineralogical, chemical and isotopic analysis (Gaffey and Bronnimann, 1993). Carbonate removal treatment was used to prepare the samples for CHNS analysis to estimate the organic content present in the sediments. I used the pretreatment also to have an estimation of the carbonate content of samples. Carbonate content was obtained by acid (hydrochloric acid HCl) fumigation, as detailed in Brancaleoni *et al.* (2022). I also estimated the organic matter content by sediment treatment with hydrogen peroxide (H<sub>2</sub>O<sub>2</sub>). These treatments are relatively simple and do not require sophisticated equipment; moreover, the reagents are commercially available. On the other hand, HCl treatment is time-consuming when dealing with carbonate-rich samples and may result in the precipitation of an acid-insoluble complex, coating and protecting residual carbonate, preventing its complete removal (Fernandes and Krull, 2008). H<sub>2</sub>O<sub>2</sub> treatment resulted in a time-consuming removal and can lead to partial dissolution of carbonate that can bias the organic content estimation (Gaffey and Bronnimann, 1993; Falster, Delean and Tyler, 2018). As an example, the results obtained for Obishir samples were null, perhaps due to the too small amount of samples employed and drying at high temperature (105°C). Drying at high temperature can indeed compromise the amount of organic matter in the sediments. It is suggested drying at temperatures below 65°C to preserve the organics.

For a more reliable estimation of the organics in the samples, CHNS analysis was employed after samples underwent HCl fumigation. The technique is employed to determine the elemental composition of CHNS in a sample. In this way, I obtained the estimation of total amount of C (TOC) and total N (TN) that I used for the characterization of sediments at Obishirian sites (Brancaleoni *et al.*, 2022, submitted). The method employs sample combustion in a high-temperature environment (Matejovic, 1993). This produces carbon dioxide (CO<sub>2</sub>), sulfur dioxide (SO<sub>2</sub>), water and nitrogen oxides (NO<sub>x</sub>) that are separated using gas chromatography and detected. Eventually, the signal is converted into concentrations, and calibration is done using standards

with known concentrations of the elements of interest. Limitations to the method can be found in Byers, Mills and Stewart (1978), Matejovic (1993), and Phillips *et al.* (2011) among others.

ICP-MS was employed to estimate the concentrations of an extensive array of elements in my sediments samples. ICP-MS uses a plasma to ionize the atoms (Holliday and Gartner, 2007) and then uses a quadrupole magnet that separates elements based on mass-to-charge ratio (Ryan, 2020), and each detector is bombarded by ions of known mass whose signal is proportional to concentration (Ryan, 2020). The signal is then converted into a mass spectrum. ICP-MS works well with heavy ions (Holliday and Gartner, 2007), and the methodology is affected by sample digestion (Holliday and Gartner, 2007). For instance, an accurate measure of phosphorus (P) concentration is partially dependent on the capacity of the reagent to liberate P molecules during digestion (Holliday and Gartner, 2007).

#### **5.6.1.1 Statistical analysis**

To unveil relationships within our geochemical data at Obishir-5, I computed a correlation matrix for the concentrations of these elements. A Correlation matrix shows correlation coefficients between variables. The correlation can be positive or negative, there is perfect positive correlation when the value is 1, and perfect negative correlation when the value is -1. Given that our dataset displayed a lack of normal distribution, I opted for the Spearman method (Friendly, 2002), a non-parametric correlation approach. These computations were conducted within the RStudio v3 environment. The resulting correlation matrix allowed to identify patterns and potential causal connections between various geochemical variables (see Supplementary Material in *Appendix C – Scientific paper 3*).

#### **5.6.2 Powder X-ray diffraction (PXRD) and Infra-Red spectroscopy (FTIR)**

Dr. Małgorzata Lempart-Drozd conducted PXRD and FTIR analysis on loose (bulk) samples at the Institute of Geological Sciences in Cracow of The Polish Academy of Sciences. FTIR was initially utilized for preliminary examinations of samples, serving to identify both inorganic and organic components, and assess the samples' purity. PXRD analysis, on the other hand, facilitated both qualitative and quantitative assessments of the minerals present in the samples. This technique enabled the tracking of mineralogical changes throughout the profile. Specifics of these techniques are described in Brancaloni *et al.* (submitted) and its supplementary materials (*Appendix C – Scientific paper 3*).

FTIR is a laboratory technique used to identify organic and inorganic compounds by measuring their absorption of infrared radiation over a range of wavelengths (e.g., 50 to 5000  $\text{cm}^{-1}$  wavenumber) (Berna, 2017). Using an interferometer, the method collects an interferogram

of sample signal, and eventually performs a Fourier transform to obtain the infrared spectrum (Berna, 2017). The location of peaks in the spectrum is characteristic of specific compounds, and moreover, spectra can be compared using reference libraries. Additionally, assessing changes in peak intensity or position between related samples can provide information on the chemical structure variation (Berna *et al.*, 2007). This provides a useful tool for the identification of site formation processes (e.g., Mallol, Mentzer and Wrinn, 2009), such as the identification of burning (e.g., Stiner *et al.*, 1995; Berna *et al.*, 2007; Mentzer, 2014) and/or diagenesis (e.g., Schiegl *et al.*, 1996; Karkanis *et al.*, 1999, 2002). The limitations are dependent on the equipment used and the experience in interpreting the spectra, for further details on limitations the reader may refer to Jananee, Thangam and Rajalakshmi (2021) and de Caritat *et al.* (2022).

PXRD is also a laboratory technique applied to powdered samples that allows the determination of mineral assemblages in sediments. The method exploits the fact that crystal bonds are of the same magnitude as X-ray wavelengths (Berthold and Mentzer, 2017), and the basic principle that the interaction of X-ray with the crystal lattice produces scattering of X-rays in specific directions. Every crystalline substance has its individual crystal structure and chemical composition, resulting in a unique pattern in an X-ray diffractogram, where intensity of the scattered X-ray beam is plotted versus the diffraction angle (Berthold and Mentzer, 2017). Limitations for these methods are set by the equipment used and experience, for further reading refer to Goehner and Nichols (1986).

At Obishir-5, while geochemical and mineralogical analyses have their merits, they failed to detect certain critical aspects captured by the microscopic method. Micromorphology has unveiled hidden facets of the sedimentary records such as the presence of bones, ash and charcoals, that other applied methodologies could not reveal (Brancaleoni *et al.*, submitted). Micro-analytical methods should be considered for the study of these sediments, as bulk sample analyses failed to detect the presence of phosphates, which were revealed in the microscopic record. The application of the micro-analytical method where the thin section can be directly analyzed is recommended for *in situ* analysis that can be compared with micromorphology results.

## 5.7 Faunal assemblage

Prof. Guzel Danukalova and Dr. Evgenia Osipova analyzed fossil mollusks according to the methodology presented in Osipova *et al.* (2021) and in Brancaleoni *et al.* (2022). Taxonomy of fossil mollusks was applied to provide palaeoecological and paleoclimatic data for the identified processes at Obishirian sites (Osipova *et al.*, 2021; Brancaleoni *et al.*, 2022).

Faunal assemblage analysis has long been of interest in archaeological studies (Casteel, 1972; Grayson, 1973). In particular, the study of terrestrial mollusk assemblages represents a

reliable tool for the study of paleoecology and paleoclimate at a location (Wu, Li and Rousseau, 2018). Terrestrial mollusks are easily found in Quaternary sediments (Moine *et al.*, 2002) and are highly sensitive to environmental changes (Wu, Li and Rousseau, 2018). For instance, Wu, Li and Rousseau (2018) assert that the mollusk record is one of the most important proxies in the paleoenvironmental and paleoclimatic reconstruction of loess-paleosol sequences in China. The analysis for interpreting the paleoenvironment is based on the information on the ecological requirements provided by modern terrestrial species (Wu, Li and Rousseau, 2018). Therefore, malacologists always refer to reference materials, which result from systematic surveys and classification of modern terrestrial mollusks (Wu, Li and Rousseau, 2018; Osipova *et al.*, 2021; Brancaleoni *et al.*, 2022). Recent advances in the field are related to isotopic studies of mollusk shell for the reconstruction of paleotemperature combined with higher accuracy of C-14 dating techniques (Loftus, Rogers and Lee-Thorp, 2015; Wu, Li and Rousseau, 2018).

Method limitations are largely related to the insufficient number of studies into the taphonomy of fossil mollusks, and into ecological surveys of modern terrestrial mollusks (Wu, Li and Rousseau, 2018), and poor preservation conditions due to post-depositional processes at a location. A possible solution is the application of complementary methods in the evaluation of paleoenvironmental conditions, or the consideration of control profiles (for example loess-paleosol sequences) in the vicinity of a site.

## 5.8 Dating methods

At Obishir-5, dating stands on several published radiocarbon dates (Taylor *et al.*, 2021). At Obishir-1, the chronometric dating was established through the optically stimulated luminescence (OSL) performed by the Nordic Laboratory for Luminescence Dating at Risø, Denmark, on six samples collected during fieldworks in 2019 (**Figure 5-1**). Sample preparation for luminescence dating is outlined in Supplementary Material of Brancaleoni *et al.* (2022). Luminescence dating was performed according to the methodology described in Brancaleoni *et al.* (2022). Chronometric dating (radiocarbon and luminescence) was used to determine the age of deposits as well as any incoherency in the date order, which may record an inter-strata mixing and re-deposition.

### 5.8.1 Radiocarbon dating

Radiocarbon C-14 is the only naturally occurring radiogenic isotope of carbon and is utilized in Earth Sciences and Archeology as a geochronometer. C-14 is produced by the nuclear reaction between the atom of a stable isotope and cosmic rays (Taylor, 1997; Ryan, 2020). C-14 eventually combines with oxygen to produce carbon dioxide (CO<sub>2</sub>), which is rapidly dispersed

and well mixed by atmospheric circulation, eventually incorporating into plants through photosynthesis or combining with water (H<sub>2</sub>O) to form carbonic acid (H<sub>2</sub>CO<sub>3</sub>). Carbonic acid precipitates to the Earth's surface and is incorporated into living organisms, minerals and water bodies. Once the organism dies and C-14 intake stops, C-14 decreases as it undergoes radioactive decay with a half time of *ca.* 5730 years. This means that after ten half-lives, only 0.1% of C-14 remains in the material, ideally setting the limitation to the methodology for materials younger than 57300 years. Age measurements by counting the decay of individual C atoms can be carried out by several methods, with the more reliable and effective one being accelerator mass spectrometry (Ryan, 2020). Radiocarbon age analysis includes sources of error in age determination, such as variation in the C-14 concentration in the atmosphere (Suess and de Vries effects), C-14 fractionation, and the reservoir effect. To reduce analytical errors, raw ages are calibrated and corrected (Stuiver, Reimer and Braziunas, 1998; Hughen *et al.*, 2004; Reimer, Brown and Reimer, 2004; Ryan, 2020). The well-preservation of the sample and its purity are paramount for the reliability of the measurements. At archaeological sites, the most common datable materials are charcoal and bones. Both can suffer from poor preservation and post-depositional processes, such as degradation and diagenesis. Furthermore, another crucial aspect is to ensure that the sample is associated with the layer or event of interest.

### **5.8.2 Optically stimulated luminescence dating (OSL)**

OSL dates crystalline materials, such as quartz or feldspar, to the last time they were exposed to sufficient heat or sunlight (Feathers, 2008). The method is based on the assumption that mineral grains were exposed to sufficient daylight during transport to reset the OSL signals (Duller, 2008). This assumes that when deposited, grains were completely “discharged” (or in jargon completely ‘bleached’) and could be recharged by ionizing radiation from surrounding sediments during burial. Therefore, OSL measures the stored energy absorbed since the last resetting, which supposedly coincides with burial.

Reliable dating can be hindered by partial bleaching of the grains resulting from limited exposure to light during the last resetting (Duller, 2008), and other post-depositional processes affecting the deposit, such as bioturbation (Moska, Adamiec and Jary, 2011; Fitzsimmons *et al.*, 2020). The application of OSL may be challenging, among others, in colluvial settings (Duller, 2008), such as at the Obishirian sites. Regarding colluvial sediments, short transport distances, on the order of few meters to tens of meters, may result in incompletely bleached sediments, hindering reliable OSL measurements (Arnold, Bailey and Tucker, 2007; Duller, 2008). To obtain more reliable results when dealing with partial bleaching of samples, single-grain optical dating is recommended (Duller, 2008).



### **5.8.2.1 Stratigraphic accumulation rate (SAR)**

SAR was estimated just for Obishir-1, where all samples were collected from one vertical column. The Obishir-1 sequence and dating measurements allowed the estimation of SAR because coherent and taken along the same vertical profile. At Obirshir-5, the estimation of SAR was considered unreliable due to various issues. These included inconsistent sampling across several vertical columns, imprecise data regarding the exact locations of certain samples, and the lack of established collagen quality parameters for some of the dated bones. The SAR estimation is described in Supplementary Material (Brancaleoni *et al.*, 2022)(*Appendix A - Scientific paper I*).

SAR refers to the speed at which sediment or geological deposits accumulate over time in a specific stratigraphic sequence. It is a measure of how quickly or slowly materials, such as minerals, organic matter, or other geological components, accumulate and build up within a particular geological context. This rate is often used in fields such as geology and archaeology to understand the temporal patterns of sedimentation and the formation of stratigraphic layers.

## **5.9 Distribution of artifacts**

In addition to the aforementioned techniques, I explored the intra-site spatial distribution of artifacts at Obishirian sites. The goal was to assess whether the arrangement of artifacts could be attributed to natural or anthropogenic processes. For instance, the disposition of artifacts on a distinct surface implies the initial anthropogenic deposition on a living floor, with anticipated concentrations in specific areas. Arrangements along lineaments may indicate erosion and subsequent redeposition by water run off or mudflow/debris flow. A disordered three-dimensional arrangement resembling a cloud signifies post-depositional scattering in sediment, possibly caused by bioturbation, cryoturbation, or mass movements.

Spatial distribution analysis deals with the use of space in the past (Gaydarska, 2014) and the analysis is concerned in finding patterns of distribution of objects. It can be performed at two main scales: site and landscape scale. The latter involves for example the use of GIS-based mapping (Gaydarska, 2014). At the site scale, plotting the artifacts on a graph can allow the identification of different use of the space (Gaydarska, 2014) and site formation processes of a site (Mcpheeron, 2018). Limitations lie in the proper recording of locations during excavations and the correct understanding of contextual elements such as taphonomy and deposition which may displace the primary position of artifacts (Gaydarska, 2014).

# 6 Results

## 6.1 Introduction

The three papers that comprise this thesis collectively contain the results of this study. The results for the Obishir-1 site were published in Brancaleoni *et al.* (2022) and Supplementary material in *Appendix A - Scientific paper 1*). The results for the Obishir-5 were partially published in Brancaleoni *et al.* (2023) *Appendix B – Scientific paper 2*, and fully included in Brancaleoni *et al.* (submitted) and its Supplementary material in *Appendix C – Scientific paper 3*. The full author contribution statement is in *Appendix D – Author contribution statement*. This Chapter is divided into three sub-sections, each encompassing the content of the three papers that collectively constitute this thesis, and a final fourth chapter summarizing the most important findings. For each paper, the contribution of each author is given together with a summary and discussion of the results.

## 6.2 Depositional history of a talus cone in an arid intermontane basin in Central Asia: An interdisciplinary study at the Late Pleistocene–Late Holocene Obishir-I site, Kyrgyzstan

*Brancaleoni, G., Shnaider, S., Osipova, E., Danukalova, G., Kurbanov, R., Deput, E., Alisher kyzy, S., Abdykanova, A., & Krajcarz, M. T. (2022). Depositional history of a talus cone in an arid intermontane basin in Central Asia: An interdisciplinary study at the Late Pleistocene–Late Holocene Obishir-I site, Kyrgyzstan. Geoarchaeology, 37, 350–73. <https://doi.org/10.1002/gea.2189>*

The site formation at Obishir-1 location is the focus of the first published paper of this dissertation titled ‘Depositional history of a talus cone in an arid intermontane basin in CA: An interdisciplinary study at the Late Pleistocene–Late Holocene Obishir-I site, Kyrgyzstan’ and co-authored by me, Greta Brancaleoni, with a contribution of 50% (*Appendix A - Scientific paper 1*). My contribution included designing the research, fieldworks, data analysis and interpretation (stratigraphy, sedimentology, micromorphology, geochemistry), and drafting and revision of the manuscript. Dr. Svetlana Shnaider contributed with the archaeological assemblage analysis and interpretation. Dr. Evgenia Osipova and Prof. Guzel Danukalova analyzed and interpreted the mollusk assemblages. Dr. Redzhep Kurbanov carried out the OSL analysis. Ewa Deput produced the thin sections for micromorphology. Dr. Saltanat Alisher kyzy and Prof. Aida Abdykanova

guaranteed access to the excavation site. Dr. Maciej T. Krajcarz designed and supervised the research, drafted the manuscript and analyzed chronometric data.

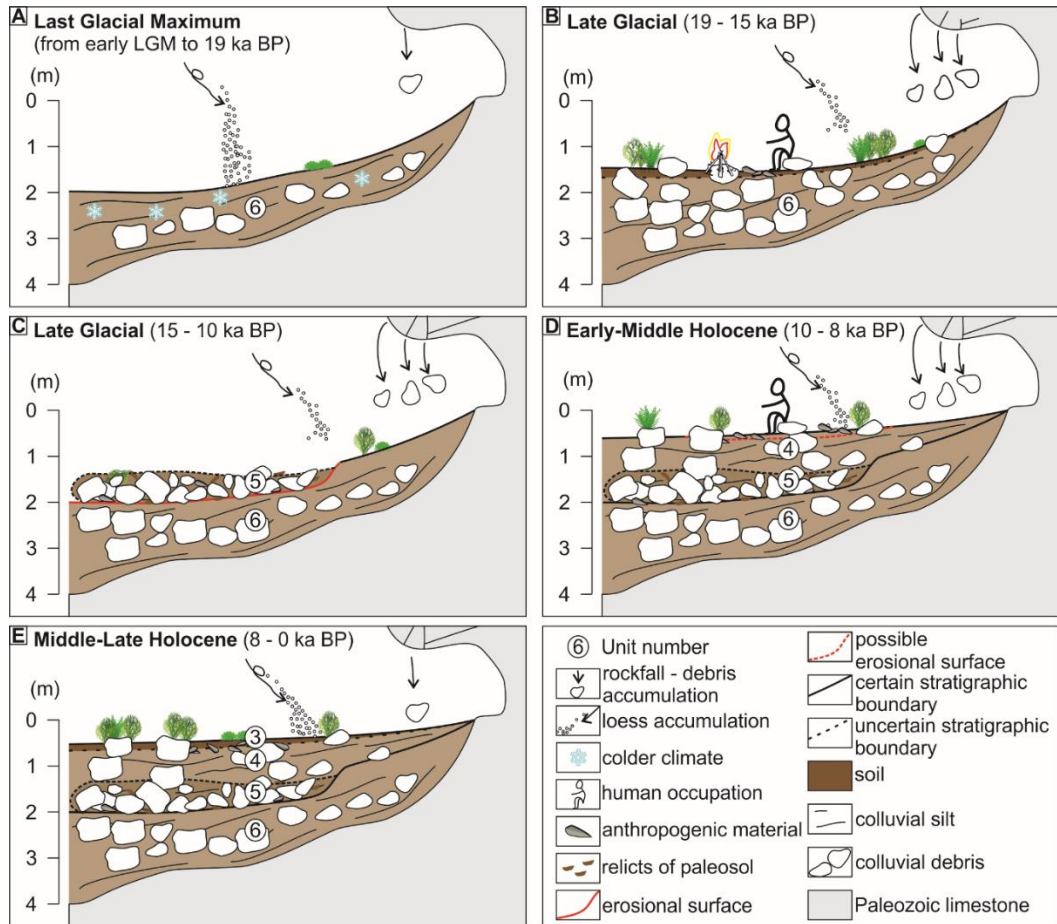
## 6.2.1 Summary

The methodology applied allowed a reasonable account of the Quaternary talus cone at Obishir-1 (Brancaleoni *et al.*, 2022). I was able to recognize the main site formation processes. I corroborated the geological and archaeological interpretation, and have been able to reconstruct the depositional history of the site (**Figure 6-1**). Importantly, from the analysis of the spatial distribution of artifacts, I identified two human occupation sequences within the talus cone deposits. The former occurred between 19000 and 15000 BP and resembles the Upper Paleolithic up to the early Neolithic complexes of CA. The latter, embedded mainly in SU4 *ca.* 10000–8000 BP, is similar to the final Epipaleolithic – early Neolithic Obishirian complex from the neighbor Obishir-5 (Shnaider *et al.*, 2017), as well as to the Oshkhona site (Pamir mountains).

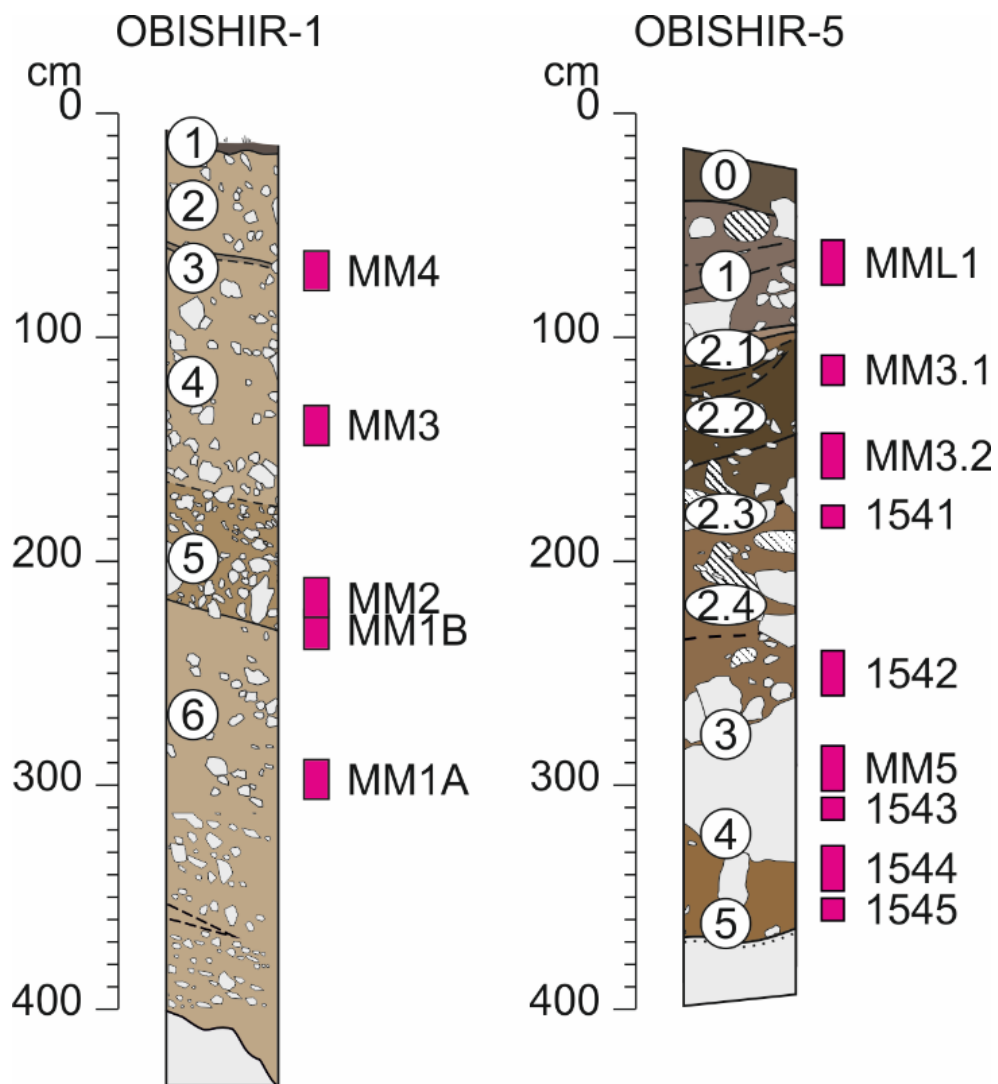
The Quaternary succession at the Obishir-1 site is quite uniform. It comprises mainly unconsolidated, poorly sorted talus deposits, namely diamicton of differing textures. Even though differences between units were subtle, six units were distinguished (SUs from 1 to 6, descending) (**Figure 6-2**). For a detailed description of the stratigraphic units please refer to Brancaleoni *et al.* (2022) in *Appendix A - Scientific paper 1*. SU6, SU5 and SU4 represent the actual talus deposit, accumulated between the end of the Late Pleistocene and the early Middle Holocene. SU3 and SU1 are, respectively, a paleosol weakly developed before Soviet archaeological campaigns and the current topsoil. SU2 is an artificial modern deposit left by Soviet excavators. Interestingly, for SU6 and SU5, a not *in situ* paleosol was recorded, which provided important information about the depositional history reconstruction (**Figure 6-3**).

Generally, I assumed that the talus is a rockfall cone, that is, accumulated thanks to rockfall events from the adjacent cliff, with infiltrated finer material of allochthonous (aeolian) and autochthonous (illuviation and/or recrystallization) origins. The fine infiltrated material resulted from aeolian and endogenous sedimentation (e.g., limestone weathering and illuviation). The former possibly accumulated simultaneously with the debris, whereas the latter occurred mainly *in situ* when the climate shifted to more humid conditions. Due to the presence of some diagnostic microfeatures (not *in situ* soil), I can assume that a rapid and local mass movement may have possibly occurred subsequently to land clearance. Effects of this movement are recorded in the arrangement of artifacts within the units (**Figure 6-4**). The lithic artifacts are unevenly distributed within the vertical profile. Two main horizons are identified (1st and 2nd occupation) of which the boundaries are difficult to draw, therefore the artifacts between the two horizons are difficult to attribute to one or the other occupation (1st or 2nd occupation – orange

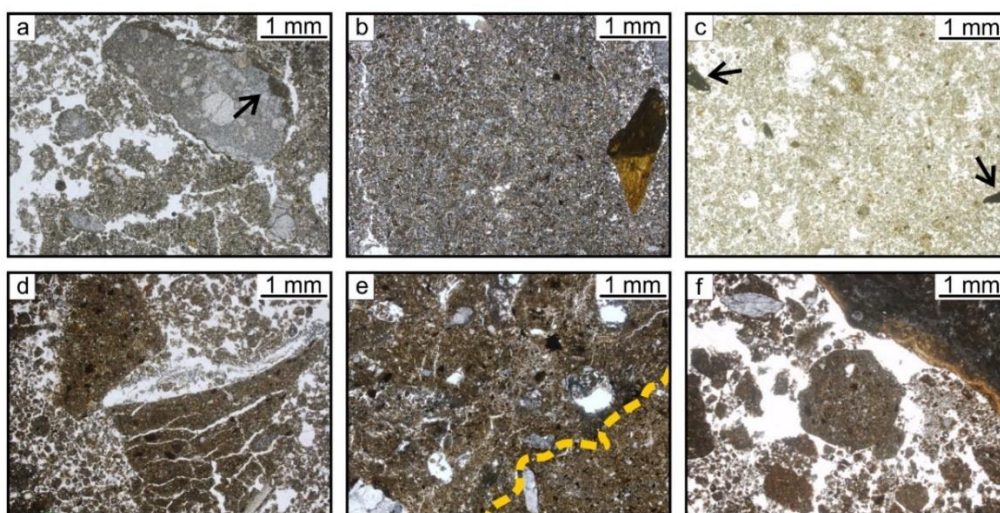
points). The lower horizon comprises less than 20 specimens and is situated near the boundary between SU5 and SU6. The upper horizon comprises a major portion of the lithics and is connected to the middle – upper part of SU4. Some artifacts, loosely scattered within SU4, SU5, and SU6, may also belong to these two horizons and represent post-depositional disturbances.



**Figure 6-1** Depositional history of Obishir-1 after Brancaloni et al. (2022). **a)** Last Glacial Maximum (LGM). Accumulation of the bottom part of Unit 6 under cold and periglacial conditions where aeolian processes were dominant. **b)** Late Glacial. Accumulation of the top part of SU6. Shifting to more humid conditions with a weakly formed soil, more efficient frost cracking and the first human occupation horizon (unknown Paleolithic). **c)** Late Glacial. Accumulation of SU5 possibly due to an erosional event after fire-related events. **d)** Early – Middle Holocene. Accumulation of SU4. Onset of the Holocene. Second cultural occupation horizon (Obishirian). **e)** Middle – Late Holocene. Soil formation and consequently cease of accumulation (SU3).

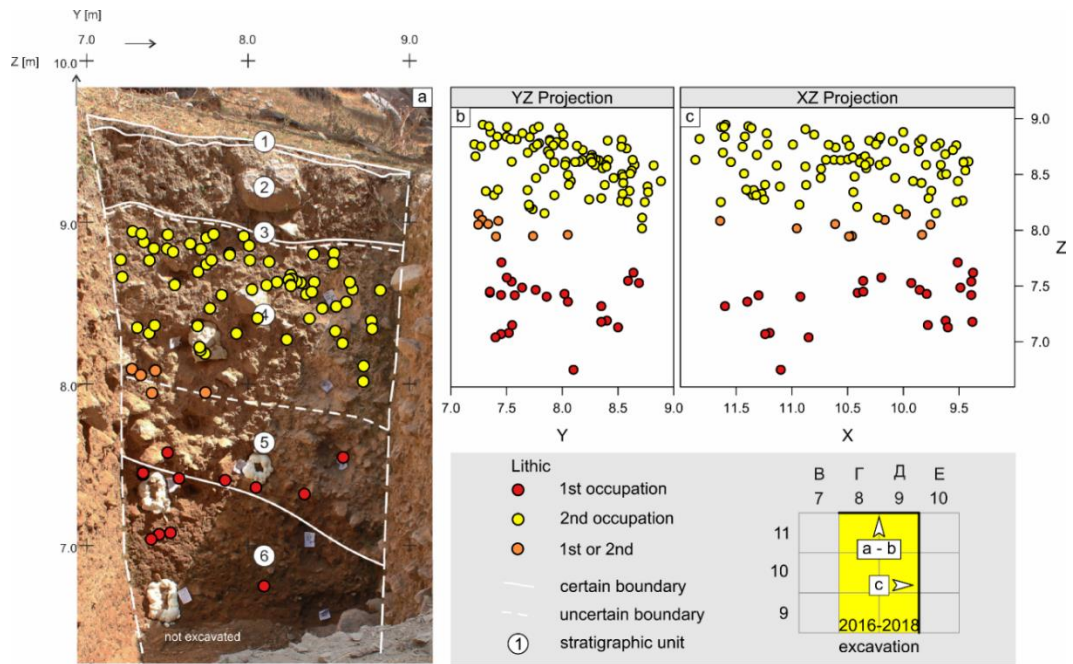


**Figure 6-2** Schematic stratigraphic profiles at the studied locations after *Brancaleoni et al. (2023)* with location of micromorphology sampling.



**Figure 6-3 a–b)** Siltic-textured soil characterizing the central part of SU6, vuggy and blocky alternating massive microstructure, vertical planes, clay capping (arrow) and

vertical oriented clasts (b) were interpreted as frost action microfeatures (thin section: MM1A II). c) Yellowish more loamy soil with fine granular microstructure with low degree of separation of aggregates and angular charcoal fragments (arrows) represents the not in situ soil noticed in the upper part of SU6, just below the scour structure (Unit 5 lower boundary – MM1B II). d) Early and Mid-Holocene soil is more brownish with loamic texture characterized by large soil mesofauna structures in which coarse pedons (to notice is the different internal fabric) are surrounded by finer organo-mineral excrements (MM3 I). e) Boundary (dashed line) between SU4 and SU3 (dark paleosol below Islamov’s dump), the microstructure of SU3 is complex whereas SU4 shows mainly a massive structure (MM4 I). f) Coarse granular microstructure with a high degree of separation as an effect of soil fauna activity characterizes the top of SU3 (MM4 II). The micro photos are in plane polarized light after Brancaleoni et al. (2022).



**Figure 6-4** Artefact distribution within the profile at Obishir-1. a) Projected lithic artifacts from 0–1.5 m distance from the E wall of the 2016–2018 excavation. b) – c) Scatter plots of all recorded lithic artifacts. From Brancaleoni et al. (2022).

## **6.3 A closer look at clasts and groundmass: Micromorphological features in sediments with archaeological significance in Obishir and Katta Sai complexes (Central Asia)**

*Brancaleoni, G., Kot, M., Shnaider, S., Mroczek, P., Kurbanov, R., Abdykanova, A., Alisher kyzy, S., Khudjanazarov, M., Pavlenok, K., Krajcarz, M. T. (2023). A closer look at clasts and groundmass: Micromorphological features in sediments with archaeological significance in Obishir and Katta Sai complexes (Central Asia), Journal of Archaeological Science: Reports, 51, 104118, <https://doi.org/10.1016/j.jasrep.2023.104118>.*

The second published paper in this dissertation titled ‘A closer look at clasts and groundmass: Micromorphological features in sediments with archaeological significance in Obishir and Katta Sai complexes (CA)’ is a methodology-oriented paper (*Appendix B – Scientific paper 2*). The initial work at Obishir-1 location revealed the complexity of matrix-clast contacts prompting a comprehensive micromorphological examination for the identification and classification of this partial fabric. Some of the findings from this analysis have been incorporated into the third paper, which focuses on the study of site formation at the Obishir-5 location.

The paper was co-authored by me, Greta Brancaleoni, with a contribution estimated to be around 68%. My contribution included designing the research, fieldworks, data analysis and interpretation (sedimentology and micromorphology), and drafting and revision of the manuscript. Dr. Svetlana Shnaider, Dr. Małgorzata Kot, Prof. Aida Abdikanova, Dr. Saltanat Alisher kyzy, Prof. Mhukkidin Khudjanazarov and Dr. Konstantin Pavlenok guaranteed access to the excavation sites. Dr. Małgorzata Kot partially sampled Katta Sai complex profiles. Dr. Redzhep Kurbanov and Dr. Przemisław Mroczek conducted grain size analysis. Dr. Maciej T. Krajcarz designed and supervised the research.

### **6.3.1 Summary**

















I studied a specific aspect of colluvial sediments in this region, such as the presence of gravel and silt and their mutual relationship. Obishir-1 and Obishir-5 were chosen together with two other archaeological sites (Katta Sai 1 and 2) in CA for their distinctive modes of sediment accumulation: aeolian and colluvial. The methodology used included grain size analysis and, more importantly, micromorphology, which enabled the examination of the matrix-clast contacts in these sediments.

Micro-features on the surfaces of clasts were identified and classified into four main types: loamy cappings, loamy coatings, secondary calcium carbonate accumulations, cracks

(Brancaleoni *et al.*, 2023). The contact between the coarse and fine material was frequently altered and marked by features related to mineral grain alteration, frost action, redeposition, pedogenetic processes, and anthropogenic activity. The processes affecting gravelly geogenic components and their micro-features may also reflect those impacting gravelly archaeological artifacts, such as secondary calcium carbonate accumulations. A tentative relative chronology and history based on the identified micro-features was proposed.

By analyzing micro-features related to the contact between the coarser mineral components and finer groundmass around, we observed a wide range of processes at this contact. However, we found that the same features were often attributed to different processes, demonstrating the complexity of the formation processes (**Figure 6-5**). My study addresses the issue of equifinality in interpreting site formation and site-specific conditions, as highlighted in previous researches (e.g., Kielhofer *et al.*, 2020).



Micro feature		Archaeological importance							Notes	
		Reorientation of clasts	Redeposition, transport	Relocation of fine material	Frost action (cold climate proxy)	Unidentified physical disturbances	Chemical weathering (humid climate proxy)	Bioturbation		Human/animal activity
No specific features										Clast not affected by post-sedimentary processes
Voids around the clast						yes		yes?		Relative movement between clast and groundmass
Loamy capping		no	no		yes					Frost action after deposition, no transport after
Loamy capping in non-upside position		yes	yes?		yes					Clast reoriented after development of capping
Loamy coating			yes							Possibly rotation
Fragmentary loamy capping or coating			yes					yes?		Erosion after development of capping or coating
Dusty coating							yes			Chemical alteration of limestone
Loamy coating and bio-gallery		no	no	no				yes		Bioturbation contributing to formation of coating
Loamy phosphatic coating		no	no	no					yes	Leaching of P-rich waters
CaCO <sub>3</sub> coat on the under-side		no	no	no						Accumulation of calcium carbonate
CaCO <sub>3</sub> coat on top		yes?	yes?	no						Transport? after accumulation of calcium carbonate
In situ shattering		no	no		yes					Frost action after deposition, no transport after
Shattering cracks filled with groundmass		no	no	yes	yes					Relocation of fines after frost action, no transport after
Shattering cracks empty		no	no	no	yes					Frost action after deposition, no transport after
Shattering cracks with recrystallization		no	no	no	yes		yes			Frost action after deposition, no transport after

**Figure 6-5** A summary of observed features in sediments at the Obishir and Katta Sai complexes from Brancaleoni et al. (2023)

## 6.4 Geoarchaeological approach for tackling the function and preservation state of the Obishir-5 site, the earliest Neolithic site in the Fergana Valley

*Brancaleoni, G., Shnaider, S., Lempart-Drozd, G., Deput, E., Abdykanova, A., Krajcarz, M. T. Geoarchaeological approach for tackling the function and preservation state of the Obishir-5 site, the earliest Neolithic site in the Fergana Valley, submitted on 23<sup>rd</sup> October 2023 at the Journal of Archaeological and Anthropological Sciences*

The site formation at Obishir-5 location is the focus of the third (submitted) paper of this dissertation titled ‘Geoarchaeological approach for tackling the function and preservation state of the Obishir-5 site, the earliest Neolithic site in the Fergana Valley’ and co-authored by me, Greta Brancaleoni, with a contribution of 70% (*Appendix C – Scientific paper 3*). My contribution included designing the research, fieldworks, data analysis and interpretation (stratigraphy, sedimentology, micromorphology, geochemistry), and drafting and revision of the manuscript. Dr. Svetlana Shnaider and Prof. Aida Abdykanova guaranteed access to the excavation site. Ewa Deput produced the thin sections for micromorphology. Dr. Małgorzata Lempart-Drozd performed mineralogical analysis (PXRD and FTIR). Jan Goleń, MSc assisted during observations under epifluorescence microscopy. Dr. Maciej T. Krajcarz designed and supervised the research.

### 6.4.1 Summary

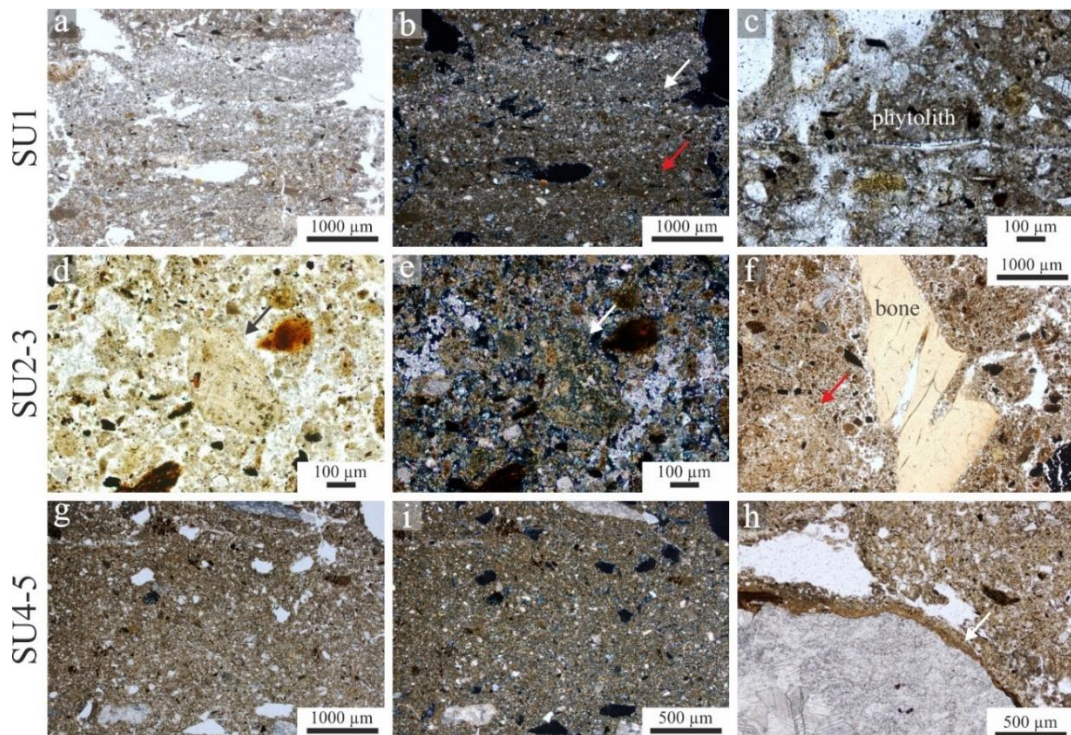
The Obishir-5 is one of the earliest Neolithic sites investigated in Kyrgyzstan and it holds evidence of domestic animals. The Obishir-5 site is embedded in talus deposits in front of two rockshelters at the toe of a heavily fractured and largely karstified limestone cliff. The stratigraphic sequence at the site was originally characterized by U. Islamov (Islamov, 1980), who identified nine stratigraphic units. However, during the 2016 field campaign, a reevaluation of the stratigraphy led to the recognition of six stratigraphic units (Osipova *et al.*, 2021; Taylor *et al.*, 2021). In this study, I adhere to the same stratigraphic scheme (**Figure 6-2**), consisting of stratigraphic units (SU) from SU0 to SU5 (from top to bottom), with SU2 being further divided into four subunits (Sub2.1, Sub2.2, Sub2.3 and Sub2.4).

SU5 and SU4, both hosting the Epipaleolithic cultural horizon, were affected by low sedimentation rates, mostly resulting from the accumulation of debris and fine particles due to erosion, weathering and aeolian processes. Secondary processes included impregnation and

bioturbation. These units were characterized by low-intensity human occupation, which resulted in the absence of archaeologically important components.

SU3 and SU2, representing the Obishirian cultural horizon, showed syn- or post-depositional accumulation of anthropogenic material within the talus. SU3 showed accumulation of bones, charcoals, and ash, but their chaotic arrangement and the fact that they are mixed with geogenic material suggested secondary reworking. In SU2, I observed the presence of herbivore dung material along with the presence of fire by-products and bone fragments. The general arrangement of the fabric suggested reworking processes. Geochemical analyses revealed the presence of a former ground surface at the top of SU2, suggesting a halt in the accumulation and consequently soil formation (**Fig. 4** in Brancaloni *et al.* submitted; *Appendix C – Scientific paper 3*).

In SU1 (Bronze Age and Middle Ages), the archaeological material, especially dung pellets, exhibited horizontal alignment, and the fabric displayed evidence of trampling (e.g., subparallel micro laminated and platy microstructure, alignment of components), as well as bioturbation by soil fauna. The presence of dung droppings, along with elongated phytoliths, suggests animal foddering. Therefore, SU1 likely served as living floors where livestock congregated and grazed. During archaeological excavations, a complex archaeological stratification was revealed made of several different cultural assemblages, that are Paleolithic (SU5 and SU4), Obishirian (SU3 and SU2), Bronze Age and Middle Ages (SU1) (**Figure 6-6**). This may have led also to mixing and contaminations amongst the aforementioned cultural assemblages.



**Figure 6-6** Microphotographs illustrating occupational facies; **a c**) Bronze and Middle Ages (SU1) facies is characterized by an horizon with (ab) micro laminated structure with differing b-fabric, white arrow is indicating a whitish gray crystallitic b-fabric due to sorted mineral grains (mainly quartz and calcite), red arrow is indicating steeple speckled due to loamy brown material; and (c) broken elongated phytolith, evidence of post-depositional modifications due to trampling; **d-f**) Obishirian (SU2 and SU3), total reworking reflects the chaotic arrangement and typical granular microstructure of the fabric, (de) groundmass made of biological droppings, black and white arrows point a dung aggregate in ppl and xpl respectively, fecal spherulites occur within the aggregate and in the surrounding groundmass, (e) b-fabric is dotted due to fecal spherulites, except for voids which are partially filled by micritic calcite; (f) this facies is featured by typical association of components, that are dung aggregates (red arrow), bone (white arrow) and charcoal fragments, note that the bone is in situ cracked (a close-up on the cracks is given in Fig. 5f) **g h**) Paleolithic's typical compacted micro-granular structure (SU4 and SU5) and rare amount of archaeological components and the presence of phosphatic features led to a suspected decomposition of elements, as shown in h the white arrow points a phosphatic rim characterizing a sub-rounded limestone pebble. From Brancaleoni et al. (submitted)

## 6.5 Synopsis

For the Obishir-1 site (Appendix A), archaeological excavations have allowed the study of the internal structure, chronology, and depositional history of the talus cone, as well as the relationship between the slope processes and the archaeological assemblage. I applied a multi-proxy approach, including sedimentological studies (such as micromorphology) supported by the basic geochemistry of sediments, luminescence dating, paleoecology of fossil mollusks, and archaeological analyses. The coarse sedimentary material accumulated through rockfall, and fine-

grained materials accumulated through aeolian processes, illuviation, and *in situ* weathering. Importantly, the assemblages were affected by post-depositional relocation within the slope.

For the Obishir-5 site (*Appendix B and C*), geoarchaeological investigations, including the application of textural, geochemical, mineralogical and micromorphological methods focused on the reconstruction of geogenic and anthropogenic formation processes and disturbances responsible for the alteration of the sedimentary and the archaeological record. The geogenic material accumulated through gravity-induced processes like rockfalls, alongside fine-grained sediment resulting from aeolian processes and *in situ* weathering. The archaeological material, including bones, charcoals, ash and herbivore dung is intermixed with geogenic sediments and shows evidence of reworking. This archaeological material likely originated from anthropogenic activities, such as herding and firing, and subsequently subjected to post-depositional disturbance, including bioturbation, trampling, and organic matter degradation.

A crucial finding was the observation of herbivore dropping at the Obishir-5 location. This holds a crucial significance in terms of the understanding of the Neolithization processes in the region. The presence of herbivore dung supports the interpretation that the domestic animals were present at the location. Along with the evidence purported by (Taylor *et al.*, 2021), who gave evidence of exploitation of domestic animals, our findings contribute to the assumption that the Obishirian culture relied on stabling of domesticated animals.

The presence of coarse (gravel) and fine (silt) sedimentary material is a common aspect of colluvial facies. By using micromorphology and grain size analysis at selected sites in CA, including the Obishirian sites, the study (*Appendix B*) aimed to understand the microscale processes that have affected the geogenic material and, by extension, the potential impact on the archaeological assemblages. The processes related to these features are identified as alteration of the mineral grains, frost action, redeposition, and pedogenetic and anthropogenic processes. Analogies with gravel-sized artifacts can be drawn, particularly with regard to secondary calcium carbonate accumulation.

# 7 Discussions and conclusions

## 7.1 Introduction

This thesis is built upon the study of two different locations—Obishir-1 and Obishir-5—in the same micro-region. It was shown how the methodology applied allowed to meet the defined objectives. It was possible to formulate site formation models for the two locations, highlighting important aspects concerning colluvial facies and addressing significant aspects of the Obishirian culture, such as herding practices. For instance, the main primary depositional processes at the two locations were gravity-induced processes and aeolian accumulation, along with human-related activities. It was also stressed the importance of such findings that allow the assumption of the presence of herbivore dung at Obishir-5, this allowed to infer that the Obishirian economic strategy was based on herding domestic animals.

The next step is to compare the case studies to draw generalizations and contribute to the theory-building process regarding not only the formation processes in the region but also broader implications. By comparing multiple case studies, we can identify common patterns and trends in the sedimentation and disturbances of the sedimentary record, and by extension, the archaeological record. This allows for the development of broader theories and generalizations about human-environment interactions and past landscapes. Along with generalization and theory building, there is contextual understanding. Comparing case studies, we can understand how different factors, such as climate, geology, vegetation, and human activities, interact and shape the archaeological record.

Obishir-1 and Obishir-5 are the first Obishirian sites to have been studied with a modern geoarchaeological approach. Obishir-5 is the eponymous and pivotal site of the Obishirian culture, while Obishir-1 is a site in the vicinity, sharing similar characteristics. Both sites are archaeologically stratified. The sites share similar geological and geomorphological settings, leading us to the assumption that similar physical and geological processes occurred at these locations. Both sites also belong to the same periods. Therefore, if differences are noted within the stratigraphic record, these might be site-related, and may be connected to the different human-related activities carried out at the site rather than to other factors such as the climate, which is expected to be the same at these two close locations.

In this thesis, directions for future works are also outlined. Future works might delve into a complete understanding of site formation at all Obishirian sites. The Obishirian sites are spread in an area comprising the Fergana Valley and the Pamirs (**Figure 2-5**, Chapter 2.4.3.1). This area stretches from low elevation characterizing the basin (Fergana Valley) to high elevation plateaus

(the Pamirs) (**Figure 2-5**, Chapter 2.4.3.1). Studying all other Obishirian sites located in different environments with a geoarchaeological approach can lead us to a better understanding of the Obishirian phenomenon as a whole and its relationship with the landscape. Additionally, giving the different elevations where the sites were found, we can gain insights into the different strategies adopted in response to differing and harsher environments. Given that the Obishirian might revolve around pastoral economy, different environments might have led to different economic strategies such as varied stock management. Moreover, in the area, there is evidence of different cultures that inhabited the same landscape during the same period (e.g., Surungur rockshelter site; Shnaider pers. comm.). Studying these cultures under a geoarchaeological approach might reveal similarities and differences between different cultures in the adaptation to similar environments and adoption of differing or the same economic strategies.

In this Chapter, firstly, the two case studies—Obishir-1 and Obishir-5—are compared, eventually discussing results obtained by paleoenvironmental proxies. Subsequently, the significance of this thesis is discussed. And as final remarks, possible directions for future works are outlined.

## **7.2 Case studies at comparison**

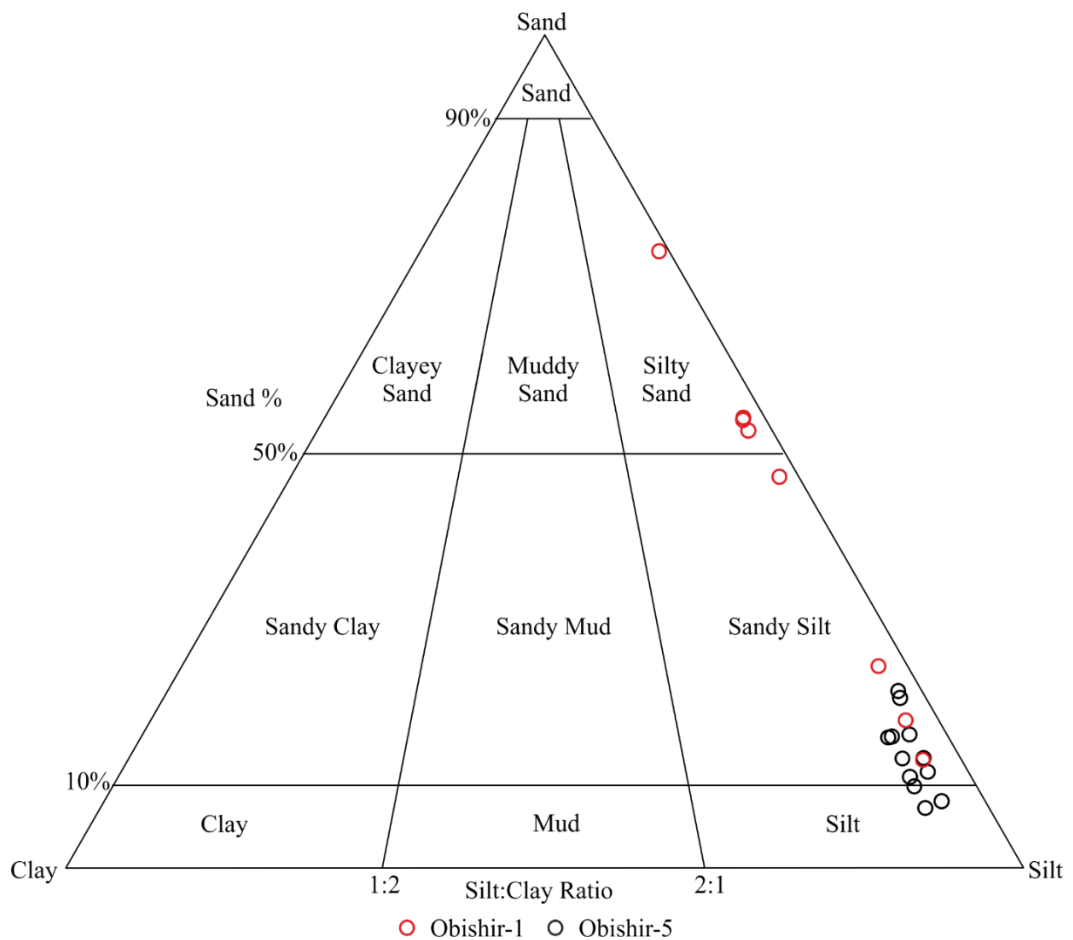
### **7.2.1 The Obishirian sites at comparison**

The scientific articles included in this thesis provide a reasonable account of the site formation histories at both Obishirian locations. Obishir-1 and Obishir-5 share a similar geomorphological setting (see **Figure 3-2**, Chapter 3.1), they are located in front of a rockshelter, facing the Obishir stream and embedded in talus deposits, and situated approximately 400 m apart. Obishir-1 yields EPP and Obishirian assemblages, while Obishir-5 contains EPP, Obishirian, and Bronze Age and Middle Ages assemblages.

Concerning macroscopic characteristics at both sites, Obishir-5 site is characterized by a greater area that opens in front of the rockshelter and has a more direct access to the Obishir river. At both sites, the sedimentary units were classified as diamictons, have fairly visible boundaries, predominantly massive structure, and weakly visible alignments of cobbles and boulders. Differences are to be found in the coloration of layers, and internal structure between the two locations. For instance, SU2 (yielding the Obishirian assemblage) at Obishir-5 has a complex structure, a similar unit was not observed at Obishir-1 (**Figure 6-2**, Chapter 6.2). At Obishir-1, the presence of an erosional surface was observed between SU6 and SU5, such a similar structure was not observed at Obishir-5. The Bronze Age and Middle Ages SU1 unit present at Obishir-5, at Obishir-1 is missing, perhaps disturbed by Soviet campaigns or more likely neglected.

Overall, at both sites, sediments exhibit a bimodal pattern with the presence of very coarse and fine sedimentary particles, typical of colluvial facies in particular taluses. The difference lies in the grain size of the fine fraction. The fine sediments for all units at Obishir-5 are much more homogeneous and clustered around the lower portion of the ternary plot showed in **Figure 7-1**, whereas those at Obishir-1 are stretched instead of being clustered. This difference was interpreted as possibly due to a higher rate of homogenization of the sedimentary material at Obishir-5 (Brancaleoni *et al.*, submitted) perhaps connected with post-depositional reworking such as bioturbation.

At Obishir-5, except for the identification of macroscopic stratigraphic units and several subunits yielding the Obishirian, the material is predominantly reworked. According to this study, it is challenging to identify minor phases of occupation within the Obishirian or recognize the original arrangement of the archaeological record. This difficulty hampers a proper recognition of functions at the site.

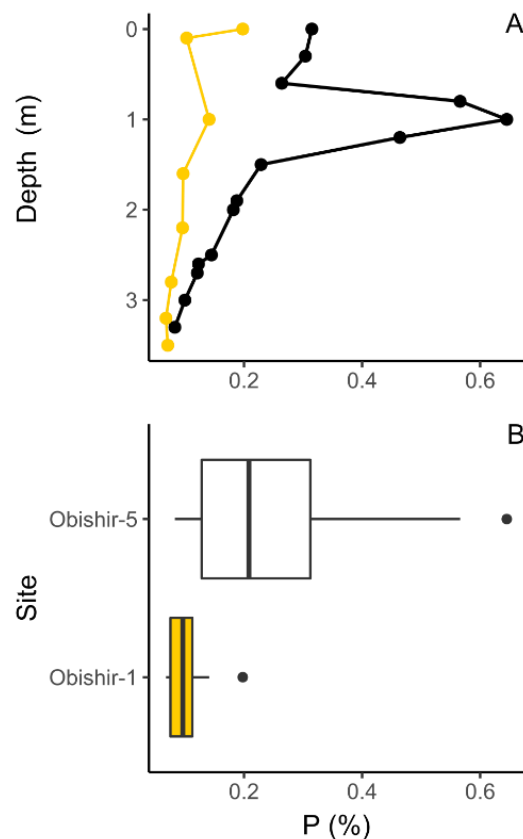


**Figure 7-1** Ternary plot after grain size analysis for the fine fraction < 2 mm from Obishir-1 and Obishir-5

Geochemically, at both sites sediments are rich in carbonates and low in organic matter content (Brancaleoni *et al.*, 2022, submitted). However, a distinction can be drawn regarding P



concentration in the sediments. Typical sources of P are bone fragments, dead plant, animal residues and droppings. At Obishir-5, P concentration reaches its peak at the top of SU2 around 1 m below the ground surface. Having a peak at this depth rules out the sole action of modern input at the site. Therefore, top of SU2 likely coincides with a former surface (see **Figure 7-2**)(Brancaleoni *et al.*, submitted) where soil formation also possibly occurred given the trend observed for other geochemical elements such as Al, Ca (the reader is refer to Fig.4 in Brancaleoni *et al.*, submitted; *Appendix C – Scientific paper 3*). On the other hand, the profile at Obishir-1 does not show such a pronounced trend (**Figure 7-2**). At Obishir-5, the paleosol has been identified just at the top of SU2 (top of the Obishirian bearing unit), and not within the unit itself. This indicates either a rapid deposition rate of SU2, or subsequent reworking, followed by a stabilization phase, that facilitated soil formation. Both explanations contribute to the conclusion of homogeneity, as indicated by grain size analysis.



**Figure 7-2** Phosphorus profiles at the selected locations. **a)** Phosphorous profiles at Obishir-1 (in yellow) and Obishir-5 (in black); **b)** Boxplot showing the P mean values for Obishir-1 and Obishir-5.

Micromorphology provided an in-depth study of characteristics at the sites (Brancaleoni *et al.*, 2022, submitted). At Obishir-1, the Obishirian assemblage was retrieved from SU4. Micromorphological observations did not point to any anthropogenic input within this unit.

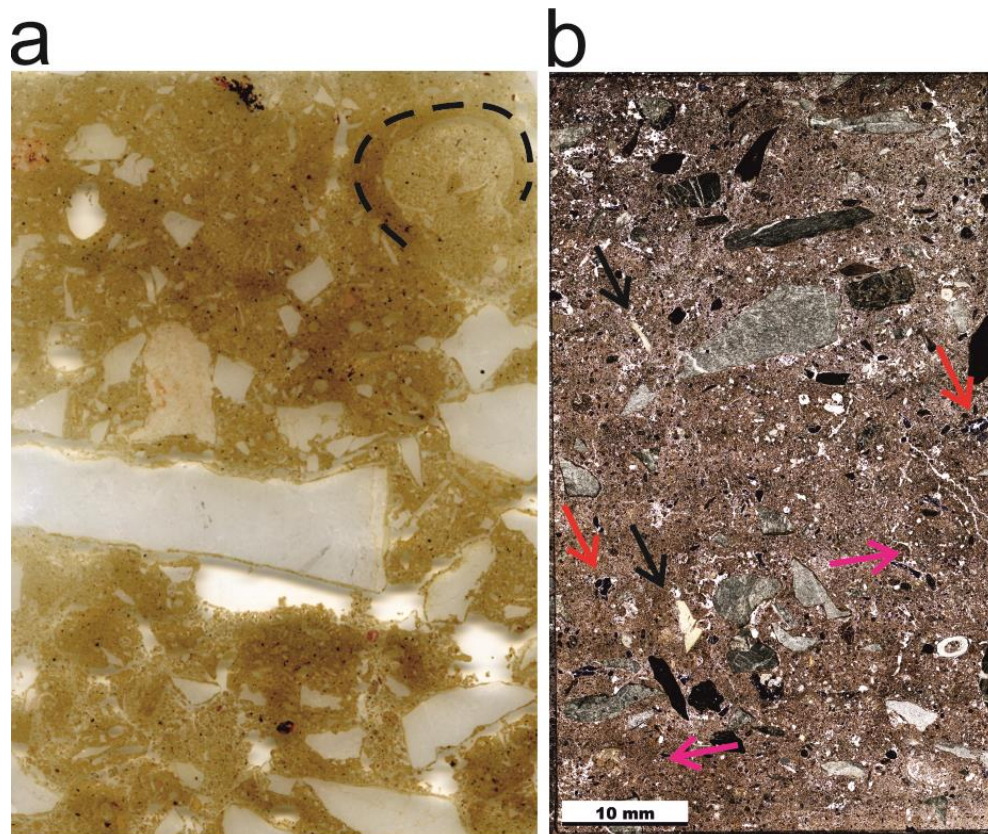
Micro-features pointed out a melioration of the climatic conditions, in line also with the mollusk assemblage analysis. This might lead to the conclusion that the Obishirian culture at Obishir-1 is not well-preserved in the sedimentary record, perhaps due to reworking processes or more likely to a different use of that specific area at the site (**Figure 7-3a**).

On the contrary, at Obishir-5, elements related with the Obishirian culture were recorded in the sedimentary record (**Figure 7-3b**). Within sediments of SU2, there is evidence of the use of fire and the presence of livestock, this was purported by the presence of bones, fire by-products (charcoals, char material and ash), and herbivore dung pellets (Brancaleoni et al., submitted). The use of livestock at the site was previously tested by the application of proteomics analysis (Taylor *et al.*, 2021). The presence of herbivore dung pellets within the sedimentary record at the site provides evidence of herding, meaning that livestock, herbivores, were present alive at the site. This supports the hypothesis that the Obishirian people likely relied on herding of these animals rather than hunting them or importing meat from elsewhere.

Overall, the archaeological record of the Obishirian at both sites is poorly preserved, characterized by bioturbation, fragmentation, and significant reworking (**Figure 7-3**). For example, at Obishir 5, micro-indicators associated with firing are not in their original, intact state but rather disassembled. The same holds true for dung droppings and bones. Furthermore, their arrangement appears chaotic, indicating mixing and reworking. These observations align with the findings from grain size and geochemical analyses.

The comparison of the two sites revealed differences in land use during the Obishirian occupation. Obishir-5 yields evidence of grazing, roaming animals, and firing activity (*Appendix C – Scientific paper 3*). In contrast, Obishir-1 lacks such evidence, with limited by-products of firing and no noticeable herbivore animal dung. This distinction suggests that Obishir-1 may have served primarily as a lithic workshop or had a different functional role within the culture.

The EPP assemblages are scarce at both sites, with poor evidence recorded in the sedimentary material. At Obishir-1, the assemblage is limited, and the top of SU6 likely underwent erosion and transportation, given that an erosional surface at this stratigraphic position was identified (**Figure 6-1**, Chapter 6.2.1). The bottom part of SU6 accumulated during the LGM and shows weak traces of cold and arid conditions. At Obishir-5, evidence of large mass movement was not noted. The archaeological components within the sediments are scarce and nearly absent, preventing any strong interpretation. Micromorphological evidence, such as root-related calcite and rims around coarse rock fragments (see Supplementary material in *Appendix C – Scientific paper 3*), points toward arid conditions and low sedimentation rate for the units bearing the EPP assemblage at Obishir-5.



**Figure 7-3** Example of micromorphological thin sections from the two locations. **a)** Obishir-1, thin section MM3.1, SU4, the thin section is almost sterile, high amount of coarse limestone fragments and coarse burrows (example in dash line); **b)** Obishir-5, thin section MM3.1, SU2.2, the coloration is much darker, and there is the presence of coarse bone and charcoal fragments (black and red arrows), as well as the presence of dung pellets (pink arrow).

## 7.2.2 Local paleoenvironmental conditions

In line with the ecological interpretation proposed by Osipova *et al.* (2021) for Obishir-5, in SU4's top part, I observed rare root-related calcite, indicating xeric conditions—shrub-dominated vegetation and low moisture (Khormali, Abtahi and Stoops, 2006; Barta, 2011). The absence of clay coatings around voids along the profile suggests lack of humid conditions, ruling out significant fluctuations in humidity and temperature during the Holocene. The few dusty coatings observed in the stratigraphy may be related to turbulent water infiltration from high-intensity rainfall, common in arid and semi-arid settings (Stahlschmidt *et al.*, 2017). In addition, relic papules might have been recycled from an older “pre-Holocene” argic horizon testifying a more humid paleoclimate (mostly linked with interstadial conditions).

Analyses conducted at Obishir-1, indicated periglacial conditions during the LGM, followed by relatively moist interstadial conditions during the Late Glacial (Brancaleoni *et al.*, 2022). Unfortunately, the main excavation trench at Obishir-5 did not uncover such old sediments, preventing further data for this period. According to the data from Obishir-1 and other regional

studies (such as Heinecke *et al.*, 2017; Li *et al.*, 2020), the region experienced the onset of more humid conditions at the Pleistocene/Holocene transition (Brancaleoni *et al.*, 2022).

Obishir-5 recorded an increase in the accumulation of archaeological material (e.g., bones, charcoals and dung material in SU2 and SU3), along with leaching of P-solutions from SU2, corresponding to the Early/Middle Holocene. This period is linked to slightly warmer and wetter conditions according to Osipova *et al.* (2021), possibly leading to an overgrown of steppe grass, shrubs and single trees and increased water supply, making it suitable conditions for herding activities. The micromorphological data from Obishir-1 align with Osipova *et al.* (2021) findings, suggesting an overall increase in humidity and temperature in the study region. However, regional records and studies do not universally agree on moisture conditions (Brancaleoni *et al.*, 2022; Spate, Leipe and Motuzaitė Matuzevičiūtė, 2022).

Proxy studies from lakes in north-eastern Tajikistan and north-eastern and central Kyrgyzstan have reconstructed a phase of increasing humidity between approximately 5000 and 4000 BP (Beer, Heiri and Tinner, 2007; Heinecke *et al.*, 2018; Laug *et al.*, 2020; Leroy and Giralt, 2021; Spate, Leipe and Motuzaitė Matuzevičiūtė, 2022). However, for the same period, other records suggest contradicting moisture trends (Mathis *et al.*, 2014; Heinecke *et al.*, 2017; Spate, Leipe and Motuzaitė Matuzevičiūtė, 2022). Recent pollen data and analyses, indicate an overall drying trend between approximately 6000 and 3000 BP, followed by increasing moisture conditions after 3000 BP (Spate, Leipe and Motuzaitė Matuzevičiūtė, 2022). The period from 4000 years to the present is characterized by an overall increase in humidity, with minor drier fluctuations around 2700 and 1700 BP (Spate, Leipe and Motuzaitė Matuzevičiūtė, 2022). Furthermore, after 1500 BP, the pollen data recorded increased moisture conditions. The Middle Holocene (Northgrippian) is not fully represented in the Obishir-5 sequence either due to a halt in the accumulation of sedimentary material (geogenic and anthropogenic) or erosional processes, and eventually soil formation. The presence of herding activities in high elevated mountainous regions of Inner Asia has been interpreted as a response to overall regional aridification that probably pushed herding and hunting populations on higher elevations in search of higher moisture levels (Spate, Leipe and Motuzaitė Matuzevičiūtė, 2022).

## **7.3 Implication and significance of this thesis**

This PhD dissertation on the geoarchaeology of selected archaeological sites in CA has several significant implications and contributions to the field of archaeology and our understanding of the region's history and environment. Here are some of the key contributions and implications:

1. Obishir-1 primarily accumulated through a combination of gravity-induced processes, in situ weathering, and aeolian contributions. The sequence at Obishir 1 exhibited signs of mass movement translocation.
2. The sediments at both locations are characterized by coarse (gravel) and fine (silt) particles, at the contact clast-matrix were recognized varying processes such as mineral grain alteration, frost action, redeposition, pedogenetic processes, and anthropogenic activity. The processes affecting gravelly geogenic components and their micro-features may also reflect those impacting gravelly archaeological artifacts, such as secondary calcium carbonate accumulations
3. Obishir-5 primarily accumulated through a mix of gravity-induced processes, in situ weathering, and aeolian contributions. Additionally, the site witnessed the accumulation of archaeologically significant materials, such as charcoals, bones, and dung pellets, likely influenced by firing and potentially herding activities.
4. The Obishirian sequence at Obishir-5 (stratigraphic units: 3, 2.4, 2.3, 2.2, and 2.1) displayed evidence of post-depositional reworking. This is supported by the grain size homogeneity of fine fractions, the absence of paleosols or living floors recorded in geochemistry within the sequence, and the presence of re-working micromorphological features.
5. Obishir-5 was utilized by the Obishirian people as a stable for keeping sheep and/or goats, as indicated by the preserved herbivore dung within the sediments. In contrast, Obishir-1 lacks such evidence, exhibiting limited firing by-products and no noticeable herbivore animal dung. This distinction suggests that Obishir-1 may have primarily served as a lithic workshop or had a different functional role within the culture.
6. The Obishirian culture engaged in animal herding, as evidenced at Obishir-5. This supports the prior conclusion by Taylor *et al.* (2021) regarding the use of domestic animals' meat and provides crucial data for categorizing the Obishirian as a fully Neolithic unit.

In summary, this dissertation contributes to the growing body of knowledge about CA's rich archaeological history, environmental conditions, and cultural interactions. It highlights the need for continued research, interdisciplinary collaboration, and the preservation of these valuable archaeological sites. The study challenges previous assumptions about the Obishirian culture, originally thought to be an Epipaleolithic culture. Thanks to the evidence presented in this study, it suggests that the Obishirian culture is more likely an early Neolithic culture relying on herding

activities. This reevaluation has broad implications for understanding the cultural and economic history of CA. The study also provides valuable insights into the environmental conditions at the sites. It suggests that the high mountains of CA might have served as refuges during adverse environmental conditions, providing water and vegetation resources for herding. This understanding of past environmental dynamics can inform broader discussions of human-environment interactions in the region. The application of a multi-aspect approach highlights the advantages and disadvantages of certain techniques in the Central Asian context. For example, the study underscores the importance of micro-analytical methods and suggests the application of biomarkers in future research, especially given the central role of domesticated animals in the Obishirian culture. The study exemplifies the benefits of interdisciplinary collaboration between researchers from different fields. This collaboration contributed to a more comprehensive understanding of the archaeology and history of the studied sites.

CA has a rich history as a crossroads for different civilizations, where trade and cultural exchange likely occurred. Although not the primary focus, this study hints at the movement of people, goods, and ideas. It sets the stage for further research into the cultural interactions and exchanges that took place in the region. The study emphasizes the importance of preserving and promoting crucial archaeological sites in CA, such as Obishir-5. It also underscores the need for government policies and heritage management to protect and sustainably develop these areas, which hold significant aspects of Kyrgyzstan's identity and heritage. This study is one of the few in CA that takes into account the site formation history of archaeological sites. As such, it holds crucial importance in advancing our understanding of the region's archaeological heritage and its place in the broader context of world history.

## **7.4 Future work**

### **7.4.1 Other Obishirian sites**

So far, only two sites bearing the Obishirian culture have been analyzed with a micro-stratigraphic approach as the one shown in this thesis. But there are more Obishirian sites as illustrated in **Figure 2-5** (Chapter 2.4.3.1). A future aim is to apply similar research to all Obishirian sites. This may also include the so-called “Pre-Obishirian” sites (Aygyrzhal and Alamishik) in central Kyrgyzstan. A holistic study of all Obishirian sites would provide a comprehensive understanding of this culture, including its geographical distribution, temporal evolution, and site-specific variations. It would help create a more detailed and nuanced picture of the Obishirian phenomenon.

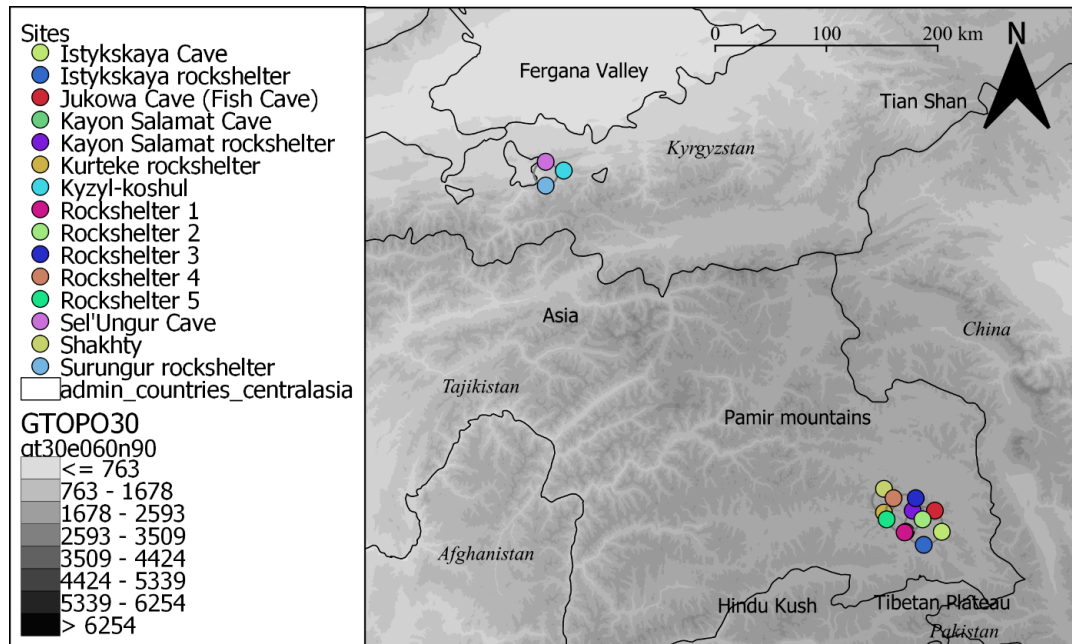
The Obishirian sites are spread in an area comprising the Fergana Valley and the Pamirs (**Figure 2-5**), therefore stretching from a basin (Fergana Valley) with average elevation of 400 m asl to high elevation plateau with average elevation of 4000 m asl. By studying Obishirian sites at different elevations, one can gain insights into how human populations adapted to varying environmental conditions. This research can shed light on the strategies employed for herding, hunting, and fishing at different altitudes, which is essential for understanding human-environment interactions. Moreover, in the area there is evidence of different cultures that inhabited the same landscape during the same period (Shnaider pers. comm.). This evidence was found at Surungur rockshelter (Dedov *et al.*, 2021; Shnaider *et al.*, 2021). Studying the Surungur site with a geoarchaeological approach might reveal similarities and differences between different cultures in the adaptation to similar environments.

#### **7.4.2 Central Asian fumiers**

Surungur archaeological site has a similar geomorphic setting to the one characterizing the Obishirian sites and similar age (Dedov *et al.*, 2021; Shnaider *et al.*, 2021). The site has revealed the presence of thick sedimentary succession resembling *fumiers*. *Fumiers* are stratified burnt and unburnt sediments, often containing burnt animal dung and vegetal remains. These deposits are typically found in karstic environments and are well-documented in the Mediterranean area, dating back to the Early Neolithic and Bronze Age (Boschian and Montagnari-Kokelj, 2000; Angelucci *et al.*, 2009; Del Valle *et al.*, 2022; Fernández-Palacios *et al.*, 2023). *Fumiers* are typically associated with herding practices and management, exhibiting complex structures with abrupt vertical and lateral changes, displaying different chromatism and often showing bedding. Due to their complexity, the study of these deposits poses challenges, making it difficult to establish a unified model for their formation. For instance, at Obishir-5, the sedimentary record revealed indications of animal stabling, and certain aspects of the sedimentary fabric bore resemblance to *fumiers* (Brancaleoni *et al.*, submitted). However, a significant distinction exists, as the sediment did not exhibit well-stratified characteristics. This raises the possibility of a degraded fumiers facies or traces of a paleo-fumier recorded in the reworked sediment. Such traces may only be traceable using in-depth methods, such as microstratigraphy.

During surveys in CA, a number of archaeological sites were explored comprising stabling facies, their locations are illustrated in **Figure 7-4**. The study of these sites, particularly Surungur, holds the potential to provide valuable evidence for early forms of herding in the region, thus shedding light on the pastoral practices that were carried out. By examining the composition of sediments, particularly the presence of fecal matter, we can provide information about the type of animals, their presence and their diet. Along with analyzing the composition and quantity of dung within sediment layers, we can make inferences about the size of the herd. And, by examining the

extent and distribution of trampled or compacted sediments and presence of foddering evidence, we can gain clues about where animals congregated and grazed. This information can be used to estimate the size and movement patterns of the herd. Moreover, the recognition of other types of sediment, such as standing water bodies, bird and/or bat guano, aeolian dust, or alluvial deposits interbedded in the *fumier* sequence can provide useful information on the frequency of site use and seasonality. These pieces of information should be considered in conjunction with other evidence and interdisciplinary approaches, such as biomarkers and isotopic composition.



**Figure 7-4** Archaeological sites with stabling facies, DEM depths are in m asl.



# **Bibliography**

Abell, J. T. *et al.* (2019) ‘Urine salts elucidate Early Neolithic animal management at Aşikli Höyük, Turkey’, *Science Advances*, 5(4). doi: 10.1126/sciadv.aaw0038.

Andreeva, T. V *et al.* (1990) ‘Genomic analysis of a novel Neanderthal from Mezmaiskaya Cave provides insights into the genetic relationships of Middle Palaeolithic populations’, (6). doi: 10.1038/s41598-022-16164-9.

Angelucci, D. E. *et al.* (2009) ‘Shepherds and karst: The use of caves and rock-shelters in the Mediterranean region during the Neolithic’, *World Archaeology*, 41(2), pp. 191–214. doi: 10.1080/00438240902843659.

Arnold, L. J., Bailey, R. M. and Tucker, G. E. (2007) ‘Statistical treatment of fluvial dose distributions from southern Colorado arroyo deposits’, *Quaternary Geochronology*. Elsevier, 2(1–4), pp. 162–167. doi: 10.1016/J.QUAGEO.2006.05.003.

Barta, G. (2011) ‘Secondary carbonates in loess-paleosol sequences: A general review’, *Central European Journal of Geosciences*, 3(2), pp. 129–146. doi: 10.2478/s13533-011-0013-7.

Beer, R., Heiri, O. and Tinner, W. (2007) ‘Vegetation history, fire history and lake development recorded for 6300 years by pollen, charcoal, loss on ignition and chironomids at a small lake in southern Kyrgyzstan (Alay Range, Central Asia)’, *Holocene*, 17(7), pp. 977–985. doi: 10.1177/0959683607082413.

Beeton, T. A. *et al.* (2014) ‘The fundamental hominin niche in late Pleistocene Central Asia: A preliminary refugium model’, *Journal of Biogeography*, 41(1), pp. 95–110. doi: 10.1111/jbi.12183.

Berna, F. *et al.* (2007) ‘Sediments exposed to high temperatures: reconstructing pyrotechnological processes in Late Bronze and Iron Age Strata at Tel Dor (Israel)’, *Journal of Archaeological Science*. Academic Press, 34(3), pp. 358–373. doi: 10.1016/J.JAS.2006.05.011.

Berna, F. (2017) ‘FTIR Microscopy’, in Nicosia, C. and Stoops, G. (eds) *Archaeological Soil and Sediment Micromorphology*. First. John Wiley & Sons Ltd., pp. 411–415.

Berthold, C. and Mentzer, S. M. (2017) ‘X-ray Microdiffraction’, in Nicosia, C. and Stoops, G. (eds) *Archaeological Soil and Sediment Micromorphology*. First. John Wiley & Sons Ltd., pp. 417–429.

Bertran, P. *et al.* (1997) ‘Fabric characteristics of subaerial slope deposits’, *Sedimentology*, 44(1), pp. 1–16. doi: 10.1111/j.1365-3091.1997.tb00421.x.

Bertran, P. and Texier, J. P. (1999) 'Facies and microfacies of slope deposits', *Catena*, 35(2–4), pp. 99–121. doi: 10.1016/S0341-8162(98)00096-4.

Blott, S. J. and Pye, K. (2001) 'GRADISTAT: A GRAIN SIZE DISTRIBUTION AND STATISTICS PACKAGE FOR THE ANALYSIS OF UNCONSOLIDATED SEDIMENTS', 26, pp. 1237–1248. doi: 10.1002/esp.261.

Boschian, G. and Montagnari-Kokelj, E. (2000) 'Prehistoric Shepherds and Caves in the Trieste Karst (Northeastern Italy)', *Geoarchaeology - An International Journal*, 15(4), pp. 331–371. doi: 10.1002/(SICI)1520-6548(200004)15:4<331::AID-GEA3>3.0.CO;2-H.

Brancaleoni, G. *et al.* (2022) 'Depositional history of a talus cone in an arid intermontane basin in Central Asia: An interdisciplinary study at the Late Pleistocene–Late Holocene Obishir-I site, Kyrgyzstan', *Geoarchaeology*. John Wiley and Sons Inc, 37(2), pp. 350–373. doi: 10.1002/gea.21892.

Brancaleoni, G. *et al.* (2023) 'A closer look at clasts and groundmass: Micromorphological features in sediments with archaeological significance in Obishir and Katta Sai complexes (Central Asia)', *Journal of Archaeological Science: Reports*. Elsevier, 51, p. 104118. doi: 10.1016/j.jasrep.2023.104118.

Brancaleoni, G. *et al.* (submitted) 'Geoarchaeological approach for tackling the function and preservation state of the Obishir-5 site, the earliest Neolithic site in the Fergana Valley'.

Branch, N. (2015) *Environmental Archaeology*. Second Edi, *International Encyclopedia of the Social & Behavioral Sciences: Second Edition*. Second Edi. Elsevier. doi: 10.1016/B978-0-08-097086-8.13031-4.

Brönnimann, D. *et al.* (2017) 'Excrements of Herbivores', *Archaeological Soil and Sediment Micromorphology*. John Wiley & Sons, Ltd, pp. 55–65. doi: 10.1002/9781118941065.CH6.

Brunet, F. (2012) 'The technique of pressure knapping in Central Asia: Innovation or diffusion?', *The Emergence of Pressure Blade Making: From Origin to Modern Experimentation*, 9781461420(May), pp. 307–328. doi: 10.1007/978-1-4614-2003-3\_12.

Brunet, F. (2021) 'The Neolithisation of Central Asia : Emergence of cultural identities and long-distance networks'. Brepols Publishers, pp. 43–60. Available at: <https://halshs.archives-ouvertes.fr/halshs-03096327> (Accessed: 24 October 2022).

Brunet, M. F., Sobel, E. R. and Mccann, T. (2017) 'Geological evolution of Central Asian Basins and the western Tien Shan Range', *Geological Society Special Publication*, 427(1), pp. 1–17. doi: 10.1144/SP427.17.

Bullock, P. *et al.* (1985) 'Handbook for soil thin section description.', *Handbook for soil thin section description*. Waine Research.

Byers, S. C., Mills, E. L. and Stewart, P. L. (1978) 'A comparison of methods of determining organic carbon in marine sediments, with suggestions for a standard method', *Hydrobiologia*, 58(1), pp. 43–47. doi: 10.1007/BF00018894.

Canti, M. and Huisman, D. J. (2015) 'Scientific advances in geoarchaeology during the last twenty years', *Journal of Archaeological Science*. Academic Press, 56, pp. 96–108. doi: 10.1016/J.JAS.2015.02.024.

de Caritat, P. *et al.* (2022) 'P A P E R Forensic soil provenancing in an urban/suburban setting: A simultaneous multivariate approach', *J Forensic Sci*, 67, pp. 927–935. doi: 10.1111/1556-4029.14967.

Casteel, R. W. (1972) 'Some biases in the recovery of archaeological faunal remains', *Proceedings of the Prehistoric Society*, 38(May 2014), pp. 382–388. doi: 10.1017/S0079497X00012172.

Comas, D. *et al.* (1998) 'Trading genes along the silk road: mtDNA sequences and the origin of central Asian populations', *American Journal of Human Genetics*, 63(6), pp. 1824–1838. doi: 10.1086/302133.

Cooke, R., Warren, A. and Goudie, A. (1993) *Desert Geomorphology*. London: UCL Press.

Courty, M. A., Goldberg, P. and Macphail, R. I. (1989) *Soils and Micromorphology in Archaeology*. Cambridge: Cambridge University Press.

Cowan, P. J. (2007) 'Geographic usage of the terms Middle Asia and Central Asia', *Journal of Arid Environments*, 69(2), pp. 359–363. doi: 10.1016/j.jaridenv.2006.09.013.

Cuthbertson, P. *et al.* (2021) 'Finding karstic caves and rockshelters in the Inner Asian mountain corridor using predictive modelling and field survey'. doi: 10.1371/journal.pone.0245170.

Davis, R. S. and Ranov, V. A. (1999) 'Recent work on the paleolithic of Central Asia', *Evolutionary Anthropology*, 8(5), pp. 186–193. doi: 10.1002/(SICI)1520-6505(1999)8:5<186::AID-EVAN6>3.0.CO;2-R.

Dedov, I. E. *et al.* (2021) 'Multidisciplinary Study of Burnt Deposits at Surungur, Fergana Valley, Southern Kyrgyzstan', *Archaeology, Ethnology and Anthropology of Eurasia*, 49(4), pp. 24–36. doi: 10.17746/1563-0110.2021.49.4.024-036.

Dincauze, D. F. (2000) 'Environmental Archaeology: Principles and Practice'. Cambridge

University Press. doi: 10.1017/CBO9780511607837.

Dlussky, K. G. (2009) 'Loess Deposits', *Encyclopedia of Earth Sciences Series*. Springer, Dordrecht, pp. 522–524. doi: 10.1007/978-1-4020-4411-3\_130.

Dodonov, A. E. (1991) 'Loess of Central Asia', *GeoJournal*, 24(2), pp. 185–194. doi: 10.1007/BF00186015.

Duller, G. A. T. (2008) 'Single-grain optical dating of Quaternary sediments: Why aliquot size matters in luminescence dating', *Boreas*, 37(4), pp. 589–612. doi: 10.1111/J.1502-3885.2008.00051.X.

Égüez, N. *et al.* (2020) 'A pilot geo-ethnoarchaeological study of dung deposits from pastoral rock shelters in the Monti Sibillini (central Italy)', *Archaeological and Anthropological Sciences*. Springer Science and Business Media Deutschland GmbH, 12(6). doi: 10.1007/S12520-020-01076-4.

Falster, G., Delean, S. and Tyler, J. (2018) 'Hydrogen Peroxide Treatment of Natural Lake Sediment Prior to Carbon and Oxygen Stable Isotope Analysis of Calcium Carbonate', *Geochemistry, Geophysics, Geosystems*, 19(9), pp. 3583–3595. doi: 10.1029/2018GC007575.

Feathers, J. (2008) 'LUMINESCENCE DATING', *Encyclopedia of Archaeology*. Academic Press, pp. 1590–1592. doi: 10.1016/B978-012373962-9.00306-X.

Fedorchenko, A. Y. *et al.* (2018) 'Personal ornament production technology in the early holocene complexes of western central Asia: Insights from Obishir-5', *Archaeology, Ethnology and Anthropology of Eurasia*, 46(1), pp. 3–15. doi: 10.17746/1563-0110.2018.46.1.003-015.

Fernandes, M. and Krull, E. (2008) 'How does acid treatment to remove carbonates affect the isotopic and elemental composition of soils and sediments?', *Environmental Chemistry*, 5(1), pp. 33–39. doi: 10.1071/EN07070.

Fernández-Palacios, E. *et al.* (2023) 'Reconstructing formation processes at the Canary Islands indigenous site of Belmaco Cave (La Palma, Spain) through a multiproxy geoarchaeological approach', *Geoarchaeology*. doi: 10.1002/gea.21972.

Finestone, E. M. *et al.* (2022) 'Paleolithic occupation of arid Central Asia in the Middle Pleistocene', *PLoS ONE*, 17(10 October). doi: 10.1371/journal.pone.0273984.

Fitzsimmons, K. E. *et al.* (2020) 'Thinking Outside the Box at Open-Air Archeological Contexts: Examples From Loess Landscapes in Southeast Romania', *Frontiers in Earth Science*, 8. doi: 10.3389/feart.2020.561207.

Folk, R. L. and Ward, W. C. (1957) 'Brazos River bar [Texas]; a study in the significance

of grain size parameters', *Journal of Sedimentary Research*. Society for Sedimentary Geology, 27(1), pp. 3–26. doi: 10.1306/74D70646-2B21-11D7-8648000102C1865D.

Frachetti, M. D. *et al.* (2017) 'Nomadic ecology shaped the highland geography of Asia's Silk Roads', *Nature Publishing Group*. doi: 10.1038/nature21696.

French, C. (2019) *A Handbook of Geoarchaeological Approaches to Settlement Sites and Landscapes*, *A Handbook of Geoarchaeological Approaches to Settlement Sites and Landscapes*. Oxford: Oxbow Books. doi: 10.2307/j.ctvh1dthr.

Friedman, G. M. (1979) 'Differences in size distributions of populations of particles among sands of various origins: addendum to IAS Presidential Address', *Sedimentology*, 26(6), pp. 859–862. doi: 10.1111/j.1365-3091.1979.tb00979.x.

Friendly, M. (2002) 'Corrgrams: Exploratory displays for correlation matrices', *The American Statistician*, 56, pp. 316–324.

Friesem, D. E. (2016) 'Geo-ethnoarchaeology in action', *Journal of Archaeological Science*. Academic Press, 70, pp. 145–157. doi: 10.1016/J.JAS.2016.05.004.

Fu, Q. *et al.* (2014) 'Genome sequence of a 45,000-year-old modern human from western Siberia', *Nature*, 514(7253), pp. 445–449. doi: 10.1038/nature13810.

Gaffey, S. J. and Bronnimann, C. E. (1993) 'Effects of bleaching on organic and mineral phases in biogenic carbonates', *Journal of Sedimentary Petrology*, 63(4), pp. 752–754. doi: 10.1306/d4267be0-2b26-11d7-8648000102c1865d.

Gaydarska, B. (2014) 'Spatial Analysis in Field Archaeology', *Encyclopedia of Global Archaeology*. Edited by C. Smith. New York, NY: Springer New York. doi: 10.1007/978-1-4419-0465-2\_219.

Ghasidianid, E. *et al.* (2023) 'Modelling Neanderthals' dispersal routes from Caucasus towards east'. doi: 10.1371/journal.pone.0281978.

Goehner, R. P. and Nichols, M. C. (1986) 'X-Ray Powder Diffraction', *Materials Characterization*. Edited by R. E. Whan. ASM International, p. 0. doi: 10.31399/asm.hb.v10.a0001757.

Goldberg, P. *et al.* (2009) 'Bedding, hearths, and site maintenance in the Middle Stone Age of Sibudu Cave, KwaZulu-Natal, South Africa', *Archaeological and Anthropological Sciences*, 1(2), pp. 95–122. doi: 10.1007/s12520-009-0008-1.

Goldberg, P. and Aldeias, V. (2018) 'Why does (archaeological) micromorphology have such little traction in (geo)archaeology?', *Archaeological and Anthropological Sciences*.

Archaeological and Anthropological Sciences, 10(2), pp. 269–278. doi: 10.1007/s12520-016-0353-9.

Goldberg, P. and Berna, F. (2010) ‘Micromorphology and context’, *Quaternary International*. Pergamon, 214(1–2), pp. 56–62. doi: 10.1016/J.QUAINT.2009.10.023.

Goldberg, P. and Macphail, R. I. (2006) *Practical and Theoretical Geoarchaeology*. Malden, MA USA: Blackwell Publishing Ltd. doi: 10.1002/9781118688182.

Goldberg, P., Miller, C. E. and Mentzer, S. M. (2017) ‘Recognizing fire in the paleolithic archaeological record’, *Current Anthropology*, 58, pp. S175–S190. doi: 10.1086/692729.

Goldstein, J. I. *et al.* (2017) *Scanning electron microscopy and x-ray microanalysis, Scanning Electron Microscopy and X-ray Microanalysis*. doi: 10.1007/978-1-4939-6676-9.

Gorbunov, A. P. and Seversky, E. V. (1999) ‘Solifluction in the mountains of Central Asia: Distribution, morphology, processes’, *Permafrost and Periglacial Processes*, 10(1), pp. 81–89. doi: 10.1002/(SICI)1099-1530(199901/03)10:1<81::AID-PPP307>3.0.CO;2-3.

Grayson, D. K. (1973) ‘Methodology of Faunal Analysis’, *American Antiquity*, 39(4), pp. 432–439.

Hamon, C. and Manen, C. (2021) ‘The Mechanisms of Neolithisation of Western Europe: Beyond a South/North Approach’, *Open Archaeology*. De Gruyter Open Ltd, 7(1), pp. 718–735. doi: 10.1515/opar-2020-0164.

Hassan, F. A. (1974) ‘Sediments in archaeology’, *Nature*, 247(5439), p. 256. doi: 10.1038/247256a0.

Heinecke, L. *et al.* (2017) ‘Climatic and limnological changes at Lake Karakul (Tajikistan) during the last ~29 cal ka’, *Journal of Paleolimnology*. Springer Netherlands, 58(3), pp. 317–334. doi: 10.1007/s10933-017-9980-0.

Heinecke, L. *et al.* (2018) ‘Vegetation change in the eastern Pamir Mountains, Tajikistan, inferred from Lake Karakul pollen spectra of the last 28 kyr’, *Palaeogeography, Palaeoclimatology, Palaeoecology*, 511, pp. 232–242. doi: 10.1016/j.palaeo.2018.08.010.

Hewitt, K. (2002) *Postglacial Landform and Sediment Associations in a Landslide-Fragmented River System: The Transhimalayan Indus Streams, Central Asia*. doi: 10.1007/978-94-017-2037-3\_4.

Hnylko, O. *et al.* (2019) ‘A late carboniferous olistostrome at the front of the Southern Tian Shan nappes (Kadamzhai and Khaidarkan deposits, Kyrgyzstan)’, *Geological Quarterly*, 63(2), pp. 407–423. doi: 10.7306/gq.1478.

Holliday, V. T. and Gartner, W. G. (2007) 'Methods of soil P analysis in archaeology', *Journal of Archaeological Science*. Academic Press, 34(2), pp. 301–333. doi: 10.1016/J.JAS.2006.05.004.

Hughen, K. *et al.* (2004) '14C Activity and Global Carbon Cycle Changes over the Past 50,000 Years', *Science*, 303(January), pp. 202–207. doi: 10.1126/science.1090300.

Iovita, R. *et al.* (2020) 'In search of a Paleolithic Silk Road in Kazakhstan', *Quaternary International*. Elsevier Ltd, 559, pp. 119–132. doi: 10.1016/j.quaint.2020.02.023.

Islamov, U. I. (1972) 'Mesoliticheskie pamyatniki Ferganskoy doliny', *Istoriya materialnoy kultury Uzbekistana*, (9), pp. 21–28.

Islamov, U. I. (1980) *Obishirskaya kultura (Obishir culture)*. Tashkent: Tashkent: Phan.

Jananee, B., Thangam, V. and Rajalakshmi, A. (2021) 'Investigation of soils by thermal and spectroscopic analysis', *Chemical Engineering Communications*. Taylor & Francis, 208(6), pp. 812–821. doi: 10.1080/00986445.2019.1680370.

Karkanias, P. *et al.* (1999) 'Mineral assemblages in Theopetra, Greece: A framework for understanding diagenesis in a prehistoric cave', *Journal of Archaeological Science*. Academic Press, 26(9), pp. 1171–1180. doi: 10.1006/jasc.1998.0354.

Karkanias, P. *et al.* (2002) 'Ash bones and guano: A study of the minerals and phytoliths in the sediments of Grotte XVI, Dordogne, France', *Journal of Archaeological Science*. Academic Press, 29(7), pp. 721–732. doi: 10.1006/jasc.2001.0742.

Karkanias, P. and Goldberg, P. (2018) *Reconstructing Archaeological Sites, Reconstructing Archaeological Sites*. Wiley-Blackwell. doi: 10.1002/9781119016427.

Kasymov, M. R. (1972) 'Resultaty archeologicheskikh rabot d doline reki Sokh v 1966-1967 gg', *Istoriya materialnoy kultury Uzbekistana*, (9), pp. 16–20.

Khormali, F., Abtahi, A. and Stoops, G. (2006) 'Micromorphology of calcitic features in highly calcareous soils of Fars Province, Southern Iran', *Geoderma*, 132(1–2), pp. 31–46. doi: 10.1016/j.geoderma.2005.04.024.

Kielhofer, J. *et al.* (2020) 'The micromorphology of loess-paleosol sequences in central Alaska: A new perspective on soil formation and landscape evolution since the Late Glacial period (c. 16,000 cal yr BP to present)', *Geoarchaeology*, 35(5), pp. 701–728. doi: 10.1002/gea.21807.

Kolobova, K. A. *et al.* (2013a) 'The Kulbulak bladelet tradition in the upper paleolithic of central asia', *Archaeology, Ethnology and Anthropology of Eurasia*. No longer published by

Elsevier, 41(2), pp. 2–25. doi: 10.1016/j.aeae.2013.11.002.

Kolobova, K. A. *et al.* (2013b) ‘The Kulbulak bladelet tradition in the upper paleolithic of central asia’, *Archaeology, Ethnology and Anthropology of Eurasia*. Elsevier Srl, 41(2), pp. 2–25. doi: 10.1016/j.aeae.2013.11.002.

Konert, M. and Vandenberghe, J. (1997) ‘Comparison of laser grain size analysis with pipette and sieve analysis: a solution for the underestimation of the clay fraction’, *Sedimentology*. John Wiley & Sons, Ltd, 44(3), pp. 523–535. doi: 10.1046/J.1365-3091.1997.D01-38.X.

Kot, M. *et al.* (in press) ‘New data for asymmetric core reduction in western Tian Shan piedmonts: Ertash Sai 2 open-air site.’, *Lithic Technology*.

Krajcarz, M. T. *et al.* (2016) ‘Middle Paleolithic sites of Katta Sai in western Tian Shan piedmont, Central Asiatic loess zone: Geoarchaeological investigation of the site formation and the integrity of the lithic assemblages’, *Quaternary International*, 399, pp. 136–150. doi: 10.1016/j.quaint.2015.07.051.

Krajcarz, M. T. *et al.* (2020) *Shelter in Smoleń III - A unique example of stratified Holocene clastic cave sediments in Central Europe, a lithostratigraphic stratotype and a record of regional paleoecology*, *PLoS ONE*. doi: 10.1371/journal.pone.0228546.

Krap, T. *et al.* (2017) ‘Luminescence of thermally altered human skeletal remains’, *International Journal of Legal Medicine*, 131(4), pp. 1165–1177. doi: 10.1007/s00414-017-1546-1.

Krause-Kyora, B. *et al.* (2013) ‘Use of domesticated pigs by Mesolithic hunter-gatherers in northwestern Europe’, *Nature Communications*, 4. doi: 10.1038/ncomms3348.

Krause, J. *et al.* (2007) ‘Neanderthals in central Asia and Siberia’, *Nature* 2007 449:7164. Nature Publishing Group, 449(7164), pp. 902–904. doi: 10.1038/nature06193.

Krivoshapkin, A. *et al.* (2020) ‘Middle Paleolithic variability in Central Asia: Lithic assemblage of Sel’Ungur cave’, *Quaternary International*. Elsevier, 535(August), pp. 88–103. doi: 10.1016/j.quaint.2018.09.051.

Lambrecht, G. and Mallol, C. (2020) ‘Autofluorescence of experimentally heated bone: Potential archaeological applications and relevance for estimating degree of burning’, *Journal of Archaeological Science: Reports*. Elsevier Ltd, 31. doi: 10.1016/J.JASREP.2020.102333.

Lancaster, N. (2020) ‘On the formation of desert loess’, *Quaternary Research*. Cambridge University Press, 96, pp. 105–122. doi: 10.1017/QUA.2020.33.

Laug, A. *et al.* (2020) ‘Ecosystem shifts at two mid-Holocene tipping points in the alpine



Lake Son Kol (Kyrgyzstan, Central Asia)', *Holocene*, 30(10), pp. 1410–1419. doi: 10.1177/0959683620932973.

Leroy, S. A. G. and Giralt, S. R. (2021) 'Humid and cold periods in the last 5600 years in Arid Central Asia revealed by palynology of *Picea schrenkiana* from Issyk-Kul', *Holocene*, 31(3), pp. 380–391. doi: 10.1177/0959683620972776.

Li, Y. *et al.* (2020) 'Moisture evolution in Central Asia since 26 ka: Insights from a Kyrgyz loess section, Western Tian Shan', *Quaternary Science Reviews*. Elsevier Ltd, 249, p. 106604. doi: 10.1016/j.quascirev.2020.106604.

Lioubimtseva, E. and Henebry, G. M. (2009) 'Climate and environmental change in arid Central Asia: Impacts, vulnerability, and adaptations', *Journal of Arid Environments*. Elsevier Ltd, 73(11), pp. 963–977. doi: 10.1016/j.jaridenv.2009.04.022.

Loftus, E., Rogers, K. and Lee-Thorp, J. (2015) 'A simple method to establish calcite: Aragonite ratios in archaeological mollusc shells', *Journal of Quaternary Science*, 30(8), pp. 731–735. doi: 10.1002/jqs.2819.

Macphail, R. I. *et al.* (1997) 'The soil micromorphological evidence of domestic occupation and stabling activities', *Memorie dell'Istituto Italiano di Paleontologia Umana*, V, pp. 53–88.

Macphail, R. I. and Goldberg, P. (2017) *Applied soils and micromorphology in archaeology*, *Applied Soils and Micromorphology in Archaeology*. Cambridge University Press. doi: 10.1017/9780511895562.

Mallol, C. and Goldberg, P. (2017) 'Cave and Rock Shelter Sediments', in *Archaeological Soil and Sediment Micromorphology*. John Wiley & Sons, Ltd, pp. 359–381. doi: 10.1002/9781118941065.ch34.

Mallol, C., Mentzer, S. M. and Wrinn, P. J. (2009) 'A micromorphological and mineralogical study of site formation processes at the Late Pleistocene site of Obi-Rakhmat, Uzbekistan', *Geoarchaeology*. John Wiley and Sons Inc., 24(5), pp. 548–575. doi: 10.1002/GEA.20280/FORMAT/PDF.

March, Ramiro Javier *et al.* (2014) 'Processes of Formation and Alteration of Archaeological Fire Structures: Complexity Viewed in the Light of Experimental Approaches', *J Archaeol Method Theory*, 21, pp. 1–45. doi: 10.1007/s10816-012-9134-7.

Matejovic, I. (1993) 'Determination of Carbon, Hydrogen, and Nitrogen in Soils by Automated Elemental Analysis (Dry Combustion Method)', *Communications in Soil Science and Plant Analysis*, 24(17–18), pp. 2213–2222. doi: 10.1080/00103629309368950.

Mathis, M. *et al.* (2014) 'Regional vegetation patterns at lake Son Kul reveal Holocene climatic variability in central Tien Shan (Kyrgyzstan, Central Asia)', *Quaternary Science Reviews*, 89, pp. 169–185. doi: 10.1016/j.quascirev.2014.01.023.

Matthews, W. *et al.* (1997) 'Microstratigraphic traces of site formation processes and human activities', *World Archaeology*, 29(2), pp. 281–308. doi: 10.1080/00438243.1997.9980378.

McAdams, C. (2020) *The Pleistocene geoarchaeology and geochronology of Con Moong Cave, North Vietnam: Site formation processes and hominin activity in the humid tropics*. University of Wollongong (UOW).

Mcpherron, S. P. (2018) 'Additional statistical and graphical methods for analyzing site formation processes using artifact orientations'. doi: 10.1371/journal.pone.0190195.

Mentzer, S. M. (2014) 'Microarchaeological Approaches to the Identification and Interpretation of Combustion Features in Prehistoric Archaeological Sites', *Journal of Archaeological Method and Theory*, 21(3), pp. 616–668. doi: 10.1007/s10816-012-9163-2.

Mentzer, S. M. (2017) 'Rockshelter settings', *Encyclopedia of Earth Sciences Series*. Springer Netherlands. doi: 10.1007/978-1-4020-4409-0\_159.

Miller, B. A. and Juilleret, J. (2020) 'The colluvium and alluvium problem: Historical review and current state of definitions', *Earth-Science Reviews*. Elsevier, 209(July), p. 103316. doi: 10.1016/j.earscirev.2020.103316.

Miller, C. E. (2015) *A Tale of Two Swabian Caves : Geoarchaeological Investigations at Hohle Fels an Geissenkloesterle*. Tübingen: Kerns Verlag.

Moine, O. *et al.* (2002) 'Paleoclimatic Reconstruction Using Mutual Climatic Range on Terrestrial Mollusks', *Quaternary Research*. No longer published by Elsevier, 57(1), pp. 162–172. doi: 10.1006/QRES.2001.2286.

Morley, M. W. *et al.* (2019) 'Hominin and animal activities in the microstratigraphic record from Denisova Cave (Altai Mountains, Russia)', *Scientific Reports*, 9(1), pp. 1–6. doi: 10.1038/s41598-019-49930-3.

Morrissey, P., Mentzer, S. M. and Wurz, S. (2022) *A Critical Review of the Stratigraphic Context of the MSA I and II at Klasies River Main Site, South Africa*, *Journal of Paleolithic Archaeology*. Springer International Publishing. doi: 10.1007/s41982-022-00110-2.

Moska, P., Adamiec, G. and Jary, Z. (2011) 'OSL dating and lithological characteristics of loess deposits from bialy kosciól', *Geochronometria*, 38(2), pp. 162–171. doi: 10.2478/s13386-

011-0013-x.

Mücher, H., Steijn, H. van and Kwaad, F. (2010) 'Colluvial and Mass Wasting Deposits', in *Interpretation of Micromorphological Features of Soils and Regoliths*. Elsevier B.V., pp. 37–48. doi: 10.1016/B978-0-444-53156-8.00003-9.

Nasab, H. V., Clark, G. A. and Torkamandi, S. (2013) 'Late Pleistocene dispersal corridors across the Iranian Plateau: A case study from Mirak, a Middle Paleolithic site on the northern edge of the Iranian Central desert (Dasht-e Kavir)', *Quaternary International*. Pergamon, 300, pp. 267–281. doi: 10.1016/J.QUAINT.2012.11.028.

Nishiaki, Y. *et al.* (2022) 'Neolithization during the 6th millennium BCE in western Central Asia: New evidence from Kaynar Kamar Rockshelter, Hissar Mountains, Southeast Uzbekistan', *Archaeological Research in Asia*. Elsevier, 30, p. 100352. doi: 10.1016/j.ara.2022.100352.

Olenchenko, V. *et al.* (2017) 'Geoelectric Structure of the Obishir-5 Archaeological Site (Kyrgyzstan) Based on Electrotomography Data', *Teoriya i praktika arkheologicheskikh issledovaniy*, 4(4), pp. 150–157. doi: 10.14258/tpai(2017)4(20).-11.

Olszewski, D. I. (2012) 'The Zarzian in the Context of the Epipaleolithic Middle East', *Intl. J. Humanities*, 19(193), pp. 1–20.

Osipova, E. *et al.* (2021) 'Palaeoenvironmental conditions of the Palaeolithic–Neolithic transition in the Fergana Valley (Central Asia) – New data inferred from fossil molluscs in Obishir-V rockshelter (Kyrgyzstan)', *Quaternary International*. Pergamon, 605–606, pp. 287–299. doi: 10.1016/J.QUAINT.2020.11.009.

Pécsi, M. (1990) 'Loess is not just the accumulation of dust', *Quaternary International*. Pergamon, 7–8(C), pp. 1–21. doi: 10.1016/1040-6182(90)90034-2.

Phillips, S. C. *et al.* (2011) 'Improving CHN measurements in carbonate-rich marine sediments', *Limnology and Oceanography: Methods*, 9(MAY), pp. 194–203. doi: 10.4319/lom.2011.9.194.

Prudnikova, T. N. (2017) 'Ancient agriculture and paleographic characteristics of the Ubsunurskaya depression', *Geography and Natural Resources*. © Pleiades Publishing, 38(1), pp. 93–100. doi: 10.1134/S1875372817010127.

Pye, K. (1987) 'LOESS', *Aeolian Dust and Dust Deposits*. Academic Press, pp. 198–265. doi: 10.1016/B978-0-12-568690-7.50013-2.

Pye, K. (1995) 'The nature, origin and accumulation of loess', *Quaternary Science Reviews*. Pergamon, 14(7–8), pp. 653–667. doi: 10.1016/0277-3791(95)00047-X.

Ranov, V. A. and Davis, R. S. (1979) 'Toward a New Outline of the Soviet Central Asian Paleolithic', *Current Anthropology*, 20(2), pp. 249–270. doi: 10.1086/202265.

Rapp, G. and Hill, C. H. (2006) *Geoarchaeology: The Earth-Science Approach to Archaeological Interpretation*. Second. Yale University Press.

Reimer, P. J., Brown, T. A. and Reimer, R. W. (2004) 'Discussion: Reporting and calibration of post-bomb 14C data', *Radiocarbon*, 46(3), pp. 1299–1304. doi: 10.1017/S0033822200033154.

Richter, T. (2009) *Marginal Landscapes ? The Azraq Oasis and the cultural landscapes of the final Pleistocene southern Levant*. University College London.

Rowley-Conwy, P. (2011) 'Westward Ho!: The spread of agriculture from central Europe to the Atlantic', *Current Anthropology*, 52(SUPPL. 4). doi: 10.1086/658368.

Ryan, P. (2020) *Environmental and Low-Temperature Geochemistry*. Second. Middlebury, VT: Wiley-Blackwell.

Sanders, D. (2010) 'Sedimentary facies and progradational style of a Pleistocene talus-slope succession, Northern Calcareous Alps, Austria', *Sedimentary Geology*. Elsevier B.V., 228(3–4), pp. 271–283. doi: 10.1016/j.sedgeo.2010.05.002.

Sanders, D., Ostermann, M. and Kramers, J. (2009) 'Quaternary carbonate-rocky talus slope successions (Eastern Alps, Austria): Sedimentary facies and facies architecture', *Facies*, 55(3), pp. 345–373. doi: 10.1007/s10347-008-0175-z.

Sarianidi, V. (1992) 'FOOD-PRODUCING AND OTHER NEOLITHIC COMMUNITIES IN KHORASAN AND TRANSOXANIA: EASTERN IRAN SOVIET CENTRAL ASIA AND AFGHANISTAN', in Dani, A. H. and Masson, V. M. (eds) *HISTORY OF CIVILIZATIONS OF CENTRAL ASIA The dawn of civilization: earliest times to 700 B.C.* UNESCO Publishing, pp. 105–122.

Sayfullaev, B. K. (2017) 'Les nouveaux sites paléolithiques de la vallée de Ferghana', *Anthropologie (France)*. Elsevier Masson SAS, 121(4), pp. 288–299. doi: 10.1016/J.ANTHRO.2017.09.004.

Schiegl, S. *et al.* (1996) 'Ash deposits in Hayonim and Kebara caves, Israel: Macroscopic, microscopic and mineralogical observations, and their archaeological implications', *Journal of Archaeological Science*. Academic Press, 23(5), pp. 763–781. doi: 10.1006/jasc.1996.0071.

Schiffer, M. B. (1987) *Formation Processes of the Archaeological Record*. Salt Lake City: University of Utah Press. doi: 10.2307/3034040.

Selin, D. V. *et al.* (2023) ‘Новые данные по Чустской культуре Памиро - Алая (Южный Кыргызстан) New evidence for the Chust culture in the Pamiro-Alay mountains (South Kyrgyzstan)’, *Tomsk State University Journal of History*, (84), pp. 175–183. doi: 10.17223/19988613/84/22.

Serdyuk, N. V. *et al.* (2023) ‘Holocene vertebrate fauna in Fergana Valley, Kyrgyzstan, based on fossils from the Obishir-5 rock shelter’, *Geobios*. Elsevier Masson. doi: 10.1016/J.GEOBIOS.2023.01.002.

Shahack-Gross, R. (2011) ‘Herbivorous livestock dung: Formation, taphonomy, methods for identification, and archaeological significance’, *Journal of Archaeological Science*. Academic Press, 38(2), pp. 205–218. doi: 10.1016/J.JAS.2010.09.019.

Shahack-Gross, R. (2017) ‘Archaeological formation theory and geoarchaeology: State-of-the-art in 2016’, *Journal of Archaeological Science*, 79, pp. 36–43. doi: 10.1016/j.jas.2017.01.004.

Shi, L. *et al.* (2020) ‘Temporal variation of dust emissions in dust sources over Central Asia in recent decades and the climate linkages’, *Atmospheric Environment*. Pergamon, 222, p. 117176. doi: 10.1016/J.ATMOENV.2019.117176.

Shillito, L. M., Bull, I. D., *et al.* (2011) ‘Biomolecular and micromorphological analysis of suspected faecal deposits at Neolithic Çatalhöyük, Turkey’, *Journal of Archaeological Science*. Elsevier Ltd, 38(8), pp. 1869–1877. doi: 10.1016/j.jas.2011.03.031.

Shillito, L. M., Matthews, W., *et al.* (2011) ‘The microstratigraphy of middens: capturing daily routine in rubbish at Neolithic Çatalhöyük, Turkey’, *Antiquity*, 85(October 2010), pp. 1024–1038.

Shnaider, S. *et al.* (2023) ‘Occupation of highland Central Asia: New evidence from Kurteke rockshelter, Eastern Pamir’, *Archaeological Research in Asia*, 34(November 2022). doi: 10.1016/j.ara.2023.100443.

Shnaider, S. V. *et al.* (2017) ‘New investigations of the Epipalaeolithic in western Central Asia: Obishir-5’, *Antiquity*. Antiquity Publications, 91(360). doi: 10.15184/aqy.2017.213.

Shnaider, S. V. *et al.* (2019) ‘Results of Field Studies at the Obishir-5 Site in 2018–2019’, *Problems of Archaeology, Ethnography, Anthropology of Siberia and Neighboring Territories*, XXV, pp. 286–292.

Shnaider, S. V. *et al.* (2020) ‘New insights into the Epipaleolithic of western Central Asia: The Tutkaulian complex’, *Quaternary International*. Elsevier Ltd, 535, pp. 139–154. doi: 10.1016/j.quaint.2018.10.001.

Shnaider, S. V. *et al.* (2021) 'Surungur - New Early Holocene Archaeological Site in Fergana Valley', *Stratum Plus*, 25(2), pp. 319–337. doi: 10.55086/sp212319337.

Slon, V. *et al.* (2018) 'The genome of the offspring of a Neanderthal mother and a Denisovan father', *Nature*. Springer US, 561(7721), pp. 113–116. doi: 10.1038/s41586-018-0455-x.

Song, Y. *et al.* (2021) 'Preface (volume I): Quaternary paleoclimate and paleoenvironmental changes in Central Asia', *Palaeogeography, Palaeoclimatology, Palaeoecology*. Elsevier B.V., 568(February), p. 110319. doi: 10.1016/j.palaeo.2021.110319.

Spate, M., Leipe, C. and Motuzaitė Matuzevičiūtė, G. (2022) 'Reviewing the Palaeoenvironmental Record to Better Understand Long-Term Human-Environment Interaction in Inner Asia During the Late Holocene', *Frontiers in Ecology and Evolution*, 10(July). doi: 10.3389/fevo.2022.939374.

Spengler, R. N. (2014) 'Niche Dwelling vs. Niche construction: Landscape modification in the Bronze and iron ages of central Asia', *Human Ecology*, 42(6), pp. 813–821. doi: 10.1007/s10745-014-9697-x.

Stahlschmidt, M. C. *et al.* (2017) 'Site formation processes and Late Natufian domestic spaces at Baaz Rockshelter, Syria: A micromorphological perspective', *Journal of Archaeological Science: Reports*. Elsevier, 12, pp. 499–514. doi: 10.1016/j.jasrep.2017.03.009.

Stiner, M. C. *et al.* (1995) 'Differential Burning, Recrystallization, and Fragmentation of Archaeological Bone', *Journal of Archaeological Science*, 22(2), pp. 223–237. doi: 10.1006/jasc.1995.0024.

Stoops, G. (2003) *Guidelines for analysis and description of soil and regolith thin sections*. Madison, Wisconsin: Soil Science Society of America Inc.

Stoops, G. (2021) *Guidelines for Analysis and Description of Soil and Regolith Thin Sections*. Second Edi. Wiley.

Stoops, G., Marcellino, V. and Mees, F. (2010) 'Micromorphological Features and Their Relation to Processes and Classification: General Guidelines and Keys', in Stoops, G., Marcellino, V., and Mees, F. (eds) *Interpretation of Micromorphological Features of Soils and Regoliths*. 1st edn. Oxford: Elsevier, pp. 15–33.

Stoops, Georges (2017) 'Fluorescence Microscopy', in Nicosia, C. and Stoops, G. (eds) *Archaeological Soil and Sediment Micromorphology*. John Wiley & Sons, Ltd, pp. 393–398.

Strom, A. and Wang, G. (2022) 'Some Earthquake-Induced Rockslides in the Central Asia

Region'. Springer, Singapore, pp. 143–168. doi: 10.1007/978-981-19-6597-5\_6.

Stübner, K. *et al.* (2021) 'Unravelling the Pleistocene glacial history of the Pamir mountains, Central Asia', *Quaternary Science Reviews*. Elsevier Ltd, 257, p. 106857. doi: 10.1016/j.quascirev.2021.106857.

Stuiver, M., Reimer, P. J. and Braziunas, T. F. (1998) 'High-precision radiocarbon age calibration for terrestrial and marine samples', *Radiocarbon*, 40(3), pp. 1127–1151. doi: 10.1017/S0033822200019172.

Suska-Malawska, M. *et al.* (2022) 'Potential impact of Holocene climate changes on camel breeding practices of Neolithic pastoralists in the Central Asian drylands: A preliminary assessment', *Holocene*. SAGE Publications Ltd, 32(11), pp. 1132–1143. doi: 10.1177/09596836221114289/ASSET/IMAGES/LARGE/10.1177\_09596836221114289-FIG2.JPEG.

Taylor, R. E. (1997) 'Radiocarbon Dating', in Taylor, R. E. and Aitken, M. J. (eds) *Chronometric Dating in Archaeology*. New York, NY: Plenum Press, pp. 65–96.

Taylor, W. T. T. *et al.* (2020) 'Early Pastoral Economies and Herding Transitions in Eastern Eurasia', *Scientific Reports*, 10(1), p. 60516. doi: 10.1038/s41598-020-57735-y.

Taylor, W. T. T. *et al.* (2021) 'Evidence for early dispersal of domestic sheep into Central Asia', *Nature Human Behaviour*. doi: 10.1038/s41562-021-01083-y.

Turner, A. K. (1996) 'COLLUVIUM AND TALUS', in Turner, A. K. and Schuster, R. L. (eds) *Landslides : investigation and mitigation*. Washington, DC: Transportation Research Board, p. 686.

UNEP, UNITAR and Zoï E. Network (2009) *Khaidarkan Mercury: Addressing Primary Mercury Mining in Kyrgyzstan*.

Del Valle, H. *et al.* (2022) 'ATR-FTIR to distinguish Holocene fumier facies. A perspective from bone diagenesis at El Mirador cave (Sierra de Atapuerca, Spain)', *Journal of Archaeological Science*. Elsevier Inc., 141. doi: 10.1016/J.JAS.2022.105582.

Varis, A. *et al.* (2022) 'The effect of formation processes on the frequency of palaeolithic cave sites in semiarid zones: Insights from Kazakhstan', *Geoarchaeology*, 37(4), pp. 594–616. doi: 10.1002/gea.21909.

Varnes, D. (1978) 'Slope Movement Types and Processes', in Schuster, R. and Krizek, R. (eds) *Landslides, analysis and control, special report*. Washington, DC: Transportation research board, National Academy of Science, pp. 11–33.

Ventra, D., Diaz, G. C. and De boer, P. I. (2013) 'Colluvial sedimentation in a hyperarid setting (Atacama Desert, northern Chile): Geomorphic controls and stratigraphic facies variability', *Sedimentology*, 60(5), pp. 1257–1290. doi: 10.1111/sed.12029.

Verrecchia, E. P. and Trombino, L. (2021) *A Visual Atlas for Soil Micromorphologists, A Visual Atlas for Soil Micromorphologists*. doi: 10.1007/978-3-030-67806-7.

Vigne, J. D. (2015) 'Early domestication and farming: What should we know or do for a better understanding?', *Anthropozoologica*, 50(2), pp. 123–150. doi: 10.5252/az2015n2a5.

Villagran, X. S. *et al.* (2017) 'Bone and Other Skeletal Tissues', in Nicosia, C. and Stoops, G. (eds) *Archaeological Soil and Sediment Micromorphology*. First. John Wiley & Sons Ltd., pp. 11–38.

Weihrauch, C., Söder, U. and Stoddart, S. (2022) 'The identification of archaeologically interesting depths from vertical soil phosphorus prospections in geoarchaeology', *Geoderma*. Elsevier, 418, p. 115850. doi: 10.1016/j.geoderma.2022.115850.

Wu, N., Li, F. and Rousseau, D. D. (2018) 'Terrestrial mollusk records from Chinese loess sequences and changes in the East Asian monsoonal environment', *Journal of Asian Earth Sciences*. Elsevier, 155(November 2017), pp. 35–48. doi: 10.1016/j.jseas.2017.11.003.

Zavala, E. I. *et al.* (2021) 'Pleistocene sediment DNA reveals hominin and faunal turnovers at Denisova Cave', *Nature*, 595, p. 399. doi: 10.1038/s41586-021-03675-0.

Zhimin, A. (1992) 'NEOLITHIC COMMUNITIES IN EASTERN PARTS OF CENTRAL ASIA', in Dani, A. H. and Masson, V. M. (eds) *HISTORY OF CIVILIZATIONS OF CENTRAL ASIA The dawn of civilization: earliest times to 700 B.C.* UNESCO Publishing, pp. 148–162.









Zwyns, N. *et al.* (2019) 'The Northern Route for Human dispersal in Central and Northeast Asia: New evidence from the site of Tolbor-16, Mongolia', *Scientific Reports*, 9(1). doi: 10.1038/s41598-019-47972-1.



## ***Appendix A - Scientific paper 1***

Brancaleoni, G., Shnaider, S., Osipova, E., Danukalova, G., Kurbanov, R., Deput, E., Alisherkyzy, S., Abdykanova, A., & Krajcarz, M. T. (2022). Depositional history of a talus cone in an arid intermontane basin in Central Asia: An interdisciplinary study at the Late Pleistocene–Late Holocene Obishir-I site, Kyrgyzstan. *Geoarchaeology*, 37, 350–73.  
<https://doi.org/10.1002/gea.2189>

# Depositional history of a talus cone in an arid intermontane basin in Central Asia: An interdisciplinary study at the Late Pleistocene–Late Holocene Obishir-I site, Kyrgyzstan

Greta Brancaleoni<sup>1</sup>  | Svetlana Shnaider<sup>2,3</sup>  | Evgeniya Osipova<sup>4</sup>  |  
 Guzel Danukalova<sup>4</sup>  | Redzhep Kurbanov<sup>5,6</sup>  | Ewa Deput<sup>1</sup> |  
 Saltanat Alisher kyzy<sup>3</sup>  | Aida Abdykanova<sup>7</sup>  | Maciej T. Krajcarz<sup>1</sup> 

<sup>1</sup>Institute of Geological Sciences, Polish Academy of Sciences, Warszawa, Poland

<sup>2</sup>ArchaeoZOOlogy in Siberia and Central Asia—ZooSCAN, CNRS—IAET SB RAS International Research Laboratory, Novosibirsk, Russia

<sup>3</sup>Institute of Archaeology and Ethnography SB RAS, Novosibirsk, Russia

<sup>4</sup>Institute of Geology, Ufimian Federal Research Centre of Russian Academy of Sciences (RAS), Ufa, Russian Federation

<sup>5</sup>Faculty of Geography, Lomonosov Moscow State University, Moscow, Russia

<sup>6</sup>Institute of Geography, RAS, Moscow, Russia

<sup>7</sup>American University of Central Asia, Bishkek, Kyrgyzstan

## Correspondence

Greta Brancaleoni, Institute of Geological Sciences, Polish Academy of Sciences, Warszawa 00-818, Poland.  
 Email: [greta.brancaleoni@twarda.pan.pl](mailto:greta.brancaleoni@twarda.pan.pl)

## Funding information

Narodowe Centrum Nauki;  
 Russian Science Foundation;  
 Russian State Program

## Abstract

Cliff-related talus accumulations are often highly affected by post-depositional processes, and the sedimentological characteristics are poorly documented, especially in arid settings. In the southern margin of the Fergana Valley, Kyrgyzstan, the Obishir-I is an archaeological site of the Epipaleolithic Obishirian industry, located within a talus cone. Archaeological excavations have allowed us to study the internal structure, chronology, and depositional history of the cone as well as the relationship between the slope processes and the archaeological assemblage. We applied a multiproxy approach, including sedimentological studies supported by the basic geochemistry of sediments, luminescence dating, paleoecology of fossil mollusks, and archaeological analyses. The Obishir-I rockfall talus accumulated from the Last Glacial Maximum to the early part of the Middle Holocene. The talus onlaps the bedrock at the foot of a limestone cliff, and its chronology is coherent, spanning from ca. 19–8 ka B.P. The material is an unconsolidated, poorly sorted mixture of angular rock fragments accumulated by rockfall and fine-grained materials accumulated by aeolian processes, illuviation, and in situ weathering. The sequence bears an archaeological collection attributed to two settlement phases: unidentified Upper Paleolithic and the Obishirian. Both assemblages are affected by post-depositional relocation within the slope.

## KEYWORDS

Epipaleolithic, micromorphology, Obishirian, site formation, talus

Scientific editing by Vance Holliday.

This is an open access article under the terms of the Creative Commons Attribution-NonCommercial-NoDerivs License, which permits use and distribution in any medium, provided the original work is properly cited, the use is non-commercial and no modifications or adaptations are made.

© 2021 The Authors. *Geoarchaeology* published by Wiley Periodicals LLC

## 1 | INTRODUCTION

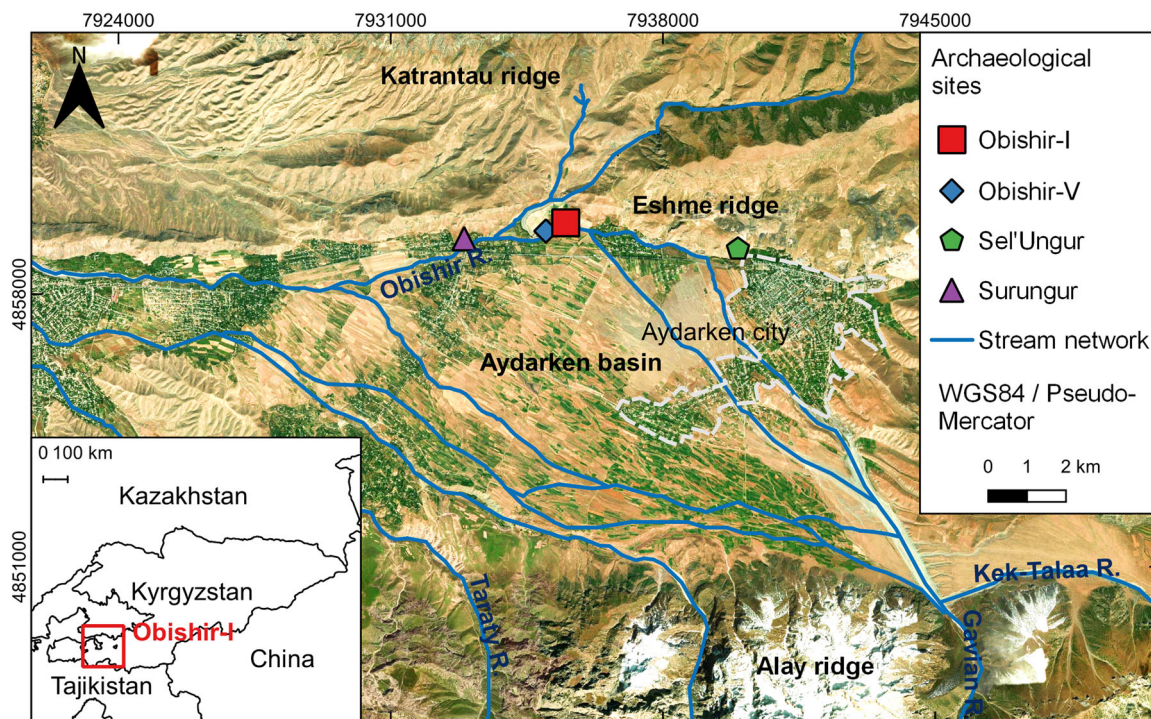
The term talus or scree generally refers to coarse-grained deposits located along and at the toe of a slope resulting from rockfall and other gravity-related processes (Turner, 1996; Ventra et al., 2013). In terrestrial environments, these are usually immature deposits, with typically unsorted and chaotic material, and angular rock fragments mixed with fine-grained material. Their commonly wedge-shaped geometry is controlled by the angle of repose of the material itself and its position relative to the slope. Taluses tend to be associated with steep cliffs and directly onlap the bedrock (Turner, 1996). The production of talus debris is linked to the relative rapid fragmentation of bedrock exposed on cliffs (Turner, 1996). The cliff erosion rate and thereby debris accumulation rate are indirectly related to climate (Pawelec & Ludwikowska-Kędzia, 2016; Sanders, 2010; Sanders et al., 2009). Climatic factors can be frost cracking (controlled by precipitation and temperature and indirectly related to the absolute elevation), slope exposition to insolation and winds, and seasonal snow thawing (Hales & Roering, 2005; Héту & Gray, 2000; Sander et al., 2009). Another agent responsible for triggering rockfalls is possibly earthquakes (Hales & Roering, 2005).

The study of slope deposits is difficult due to several factors. First, slopes are dynamic environments constantly affected by slope processes and therefore have complex structures. Second, at the macro- and mesoscales, the deposit (if not active) is often remodeled by weathering processes, development of vegetation and/or human activity. Finally, at the microscale, different mass movements produce

similar deposits (Bertran & Texier, 1999; Múcher et al., 2010), and the materials are often highly affected by post-depositional processes, which can erase primary structures (Bertran & Texier, 1999; Field & Banning, 1998; Múcher et al., 2010; Nelson, 1992). Therefore, macro- and micromorphological aspects of slope deposits are still poorly documented (Múcher et al., 2010). This is true for slope deposits in arid settings (Ventra et al., 2013), especially for those generated by rockfalls, because they usually lack enough abundant matrix to permit their study.

For archaeological studies, slope deposits are important for their relationship with climatic conditions, and they usually tend to preserve buried surfaces (Field & Banning, 1998; French, 2019; Goldberg & Macphail, 2013). When combined with knowledge of soil formation, they can provide important information for the understanding of the geomorphic and paleoenvironmental history of the site (Courty et al., 1989; Múcher et al., 2010).

Here, we present a study conducted on a rockfall talus cone at a Late Pleistocene–Late Holocene site—Obishir-I—in an arid intermountain basin (Aydarken Basin) in Central Asia. Importantly, Obishir-I is one of several archaeological sites (e.g., Obishir-V; Sel'Ungur; Surungur) located within the microregion (Figure 1). To reconstruct the depositional history of the site, this study aims to (a) establish the stratigraphy of clastic sediments, paying special attention to talus deposits, (b) recognize and distinguish which processes were relevant in the site formation, and (c) reconstruct the paleoclimatic and paleoenvironmental conditions of deposition. Indirectly, we also aim to contribute to further documentation of talus deposits.



**FIGURE 1** Location of the research area, Obishir-I, and the other archaeological sites. Esri satellite imagery was used as the base map [Color figure can be viewed at [wileyonlinelibrary.com](http://wileyonlinelibrary.com)]

Based on existing methodologies and our experience regarding local conditions, we report the results obtained from our interdisciplinary study. This study considered the following:

- (i) identification of macro sedimentary structures, focusing on re-deposition events, sources of material, and possible hiatuses;
- (ii) grain size distribution to gain a better understanding of the material sorting, possibly due to sedimentary processes and the coexistence of different deposition modes;
- (iii) chemical composition of sediments to identify pedogenic or weathering horizons and indirectly any temporary ceasing of sedimentary action;
- (iv) diagnostic microfeatures as a supporting tool in the recognition of site formation processes;
- (v) analysis of archaeological assemblages and inter-strata refitting together with the analysis of the distribution of finds to detect any possible disturbance of the assemblage integrity, and to identify any preserved original depositional horizon;
- (vi) taxonomy of fossil mollusks to provide paleoecological and paleoclimatic data for the identified processes; and
- (vii) chronometric dating to determine the age of deposits and their accumulation rate.

## 2 | STUDY SITE

### 2.1 | Regional and geomorphological setting

Located at the foothills of the Pamir-Alay mountain range in the southern margin of the Fergana Valley, Obishir-I (39°57'28.6"N, 71°17'08.9"E; 1731 masl) is an Epipaleolithic site just at the toe of a heavily fractured and karstified limestone cliff (Lower Carboniferous), which is characterized by a rock shelter (Figure 2). Specifically, the site is located at the foothills of an ENE-WSW-oriented Eshme ridge (indicated as Eshme Too in Soviet topographic maps, 1:100k). Toward the south, the ridge faces the Aydarken Basin drained by several streams, including the Obishir (Figure 1). These streams are small, braided, and temporarily recharged by meltwaters from winter snow and mountain glaciers of the Pamir-Alay Mountains (toward S), thus restricting the outflow mainly to the winter and spring seasons. The drainage was ESE-WNW that diverted within the valley (Figure 1). The basin stretches for ca. 18 km from E to W and is ca. 6 km wide. The surrounding landscape is mainly mountainous and dissected with the Aydarken Basin, which is essentially a small intermountain basin surrounded by E-W-oriented ridges to the north and the south and filled with Quaternary deposits (mostly of alluvial, aeolian, and colluvial origin). The valley closes to the west, where the streams converge into the Sokh.

Several urban areas are located in the basin. Aydarken (Rus. Khaydarkan) is one of the largest and most urbanized cities, second only to Sokh. Excluding these, standalone rural houses and farming structures are spread within the basin. Agriculture and pastoralism

comprise the most common land use types, and fruit orchards are generally grown for local commercial production. It is worth mentioning that the Eshme ridge has been extensively exploited for its mineral resources since the 1940s (UNEP et al., 2009). Therefore, the landscape is dominated by tailings piles, mines, and shafts.

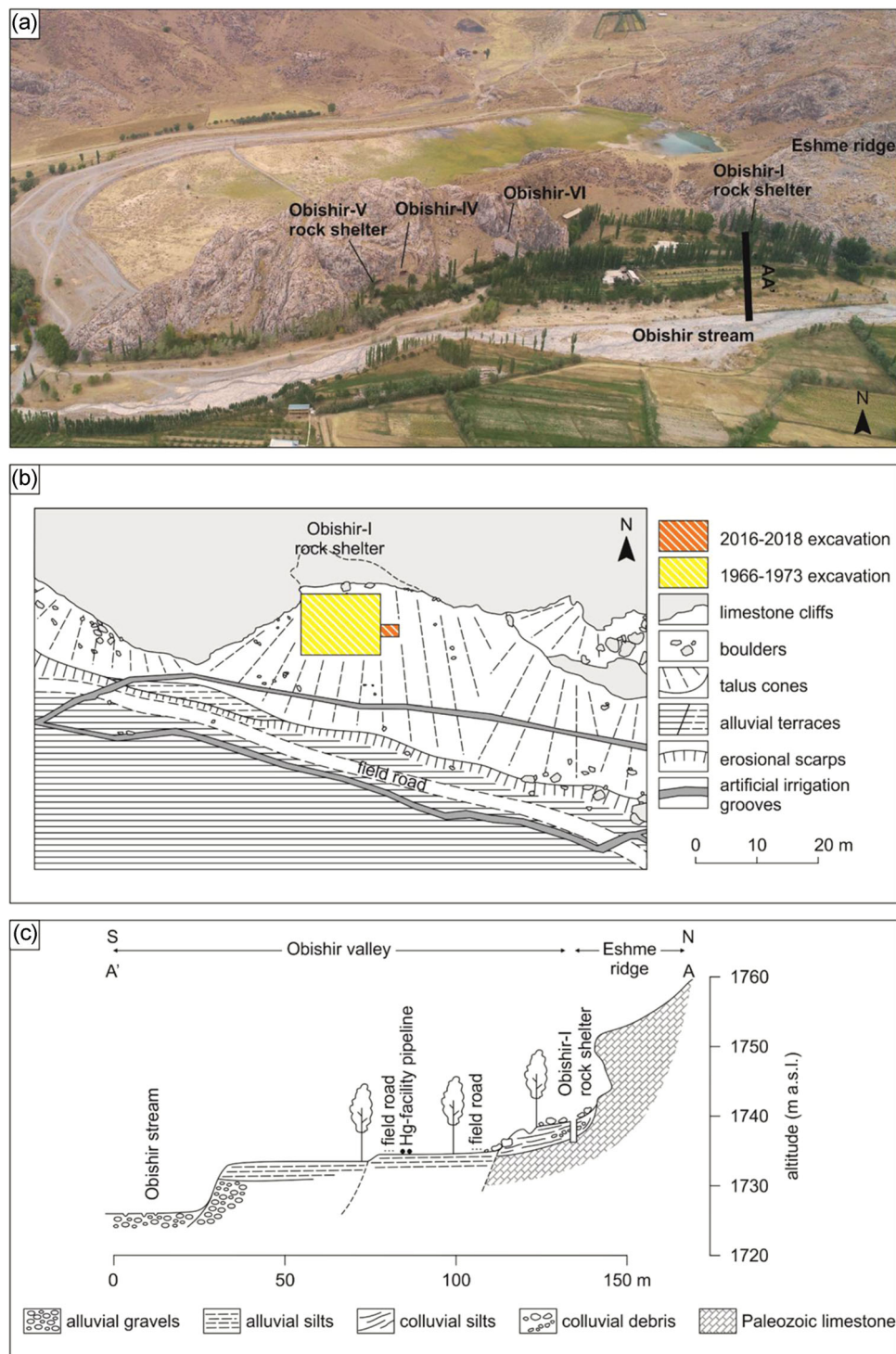
According to the present-day Köppen-Geiger map (Beck et al., 2018), the climate affecting the study area is arid (B), steppe (S), and cold (k), with a mean annual air temperature (MAT) below 18°C and a mean annual precipitation (MAP) estimated to be below 250 mm a<sup>-1</sup>. Being arid, the terrain is subjected to the development of weak and sparse surface vegetation (Cooke et al., 1993) and prone to mobilization downslope in mass movement erosive episodes (French, 2019). Moreover, in arid and semiarid environments, rock outcrops and superficial debris are commonly affected by flaking, spalling, splitting, and granular disintegration (Cooke et al., 1993).

Rock shelters and small caves are ubiquitous in the Eshme Ridge. Significantly, several archaeological sites (e.g., Obishir-V, Sel'Ungur, Surungur) are on the southern flank of the Eshme ridge (Figure 1), and they all have a geomorphological setting similar to that characterizing Obishir-I (Figure 2b). They are located at the foot of a steep cliff, in front of a rock shelter niche or a cave entrance, where associated scree deposits overlay the bedrock or a flat alluvial terrace. The steep cliffs face mainly the south, and their heights range from 20 to 30 m. The Obishir stream flows just in front of the Obishir-I, approximately 150 m away toward the south (Figure 2a,c). Its flat terraces are used for agriculture and pastoralism.

At Obishir-I, the talus cone is approximately 60 m wide and spans the circa 30 m downslope from the cliff toe toward the south, where greater boulders overlap a flat alluvial terrace (Figure 2b,c). Its total thickness is up to circa 4 m. After comparing our data with the literature, we found that the Obishir-I talus is immature, as the relationship between the slope height (15–25 m) and the average talus height (ca. 4 m) does not satisfy the equation proposed by Sanders et al. (2009). It is also possible that the cone originally had a greater length, which was reduced by later fluvial erosion, but no evidence supporting this was possibly observed in the field.

### 2.2 | Previous investigations

Obishir-I was first discovered in the mid-20th century by Islamov (1972), who subsequently also studied the site during three archaeological excavation seasons between 1966 and 1973 (Islamov, 1980; Figure 2b), yielding a substantial collection of lithic finds (2,511 artifacts) and providing preliminary geological and archaeological interpretations. In the aftermath, the stratigraphic units were described as in situ, and the archaeological assemblage was attributed to the Mesolithic tradition (final Pleistocene–earliest Holocene) based on technical and typological comparisons with other sites in the vicinity. Furthermore, lithic assemblage similarities were recognized among Obishir-I and Obishir-V sites, attributed to a unique cultural unit, named Obishirian.



**FIGURE 2** (a) Drone imagery taken in the field showing the Eshme ridge southern flank where Obishirian sites are situated. (b) Excavation plans of Obishir-I with the main features characterizing the site. (c) Schematic cross-section showing the main features present in the field from the Eshme slope to the Obishir stream [Color figure can be viewed at [wileyonlinelibrary.com](http://wileyonlinelibrary.com)]

A new joint Russian–Kyrgyz archaeological expedition, led by S. V. Shnaider and A. Abdykanova, was carried out during 2016–2018 (Figure 2b). This new research involved an excavation area of 6 m<sup>2</sup>, in which the excavation was conducted according to modern

excavation and documentation techniques. This provided access to the internal part of the talus cone and allowed us to study its geological structure, sampling for luminescence dating, and analysis of fossil mollusks.

### 3 | MATERIALS AND METHODS

#### 3.1 | Archaeological excavation and techno- and typological analyses of the lithic assemblage

Field excavations were conducted according to the methods and standards previously used by the research team at the Obishir-V site (Taylor et al., 2021). Photo fixations were taken using a camera (Canon D600) and a quadcopter (DJI Phantom 4 Pro). To retrieve small artifacts and shell fragments, the sediments were sieved through a 1×1 mm mesh. The techno- and typological lithic collection analyses were performed according to the methodology of Monigal (2002, unpublished data).

#### 3.2 | Distribution of artifacts

During the 2016–2018 excavation campaigns, the detailed position of each artifact was recorded with the Total Station (Leica TS02 plus) in tandem with Trimble (software EDM Mobile). A numerical database of the X, Y, and Z coordinates of the finds (vs. the site datum) was then produced (Supporting Information material S1). The database was processed, and the distribution of artifacts was obtained using QGIS v3.08 and R v.3.6.

#### 3.3 | Field geological analyses

The study of the Quaternary infill was conducted in 2019 within the current archaeological trench, which uncovered a profile (circa 4 × 1.5 m) just in front of the rock shelter (Figure 2b). The site was investigated using a common geological approach (Goldberg & Macphail, 2013; Karkanas & Goldberg, 2018; Krajcarz et al., 2020; Macphail & Goldberg, 2017). The stratigraphic units (Table 1) were identified using both lithostratigraphic characteristics (differences in texture, color, and small sedimentary structures) and an allostratigraphic approach (presence of unconformities) according to the recommendations of Hughes (2010) and Räsänen et al. (2009). We independently described the matrix (<2 mm) and skeleton (>2 mm) for each stratigraphic unit. The former was characterized by the main composition, texture, color (Munsell Rock Color Chart), and hydrochloric acid (HCl) test. The latter was described by noting the petrographic composition, shape, and roundness, measuring the orientation of rock fragments with a classic compass, recording possible rock fragment alignments, and taking notes of the maximum and minimum diameters (Table 1). Observations, measurements, and sketches were noted in the field notebook and documented using a photographic camera.

#### 3.4 | Sampling

Sampling was conducted during the 2018 and 2019 campaigns. Most of the samples were taken from the eastern wall of the

excavation, except for the weakly available uppermost and lowermost parts, which were sampled in the cleaned-up walls of the old 1973 trench (Figure 3). Unit 3 was sampled only for micro-morphological analysis, as it was thin and weakly detectable in the field. A total of 127 samples were collected at various depths, including eight bulk sediment samples, five undisturbed monoliths, 108 mollusk samples from 35 levels (Figure S3 in the Supporting Information Material S2), and six samples for luminescence dating.

#### 3.5 | Grain size analyses

The volume for each sample was approximately 5 L; therefore, the samples could not adequately represent the material heterogeneity. To obtain information about the cobbles and boulders greater than 50 mm, the maximum diameter of the clasts was annotated during the field survey (Table 1). Preliminary dry sieving with a 2 mm sieve was performed at the site to divide the coarse fraction from the fine fraction. The coarse fraction was then dry-sieved (using 2, 5, 10, 20, and 50 mm sieves) at the site. The fine fraction (<2 mm) was dried at 105°C in the laboratory and representatively split into several subsamples intended for archiving, grain size analysis, and chemical analyses. The set of subsamples for grain size analysis ( $n = 8$ , ≈5 g each) was analyzed by laser diffraction (range 0.01–2000 μm) at the certified Laboratory Jars S.A. (Poland). Rapid grain size analyses and statistical calculations were performed using GRADISTATv9.1 (Blott & Pye, 2001, Supporting Information Materials S3 and S4).

#### 3.6 | Basic geochemistry

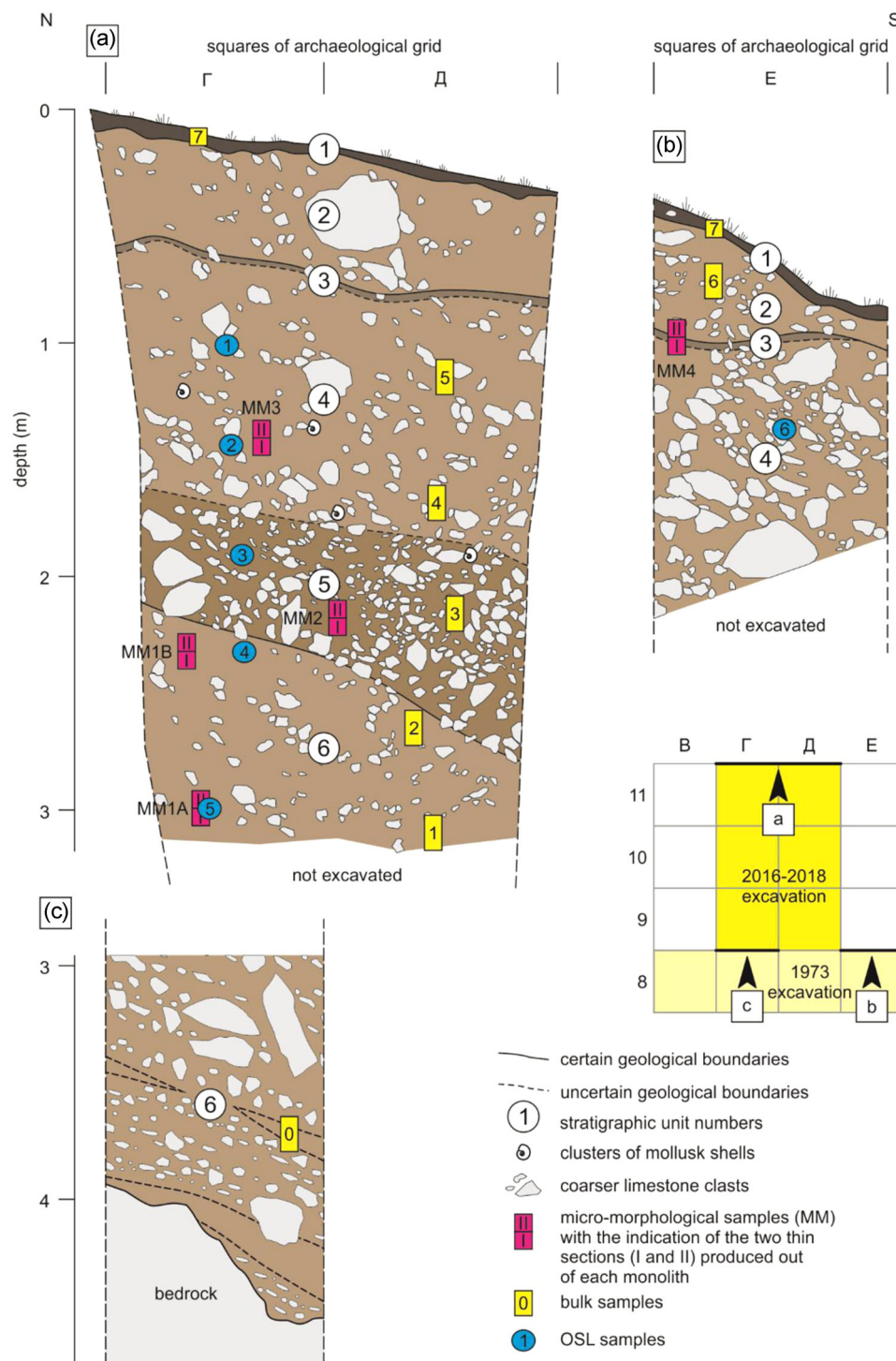
The subsamples intended for geochemical analyses were homogenized using an automatic agate ball mill. One set (≈1 g each) was pretreated with 1 M HCl to remove carbonates and thus estimate the carbonate content. Another set (≈1 g each) was decomposed with 30% hydrogen peroxide (H<sub>2</sub>O<sub>2</sub>) to remove and estimate the amount of organic matter. Pretreatments were performed according to existing methodologies (Krajcarz et al., 2020). For the estimation of organic carbon (TOC) and organic nitrogen (TN), elemental analysis (Vario MicroCUBE CHNS analyzer) was performed for the HCl-pretreated sediment samples (≈4 mg each). A set of non-pretreated subsamples (≈1 g each) was subjected to chemical analysis by coupled plasma mass spectrometry (ICP-MS) according to Krajcarz (2019) at the Bureau Veritas Minerals Laboratory (Vancouver, Canada).

#### 3.7 | Micromorphology

Ten petrographic thin sections were produced from the five monoliths. We followed the procedure modified by Krajcarz et al. (2016) and

TABLE 1 Detailed description of the stratigraphic units

Unit n.	Maximum thickness (cm)	Matrix grain size (nomenclature according to R. L. Folk, 1954)	Matrix Munsell color dry; moist	Skeleton	Lower boundary	Compounds	General description
1	10	Poorly sorted, silty fine sand	5YR 4/1; 5YR 3/1	Angular and subangular pebbles of different sizes	Irregular following the sloping ground; the lower boundary is gradual	Roots	Topsoil (O and A soil horizons) of a Mollisol, with moss and thin vegetation, sandy silt material, organic matter
2	50	Poorly sorted, silty very fine sand	10YR 6/3; 10YR 5/3	Angular gravel-and-cobble-sized limestone, extremely poorly sorted	Fairly visible and erosional		Matrix-supported, massive, clast moderate, gravelly diamicton (Islamov's dump)
3	5	Loose sandy silt	10YR 5/2; 10YR 4/2	Angular and sub rounded gravel-sized limestone from 2 mm to 2 cm	Gradual	Roots, pebbles	Paleosol (A soil horizon) below the pre-1970s ground surface, darker than the surrounding material, characterized by small aligned pebbles and cobbles; the thickness is irregular
4	100	Very poorly sorted to poorly sorted, silty fine sand	10YR 7/3; 10YR 5/4	Angular gravel-sized limestone, extremely poorly sorted, chaotic structure. $D_{\min}$ 2 mm, $D_{\max}$ 30 cm	Fairly visible, inclined, and gradual	Snail shells, Rhizolites (5–2 mm), artifact	From clast-supported to matrix-supported, massive, clast-rich, gravelly diamicton. In the middle, rock fragments were poorly aligned
5	80	Poorly sorted, sandy very coarse silt	10YR 6/4; 10YR 5/4	Angular gravel-and-cobble-sized limestone. $D_{\min}$ 2 mm, $D_{\max}$ 19 cm	Fairly visible, inclined, and erosional	Snail shells	Matrix-supported very close to being grain-supported, massive, gravelly diamicton with 76% of clast, poorly sorted material
6	200	Poorly sorted, sandy from very coarse to coarse silt	10YR 7/3; 10YR 5/4	Angular gravel-and-cobble-sized limestone, chaotic distribution. Bottom: Minimum diameter ( $D_{\min}$ ) 2 mm, Maximum diameter ( $D_{\max}$ ) 8 cm. Top: from 2 mm to 14 cm	Bedrock	Snail shells, rounded pebbles 0.7 g	Matrix-supported, massive, gravelly diamicton. An increase in the clast amount from the bottom to the top, poorly sorted material; lenses of silty material, and weakly visible lamination in the lowermost part



**FIGURE 3** Stratigraphic sequence at Obishir-I: (a) the main profile exposed after the 2016–2018 archaeological campaign. (b) and (c) Profiles exposed after the 1973 archaeological campaign and cleaned-up in 2016. The lowermost part (c) was weakly preserved, so only one sample of limited reliability has been collected from a silty lens [Color figure can be viewed at [wileyonlinelibrary.com](http://wileyonlinelibrary.com)]

Morley et al. (2017), as described in Supporting Information Material S2. Thin-section analysis was conducted using a polarization microscope (ECLIPSE LV100POL, magnification ranging from 2.5 to 50). A systematic description was performed according to Stoops (2003). Secondary calcium carbonate accumulations were identified using the

recommendations of Blank and Fosberg (1990). Quantitative analyses were conducted, such as point counting for the coarser fraction and porosity, using image analysis (Adobe Photoshop package), following the method described by Mroczek (2008) and Zhang et al. (2014) described in the Supporting Information Material S2.



### 3.8 | Mollusk taphonomy and assemblage

Fossil mollusks were analyzed according to the methodology presented by Osipova et al. (2021). The shell abundance was determined according to the method of Ložek (1964). The mollusk species were identified as described by Likharev and Rammelmeier (1952), Likharev and Viktor (1980), Shileyko (1984), Shileyko and Rymzhanov (2013), and Sysoev and Shileyko (2009). Each specimen was identified to the genus, and, if possible, species.

### 3.9 | Chronometric dating

The chronometric dating includes six optically stimulated luminescence (OSL) dates. Sample preparation for luminescence dating is outlined in the Supporting Information Material S2. Luminescence dating was performed in the Nordic Laboratory for Luminescence Dating at Risø, Denmark, according to the methodology described in the Supporting Information Material S2.

### 3.10 | Stratigraphic accumulation rate (SAR)

The SAR, reported in  $\text{cm a}^{-1}$ , approximates the sedimentary rate. We used SAR instead of the sedimentary rate because it includes three independent factors that are difficult to separate in the studied sediment types: (i) aggradative accumulation (i.e., representing the sedimentary rate as a simple function of thickness and age), (ii) sedimentary gaps, and (iii) erosion (Johnstone et al., 2019). SAR was calculated between two dated points of the same stratigraphic section, as described in the Supporting Information Material S2.

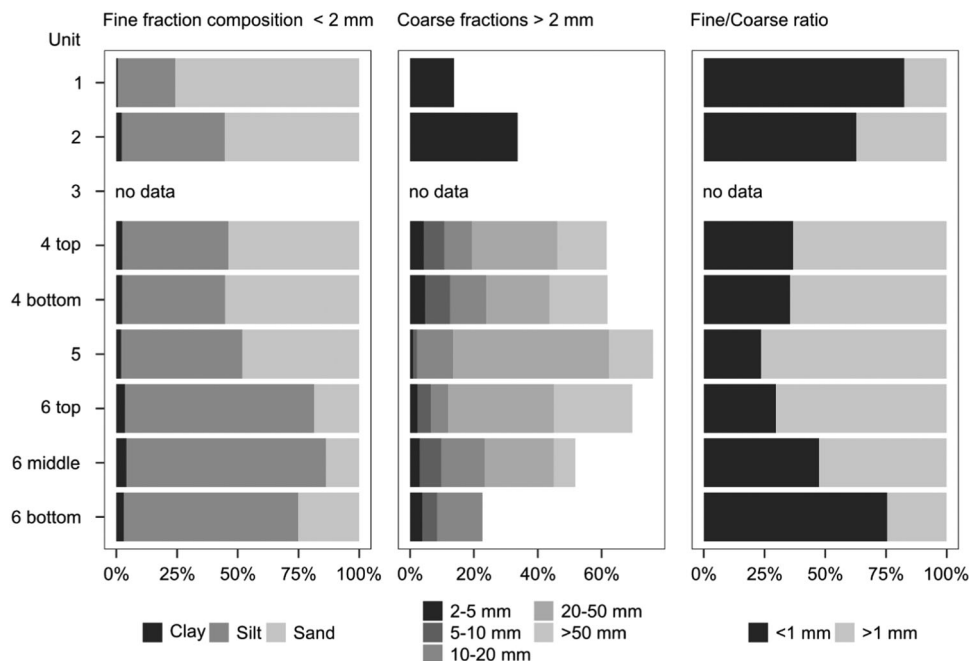
## 4 | RESULTS

### 4.1 | Quaternary sequence

The Quaternary clastic sequence comprises six calcareous, gravel-rich stratigraphic units (diamicton), namely, Unit 1 to Unit 6 (Table 1; Figure 3). The poorly sorted material is uniform throughout the sequence. The skeleton is generally represented by the angular limestone clasts. The loose matrix was mainly calcareous, with sparse quartz and mica grains. The texture varied from sandy silt to silty sand. The infill directly overlies the Paleozoic bedrock, and its internal stratification is fairly visible. The overall structure dips approximately  $10^\circ$  toward the valley (SW) and the bedding, and boulders generally lie parallel to the local slope inclination. Two erosional surfaces were recognized within the profile: one at the contact between Units 6 and 5 and the second at the boundary between Units 3 and 2 (Table 1; Figure 3). Unit 5 possibly had a lenticular geometry (Figure S2 in the Supporting Information Material S2). At approximately 50 cm below the ground surface, we recognized a paleosol (Unit 3–A horizon), possibly a soil occurring before Islamov's excavations during 1966–1973, and covered by Unit 2. Unit 2 is therefore an artificially disturbed sediment, recognized by archaeologists as the dump left after Islamov's campaigns. The sequence closes with the current topsoil (Unit 1—O and A horizons).

### 4.2 | Grain size analyses

The results (Figure 4) show that Units 6, 5, and 4 have textural features typical of talus cone deposits. Overall, the matrix is poorly sorted and has a weak coarsening upward tendency from sandy silt to silty sand.



**FIGURE 4** Grain size results for each unit, except for Unit 3, which was not characterized by bulk samples because of its small thickness

The clay content was low. The highest amount was found in Unit 6 (4% of the fine fraction). Unit 6 also had the highest silt content ( $\approx 70\%$  of the fine fraction). The skeleton amount is greater than 50% at the central top part of Unit 6, in Units 5 and 4 (Figure 4, fine/coarse ratio). Units 6 to 4 have a dominant  $>10$  mm fraction, and consistent  $>50$  mm fraction. The sample representative of the loess-like lens material lacks gravel content; the same is true for Units 2 and 1. For Units 2 and 1, this is possibly due to nonrepresentative samples.

### 4.3 | Chemical composition of sediments and semiquantitative geochemical indices

The results, shown in Figure 5, represent sediments with poor organic matter content, except for Unit 1 (topsoil), and high  $\text{CaCO}_3$  content. The organic content is represented by the biogeochemical proxies, % TOC, and % TN. Their overall trend decreased downward, and the same was true for % P. The Ca concentration (lrb % Ca) varied from 10% to 15% throughout the profile, with the upper part of Unit 4 showing the highest concentration (Figure 5). The observed discrepancies between the  $\text{CaCO}_3$  content and % Ca may result from different sensitivities of the applied method and from the fact that some Ca can be bound within noncarbonate compounds (e.g., in detrital plagioclase). Additionally, in an attempt to reconstruct the alteration trend related to past climate variability within the Obishir-I profile, we calculated semiquantitative geochemical indices such as chemical proxy alteration (CPA) (Buggle et al., 2011), and  $\text{Al}_2\text{O}_3/\text{TiO}_2$  and  $\text{K}_2\text{O}/\text{Na}_2\text{O}$  ratios (Krajcarz et al., 2016), which we believed to be the most appropriate for our case (see the Supporting Information Material S2). The results are shown in Figure 5.

## 4.4 | Micromorphology of sediments

### 4.4.1 | Lithological composition and structure

The lithological composition was similar for all thin sections. Dominant limestone and travertine pieces and heavily altered rock fragments represent the very coarse fraction ( $>2$  mm) (Supporting Information Material S2: Figure S6a,c,d). Their color varies from

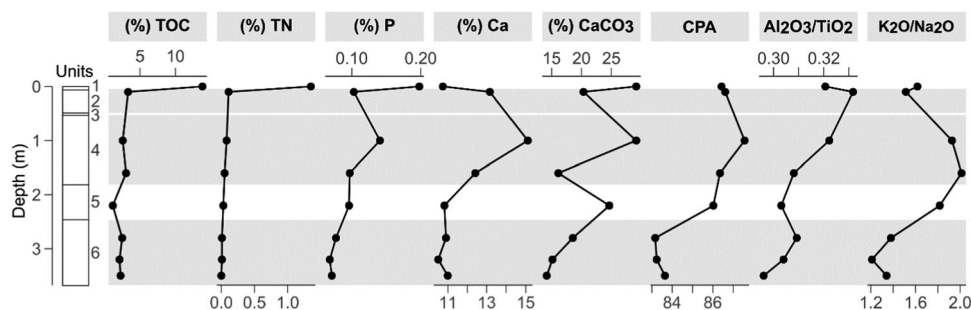
light gray to brownish red as a function of the oxidation process. The shape is generally platy, angular, and subangular (Figure S6a,c,i,j,k,o). Well-rounded clasts also occur, but they are generally smaller in size and less abundant (Figure S6o). The groundmass is mostly represented by calcareous clayey silt and sand ranging from fine to coarse. Fine to coarse sand-sized calcite, quartz, mica, and feldspar associations were observed dispersed in the groundmass (Figure S6b). The calcite grains were rounded (Figure S6b,i,m).

Vesicles, small channels, and chambers (Figures 6 and S6a,h,i) of variable sizes ( $70\ \mu\text{m}$  to 2 mm) occur very commonly throughout the profile. These voids are generally intrapedal and are most likely produced by plant and soil faunal activity. The mesoscale porosity characterized by vertically and laterally continuous channels or planes (Figures 6 and S6f) is transpedal and controlled by very coarse compounds. This phenomenon is visible both at the mesoscale (in the field) and in the macro scans of the thin sections (Supporting Information Material S2) and at the microscale in thin sections (Figure S6f,j). Packing voids can occur amid coarse clasts and coarse aggregates, and they are generally intra- and transpedal (Figure S6h). Intrapedal planes also occur, but they are not laterally continuous. The resulting microstructure is complex and very difficult to classify; it varies from weakly developed angular blocky, massive, granular, vughy, to locally weakly platy (Figures 6 and S6e-h). Lamination and/or sorting were not observed.

Overall, the micromass showed a high calcareous content (Figure S6b). The color varies from light brown to dark as a function of the increasing amount of organic matter, clay, and/or the presence of Mn/Fe oxides (Figure S6). The C/f-related distribution varies upward from porphyric to chitonic and eunalic (Figure S6e-h). There are two main types of b-fabric: crystallitic and stipple-speckled (Figure S6b,p).

### 4.4.2 | Diagnostic features

The key features are shown in Figure 6 and illustrated in Figure S6 (Supporting Information Material S2). They are generally related to various pedogenic processes, translocation, minor human activity, soil biological activity, and frost action.



**FIGURE 5** Geochemical data for the  $<2$  mm fraction. Unit 3 was not sampled. The  $\text{Al}_2\text{O}_3/\text{TiO}_2$  ratio decreases with increasing alteration, whereas  $\text{K}_2\text{O}/\text{Na}_2\text{O}$  and chemical proxy alteration increase with increasing alteration and pedogenesis. The indices possibly revealed a low alteration at the bottom of the profile (Unit 6), with an increase in alteration starting at the Unit 6–5 transition

Unit n.	Sample n.	Porosity (%)	Voids	Micro-structure	CL/f	Coarse grain count	Pedogenesis				Transport			Human activity			Bioturbation		Frost Action
							Secondary CaCO <sub>3</sub> clay and MnFe nodules	Calcareous infilling	Rounded aggregate	Reoriented grain with coat	Coated grain	Limpic clayey fragment	Dusty capping	Charcoal fragment	Bone fragment	Coprolite fragment	Biogenic carbonate	Plant fragment	Organic organo-mineral excrement
2/3	MM4 II	25	pk/vu/pl	g/v	0.8	26	+++	+++	++	+++	+	+++	++	+++	++	++	+++	+++	+++
3/4	MM4 I	26	ch/vu/ve/pl	m/b	1.0	35	+++	+++	++	+++	++	+++	++	+++	++	++	+++	+++	+++
4	MM3 II	21	pl/vu/pk/ve/ch	m/b	2.1	10	+++	+++	+++	++	++	++	++	++	++	+++	+++	+++	+++
4	MM3 I	25	ve/ch/vu/cha	m/v	0.6	36	++	++	++	+++	+	++	++	++	++	++	+++	+++	+++
5	MM2 II	23	ve/ch/vu	m	0.7	7	+	++	++	+++	+	++	+	+	++	+	++	+	+
5	MM2 I	14	ve/ch/vu	m	0.6	20	++	++	++	++	+	+	++	++	++	+++	++	++	++
6	MM1B II	11	vu/ve/pl	b/v	0.6	27	+	++	++	++	+	++	++	+	w.d.	++	+	+	++
6	MM1B I	9	ve/vu/ch	m/b	0.6	21	+	++	++	++	+	++	++	++	++	+	+	+	++
6	MM1A II	6	pl/vu	m/b	0.8	11	+	++	+	+	+	++	++	+	+	+	+	+	+
6	MM1A I	8	pl/vu	m/b	1.3	19	+	++	+	+	+	+	++	+	+	+	+	+	+

**Voids**  
**ch** - channels  
**cha** - chambers  
**pk** - packed  
**pl** - planes  
**ve** - vesicles  
**vu** - vughs  
**Structure**  
**b** - blocky  
**g** - granular  
**m** - massive  
**v** - vughy  
**Frequency**  
**+** rare to few  
**++** common  
**+++** frequent to dominant  
**c** clay  
**l** iron  
**w.d.** well developed  
**h** plant fragment oriented horizontally;  
**v** plant fragment oriented vertically

**FIGURE 6** Micromorphological diagnostic features. The porosity (%), the CL/f ratio, and the coarse-grain count were estimated using Photoshop v.C5. The porosity was estimated at the microscale, whereas the CL/f ratio and the coarse-grain count were estimated at the mesoscale, that is, using scans of thin sections. CL, coarse limestone; f, fine [Color figure can be viewed at [wileyonlinelibrary.com](http://wileyonlinelibrary.com)]

#### 4.5 | Techno- and typological analyses of the lithic assemblage and its distribution

According to the techno- and typological analyses of the lithic assemblage and its distribution, two horizons were distinguished: the former related to Units 6 and 5, and the latter to Unit 4. The lithic assemblage is described in the Supporting Information Material S2, and its distribution is illustrated in Figure 7.

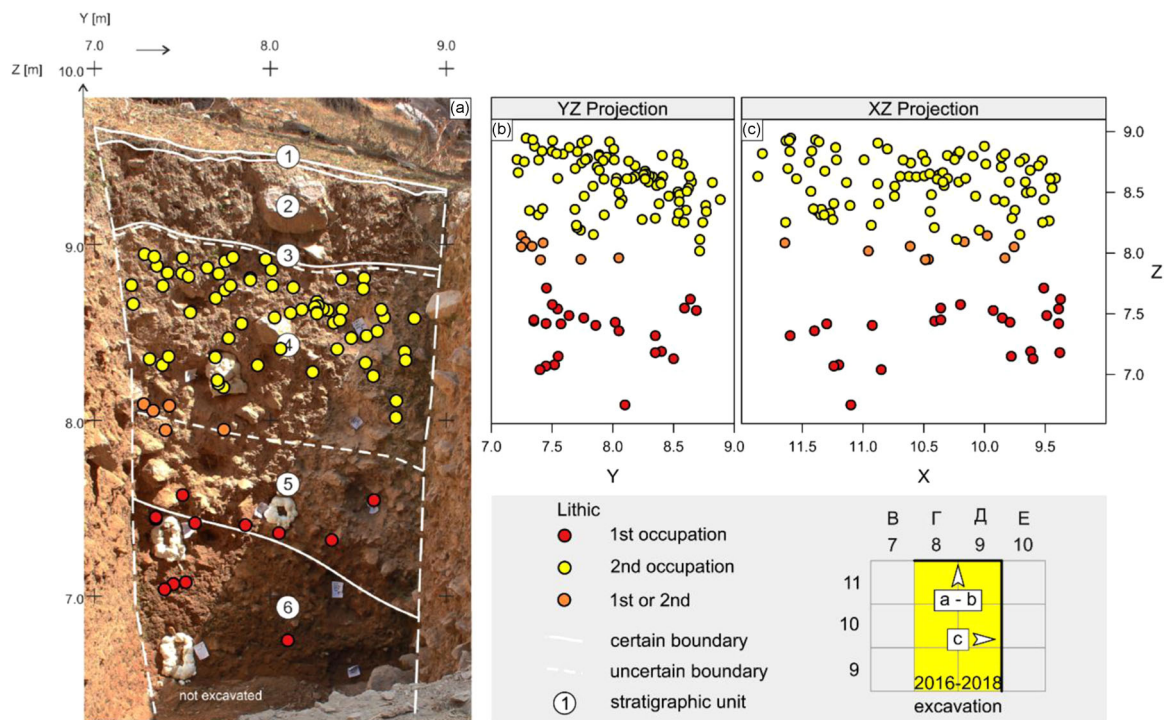
#### 4.6 | Mollusk taxonomic composition

A total of 2301 complete shells and shell fragments represented the mollusk assemblage. The number of extracted shells per sample varied depending on the investigated level (Supporting Information Material S5). Nine terrestrial mollusk species were identified in sections D11 and Γ11. They belong to six genera of four families (Puppilloidea, Enidae, Parmacellidae, Bradybaenidae)

attributed to the class Gastropoda. The best-represented species are *Gibbulinopsis signata* (Mousson, 1873), *Candaharia (Levanderiella) levanderi* (Simroth, 1901), *Pseudonapaeus cf. asiaticus* (Mousson in Martens, 1880), *Ps. secalinus* (Mousson in Martens, 1880), and *Fruticicola* sp., whereas *Pseudonapaeus stabilis chatkalicus* (Kuznetsov, 1999) and *Ps. sogdianus* (Martens, 1874) were fewer. The rest of the species were represented by single shells (Table 2).

#### 4.7 | Chronometric dating and accumulation rate

The dating results are shown in Table 3, and the age-depth model is shown in Figure 8. Units 6 and 5 showed the Late Pleistocene OSL age (~19–15 ka), while Unit 4 showed the Early Holocene OSL age (~9.5–9 ka). The SARs are high for Units 6 and 4 (270 and 140 cm ka<sup>-1</sup>), with high error values, but low for the middle part of the sequence (13 and 9 cm ka<sup>-1</sup>).



**FIGURE 7** (a) Projected lithic artifacts from 0 to 1.5 m distance from the E wall of the 2016–2018 excavation. (b)–(d) Scatter plots of all recorded lithic artifacts. The lithic artifacts are unevenly distributed within the vertical profile. Two main horizons are identified (first and second occupation), of which the boundaries are difficult to draw; therefore, the artifacts between the two horizons are difficult to attribute to one or the other occupation (first or second occupation—orange points). The lower horizon includes less than 20 specimens and it is situated near the boundary between Units 5 and 6. The upper horizon includes a major portion of the lithics and is connected to the middle-upper part of Unit 4. Some artifacts, loosely scattered within Units 4, 5, and 6, may also belong to these two horizons and represent post-depositional disturbances [Color figure can be viewed at [wileyonlinelibrary.com](http://wileyonlinelibrary.com)]

In terms of the reliability of our dates, the quartz OSL signal of sand-sized grains from all the samples is sensitive, and dominated by the fast component. Dose recovery measurements were performed using six aliquots of each sample and given doses varying between 25 and 35 Gy (as appropriate, based on the approximate  $D_e$ ). Overall, dose recovery ratios are close to unity ( $1.02 \pm 0.02$ ,  $n = 24$ ), which suggests that our protocol is able to accurately measure a known dose given before any thermal treatment. The quartz  $D_e$  estimates (arithmetic averages) obtained using our selected protocol are summarized in Table 3, together with the standard deviations of the mean (standard errors) and the number of aliquots used to calculate the mean. The degree of bleaching was investigated using the differential resetting rates of quartz and feldspar. Based on Murray et al. (2012) and Möller and Murray (2015), we considered those samples for which the  $IR_{50}$  age is less than or equal to the quartz age (see Table 3: IR/Q column) to be probably well bleached, and those for which the  $pIRIR_{290}$  age was less than or equal to the quartz age (Table 3:  $pIRIR/Q$  column) to be well bleached. Therefore, five of the six studied samples are well bleached. In addition, the age of the sample OBS-I-5, at the bottom of the sequence, could be overestimated. To conclude, it appears that the quartz, in most of the samples, sufficiently bleached before deposition, and that any uncertainties in bleaching do not significantly contribute to the reliability of the quartz luminescence ages presented in this study.

## 5 | DISCUSSION

### 5.1 | Depositional processes

#### 5.1.1 | Colluvial and aeolian deposition

At Obshir-I, it is clear that the overhanging limestone cliff is the main source of coarse clastic material. Deposits such as those at this site, lacking lamination and sorting, are typical for mass movements, such as debris flow, rock avalanches, or dry grain flow (Bertran & Texier, 1999). In our case, the overall cone characteristics (i.e., landform, debris or diamicton texture, fairly visible stratification, clasts weakly parallel to the local slope) led to the conclusion that the site was, and still is, characterized by rockfall events.

The matrix, which fills the space between limestone clasts, has macroscopic characteristics of yellowish-brown silt or silty loam (Table 1). Its color and consistency resemble loess deposits from the region, known, for instance, from the nearby Sel'Ungur Cave (Krivoshapkin et al., 2020). This material could have been either accumulated directly by wind simultaneously to the debris accumulation or primarily accumulated by wind and later relocated downward into the empty spaces of the original debris open-work structure. The translocation into voids could have been caused by washing, illuviation, crumbling, and falling. Dust activity and emissions in Central

TABLE 2 List of species and summarized number of mollusk shell remains found in two D11 and T11 sections of the Obshir-I rock shelter site

Stratigraphic unit	IG UFRC RAS <sup>1</sup> Registration number	Archaeological horizon	Depth (m)	Fruticola cf. fedtschenkoi (Martens, 1874)	Fruticicola sp.	Candaharia (Levanderella levanderi (Simroth, 1901)	Gibbulinopsis signata (Mousson, 1873)	Leucozonella sp.	Pseudo-napaeus asiaticus (Mousson, 1880)	Pseudo-napaeus secalinus (Mousson, 1880)	Pseudo-napaeus in Martens, 1874)	Pseudonapaeus sogdianus (Martens, 1874)	Pseudonapaeus chatkalicus (Kuznetsov, 1999)	Turana mar-tensiana (Ancey, 1886)	Total number of mollusk shells
2	6442, 6443	T11	0.40-0.45	1	13	5	-	-	9	-	-	2	2	2	32
3	6422-6-424	T11	0.52-0.62	-	3	-	-	-	12	-	-	-	-	-	15
			Sum of shells	1	16	5	-	-	21	-	-	2	2	2	47
4	6449-6-452	T11	0.62-0.69	3	8	-	-	-	6	88	-	-	-	-	105
4	6447, 6448	T11	0.69-0.77	5	1	3	-	-	3	103	-	-	-	-	115
4	6437-6-439	T11	0.77-0.91	2	9	2	1	1	6	76	-	-	1	-	97
4	6411-6-417	T11	0.91-1.00	6	1	-	-	-	6	112	-	-	-	2	127
4	6434-6-436	T11	1.00-1.21	5	2	1	-	-	3	92	-	-	2	1	106
4	6646	T11	1.21-1.34	-	-	22	-	-	1	-	-	-	-	-	23
			Sum of shells	21	21	29	1	1	24	472	-	-	3	3	573
5	6453, 642-5-6-427	T11	1.61-1.71	4	-	1	-	-	1	19	-	-	4	-	29
5	6644, 6645	T11	1.71-2.04	2	-	3	-	-	4	41	-	-	-	-	50
5	6432, 6433	T11	2.04-2.15	1	3	-	-	-	3	18	-	1	-	-	26
			Sum of shells	1	9	4	-	-	8	78	-	1	4	-	105

TABLE 2 (Continued)

Stratigraphic unit	IG UFRS	Registration number	Archaeological horizon	Depth (m)	Fruticicola cf. fedtschenkoi (Martens, 1874) sp.	Candaharia (Levanderiella) nopsis (Simroth, 1901) sp.	Gibbulinopsis (Mousson, 1873) sp.	Leucozonella sp.	Pseudonapaeus asiaticus (Mousson, 1880) in Martens, 1880	Pseudonapaeus secalinus (Mousson, 1880) in Martens, 1880	Pseudonapaeus sogdianus (Martens, 1874) sp.	Pseudonapaeus stabilis chatkalicus (Kuznetsov, 1999) sp.	Turana mar-tensiana (Ancey, 1886) shells	Total number of mollusk shells
6	6440,	Г11	14	2.15-2.27	-	3	-	-	3	19	-	-	-	25
		6441												
6	6418-6-	Г11	15	2.27-2.50	-	1	-	-	4	22	-	-	-	27
		421												
6	6428-6-	Г11	16	2.50-2.74	-	1	-	-	3	18	-	-	2	24
		431												
				Sum of shells	-	5	-	-	10	59	-	-	2	76
4	6391-6-	Д11	3	0.61-0.73	-	6	9	1	4	29	1	1	-	51
		394												
4	6372	Д11	4	0.73-0.80	-	1	-	-	-	-	-	-	-	1
4	6403-6-	Д11	5	0.80-0.93	-	5	15	4	7	82	-	-	-	113
		406												
4	6397-6-	Д11	6	0.93-1.02	-	5	10	3	7	61	-	-	-	86
		402												
4	6373-6-	Д11	8	1.00-1.28	-	7	14	27	15	243	-	2	-	308
		378												
4	6371	Д11	9	1.29-1.52	-	3	-	-	1	7	-	-	-	11
4	6379,	Д11	10	1.52-1.71	-	2	1	-	2	52	-	1	-	58
		6380												
				Sum of shells	-	29	49	35	36	474	1	4	-	628
5	6395,	Д11	11	1.71-1.90	-	4	1	1	2	29	-	-	-	37
		6396												
5	6381-6-	Д11	12	1.90-2.16	-	5	2	2	12	52	15	-	1	89
		383												
5	6407-6-	Д11	13	2.16-2.26	-	11	-	2	4	180	-	-	-	339
		410												

(Continues)

TABLE 2 (Continued)

Stratigraphic unit	IG UFRS' Registration number	Archaeological horizon	Depth (m)	Fruticola cf. fedtschenkoi (Martens, 1874) sp.	Candaharia (Levanderiella) levanderi (Simroth, 1901) sp.	Gibbulinopsis signata (Mousson, 1873) sp.	Pseudonapaeus asiaticus (Mousson in Martens, 1880) sp.	Pseudonapaeus secalinus (Mousson in Martens, 1880) sp.	Pseudonapaeus sogdianus (Martens, 1874) sp.	Pseudonapaeus stabilis chatkalicus (Kuznetsov, 1999) sp.	Pseudonapaeus turanensis (Ancey, 1886) sp.	Total number of mollusk shells
			Sum of shells	20	3	5	156	261	15	-	1	465
6	6384-6-387	D11 16	2.54-2.74	2	2	2	7	50	2	-	-	65
6	6388-6-390	D11 17	2.74-2.92	9	15	8	7	34	6	2	-	81
			Sum of shells	11	17	10	14	84	8	2	-	146

Asia are a result of vertical wind shear caused by wind patterns between the westerly jet stream and the western extension of a massive collection of cold air (i.e., Siberian high) (Shi et al., 2020). According to Li et al. (2020), the Siberian high had a noticeable impact on wind dynamics and therefore on loess accumulation up to the Late Glacial in western Tien Shan.

### 5.1.2 | Macrostructural and textural markers of depositional processes

Among the six stratigraphic units identified in the field, one represents an artificial modern deposit (Unit 2, a dump left by Soviet excavations in the 1960s-1970s) and two are soil horizons (Unit 1: recent post-Soviet excavation topsoil, Unit 3: pre-Soviet excavation soil). Within the actual talus deposits, we identified only three stratigraphic units (Units 6, 5, and 4). They differ slightly from each other mostly in terms of the grain size distribution, that is, the ratio between the skeleton (gravel- and boulder-sized limestone clasts) and the matrix (mostly silty and sandy material). Sedimentary structures are almost lacking. The only ones recorded are as follows:

1. weak lamination, weakly aligned coarse clasts, and presence of lenses of loess-like material in the lowermost part of Unit 6;
2. erosional bottom of Unit 5;
3. weakly aligned coarse clasts locally within Units 4 and 5.

Some of these structures may indicate the temporal activity of water-related erosion and/or accumulation, such as linear erosion and sheet washing. Except for these poorly visible structures, the entire sequence was homogeneous. The sediments showed diamicton characteristics. The sorting is very poor; however, two grain size fractions are predominant: >10 and <1 mm. The intermediate fraction, that is, 1-10 mm, rarely exceeded 15% of the sediment weight. The two predominant fractions likely correspond to two main depositional processes, namely, colluvial deposition (rockfalls and related processes) and aeolian accumulation (Krajcarz et al., 2014). Therefore, the proportion between these two components may serve as a rough approximation of the contributions of the two main depositional processes. However, this must be considered with caution, as other processes could have possibly been involved and could have distorted the proportion between the two fractions (e.g., secondary physical disintegration of coarse limestone clasts into finer particles; vertical movement of fine particles, for instance via illuviation; earthquakes responsible for rapid accumulation of coarse clasts; mixing by bioturbation and/or cryoturbation, etc.).

The analysis of coarse (>10 mm) and fine (<1 mm) fraction ratios in the sequence (Figure 4) revealed a general coarsening-upward tendency in Units 6-5 and relative stabilization in Units 5-4. We considered this as a preponderance of aeolian deposition during the early stage (Unit 6, mostly the lower part), progressively replaced by the accumulation of debris, with a peak of debris accumulation recorded in Unit 5.

**TABLE 3** OSL dating results

Sample	Stratigraphic unit	Depth (cm)	Lab ID	Dose (Gy)	<i>n</i>	Quartz dose (Gy ka <sup>-1</sup> )	Age (ka)	pIRIR/Q	IR/Q	Q well-bleached
OBS-I-6	4	70	188296	33.0 ± 2.2	16	3.5 ± 0.2	9.5 ± 0.8	1.3 ± 0.1	0.6 ± 0.1	+
OBS-I-1	4	80	188253	23.0 ± 0.5	17	2.6 ± 0.1	8.8 ± 0.5	1.0 ± 0.1	0.6 ± 0.1	+
OBS-I-2	4	140	188254	30.3 ± 1.6	14	3.2 ± 0.1	9.3 ± 0.7	1.0 ± 0.1	0.5 ± 0.1	+
OBS-I-3	5	190	188255	24.1 ± 0.7	22	1.6 ± 0.1	14.9 ± 0.8	1.0 ± 0.1	0.5 ± 0.1	+
OBS-I-4	6	240	188256	24.5 ± 0.5	14	1.3 ± 0.1	18.9 ± 1.0	1.1 ± 0.1	0.6 ± 0.1	+
OBS-I-5	6	320	188297	27.3 ± 1.3	17	1.4 ± 0.1	19.2 ± 1.3	5.2 ± 0.4	0.8 ± 0.1	

Note: The protocol for estimating quartz (Q) bleaching is presented in Section 4.7.

### 5.1.3 | Micromorphological indicators of depositional processes

Evidence of colluvial processes is found in the high frequency of coarse platy limestone rock fragments randomly distributed in thin sections, as suggested by the high numbers of coarse grain count and the CL/f-related distribution, which is mainly porphyric (Figure 6). Moreover, at the microscale, the lack of sedimentological structures such as lamination, layering, and/or sorting, the massive or blocky microstructure, where distinguishable and not obliterated by bioturbation (Figure S6e,f), are all indicators of colluvial deposition (Bertran & Texier, 1999).

Micromorphological analyses also revealed clay-coated pieces within the sediments (Figure 6). This feature could be a result of various processes, for instance of saltation processes typical for rockfalls before the debris finally ends its downslope run, aeolian accumulation of dust on exposed clast surfaces, and post-depositional translocation processes involving the clasts and the matrix later on. Indirect evidence of colluvial processes may come from the orientation of rock fragments commonly characterized by carbonate rinds, coats, and in one case, pendants (Blank & Fosberg, 1990). Importantly, throughout the entire profile, coats, which usually accumulate on the undersides of fragments (1990), can present different orientations (Figure S6a,d,i,j). Post-depositional translocation processes may have been responsible for the reorientation of grains and, therefore, for the different orientations of their accumulations (Figure 6). Supporting post-depositional translocation, we also observed fragments of limpid yellow/orange clayey material (Figure S6n,r), common in the entire sequence, and coated grains (Figures 6 and S6b,h,i). Importantly, we recorded horizontally oriented plant fragments in Units 5, 4, and 3 (Figure 6).

Most of the carbonate accumulations are physically damaged and/or eroded (Figure S6d), resulting in the detachment of smaller particles. This may be linked to post-depositional parent material disintegration in situ. Parent weathering material processes also result in cryptocrystalline calcite nodules, Mn/Fe oxide nodule formation (Figures 6 and S6l), and iron coatings. The micromorphological results also showed that the site was heavily affected by bioturbation and pedogenic processes (e.g., illuviation and iron coating). Supposedly, we recognized three pedogenic phases for the presence, relatively high frequency, and association of certain key features (e.g., pedogenic, human-related, and bioturbation features) (Figure 6):

(i) just below the erosional lower boundary of Unit 5, possibly connected to the first cultural horizon; (ii) Unit 3; and (iii) Unit 1. The micromorphological data clearly show the effect (e.g., presence of calcite infillings, iron coatings, cappings, and bone and/or coprolite fragments) (Figure 6) that these pedogenic phases had on the portion of sediments just below the recognized soil horizons (Figure 6). We may also assume that having observed a difference between secondary accumulations as described in Figure S6i,j, some accumulations may be younger than others and linked to recent biological activity and may be in situ, but this needs further study.

Rounded silt- and sand-sized calcite grains, presumably linked to aeolian activity, are associated with quartz, mica, and feldspar grains (Miller, 2015). At Obishir-I, we did not observe distinct layers of loess at the microscale. In the literature, this is considered a rather common phenomenon, especially for cave sediments being washed into the cavity (Goldberg et al., 2007; Mallol & Goldberg, 2017). In our case, the lack of distinct layers can be a result of simultaneous deposition on rock fragments, and the massive microstructure characterizing the fine material can provide evidence for redeposition downward soon after (Josephs, 2010). The low porosity in Unit 6 may also indicate the relocation of fine particles rather than original loess-like accumulation.

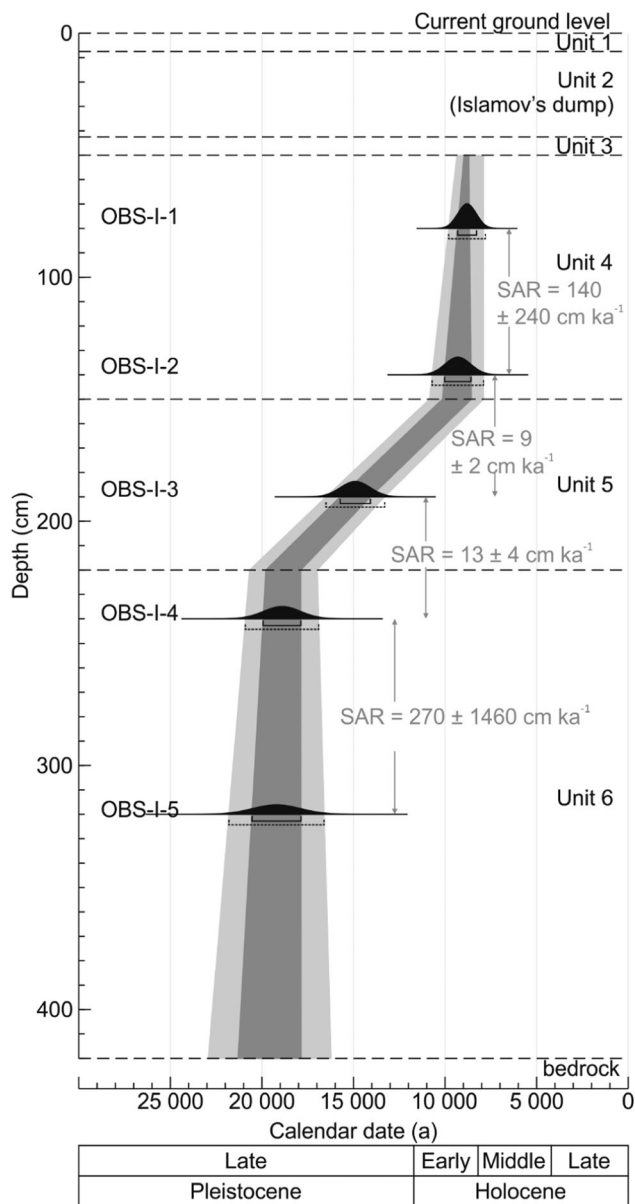
In terms of the porosity, we observed increasing values from the bottom to the top of the profile (Figure 6) as a result of both natural compaction (as suggested by the deformed shape of a shell; Figure S6m) for the lowermost deposits and faunal and plant activity, which mainly affected the uppermost units (Figure 6).

### 5.1.4 | Geochemical markers of depositional processes

While the coarse clasts at Obishir-I are almost solely Paleozoic limestone pieces of colluvial origin (relatively autochthonous), the fine material could have been deposited by several processes:

- (i) aeolian accumulation, then it is mostly allochthonous material (according to micromorphological analysis, mostly rounded calcareous, quartz, mica, and feldspar grains);
- (ii) physical disintegration of larger limestone pieces, then it is autochthonous limestone material; and





**FIGURE 8** Age–depth model for Obishir-I. The rate and its error are calculated for  $1\sigma$  (standard deviation) for OSL dates according to the method presented in the Supporting Information Material S2. The dark gray field shows the age–depth model for  $1\sigma$  for OSL dates, and the light gray field shows the age–depth model for  $2\sigma$ . The modeled SAR shown here (gray fields) was drawn as a line connecting the ends of  $1\sigma$  (standard deviations) of OSL dates within a stratigraphic unit, extrapolated further toward the top and bottom of the unit. For Unit 5, with only one date, the lines were drawn toward the lines of Units 4 and 6. Only OBS-I-1 to -5 dates have been considered in the model, due to the fact that they were collected from the same wall, whereas OBS-I-6 was collected on another wall (see Figure 3)

(iii) illuviation and/or recrystallization, which can represent variable mineral phases, including secondary autochthonous soil calcite.

Analysis of the Ca content in the fine fraction may help to distinguish type (i), which is expected to be Ca-depleted, from types (ii) and (iii), which are supposed to be Ca-enriched. In the sequence,

we observed a general increasing tendency of Ca content in the  $<1$  mm fraction (Figure 5), and similarly, an increasing  $\text{CaCO}_3$  content (Figure 5). A peak of  $\text{CaCO}_3$  content was recorded in Unit 5. This correlates well with the information derived from the grain size analysis and indicates the progressive replacement of aeolian deposition by colluvial debris during the accumulation of Units 6 and 5. In Unit 4 the  $\text{CaCO}_3$  content varied. At the bottom of the unit it is low, perhaps suggesting that the aeolian sedimentation briefly became more intense; whereas at the top of the same unit  $\text{CaCO}_3$  increased again. This peak may be contributed to secondary depositional processes related to calcite precipitation, as suggested by the micromorphological data.

### 5.1.5 | Sedimentary gaps

Several macro- and microscale features allow us to identify sedimentary hiatuses in the Obishir-I sequence. The first is the presence of erosional structures. These have only been found in two stratigraphic positions—within the lowest part of Unit 6 and at the boundary between Units 6 and 5. The presence of lamination and variable lithology in the lowest part of Unit 6 indicates numerous, possibly short-term, gaps connected to alternating erosion and accumulation. The large erosional structure between Units 6 and 5 indicates the massive and rapid removal of sediments. The edge of this structure is visible in the S wall of the excavation area (Figure S2 in the Supporting Information Material S2), which indicates that the hiatus is locally limited, and sediments removed in one place have been preserved in another.

The second indicator of sedimentary gaps, resulting from a halt of sedimentation, is the presence of soil-related features. A well-preserved paleosol A horizon (Unit 3) was found directly below the dump left by the Soviet excavators. This soil records a decline in the depositional processes after the deposition of Unit 4. Similar soil is also preserved at the top of the Soviet dump, which suggests that the paleosol of Unit 3 developed under climatic and ecological conditions similar to the present day. Connected to the soil formation in Unit 3, we recorded an upward increase in biological activity-related features at the microscale. This pedogenic event affected all the lower deposits, especially Units 5–2, whereas deeper parts were only rarely affected (lower part of Units 4 and 5), and it did not reach the deepest parts (Unit 6), because of lack of bioturbation. For instance, soil mesofauna reworked features are common in Units 5–2 (one of the several examples is shown in Figure S6q), as well as associated pedofeatures such as groundmass compaction around animal burrows (Figure S6q). Organic and organo-mineral excrements were also recorded (Figures 6 and S6j,m,q,s). Plant fragments were recorded, and their presence increased upward within the profile (Figures 6 and S6s,t). Plant activity was also recorded in the soil by well-rounded vesicles (Figure S6i,s) surrounded by hypocotings and channels filled with fine-grained calcite (Figure S6g). Features related to bioturbation are responsible for the complex microstructure (Figure S6p,s), as they cut and/or overlay the older ones. In addition, the micromorphological analysis allowed us to identify possible ex situ soil, which was not visible in the

field. This was recorded within the uppermost part of Unit 6, in MM1B II (Figures 6 and S6), by randomly distributed charcoal fragments (Figure S6n), bone fragments, and dusty textural pedofeatures (Figure S6k). The aforementioned characteristics are also common in Unit 3 (sample MM4 II), except for charcoal fragments. Pedogenic processes can also be recorded by increased concentrations of nutrients related to biological activity, such as organic matter, organic C, N, and P. All these indices show a general upward-increasing tendency (Figure 5), with a peak coinciding with the current soil (Unit 1). If we look at the geochemical proxy for the intensity of pedogenesis, that is, the  $K_2O/Na_2O$  ratio (Figure 5), pedogenic processes were fairly active at the bottom and central parts of Unit 6, with an increasing trend from the LGM–LG transition (Unit 6 uppermost part), and they reached a peak at the bottom of Unit 4, which is in line with the micromorphology data (Figure 6). The ratio also increased in Unit 1. Unfortunately, Unit 3 was not sampled for bulk analyses; therefore, the geochemical ratio showed a decreasing trend (decreasing pedogenesis) and did not confirm sedimentological results at this stratigraphic position, but we assume that this is possibly related to sampling resolution.

## 5.2 | Age of sediments and accumulation rate

According to chronometric results, the deposition of Unit 6 can be dated to late Last Glacial Maximum (LGM), as indicated by two similar OSL dates:  $19.2 \pm 1.3$  and  $18.9 \pm 1.0$  ka. The lowest sample was collected around 100 cm above the bedrock, so we cannot exclude the fact that the lower part of the sequence represents an earlier period, for example, early LGM. The date  $14.9 \pm 0.8$  ka, obtained for Unit 5, indicates the Late Glacial. The  $1\sigma$  range for this date falls within the late part of Greenland Stadial (GS) 2.1a and Greenland Interstadial (GI) 1e, up to the very beginning of GI 1d (according to the GS/GI boundaries proposed by Rasmussen et al. (2014). The e–d phases of GI 1 have been traditionally linked to the Bølling Interstadial (Björck et al., 1998). In the case of Unit 4, all achieved dates fall within a range of ~10–8 ka, representing the Early Holocene up to the very beginning of the Middle Holocene. The uppermost OSL sample was collected only 30 cm below the top of Unit 4. This suggests that later geochronological units (i.e., the remaining part of the Middle Holocene and the entire Late Holocene) are only poorly recorded or not recorded at all in the sequence of the Obishir-I talus cone.

The sedimentation rate within the sequence varied. The part of the sequence (about 250 cm thick) that was dated, accumulated between 19–8 ka. This indicates an average SAR of approximately  $25 \text{ cm ka}^{-1}$ . However, the actual deposition rate was possibly much higher, at least temporarily. This is suggested by the presence of erosional events (such as the one recorded at the bottom of Unit 5) and possibly some depositional breaks (such as those recorded by the presence of two human settlement phases). The position of the dated samples allowed us to identify three phases within the entire profile. In Units 6 and 4, the sedimentation rate was high, exceeding  $100 \text{ cm ka}^{-1}$ , whereas the middle part of the sequence (Unit 5) coincides with a low accumulation rate (Figure 8). This may lead to the conclusion that Unit 5 faced erosional processes.

## 5.3 | Paleoclimatic and paleoecological conditions of the deposition

Recently, deposition of any sort (colluvial and aeolian) at Obishir-I must have declined compared to the Late Pleistocene–Early/Middle Holocene. Some fresh limestone clasts occur at the current terrain surface, and fresh aeolian dust may be found on everyday objects. Nevertheless, the development of the paleosol (Unit 3), which continued during the decades that followed the development of Unit 1, indicates that present-day climatic conditions favor pedogenesis rather than aggradation. Considering the arid modern climate, we conclude that the past (pre-Middle Holocene) local conditions must have been more humid. This enabled increased frost action, resulting in the physical disintegration of limestone cliffs and the production of debris.

Micromorphologically, biogenic carbonates (i.e., snail shells or a few fragments and bird-egg fragments; see Figure S6i,m) increase upward in the section (Figure 6). The increasing frequency of snail shells may be further evidence of the shift toward climatic optimum conditions (Figure 6). In terms of bone and coprolite fragments (Figure 6), their size and frequency increase upward (e.g., bone fragments are medium-sand sized in Unit 6 and up to gravel-sized in Unit 3). This trend can be the result of diagenetic dissolution (Karkanas et al., 2000); if so, it should be considered with caution in the paleoclimatic interpretation.

The earliest phase, connected to increased aeolian activity during the accumulation of Unit 6, was likely linked to another climate. The conditions were possibly more arid and colder, involving desertification and the accumulation of loess material. At the microscale, a few vertically oriented coarse clasts occur in Unit 6 as well as shattered clasts (Figure S6e,c), large pores below coarse rock fragments (Figure S6f), weakly developed planes, and well-developed clay capping overhead limestone grains (Figure 6; Figure S6c) (Van Vliet-Lanoë, 1998; Van Vliet-Lanoë et al., 2004) which were not observed elsewhere.

This reasoning is also supported by mollusk results. Although the mollusk assemblage did not reveal any changes in the species structure from the LGM (Unit 6) to the Mid-Holocene strata (Units 3 and 4) (Table 2), the taxonomic composition of mollusks of different stratigraphic levels and different numbers of individuals may reveal different paleobiotopes. We may assume that the climate recorded in Unit 6 was cold and dry; it progressively changed from warm and wet (Unit 4) to dry, but still warm in Units 1–3. A similar tendency was observed at the Obishir-V site (Osipova et al., 2021). Data comparisons of mollusks from the two sections  $\Gamma 11$  and  $\Delta 11$  possibly suggest a disturbance in the lower units in section  $\Delta 11$  (Table 2). This was confirmed by the occurrence of 15 slug individuals during the LGM.

## 5.4 | Human occupation

The collection of lithics from Units 6 and 5 was not numerous, and the tool set was very poor. The types of identified artifacts, such as core flakes, bladelets, microbladelets, end-scrapers, backed microblades, and notched pieces, are common in the wide spectrum of late

Upper Paleolithic up to early Neolithic complexes of Central Asia. Analogies could be found, for example, within assemblages of the late Kulbulakian (Kolobova et al., 2013), Tutkaulian (Shnaider et al., 2020), and Obishirian industries (Shnaider et al., 2017). Although not numerous, the lithic assemblages from Units 6 and 5 were similar to each other. Most of the artifacts were found in the upper part of Unit 6, close to the boundary between Units 6 and 5, and within Unit 5 (Figure 7), leading to the conclusion that the original depositional context for these artifacts was presumably the upper part of Unit 6 or the lowermost part of Unit 5. This is also posited by micromorphological characteristics in this part of the sequence. Dusty cappings are possibly related to human activity (Figure S6k), which were recorded just below the erosional surface of Units 6 and 5, which are generally associated with exposed soils and/or soils affected by cultivation (Brammer, 1971; Gebhardt, 1988; Sauzet et al., 2016). Interestingly, charcoal fragments were recorded at the same stratigraphic position (Figures 6 and S6n), possibly as by-products of fireplace events. It is possible that a micro and angular fragment of debitage was recorded in Unit 6 (Figure S6e). It seems that the erosional event, as indicated by the erosional structure at the bottom of Unit 5, was likely responsible for the partial destruction of the integrity of the assemblage, followed by the redeposition of some artifacts at the bottom of the erosional structure (a scour). Some artifacts were also redeposited later within the sediment of Unit 5.

The collection from Unit 4 was much more abundant. According to the techno-typological characteristics, this assemblage is similar to the final Epipaleolithic-early Neolithic complex from the neighbor Obishir-V (Shnaider et al., 2017), and also to the Oshhona site (Pamir Mountains), which are dated between 10 and 7 ka B.P. (Ranov, 1988). This dating fits well with the OSL dates for Unit 4. The assemblage seems to be slightly evenly scattered throughout several dozen centimeters of the upper part of Unit 4. Several theoretical reasons for this dispersal can be considered as follows:

- (i) several repeated visits of human groups;
- (ii) colluvial redeposition of artifacts from another original position, somewhere up in the slope; and
- (iii) post-depositional disturbance of the assemblage integrity, for example, by bioturbation.

Explanation (i) seems unlikely to act solely because no clear horizons could be identified. Explanation (ii) is possible in light of the southward inclination of the assemblage, as shown in Figure 7. The visible linear arrangement of larger clasts in the middle of Unit 4, right below the lithic assemblage, may represent a residual pavement corresponding to the weakly marked erosional boundary. Following this interpretation, the upper part of Unit 4 would record a similar erosion-accumulation event as that recorded in Unit 5. Micromorphology may also support explanation (iii). Concomitant with the second and possibly last sequence of human occupation in Units 4 and 3, we recorded an increase in the soil biological activity and in the frequency and size of bone and coprolite fragments, which are often among the major material indicators of human occupation of a site

(Karkanas et al., 2002). Based on the analysis, we suggest that the cultural layers were displaced due to colluvial and bioturbation processes. The lithic collection is not numerous and is mainly represented by debris, and the small number of artifacts and its unambiguous stratigraphic context do not allow us to conclude on the functionality of the site and the term of occupation.

## 5.5 | Reconstruction of depositional history

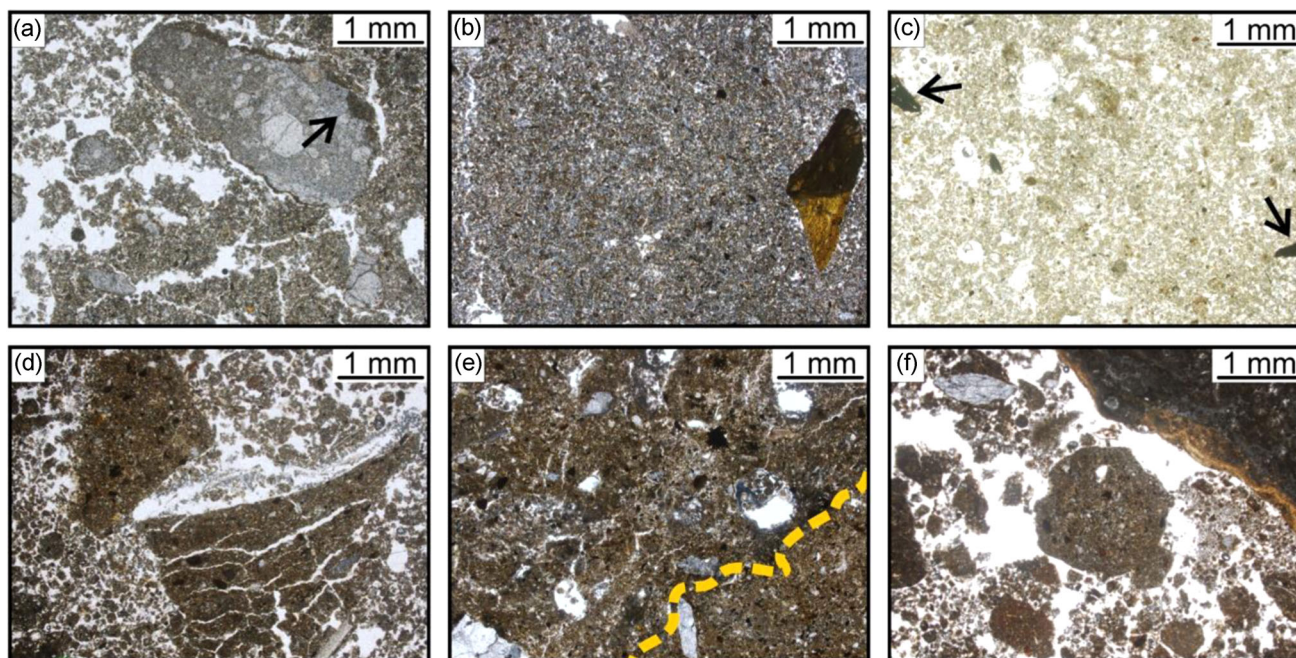
### 5.5.1 | LGM

Aeolian sedimentation is an important depositional agent, especially in the early stage of the talus cone, thus providing information about climatic conditions. Aeolian dust accumulation is typically associated with glacial activity and periglacial environments. Nonetheless, the upper part of Unit 6 dates to the late LGM, and possibly the lower part can be attributed to early LGM. The sedimentological (loess-like lenses) and grain size data (prominent silt fraction) discussed previously may confirm this interpretation. In addition, micromorphological data may record frost action by such microfeatures, such as clay capping and vertically aligned rock fragments (Figures 6 and 9a,b), even if not frequently observed. Additionally, the aeolian accumulation in the talus occurred presumably simultaneously with the coarser fraction of sediments and translocated downward only later on. Semi-quantitative geochemical proxy estimation for paleoclimate changes at Obishir-I revealed a low alteration at the bottom of the profile (Figure 5); this is in line with the assumption that only during warm and more humid periods (interstadial and/or interglacial) environmental conditions allow extensive weathering (Bugge et al., 2011). The landscape that prevailed during the accumulation of these deposits was possibly open stony habitats with grassy (steppe) vegetation cover, as suggested by the results of the mollusk data for Unit 6 (*Pseudonapaeus* species predominance; Table 2). The number of extracted individuals was low (76 in square Г11 and 142 in square Д11), which is 44 shells per sample on average. This, together with the large number of shell fragments, possibly suggests cold and dry climatic conditions.

During the time span considered here, cold climate has been recorded both globally (LGM) and regionally. For instance, dry mountain steppe vegetation and low vegetation cover were recorded in the eastern Pamir from lake Karakul (Heinecke et al., 2018). Moreover, loess deposition connected to glacial and periglacial climatic condition was recorded in the north-western part of Kyrgyzstan before ~15 ka B.P. (Li et al., 2020).

### 5.5.2 | Late glacial

Following the late LGM, micromorphological evidence of burning, that is, charcoal fragments randomly distributed in the uppermost part of Unit 6 (Figures 6, S6n, and 9c), just below the erosional



**FIGURE 9** (a) and (b) Siltic-textured soil characterizing the central part of Unit 6, vughy and blocky alternating massive microstructure, vertical planes, clay capping (arrow), and vertical oriented clasts (b) were interpreted as frost action microfeatures (thin section: MM1A II). (c) Yellowish more loamy soil with a fine granular microstructure with a low degree of separation of aggregates and angular charcoal fragments (arrows) represents the ex situ soil observed in the upper part of Unit 6, just below the scour structure (Unit 5 lower boundary—MM1B II). (d) Early and Mid-Holocene soil is more brownish with loamic texture characterized by large soil mesofauna structures in which coarse pedons (different internal fabric can be observed) are surrounded by finer organo-mineral excrements (MM3 I). (e) Boundary (dashed line) between Unit 4 and Unit 3 (dark paleosol below Islamov's dump); the microstructure of Unit 3 is complex, whereas Unit 4 shows mainly a massive structure (MM4 I). (f) Coarse granular microstructure with a high degree of separation as an effect of soil fauna activity characterizes the top of Unit 3 (MM4 II). The photomicrographs are in plane polarized light [Color figure can be viewed at [wileyonlinelibrary.com](http://wileyonlinelibrary.com)]

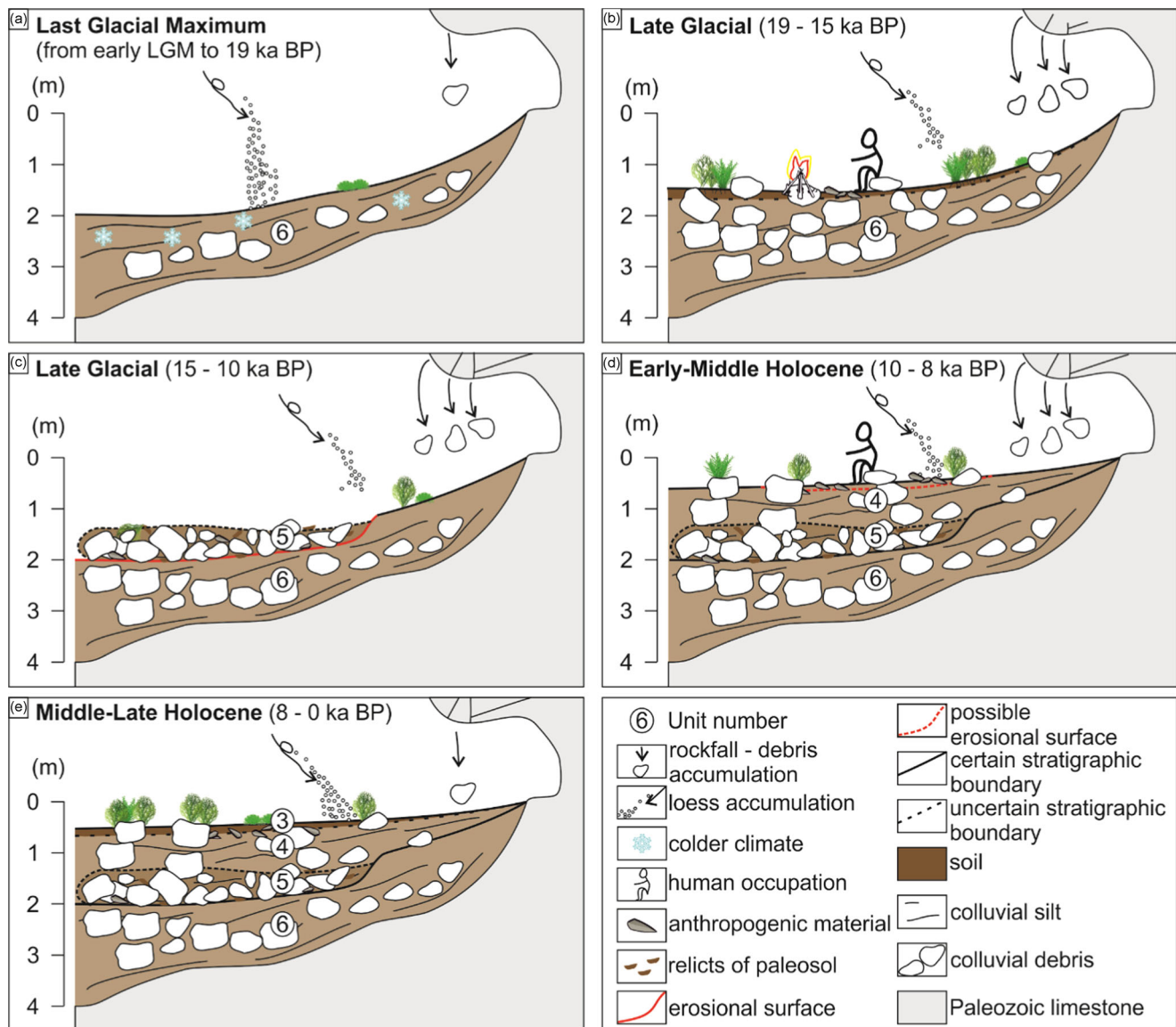
boundary of Unit 5, may support the interpretation of fire-related events, such as the presence of human activity (e.g., fireplaces) or naturally occurring wildfires. Indirectly, the aforementioned evidence may reveal the presence of soil formation, perhaps under relatively temperate interstadial conditions developed before the fire-related events. An increase in the trend of chemical alteration of minerals is showed at the LGM–LG transition (Figure 5), maybe confirming that environmental conditions were shifting toward moister conditions, therein allowing weathering processes. A logical consequence of land clearance caused by fires could have been the intensification of surface erosion, recorded by the presence of the macroerosional surface at the bottom of Unit 5, as well as by yellowish angular clayey fragments, and coated grains observed under the microscope (Figures 6 and S6n,r). This period was characterized by an increase in debris production (Figure 4). Slope processes were possibly more conspicuous in response to both relatively warmer and wetter climatic conditions, glacier retreat, and human activity, at the end of the LGM with the transition to the Late Glacial Interstadial. The upper part of Units 6 and 5 and the lower part of Unit 4 were therefore affected by a more efficient frost-cracking acting on the adjacent cliff, thereby resulting in a slightly greater amount of clast accumulation. The landscape was still characterized by open stony habitats and grassy (steppe) vegetation cover, as suggested by the mollusk assemblage (*Pseudonapaeus* species continued to prevail; Table 2). In

addition, we may assume a slight improvement in the climatic conditions, given the increasing number of total sums of shells in Unit 5 (105 at square Г11 and 465 at square Д11; on average 95 shells per sample).

The transition toward moister conditions from ~19 ka B.P. onward is in line also with the lake-level record from lake Karakul in eastern Pamir (Heinecke et al., 2017) and with an overall increasing trend of moisture from 19 to 15 ka B.P. recorded in north-western Kyrgyzstan (Li et al., 2020, Figure 8). Li et al. (2020) also proposed that climatic conditions were very different before and after ~15 ka B.P. and probably associated with migration of latitudinal climatic zones and large-scale changes in atmospheric circulation in Central Asia controlled by the Northern Hemisphere ice sheets. At Obishir-I, this transition period (~15 ka B.P.) coincides with the peak of debris accumulation (Unit 5) within the talus cone (Figure 4).

### 5.5.3 | Early–Middle Holocene

Following this instability event, the onset of a phase of stabilization enhanced burrowing (coarse soil mesofauna chambers described in Units 5 and 4), pedogenesis processes, and several successive phases of calcite dissolution and aggradation marked by calcitic infillings commonly recorded in Units 5–2 (e.g., Figures S6g and 9d).



**FIGURE 10** Reconstruction of the depositional history at the Obishir-I rock shelter. (a) Last Glacial Maximum. Accumulation of the bottom part of Unit 6 under cold and periglacial conditions where aeolian processes were dominant. (b) Late Glacial. Accumulation of the top part of Unit 6. Shifting to more humid conditions with a weakly formed soil, more efficient frost cracking and the first human occupation horizon (unknown Paleolithic). (c) Late Glacial. Accumulation of Unit 5 possibly due to a localized erosional event after fire-related events. (d) Early-Middle Holocene. Accumulation of Unit 4. Onset of the Holocene. Second cultural occupation horizon (Obishirian). (e) Middle-Late Holocene. Soil formation and consequently cease of accumulation (Unit 3) [Color figure can be viewed at [wileyonlinelibrary.com](http://wileyonlinelibrary.com)]

This is also suggested by semiquantitative proxies, for the trend of alteration started increasing at the LGM-LG transition showing a peak for Units 5 and 4 (Figure 5). Interestingly, gypsum accumulation was recorded by the high concentration of S (lrb %) recorded in the top part of Unit 6 (Supporting Information Material S3). Calcite aggradation at the top part of Unit 4 is also supported by the chemical data (Figure 5). A gradual increase in Ca is visible from the bottom part of Unit 5, with a maximum reaching the central part of Unit 4. Concomitantly, the amount of P (lrb %) also increased, thus providing evidence for greater biological activity and pedogenic processes (Figure 5). Mollusk data may support the shift toward more favorable climatic conditions during the accumulation of Unit

4. An increase in humidity and an increase in temperature might have been responsible for the increasing number of mollusks (563 in square  $\Gamma$ 11 and 626 in square  $\Delta$ 11; on average 91 shells per sample) and slugs (Table 2).

The aforementioned stability phase coincides with the onset of the Holocene and more humid conditions in the microregion (Heinecke et al., 2017; Jiang et al., 2020; Osipova et al., 2021). In line with our results, a generally wetter Early to Mid-Holocene climate was recorded from many lakes in western and arid Central Asia including north-western China and Mongolia (Chen et al., 2008; Khenzykhenova et al., 2021; Mathis et al., 2014; X. Yang & Scuderi, 2010; X. P. Yang et al., 2011). Conversely, higher moisture

availability during the Early Holocene is not reflected in the vegetation signals of Lake Karakul in eastern Pamir (Heinecke et al., 2018).

#### 5.5.4 | Middle–Late Holocene

This period supposedly coincides with a halt in the accumulation processes favoring the development of soils that we distinguished as Unit 3 (Figure 9e,f) and Unit 1. A decrease in the alteration trend is noted from the central part of Unit 4 to Unit 1 if we consider the CPA index (Figure 5); this is likely due to changes toward less moist conditions. Despite the similar mollusk species composition between the Middle and Late Holocene and the Early–Middle Holocene intervals, the number of individuals significantly decreased (from >90 shells per sample in the Early–Middle Holocene to only 15 shells in a sample collected from Unit 3), possibly indirectly demonstrating changes toward more arid climatic conditions. Mollusks inhabited open stony slopes covered by steppe vegetation. Regionally, a similar trend was noted in eastern Pamir, and central and northern Tien Shan (Heinecke et al., 2018; Ricketts et al., 2001), but was not in the lake Kichikol record in southern Tien Shan—just north of the Alay range—possibly due to local effects on climatic changes (Beer et al., 2007).

## 6 | CONCLUSIONS

The methodology applied allowed us to provide a reasonable account of the Quaternary talus cone at Obishir-I. We were able to recognize the main site formation processes and corroborate our geological and archaeological interpretation, and we have been able to reconstruct the depositional history of the site (Figure 10). The Quaternary succession at the Obishir-I site is quite uniform. It comprises mainly unconsolidated, poorly sorted talus deposits, namely, diamicton of differing textures. Six units were distinguished (Units 1–6, descending), of which Units 6 to 4 represent the actual talus deposit, accumulated between the end of the Late Pleistocene and the early Middle Holocene. Units 3 and 1 are, respectively, a paleosol weakly developed before Soviet archaeological campaigns and the current topsoil. Unit 2 is an artificial modern deposit left by Soviet excavators. Interestingly, for Units 6 and 5, we recorded an *ex situ* paleosol, which provided important information about the depositional history reconstruction. Generally, we assumed that the talus is a rockfall cone, that is, accumulated thanks to rockfall events from the adjacent cliff, with infiltrated finer material of allochthonous (aeolian) and autochthonous (illuviation and/or recrystallization) origins. The fine infiltrated material resulted from aeolian and endogenous sedimentation (e.g., limestone weathering and disintegration, and illuviation). The former possibly accumulated simultaneously with the debris, whereas the latter occurred mainly *in situ* when the climate shifted to more humid conditions. Due to the presence of some diagnostic microfeatures (*ex situ* soil formation), we can






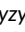


assume that a localized mass movement may have possibly occurred subsequent to land clearance. Importantly, we identified two human occupation sequences within the talus cone deposits. The former occurred between 19 and 15 ka B.P. and resembles the Upper Paleolithic up to the early Neolithic complexes of Central Asia. The latter, embedded mainly in Unit 4 ca. 10–8 ka B.P., is similar to the final Epipaleolithic–early Neolithic Obishirian complex from the neighbor Obishir-V (Shnaider et al., 2017), as well as to the Oshhona site (Pamir mountains).

Obishir-I is not the only archaeological site of the stone age in a similar setting. Situated at the foot of the Eshme Ridge are also other well-known sites such as Obishir-V and Sel'Ungur. A better understanding of the geological processes involved in the southern flank of the Eshme Ridge can therefore provide relevant knowledge of the history of archaeological sites in this microregion and possibly allows us to perform intraregion lithostratigraphic correlations. Moreover, for the first time, geological and, more importantly, micromorphological results are presented here for sediments in a semiarid mountain climate at one of the Obishirian sites and they are paleoclimatically and paleoenvironmentally correlated with neighboring regions.

### ACKNOWLEDGMENTS

We would like to express our special thanks to our colleagues: Dr. K. Kolobova and Dr. A. Krivoschapkin from the Institute of Archaeology and Ethnography SB RAS, Dr. T. Charynov from Kyrgyz National University, and Dr. B. Viola from University of Toronto for their assistance, cooperation, and friendship. We are grateful to volunteers and students from Batken University, Novosibirsk State University, and National Kyrgyz University for their hard work in the field and all people who took part in this study. We are also thankful to the anonymous reviewers for their valuable comments and suggestions. This study was funded by National Science Centre, Poland, grant number 2018/29/B/ST10/00906. Excavation, luminescence dating, and analysis of lithic materials were supported by RSF project #19-78-10053 “The emergence of food-producing economies in the high mountains of interior Central Asia.” Malacological study was performed thanks to Russian State Program N-0246-2019-0118 and N-FMRS-2022-0010.

### ORCID

Greta Brancaleoni  <http://orcid.org/0000-0002-5563-3724>  
 Svetlana Shnaider  <http://orcid.org/0000-0003-2230-4286>  
 Evgeniya Osipova  <http://orcid.org/0000-0003-3414-7409>  
 Guzel Danukalova  <http://orcid.org/0000-0001-7602-5923>  
 Redzhep Kurbanov  <https://orcid.org/0000-0001-6727-6202>  
 Saltanat Alisher kyzy  <http://orcid.org/0000-0003-3138-0942>  
 Aida Abdykanova  <http://orcid.org/0000-0002-7238-9065>  
 Maciej T. Krajcarz  <https://orcid.org/0000-0002-1240-0664>

### REFERENCES

Beck, H. E., Zimmermann, N. E., McVicar, T. R., Vergopolan, N., Berg, A., & Wood, E. F. (2018). Present and future Köppen-Geiger climate

- classification maps at 1-km resolution. *Scientific Data*, 5(1), 1–12. <https://doi.org/10.1038/sdata.2018.214>
- Beer, R., Heiri, O., & Tinner, W. (2007). Vegetation history, fire history and lake development recorded for 6300 years by pollen, charcoal, loss on ignition and chironomids at a small lake in southern Kyrgyzstan (Alay Range, Central Asia). *Holocene*, 17(7), 977–985. <https://doi.org/10.1177/0959683607082413>
- Bertran, P., & Texier, J. P. (1999). Facies and microfacies of slope deposits. *Catena*, 35(2–4), 99–121. [https://doi.org/10.1016/S0341-8162\(98\)00096-4](https://doi.org/10.1016/S0341-8162(98)00096-4)
- Björck, S., Walker, J. C., Cwynar, L. C., Johnsen, S., Knudsen, K.-L., Lowe, J. J., & Wohlfarth, B. (1998). An event stratigraphy for the Last Termination in the North Atlantic region based on the Greenland ice-core record: A proposal by the INTIMATE group. *Journal of Quaternary Science*, 13(4), 283–292. [https://doi.org/10.1002/\(SICI\)1099-1417\(199807/08\)13:4.3.CO;2-A](https://doi.org/10.1002/(SICI)1099-1417(199807/08)13:4.3.CO;2-A)
- Blank, R. R., & Fosberg, M. A. (1990). Micromorphology and classification of secondary calcium carbonate accumulations that surround or occur on the undersides of coarse fragments in Idaho (U.S.A.). *Developments in Soil Science*, 19(C), 341–346. [https://doi.org/10.1016/S0166-2481\(08\)70345-3](https://doi.org/10.1016/S0166-2481(08)70345-3)
- Blott, S. J., & Pye, K. (2001). GRADISTAT: A grain size distribution and statistics package for the analysis of unconsolidated sediments. *Earth Surface Processes and Landforms*, 26(11), 1237–1248. <https://doi.org/10.1002/esp.261>
- Brammer, H. (1971). Coatings in seasonally flooded soils. *Geoderma*, 6(1), 5–16. [https://doi.org/10.1016/0016-7061\(71\)90047-4](https://doi.org/10.1016/0016-7061(71)90047-4)
- Buggle, B., Glaser, B., Hambach, U., Gerasimenko, N., & Marković, S. (2011). An evaluation of geochemical weathering indices in loess-paleosol studies. *Quaternary International*, 240(1–2), 12–21. <https://doi.org/10.1016/j.quaint.2010.07.019>
- Chen, F., Yu, Z., Yang, M., Ito, E., Wang, S., Madsen, D. B., Huang, X., Zhao, Y., Sato, T., Birks, H. J. B., Boomer, I., Chen, J., An, C., & Wünnemann, B. (2008). Holocene moisture evolution in arid central Asia and its out-of-phase relationship with Asian monsoon history. *Quaternary Science Reviews*, 27(3–4), 351–364. <https://doi.org/10.1016/j.quascirev.2007.10.017>
- Cooke, R., Warren, A., & Goudie, A. (1993). *Desert geomorphology*. UCL Press.
- Courty, M. A., Goldberg, P., & Macphail, R. I. (1989). *Soils and micromorphology in archaeology*. Cambridge University Press.
- Field, J., & Banning, E. B. (1998). Hillslope processes and archaeology in Wadi Ziqlab, Jordan. *Geoarchaeology*, 13(6), 595–616. [https://doi.org/10.1002/\(sici\)1520-6548\(199808\)13:6.3.co;2-a](https://doi.org/10.1002/(sici)1520-6548(199808)13:6.3.co;2-a)
- French, C. (2019). *A handbook of geoarchaeological approaches to settlement sites and landscapes, a handbook of geoarchaeological approaches to settlement sites and landscapes*. Oxbow Books. <https://doi.org/10.2307/j.ctvh1dthr>
- Gebhardt, A. (1988). Evolution du paysage agricole au cours du Sub-atlantique dans la région de Redon (Morbihan, France). Apport de la micromorphologie. *Bulletin de l'Association française pour l'étude du quaternaire*, 25(4), 197–203. <https://doi.org/10.3406/quate.1988.1882>
- Goldberg, P., Laville, H., Meignen, L., & Bar-Yosef, O. (2007). *Stratigraphy and geoarchaeological history of Kebara Cave* (pp. 49–84). American School of Prehistoric Research, Peabody Museum, Harvard University Press.
- Goldberg, P., & Macphail, R. I. (2013). *Practical and theoretical geoarchaeology*. Blackwell Publishing Ltd. <https://doi.org/10.1002/9781118688182>
- Hales, T. C., & Roering, J. J. (2005). Climate-controlled variations in scree production, Southern Alps, New Zealand. *Geology*, 33(9), 701–704. <https://doi.org/10.1130/G21528.1>
- Heinecke, L., Fletcher, W. J., Mischke, S., Tian, F., & Herzschuh, U. (2018). Vegetation change in the eastern Pamir Mountains, Tajikistan, inferred from Lake Karakul pollen spectra of the last 28 kyr. *Palaeogeography, Palaeoclimatology, Palaeoecology*, 511, 232–242. <https://doi.org/10.1016/j.palaeo.2018.08.010>
- Heinecke, L., Mischke, S., Adler, K., Barth, A., Biskaborn, B. K., Plessen, B., Nitze, I., Kuhn, G., Rajabov, I., & Herzschuh, U. (2017). Climatic and limnological changes at Lake Karakul (Tajikistan) during the last ~29 cal ka. *Journal of Paleolimnology*, 58(3), 317–334. <https://doi.org/10.1007/s10933-017-9980-0>
- Hétu, B., & Gray, J. T. (2000). Effects of environmental change on scree slope development throughout the postglacial period in the Chic-Choc Mountains in the northern Gaspé Peninsula, Quebec. *Geomorphology*, 32(3–4), 335–355. [https://doi.org/10.1016/S0169-555X\(99\)00103-8](https://doi.org/10.1016/S0169-555X(99)00103-8)
- Hughes, P. D. (2010). Geomorphology and Quaternary stratigraphy: The roles of morpho-, litho-, and allostratigraphy. *Geomorphology*, 189–199. <https://doi.org/10.1016/j.geomorph.2010.07.025>
- Islamov, U. I. (1972). Mesoliticheskie pamyatniki Ferganskoy doliny. *Istoriya materialnoy kultury Uzbekistana*, (9), 21–28.
- Islamov, U. I. (1980). *Obishirskaya kultura (Obishir culture)*. Phan.
- Jiang, Q., Jianan, Z., Yufeng, Y., Wenwei, Z., & Dongliang, N. (2020). A persistently increasing precipitation trend through the Holocene in Northwest China recorded by black carbon  $\delta^{13}C$  from Sayram Lake. *Frontiers in Earth Science*, 8, 228. <https://doi.org/10.3389/feart.2020.00228>
- Johnstone, S. A., Schwartz, T. M., & Holm-Denoma, C. S. (2019). A stratigraphic approach to inferring depositional ages from detrital geochronology data. *Frontiers in Earth Sciences*, 7(7), 57. <https://doi.org/10.3389/feart.2019.00057>
- Josephs, R. L. (2010). Micromorphology of an early holocene loess-paleosol sequence, central Alaska, U.S.A. *Arctic, Antarctic, and Alpine Research*, 42(1), 67–75. <https://doi.org/10.1657/1938-4246-42.1.67>
- Karkanas, P., Bar-Yosef, O., Goldberg, P., & Weiner, S. (2000). Diagenesis in prehistoric caves: The use of minerals that form in situ to assess the completeness of the archaeological record. *Journal of Archaeological Science*, 27(10), 915–929. <https://doi.org/10.1006/jasc.1999.0506>
- Karkanas, P., & Goldberg, P. (2018). *Reconstructing archaeological sites: Understanding the geoarchaeological matrix, reconstructing archaeological sites*. Wiley-Blackwell. <https://doi.org/10.1002/9781119016427>
- Karkanas, P., Rigaud, J. P., Simek, J. F., Albert, R. M., & Weiner, S. (2002). Ash bones and guano: A study of the minerals and phytoliths in the sediments of Grotte XVI, Dordogne, France. *Journal of Archaeological Science*, 29(7), 721–732. <https://doi.org/10.1006/jasc.2001.0742>
- Khenzykhenova, F., Dorofeyuk, N., Shchetnikov, A., Danukalova, G., & Bazarova, V. (2021). Palaeoenvironmental and climatic changes during the Late Glacial and Holocene in the Mongolia and Baikal region: A review. *Quaternary International*, 605–606, 300–328. <https://doi.org/10.1016/j.quaint.2021.04.038>
- Kolobova, K. A., Flas, D., Derevianko, A. P., & Pavlenok, K. (2013). The Kulbulak bladelet tradition in the upper paleolithic of central Asia. *Archaeology, Ethnology and Anthropology of Eurasia*, 41(2), 2–25. <https://doi.org/10.1016/j.aeae.2013.11.002>
- Krajcarz, M. T. (2019). Alteration of the metal content in animal bones after 2.5-year experimental exposure to sediments. *Archaeological and Anthropological Sciences*, 11(1), 361–372. <https://doi.org/10.1007/s12520-017-0533-2>
- Krajcarz, M. T., Bosák, P., Šlechta, S., Pruner, P., Komar, M., Dresler, J., & Madeyska, T. (2014). Sediments of biśnik cave (Poland): Lithology and stratigraphy of the middle palaeolithic site. *Quaternary International*, 326–327, 6–19. <https://doi.org/10.1016/j.quaint.2013.10.017>
- Krajcarz, M. T., Kot, M., Pavlenok, K., Fedorowicz, S., Krajcarz, M., Lazarev, S. Y., Mroczek, P., Radzhabov, A., Shnaider, S., Szymanek, M., & Szycmzak, K. (2016). Middle Paleolithic sites of Katta Sai in western Tian Shan piedmont, Central Asiatic loess zone: Geoarchaeological investigation of the site formation and the integrity of the lithic assemblages. *Quaternary International*, 399, 136–150. <https://doi.org/10.1016/j.quaint.2015.07.051>

- Krajcarz, M. T., Szymanek, M., Krajcarz, M., Pereswiet-Soltan, A., Alexandrowicz, W. P., & Sudol-Procyk, M. (2020). Shelter in Smoleń III—A unique example of stratified Holocene clastic cave sediments in Central Europe, a lithostratigraphic stratotype and a record of regional paleoecology. *PLoS One*, *15*, 0228546. <https://doi.org/10.1371/journal.pone.0228546>
- Krivoshapkin, A., Viola, B., Charginov, T., & Krajcarz, M. (2020). Middle Paleolithic variability in Central Asia: Lithic assemblage of Sel'Ungur cave. *Quaternary International*, *535*, 88–103. <https://doi.org/10.1016/j.quaint.2018.09.051>
- Li, Y., Song, Y., Orozbaev, R., Dong, J., Li, X., & Zhou, J. (2020). Moisture evolution in Central Asia since 26 ka: Insights from a Kyrgyz loess section, Western Tian Shan. *Quaternary Science Reviews*, *249*, 106604. <https://doi.org/10.1016/j.quascirev.2020.106604>
- Likharev, I. M., & Rammelmeier, E. S. (1952). Nazemnye molluski fauny SSSR [Land molluscs of the fauna of the USSR]. In E. N. Pavlovsky, & A. A. Strelkov (Eds.), *Determinative tables of the USSR fauna* (pp. 511). Academy of Sciences of USSR Press.
- Likharev, I. M., & Viktor, A. I. (1980). *Slizni fauny SSSR i sopredel'nykh stran (Gastropoda terrestrial nuda) [Slugs of the fauna of the USSR and neighboring countries (Gastropoda terrestrial nuda)]*, Fauna of the USSR. *Mollusca*. Nauka Press.
- Ložek, V. (1964). 'Quartärmollusken der Tschechoslowakei', Rozpravy ústředního ústavu geologického, Sv. 31. Praha Verl. d. Tschechoslowak. Akademie d. Wissenschaften [Stuttgart]. [Schweizerbart in Komm.].
- Macphail, R. I., & Goldberg, P. (2017). *Applied soils and micromorphology in archaeology*, applied soils and micromorphology in archaeology. Cambridge University Press. <https://doi.org/10.1017/9780511895562>
- Mallol, C., & Goldberg, P. (2017). Cave and rock shelter sediments. *Archaeological Soil and Sediment Micromorphology* (pp. 359–381). John Wiley & Sons Ltd. <https://doi.org/10.1002/9781118941065.ch34>
- Mathis, M., Sorrel, P., Klotz, S., Huang, X., & Oberhänsli, H. (2014). Regional vegetation patterns at lake Son Kul reveal Holocene climatic variability in central Tien Shan (Kyrgyzstan, Central Asia). *Quaternary Science Reviews*, *89*, 169–185. <https://doi.org/10.1016/j.quascirev.2014.01.023>
- Miller, C. E. (2015). *A tale of two Swabian Caves: Geoarchaeological investigations at Hohle Fels an Geissenkloesterle*. Kerns Verlag.
- Möller, P., & Murray, A. S. (2015). Drumlinised glaciofluvial and glaciolacustrine sediments on the Småland peneplain, South Sweden—New information on the growth and decay history of the Fennoscandian Ice Sheets during MIS 3. *Quaternary Science Reviews*, *122*, 1–29. <https://doi.org/10.1016/j.quascirev.2015.04.025>
- Monigal, K. (2002). *The Levantine leptolithic: Blade technology from the Lower Paleolithic to the dawn of the Upper Paleolithic* (Unpublished Ph.D. dissertation). Southern Methodist University.
- Morley, M. W., Goldberg, P., Sutikna, T., Tocheri, M. W., Prinsloo, L. C., Saptomo, W., Jatmiko, Wasisto, S., & Roberts, R. G. (2017). Initial micromorphological results from Liang Bua, Flores (Indonesia): Site formation processes and hominin activities at the type locality of *Homo floresiensis*. *Journal of Archaeological Science*, *77*, 125–142. <https://doi.org/10.1016/j.jas.2016.06.004>
- Mroczek, P. (2008). *Interpretacja paleogeograficzna cech mikromorfologicznych neoplejstocenijskich sekwencji lessowo-glebowych*. UMCS.
- Mücher, H., van Steijn, H., & Kwaad, F. (2010). Colluvial and mass wasting deposits. In G. Stoops, V. Marcelino, & F. Mees (Eds.), *Interpretation of micromorphological features of soils and regoliths* (pp. 37–48). Elsevier B.V. <https://doi.org/10.1016/B978-0-444-53156-8.00003-9>
- Murray, A. S., Thomsen, K. J., Masuda, N., Buylaert, J. P., & Jain, M. (2012). Identifying well-bleached quartz using the different bleaching rates of quartz and feldspar luminescence signals. *Radiation measurements*, *47*(9), 688–695. <https://doi.org/10.1016/j.radmeas.2012.05.006>
- Nelson, A. R. (1992). Lithofacies analysis of colluvial sediments—An aid in interpreting the recent history of Quaternary normal faults in the Basin and Range Province, western United States. *Journal of Sedimentary Petrology*, *62*(4), 607–621. <https://doi.org/10.1306/D426796F-2B26-11D7-8648000102C1865D>
- Osipova, E., Danukalova, G., Brancaleoni, G., Krajcarz, M. T., Abdykanova, A., & Shnaider, S. (2021). Palaeoenvironmental conditions of the Palaeolithic–Neolithic transition in the Fergana Valley (Central Asia)—New data inferred from fossil molluscs in Obishir-V rockshelter (Kyrgyzstan). *Quaternary International*, *605*–606, 287–299. <https://doi.org/10.1016/j.quaint.2020.11.009>
- Pawelec, H., & Ludwikowska-Kędzia, M. (2016). Macro- and micromorphologic interpretation of relict periglacial slope deposits from the Holy Cross Mountains, Poland. *Permafrost and Periglacial Processes*, *27*(2), 229–247. <https://doi.org/10.1002/ppp.1864>
- Ranov, V. A. (1988). *Kamennyi vek Yuzhnogo Tadzhikistana i Pamira (Stone Age of southern Tajikistan and Pamir)*. Novosibirsk State University.
- Räsänen, M. E., Auri, J. M., Huitti, J. V., Klap, A. K., & Virtasalo, J. J. (2009). A shift from lithostratigraphic to allostratigraphic classification of Quaternary glacial deposits. *GSA Today*, *19*(2), 4–11. <https://doi.org/10.1130/GSATG20A.1>
- Rasmussen, S. O., Bigler, M., Blockley, S. P., Blunier, T., Buchardt, S. L., Clausen, H. B., Cvijanovic, I., Dahl-Jensen, D., Johnsen, S. J., Fischer, H., Gkinis, V., Guillevic, M., Hoek, W. Z., Lowe, J. J., Pedro, J. B., Popp, T., Seierstad, I. K., Steffensen, J. P., & Winstrup, M. (2014). A stratigraphic framework for abrupt climatic changes during the Last Glacial period based on three synchronized Greenland ice-core records: Refining and extending the INTIMATE event stratigraphy. *Quaternary Science Reviews*, *106*, 14–28. <https://doi.org/10.1016/j.quascirev.2014.09.007>
- Ricketts, R. D., Johnson, T. C., Brown, E. T., Rasmussen, K. A., & Romanovsky, V. V. (2001). The Holocene paleolimnology of Lake Issyk-Kul, Kyrgyzstan: Trace element and stable isotope composition of ostracodes. *Palaeogeography, Palaeoclimatology, Palaeoecology*, *176*(1–4), 207–227. [https://doi.org/10.1016/S0031-0182\(01\)00339-X](https://doi.org/10.1016/S0031-0182(01)00339-X)
- Sanders, D. (2010). Sedimentary facies and progradational style of a Pleistocene talus-slope succession, Northern Calcareous Alps, Austria. *Sedimentary Geology*, *228*(3–4), 271–283. <https://doi.org/10.1016/j.sedgeo.2010.05.002>
- Sanders, D., Ostermann, M., & Kramers, J. (2009). Quaternary carbonate-rocky talus slope successions (Eastern Alps, Austria): Sedimentary facies and facies architecture. *Facies*, *55*(3), 345–373. <https://doi.org/10.1007/s10347-008-0175-z>
- Sauzet, O., Cammas, C., Barbillon, P., Etienne, M.-P., & Montagne, D. (2016). Illuviation intensity and land use change: Quantification via micromorphological analysis. *Geoderma*, *266*, 46–57. <https://doi.org/10.1016/j.geoderma.2015.11.035>
- Shi, L., Zhang, J.-H., Yao, F., Zhang, D., & Guo, H. (2020). Temporal variation of dust emissions in dust sources over Central Asia in recent decades and the climate linkages. *Atmospheric Environment*, *222*, 117176. <https://doi.org/10.1016/J.ATMOENV.2019.117176>
- Shileyko, A. A. (1984). Nazemnye molluski Pupillina (Gastropoda, Pulmonata i Geophila) [Land molluscs of the Pupillina (Gastropoda, Pulmonata, and Geophila)]. *Fauna of the USSR. Mollusca* (Vol. 3, Issue 3, pp. 399). Nauka-Press.
- Shileyko, A. A., & Rymzhanov, T. S. (2013). *Fauna nazemnykh molluskov Kazakhstana i sopredel'nykh territoriy [The fauna of land molluscs of Kazakhstan and adjacent territories]*. Tovarishchestvo nauchnykh izdaniy KMK Press.
- Shnaider, S. V., Kolobova, K. A., Filimonova, T. G., & Taylor, W. (2020). New insights into the Epipaleolithic of western Central Asia: The Tutkaulian complex. *Quaternary International*, *535*, 139–154. <https://doi.org/10.1016/j.quaint.2018.10.001>
- Shnaider, S. V., Krajcarz, M. T., Viola, T. B., Abdykanova, A., Kolobova, K. A., Fedorchenko, A. Y., Alisher-kyzy, S., &



- Krivoshapkin, A. I. (2017). New investigations of the Epipalaeolithic in western Central Asia: Obishir-5. *Antiquity*, 91(360), 6–12. <https://doi.org/10.15184/aqy.2017.213>
- Stoops, G. (2003). *Guidelines for analysis and description of soil and regolith thin sections*. Soil Science Society of America Inc.
- Sysoev, A., & Shileyko, A. (2009). *Land snails and slugs of Russia and adjacent countries*. Pensoft publishers.
- Taylor, W. T. T., Pruvost, M., Posth, C., Rendu, W., Krajcarz, M. T., Abdykanova, A., Brancaleoni, G., Spengler, R., Hermes, T., Schiavinato, S., Hodgins, G., Stahl, R., Min, J., Alisher Kyzy, S., Fedorowicz, S., Orlando, L., Douka, K., Krivoshapkin, A., Jeong, C., ... Shnaider, S. (2021). Evidence for early dispersal of domestic sheep into Central Asia. *Nature Human Behaviour*, 1–11. <https://doi.org/10.1038/s41562-021-01083-y>
- Turner, A. K. (1996). Colluvium and talus. In A. K. Turner, & R. L. Schuster (Eds.), *Landslides: Investigation and mitigation* (pp. 686). Transportation Research Board.
- UNEP, UNITAR & Zoï E. Network. (2009). *Khaidarkan mercury: Addressing primary mercury mining in Kyrgyzstan*.
- Van Vliet-Lanoë, B. (1998). Frost and soils: Implications for paleosols, paleoclimates and stratigraphy. *Catena*, 34(1–2), 157–183. [https://doi.org/10.1016/S0341-8162\(98\)00087-3](https://doi.org/10.1016/S0341-8162(98)00087-3)
- Van Vliet-Lanoë, B., Fox, C. A., & Gubin, S. V. (2004). Micromorphology of Cryosols. In J. M. Kimble (Ed.), *Permafrost-affected soils* (pp. 365–390). Springer. [https://doi.org/10.1007/978-3-662-06429-0\\_18](https://doi.org/10.1007/978-3-662-06429-0_18)
- Ventra, D., Diaz, G. C., & De boer, P. L. (2013). Colluvial sedimentation in a hyperarid setting (Atacama Desert, northern Chile): Geomorphic controls and stratigraphic facies variability. *Sedimentology*, 60(5), 1257–1290. <https://doi.org/10.1111/sed.12029>
- Yang, X., & Scuderi, L. A. (2010). Hydrological and climatic changes in deserts of China since the late Pleistocene. *Quaternary Research*, 73(1), 1–9. <https://doi.org/10.1016/j.yqres.2009.10.011>
- Yang, X. P., Scuderi, L., & Paillou, P. (2011). Quaternary environmental changes in the drylands of China—A critical review. *Quaternary Science Reviews*, 30, 3219–3233. <https://doi.org/10.1016/j.quascirev.2011.08.009>
- Zhang, X., Liu, B., Wang, J., Zhang, Z., Shi, K., & Wu, S. (2014). Adobe photoshop quantification (PSQ) rather than point-counting: A rapid and precise method for quantifying rock textural data and porosities. *Computers and Geosciences*, 69, 62–71. <https://doi.org/10.1016/j.cageo.2014.04.003>

## SUPPORTING INFORMATION

Additional supporting information may be found in the online version of the article at the publisher's website.

**How to cite this article:** Brancaleoni, G., Shnaider, S., Osipova, E., Danukalova, G., Kurbanov, R., Deput, E., Alisher kyzy, S., Abdykanova, A., & Krajcarz, M. T. (2021). Depositional history of a talus cone in an arid intermontane basin in Central Asia: An interdisciplinary study at the Late Pleistocene–Late Holocene Obishir-I site, Kyrgyzstan. *Geoarchaeology*, 1–24. <https://doi.org/10.1002/gea.21892>

Detailed excavation planimetry

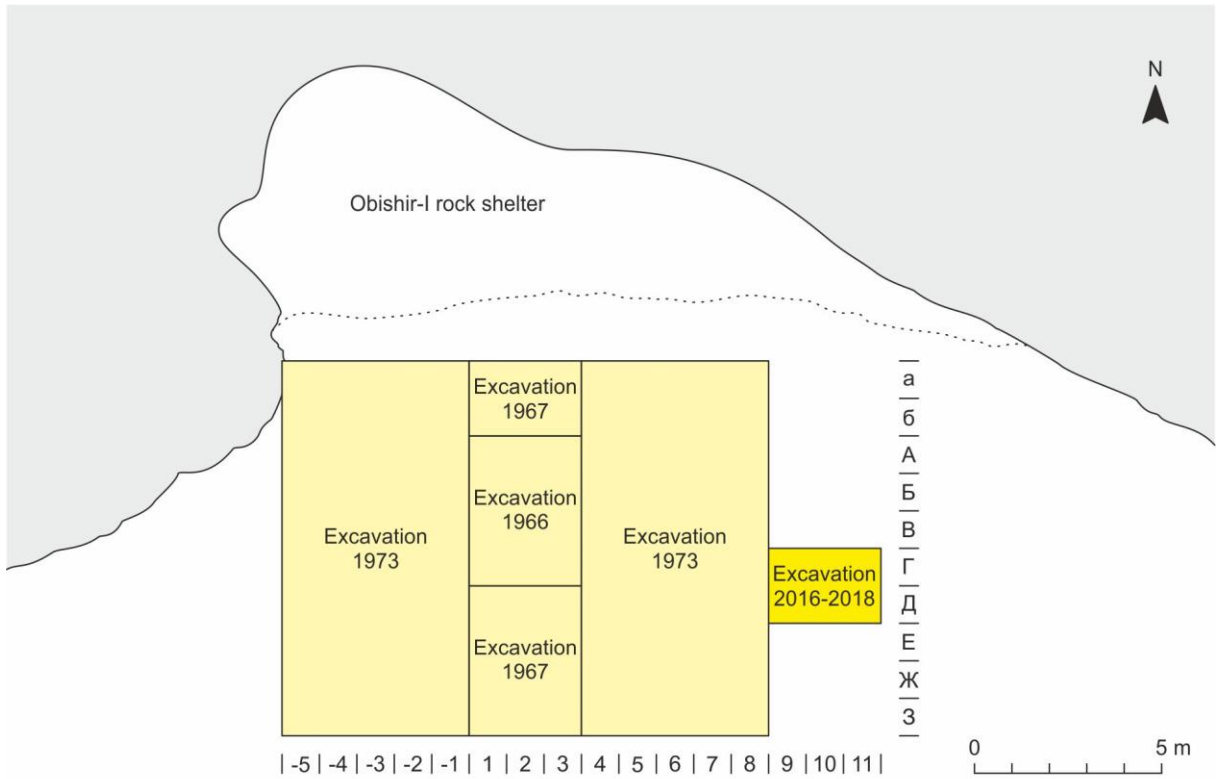


Figure S 1 Detailed excavation planimetry at Obishir-I

Sections

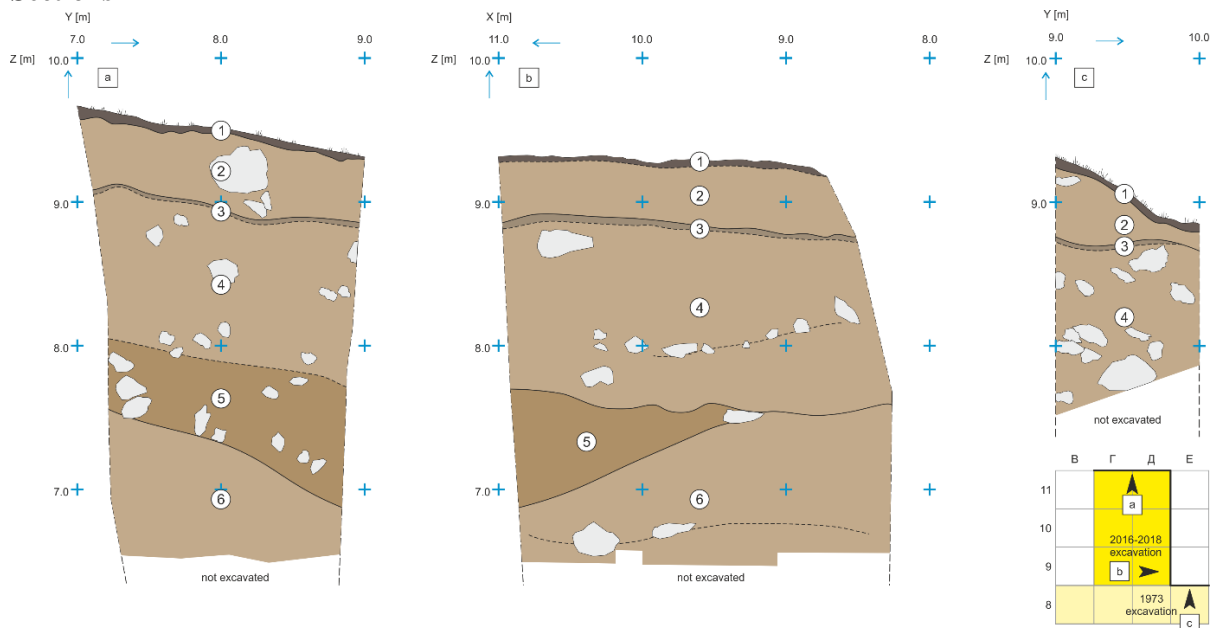


Figure S 2 Stratigraphic sequences exposed in the Eastern wall (a–c) and in the Southern wall (b).

## Sampling

The bulk samples for grain size and chemical analyses were collected with a bucket, taken in a rag sack and dried in the sunlight. The sampling weight varied between 100 g to 9 kg. Five undisturbed, oriented monoliths were extracted for micromorphological purposes. The extraction of blocks along one vertical line was not possible given the coarse nature of the deposit, for the blocks were collected where the matrix was just abundant to allow us a good extraction. We followed the sampling methodology proposed by Goldberg et al. (2003), but polyurethane foam was used instead of plaster. The foam is lighter and more elastic ensuring a safer air transport. The mollusk sampling was carried out following traditional methods during the archaeological excavations. The mollusks were collected after sieving the sediments with 5×5 mm and 1×1 mm mesh width sieves. For completeness, X, Y, Z coordinates of > 10 mm-sized shells were taken with the Total Station (Leica Total Station TS02 plus). The OSL samples were collected according to the methodology described by Nelson et al. (2015), i.e., at night with red torchlight, and secured by aluminum foil.

## Mollusk sampling

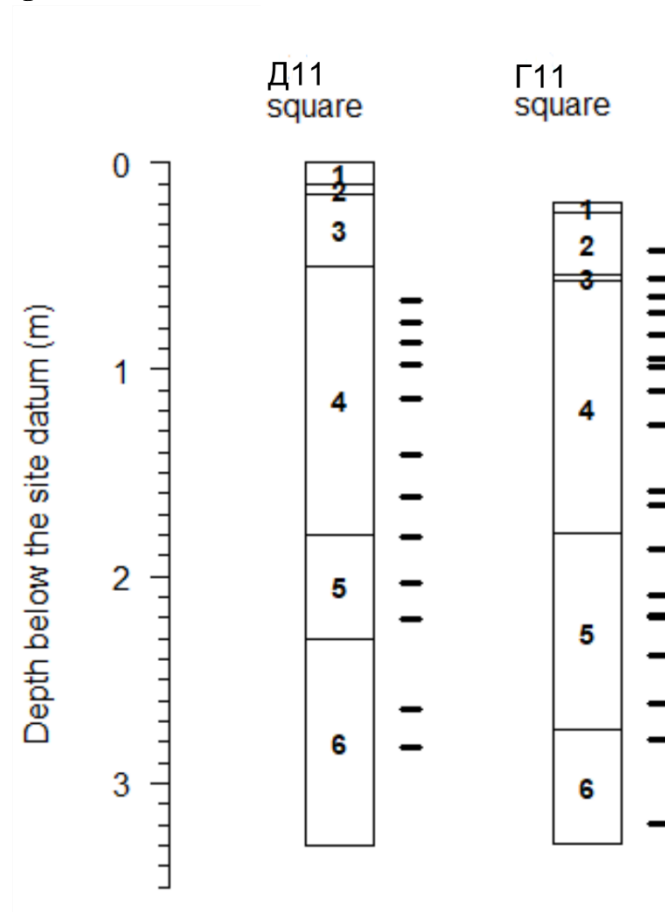


Figure S 3 Schematic stratigraphic logs with mollusk sampling location (black lines) divided per excavation squares

### Geochemical proxies

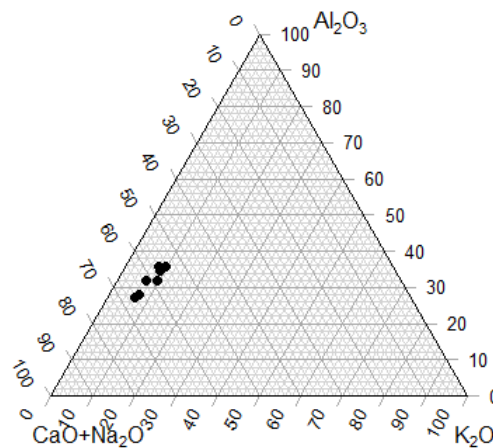
With the assumption that only warm periods and more humid periods (interstadial and/or interglacial) environmental conditions allowed extensive mineral weathering and thus soil formation (Bugge *et al.*, 2011), we calculated the following:

1. Chemical Proxy Alteration (CPA) index (molar ratio  $\text{Al}_2\text{O}_3 / (\text{Al}_2\text{O}_3 + \text{Na}_2\text{O}) \times 100$ ; Bugge *et al.*, 2011)
2.  $\text{Al}_2\text{O}_3/\text{TiO}_2$  ratio (molar proportion; Krajcarz *et al.*, 2016)
3.  $\text{K}_2\text{O}/\text{Na}_2\text{O}$  ratio (as above)

as semiquantitative proxies for paleoclimate changes at Obishir-I. As recommended by Bugge *et al.* (2011), we produced a A-CN-K diagram to check the CPA index reliability for our case (Figure S 4).

The concept of weathering indices as proxies of mineral alteration stands on the ratio of the concentration of the soluble and mobile elements to the rather immobile and non-soluble ones which we expect the soil to be enriched with (Bugge *et al.*, 2011; Krajcarz *et al.*, 2016). We chose the indices that best can be reliable in our case study. Being our sediments highly calcareous, these indices should reflect the silicate weathering and not be affected by  $\text{CaCO}_3$  dynamics within the profile. Nonetheless, they must be taken with caution being our sediments not exclusively loess deposits and the above indices are proposed for loess material.

CPA is proposed as the most appropriate index for silicate weathering and shouldn't be sensitive to dynamics of secondary carbonate and uncertainties in separating carbonate–Ca from silicate–Ca or from biases due to K–fixation (Bugge *et al.*, 2011).  $\text{Al}_2\text{O}_3/\text{TiO}_2$  ratio is described as a good paleo-weathering indicator by Krajcarz *et al.*, (2016) because fairly related with calcium dissolution/precipitation processes. Krajcarz *et al.*, (2016) also proposed  $\text{K}_2\text{O}/\text{Na}_2\text{O}$  ratio to estimate the intensity of pedogenesis at Katta Sai sites (Uzbekistan) because less independent from  $\text{Ca}^{2+}$  mobility.



**Figure S 4** The samples are plot closely together at a line parallel to A-CN, this is a typical distribution for material with different extent of chemical weathering, resulting in predominant removal of silicatic Ca and Na due to destruction of plagioclase (Bugge *et al.*, 2008)

## **Micromorphology**

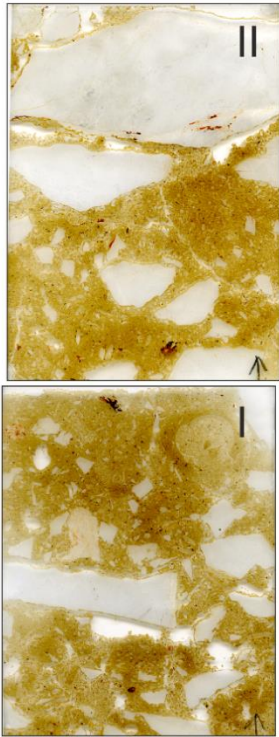
### **Thin section method**

The thin sections were produced by Ewa Deput in the sample preparation laboratory at the Institute of Geological Sciences (Polish Academy of Sciences – Warsaw). In the laboratory, the samples were carefully unwrapped and the foam was partially removed. The monoliths were air-dried for two weeks, carefully rinsed with ethanol, air-dried again, and impregnated with Araldite 2020, two-component epoxy resin. Impregnation was applied twice: once from one selected flat side, and when cured, from the opposite side. For curing, the samples were left at room temperature and under normal air pressure for 48 h each, thus enabling the epoxy to slowly infiltrate the sediment. The samples were not set in vacuum as this caused cracking during tests. For evaluating the impregnation, several millimeter-thick slabs were trimmed off from both sides of the monolith; if the inner part had not visually fully impregnated yet, the impregnation procedure was repeated. When properly impregnated, the monoliths were cut into circa 45×80 mm and 5-mm-thick slabs, using a circular saw with diamond-coated blades. The selected slabs were polished, glued onto 45×80 mm basal glass slides with Araldite 2020 and further polished with progressively finer polishing pastes to get 30 µm thin section.

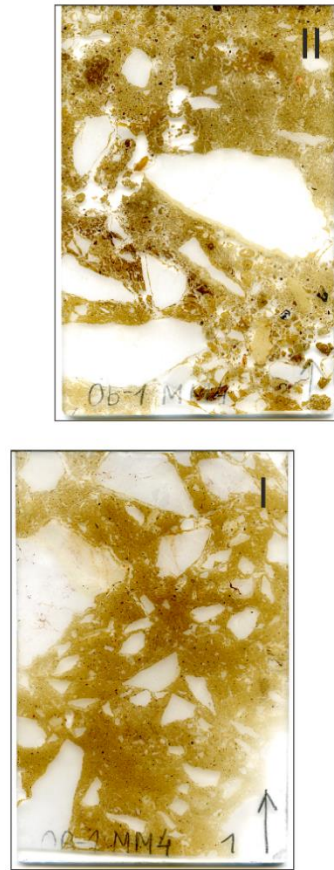
### **Quantitative analysis with Photoshop**

The porosity in percentage (empty voids) was calculated in selected microphotographs for each thin section produced, as the ratio between the total amount of pixels within the image and the pixels selected as voids with the color range tool in Photoshop v.C5, times 100. The Coarse Limestone (CL) and fine (f) ratio was calculated using the thin sections scans. First of all, due to some annotation directly taken on the thin section surface and to avoid to have the bare glass surface, the scans were resized. The bare glass surface can be easily misinterpreted for a limestone grain when using the Color Range tool. Then, the limestone grains were selected and the n. of pixels was annotated. As well as the micromass, meaning everything that was not limestone grain and porosity, was selected and the n. of pixels was annotated. The ratio was calculated between the n. of pixels for the limestone grains and the n. of pixels for the micromass. The limestone grains were counted one by one with the point counting tool within an area of 17 cm<sup>2</sup>, equal for each thin section.

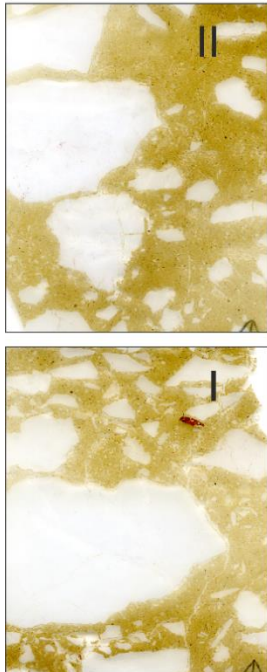
**MM 3**



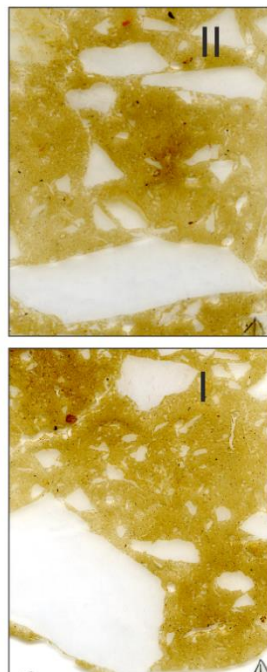
**MM 4**



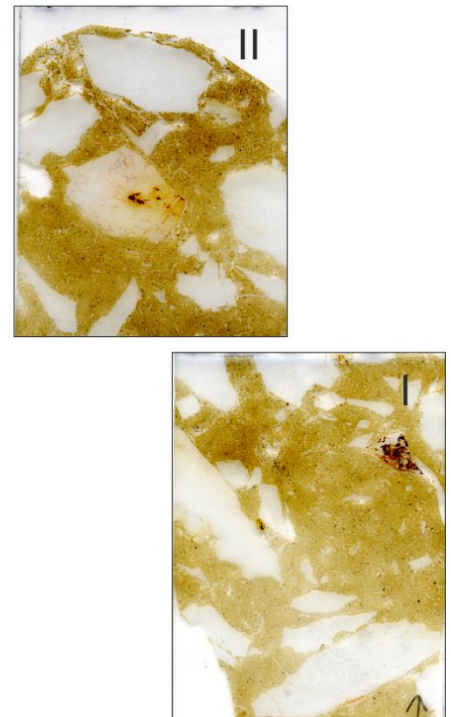
**MM 1a**



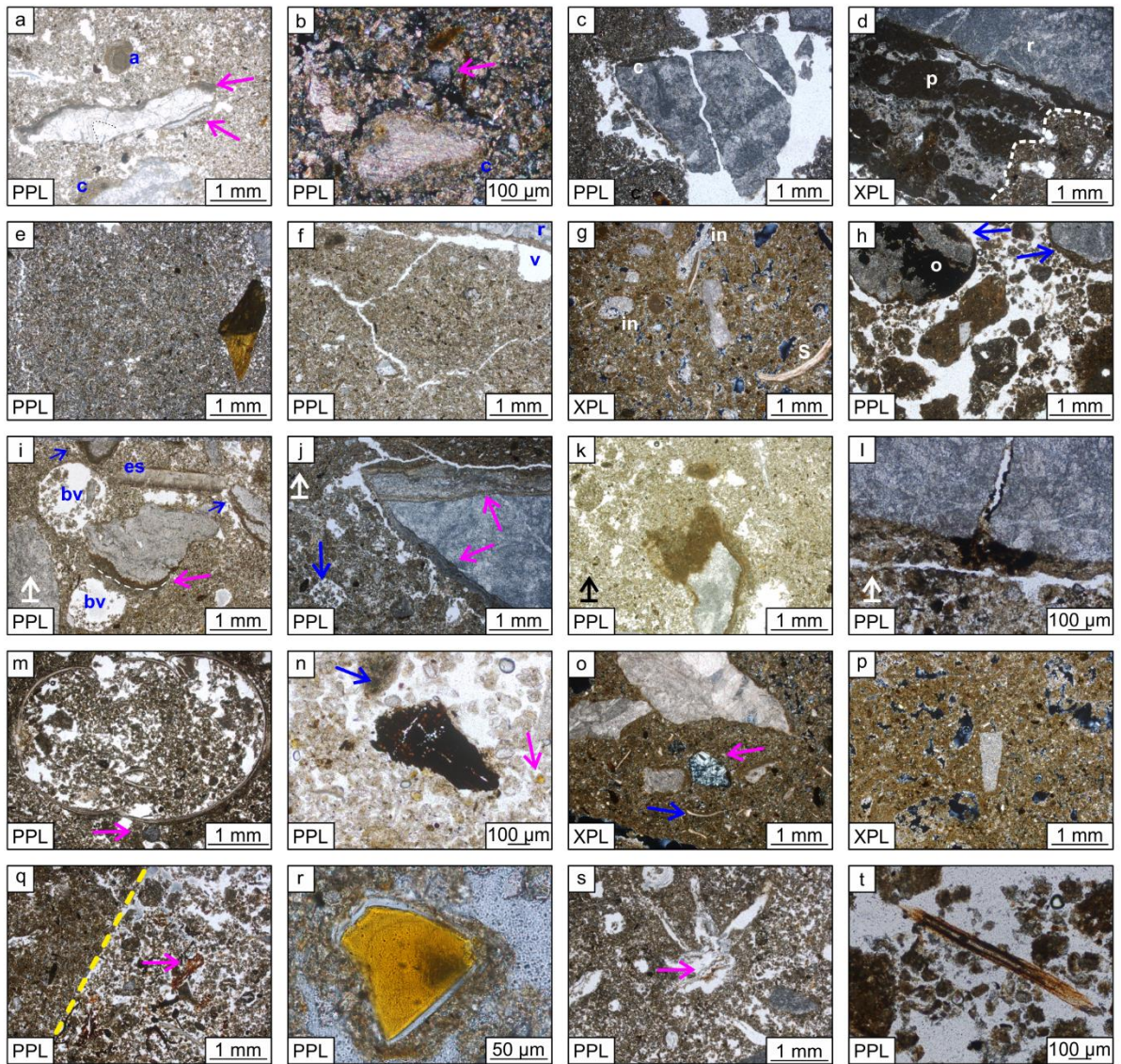
**MM 1b**



**MM 2**



**Figure S 5 Thin section scans**



**Figure S 6 Selected photomicrographs.** PPL: planar-polarized light. XPL: cross-polarized light. a) Coarse rock fragment characterized by only calcite minerals of which one is banded, the arrows indicate secondary  $\text{CaCO}_3$  accumulations overhead and underneath the clast; in the middle towards the top a gastropod-like shaped compound (a); in the middle towards the bottom another clast with a different internal fabric and a clay capping overhead on the left (c) (sample MM1A I). b) Groundmass; a quartz grain in the middle (arrow); fine-grained mica flakes are visible; the relatively coarse calcite grain is coated with clayey yellow material (c) (MM1A I). c) In situ shattered limestone fragment (MM1A II). d) Eroded coat (p) underneath a coarse limestone piece (MM3 I). e) Massive microstructure with a vertically oriented rock fragment with very sharp edges (artifact?) on the right side of the picture and a vertical plane on the left side (MM1A II). f) Weakly developed blocky structure; v – void; r – rock fragment (limestone) (MM1B I). g) Channel microstructure; voids are characterized by (in) calcite infillings, a snail shell fragment (s) is also visible (MM3 II). h) Granular microstructure characterizing Units 2 and 3, this structure is the result of soil fauna activity; blue arrows indicate coated and well-rounded limestone pieces, one of these is heavily altered by oxides (o) (MM4 II). i) “Early stage” coat (pink arrow) developed underneath a rock fragment with gradation of laminae, two rounded biogenic voids (bv) are one just below the coat and the other on the left toward the top; other coats are visible in the picture (blue arrows), interestingly an eggshell fragment (eg) is present (MM1A I). j) Coat (pink arrows) overhead and on the left side of a limestone clast, worth noticing is the difference between this coat and the one in panel i, it seems that the coat in panel j is cemented whereas it is not in i, thus it may be developed not in situ and it may be older than the one in i; the blue arrow indicates a bioturbation structure with organo-mineral excrements (MM4 I). k) Yellowish-brown dusty clay coating overhead a limestone clast, just above there is a nodule possibly detached from the coating below (MM1B II). l) Fan-shaped accumulation of oxide material illuviated from a limestone crack (MM1B II). m) Deformed and cracked snail shell, well-rounded limestone clast (arrow) (MM1B I). n) Charcoal fragment; limpid yellow clayey fragments (pink arrow), magnified in panel r, are dispersed in the groundmass; a dark rounded aggregate is visible (blue arrow) possibly due to phosphatization processes (MM1B

II. o) Coprolite fragment with bluish interference colors (pink arrow), note the coated and sub-rounded grain just toward the left; the blue arrow indicates shell fragments dispersed randomly in the groundmass (MM4 I). p) Possible artifact; the surrounding groundmass is highly affected by bioturbation (MM3 I). q) Coarse mesofauna organic and organo-mineral excrements, the structure boundary is very sharp and marked by the yellow dashed line, plant residues (pink arrow) and shell fragments are dispersed randomly inside the structure (MM2 I). r) Limpid clayey and angular fragment, with sharp edges and coated with silty and clayey material (MM1B II). s) Star-shaped vugh with calcite infillings and plant remains (pink arrow) (MM2 I). t) Longitudinal section of a burnt chaff, maybe indicating agricultural activities (MM4 II).

### **Archaeological debitage**

The lithic collection of Unit 4 consists of n. 289 artefacts, including n. 181 shatter and debris pieces (Table S 1). Amongst the cores are prismatic core and two core's shatters. According to the morphology of available cores and the composition of the blank collection, the reduction sequence was mainly performed for microbladelet production. The blanks show the following morphometric features: longitudinal flaking of the dorsal face (100%), straight (79%) or twisted and curved (21%) lateral profiles, triangular (60%) and trapezium-shaped (37%) cross-sections, and reduced punctiform (53%) or linear (13%) striking platforms. The tool assemblage totals n. 18 specimens, the highest proportions of which are retouched microbladelets. End-scrapers, burin, splinted pieces and flakes with retouches were also identified. Additionally, a blank for an axe was found in the collection. The industry is characterized by pressure knapping aimed on bladelets produced from volumetric and narrow-faced cores with a tool kit dominated by retouched microbladelets. Unit 5 lithic collection totals n. 25 artefacts. We identified core shatters, one pebble with traces of percussion, one lateral core trimming spall (Table S 1). The tool set is mainly represented by blade and bladelets with utilization retouch, one notched tool and one end-scraper. Unit 6 lithic collection contains only n. 17 artefacts, including pieces of chips and shatters (Table S 1). The assemblage contains three cores: directional core for flakes, discoidal core and semi-prismatic core for bladelets. Within the collection, three flakes, two bladelets and four microbladelets were identified. Only one backed microblade was identified in the tool set.



Table S 1 Debitage

Debitage		Unit 4 (n.)	Unit 5 (n.)	Unit 6 (n.)
Cores		3	2	3
Pebbles		-	1	-
Core trimming elements	semi-tablets	2		-
	flaking face trimming spalls	2		-
	lateral core trimming spall		1	-
	<i>eclats débordant</i>	3		-
Flakes		14	9	3
Blades		2	4	-
Bladelets		12	5	2
Microbladelets		70	-	4
Total, without debris*		108	22	8
Debris (chunks, chips, flakes less than 20mm)**		181	3	9
Total		289	25	17

### Luminescence dating

Sample preparation included wet-sieving, treatment of the sand-size fraction (180-250  $\mu\text{m}$ ) with 10% HCl, 10% H<sub>2</sub>O<sub>2</sub>, and 10% HF. A density separation of quartz and K-rich feldspar was then undertaken using a 2.58 g/cm<sup>3</sup> LST FastFloattm aqueous heavy liquid solution. Finally, the heavier quartz fraction was treated with 40% HF to remove any residual feldspar contamination, and again with HCl (10%).

Luminescence dating was performed in Nordic Laboratory for Luminescence Dating at Risø, Denmark. All measurements were made on multi-grain aliquots (quartz, 8 mm diameter; feldspar, 2 mm) mounted on stainless steel discs (quartz) or stainless steel cups (feldspar), and measured in a Risø TL/OSL reader, model TLDA 20, equipped with a calibrated beta source (Hansen *et al.*, 2018). Quartz purity was confirmed by the absence of a significant infrared-stimulated luminescence (IRSL) signal. Quartz dose estimates were made following a standard SAR protocol using blue light stimulation at 125 °C for 40 s with a 260 °C preheat for 10 s, a 220 °C cut heat and an elevated temperature (280 °C) blue-light stimulation at the end of each SAR cycle (Murray *et al.*, 2000, 2003). K-feldspar dose estimates were measured using the post-IR IRSL SAR procedure (Buylaert *et al.*, 2012) adopting preheats of 320 °C for 60 s (following regeneration doses) and 310 °C for 60 s (test doses). After preheating, the aliquots were stimulated at 50 °C with IR for 200 s (IR<sub>50</sub> signal) and subsequently stimulated again at 290 °C with IR for 200 s (post-IR IRSL<sub>290</sub> signal, pIRIR290). No correction was made for possible pIRIR290 (Buylaert *et*

*al.*, 2012) or IR<sub>50</sub> signal instability. Radionuclide concentrations were measured using high resolution gamma spectrometry (Murray *et al.*, 2018). Water content corrections were as described by Aitken (1985).

### Stratigraphic accumulation rate

SAR was calculated between two dated points of the same stratigraphic section as follow:

$$\text{SAR} = X/Y \pm \Delta\text{SAR} \quad (\text{Equation 1})$$

where X is the difference between the depths of two points, and Y is the difference between the medians of two OSL dates. The error ( $\pm$ ) for SAR was calculated according to (Harrison, 2004) as:

$$\Delta\text{SAR} = \text{SAR} \cdot \sqrt{\left(\frac{\Delta Y}{Y}\right)^2 + \left(\frac{\Delta X}{X}\right)^2} \quad (\text{Equation 2})$$

where  $\Delta Y$  is the error for the difference in OSL dates, and  $\Delta X$  is the error for the difference in depths.  $\Delta X/X$  is a very small value, because the reading error resulting from the sample size was around  $\pm 5$  cm, which gives  $\Delta X=7.07$  (calculated in the same way as  $\Delta Y$  in Equation 3 below), and further for 50–80 cm distances between samples it gives  $\Delta X/X \approx 0.01$ . Therefore, the  $(\Delta X/X)^2$  phrase could be ignored in this equation, which is then effectively reduced to:

$$\Delta\text{SAR} = \text{SAR} \cdot \Delta Y/Y. \quad (\text{Equation 2b})$$

The  $\Delta Y$  was calculated as:

$$\Delta Y = \sqrt{\Delta\text{OSL1}^2 + \Delta\text{OSL2}^2} \quad (\text{Equation 3})$$

where  $\Delta\text{OSL1}$  and  $\Delta\text{OSL2}$  are  $1\sigma$  (standard deviations) of OSL dates. Similarly, for  $\Delta X$ , the  $\Delta\text{OSL1}$  and  $\Delta\text{OSL2}$  are 5 cm reading errors, resulting from the measurement of the sample position in the field.

### References

- Buggle, B. *et al.* (2008) ‘Geochemical characterization and origin of Southeastern and Eastern European loesses (Serbia, Romania, Ukraine)’, *Quaternary Science Reviews*, 27(9–10), pp. 1058–1075. doi: 10.1016/j.quascirev.2008.01.018.
- Buggle, B. *et al.* (2011) ‘An evaluation of geochemical weathering indices in loess-paleosol studies’, *Quaternary International*, 240(1–2), pp. 12–21. doi: 10.1016/j.quaint.2010.07.019.
- Krajcarz, M. T. *et al.* (2016) ‘Middle Paleolithic sites of Katta Sai in western Tian Shan piedmont, Central Asiatic loess zone: Geoarchaeological investigation of the site formation and the integrity of the lithic assemblages’, *Quaternary International*, 399, pp. 136–150. doi: 10.1016/j.quaint.2015.07.051.
- Aitken, M. J. (1985). *Thermoluminescence Dating*. Academic Press, London, 359.
- Buylaert, J. P., Jain, M., Murray, A. S., Thomsen, K. J., Thiel, C. & Sohbat, R. (2012). A robust feldspar luminescence dating method for Middle and Late Pleistocene sediments. *Boreas* 41, 435–451.
- Hansen, V., Murray, A., Thomsen, K., Jain, M., Autzen, M. & Buylaert, J.-P. (2018). Towards

- the origins of overdispersion in beta source calibration. *Radiation Measurements* 120, 157-162.
- Harrison, D. M. (2004). Error analysis in experimental physical science [WWW Document]. Department of Physics, University of Toronto.
- Goldberg, P., Schiegl, S., Meline, K., Dayton, C., Conard, N. J. (2003). Micromorphology and Site Formation at Hohle Fels Cave, Swabian Jura, Germany. *E&G Quaternary Science Journal* 53, 1-25, doi: 10.3285/EG.53.1.01.
- Murray, A. S. & Wintle, A. G. (2000). The single aliquot regenerative dose protocol: potential for improvements in reliability. *Radiation measurements* 37, 377-381.
- Murray, A. S. & Wintle, A. G. (2003). The single aliquot regenerative dose protocol: potential for improvements in reliability. *Radiation Measurements* 37, 377-381.
- Murray, A. S., Helsted, L. M., Autzen, M., Jain, M. & Buylaert, J.-P. (2018). Measurement of natural radioactivity: Calibration and performance of a high-resolution gamma spectrometry facility. *Radiation Measurements* 120, 215-220.
- Nelson, M. S., Gray, H. J., Johnson, J.A., Rittenour, T. M., Feathers, J. K., Mahan, S. A. (2015). User guide for luminescence sampling in archaeological and geological contexts. *Advances in Archaeological Practice* 3(2), 166–177, doi: 10.7183/2326-3768.3.2.166

## ***Appendix B – Scientific paper 2***

Brancaleoni, G., Kot, M., Shnaider, S., Mroczek, P., Kurbanov, R., Abdykanova, A., Alisher kyzy, S., Khudjanazarov, M., Pavlenok, K., Krajcarz, M. T. (2023). A closer look at clasts and groundmass: Micromorphological features in sediments with archaeological significance in Obishir and Katta Sai complexes (Central Asia), *Journal of Archaeological Science: Reports*, 51, 104118, <https://doi.org/10.1016/j.jasrep.2023.10411>



## A closer look at clasts and groundmass: Micromorphological features in sediments with archaeological significance in Obishir and Katta Sai complexes (Central Asia)

Greta Brancaleoni<sup>a,\*</sup>, Małgorzata Kot<sup>b</sup>, Svetlana Shnaider<sup>c</sup>, Przemysław Mroczek<sup>d</sup>, Redzhep Kurbanov<sup>e</sup>, Aida Abdykanova<sup>f</sup>, Saltanat Alisher kyzy<sup>1</sup>, Mukhiddin Khudjanazarov<sup>g</sup>, Konstantin Pavlenok<sup>c</sup>, Maciej T. Krajcarz<sup>a</sup>

<sup>a</sup> Institute of Geological Sciences, Polish Academy of Sciences, Twarda 51/55, 00-818 Warsaw, Poland

<sup>b</sup> Faculty of Archaeology, University of Warsaw, Krakowskie Przedmieście 26/28, 00-927 Warsaw, Poland

<sup>c</sup> APSACA Laboratory, National Center of Archaeology, Uzbek Academy of Sciences, Mirzo Ulugbek, 81, Tashkent, Uzbekistan

<sup>d</sup> Institute of Earth and Environmental Sciences, Maria Curie-Skłodowska University, Al. Kraśnicka 2d, 20-718 Lublin, Poland

<sup>e</sup> Institute of Water Problems, Hydropower Engineering and Ecology, Parvin 12, Dushanbe 734063, Republic of Tajikistan

<sup>f</sup> American University of Central Asia, Bishkek 720060, Kyrgyzstan

<sup>g</sup> Institute of Archaeological Researches of the Uzbek Academy of Sciences, Mirzo Ulugbek, 81, Tashkent, Uzbekistan

### ARTICLE INFO

#### Keywords:

Micromorphology  
Grain size analysis  
Colluvial deposits  
Geoarchaeology  
Site formation

### ABSTRACT

The aim of this study is to investigate the relationship between coarse and fine material in sediments at four archaeological sites in Central Asia, which share a common characteristic of coarse clasts dispersed within a silty matrix. By using micromorphology and grain size analysis, the study aims to understand the microscale processes that have affected the geogenic material and, by extension, the potential impact on the archaeological assemblages. The four sites studied are Obishir-1, Obishir-5, Katta Sai 1, and Katta Sai 2, which are located at the toe or along a slope in Kyrgyzstan and Uzbekistan. The study focuses on the micro-features occurring on the surfaces of pebble-sized clasts and identifies four typical features: loamy cappings, loamy coatings, secondary calcium carbonate accumulations, and cracks. The processes related to these features are identified as alteration of the mineral grains, frost action, redeposition, and pedogenetic and anthropogenic processes. The study concludes that the primary contact between the two components has been disrupted in most cases, and suggests that the findings can be used to analyze site formation and post-depositional processes at archaeological sites. Furthermore, analogies with gravel-sized artifacts can be drawn, particularly with regard to secondary calcium carbonate accumulation.

### 1. Introduction

Aeolian-colluvial sediments are typically found in settings such as rock shelters, near-entrance zones of caves, rocky slopes, and toes of cliffs (Sanders, Ostermann and Kramers, 2009; Sanders, 2010; Krajcarz et al., 2016a, 2016b; Pawelec and Ludwikowska-Kędzia, 2016; Waroszewski et al., 2018; Spinapolice et al., 2022), where colluvial deposition and aeolian accumulation are common and can occur simultaneously or alternately. Colluvial debris is usually immature,

consisting of unsorted and chaotic material, and angular rock fragments mixed with infiltrated fine-grained material. Rock fragments are considered autochthonous, resulting from gravity-induced processes or derived from mechanical and/or chemical weathering of the bedrock. Loess deposits are quartz-rich, well-sorted terrestrial clastic sediments composed predominantly of silt-sized particles formed essentially by the accumulation of wind-blown dust (Dlussky, 2009; Lancaster, 2020). In such mixed deposits, the fines can have several sources, incorporating aeolian-derived particles (also known as loess-like), infiltrated particles,

\* Corresponding author.

E-mail addresses: [greta.brancaleoni@twarda.pan.pl](mailto:greta.brancaleoni@twarda.pan.pl) (G. Brancaleoni), [m.kot@uw.edu.pl](mailto:m.kot@uw.edu.pl) (M. Kot), [sveta.shnayder@gmail.com](mailto:sveta.shnayder@gmail.com) (S. Shnaider), [przemyslaw.mroczek@mail.umcs.pl](mailto:przemyslaw.mroczek@mail.umcs.pl) (P. Mroczek), [roger.kurbanov@gmail.com](mailto:roger.kurbanov@gmail.com) (R. Kurbanov), [abdykanova@gmail.com](mailto:abdykanova@gmail.com) (A. Abdykanova), [saltanat.alisher.kyzy@gmail.com](mailto:saltanat.alisher.kyzy@gmail.com) (S. Alisher kyzy), [sarmish@mail.ru](mailto:sarmish@mail.ru) (M. Khudjanazarov), [pavlenok-k@yandex.ru](mailto:pavlenok-k@yandex.ru) (K. Pavlenok), [mkrjcarz@twarda.pan.pl](mailto:mkrjcarz@twarda.pan.pl) (M.T. Krajcarz).

<sup>1</sup> Independent Researcher.

<https://doi.org/10.1016/j.jasrep.2023.104118>

Received 25 May 2022; Received in revised form 10 July 2023; Accepted 10 July 2023

Available online 5 August 2023

2352-409X/© 2023 Elsevier Ltd. All rights reserved.

products of *in-situ* weathering, and re-deposited by colluvial/alluvial, fluvial, or nival/subnival processes (e.g., Kroh et al., 2021). Thus, the fines can be classified as both autochthonous and allochthonous (Krajcarz et al., 2020; Brancaleoni et al., 2022).

Aeolian-colluvial sediments are common in mountain regions of the Central Asian loess zone, such as piedmonts of the Tien Shan and Pamir mountains (Dodonov, 2002), where a conspicuous number of important archaeological sites was discovered within such sediments. We found aeolian-colluvial sediments in slope contexts in two archaeological complexes—Katta Sai and Obishir—located at the toe or along a slope in Kyrgyzstan and Uzbekistan (Fig. 1). The complexes comprise four archaeological sites: Obishir-1, Obishir-5, Katta Sai 1 and Katta Sai 2. Recent studies on these sites provided crucial archaeological data for the prehistory of the region. For instance, the Obishir-5 is one of the first key sites that confirmed a Neolithization turnover around the 6th millennium BCE (Taylor et al., 2021; Nishiaki et al., 2022), and the issue around the Initial Upper Paleolithic is addressed at Katta Sai (Kot et al., 2022).

The occurrence of aeolian material incorporated in the colluvium, as well as the age and stratigraphy of the Quaternary sequences (Krajcarz et al., 2016b; Osipova et al., 2020; Taylor et al., 2021; Brancaleoni et al., 2022; Kot et al., 2022), have already been established at the aforementioned sites. The 'debris' component of colluvial origin is represented there by pebble-sized (and often larger) clasts derived from the bedrock, and archaeological artifacts, such as lithics and pottery sherds. Both geogenic and anthropogenic coarse components likely underwent the same post-sedimentary processes, such as reorientation, *in-situ* damage, weathering, or translocation. The identification of such processes can inform us on the preservation and the integrity evaluation of archaeological assemblages.

Micromorphological studies allow us to track the effects of such processes that are preserved at the contact between coarse components and surrounding groundmass. However, it is hardly possible to study archaeological artifacts in such a way. This is because artifacts are usually scarce and loosely scattered at these archaeological sites, thereby reducing the likelihood of having artifacts within the micromorphological monoliths. Additionally, artifacts are considered part of the valuable cultural heritage, hence limiting any destructive processes

such as the preparation of thin sections for micromorphological studies. For this reason, we adopted another approach: we tracked the micro-scale processes affecting geogenic coarse clasts for a better understanding of the general site formation processes that could have also impacted the archaeological assemblages.

This work aims to (a) analyze and classify the features that develop around the coarse clasts in these specific sediment facies and (b) describe the relationship between the coarse mineral material (mainly of colluvial origin) and the fine material of multiple geneses at their contacts. The primary methodology used in this study is micromorphology, supported by grain size analysis. We aim to determine (a) the typical micro-features at the silt-gravel contact at these sites, (b) the main processes at the contacts, and (c) the integrity of the primary contact. We may also estimate the extent to which these same processes affected the archaeological sites. Additionally, we aim to establish general trends related to the stratigraphic position, paleoenvironmental factors, weathering, and biogenic processes.

## 2. Sites

The sites are located in the Central Asian loess zone, specifically in southwestern Kyrgyzstan (Obishir-1 and Obishir-5) and eastern Uzbekistan (Katta Sai 1 and Katta Sai 2) (Fig. 1). The Obishir is a terminal Upper Pleistocene–Holocene complex located in the Aydarken valley (Batken province). The sites are located in a mountainous region to the south of the Fergana Valley, on the northern slope of the South Tien Shan (Alay Range; according to Brunet, Sobel and Mccann, (2017)). In this region, the climate is steppe semi-arid. Both sites are situated at the base of a limestone cliff (Fig. 2).

At the Obishir-1, the Quaternary sequence is represented by 4-m-thick talus material mixed with loess-like material (Fig. 2). In total, six stratigraphic units were distinguished (Table 1). The stratigraphic units were represented by poorly sorted, matrix supported, massive, and gravelly diamictons. At the bottom of the sequence, silty lenses provided evidence for aeolian accumulation (Brancaleoni et al., 2022).

At the Obishir-5, five stratigraphic units and 4 sub-units were distinguished (Osipova et al., 2020; Taylor et al., 2021). The material was poorly sorted, matrix supported, and the units were mainly fine,

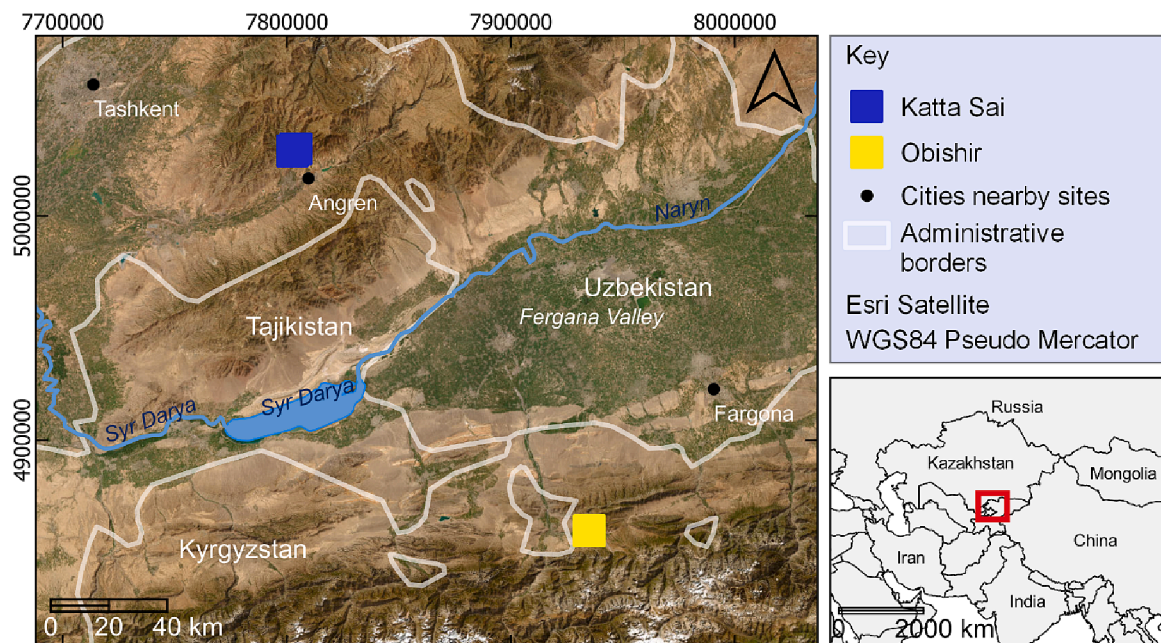
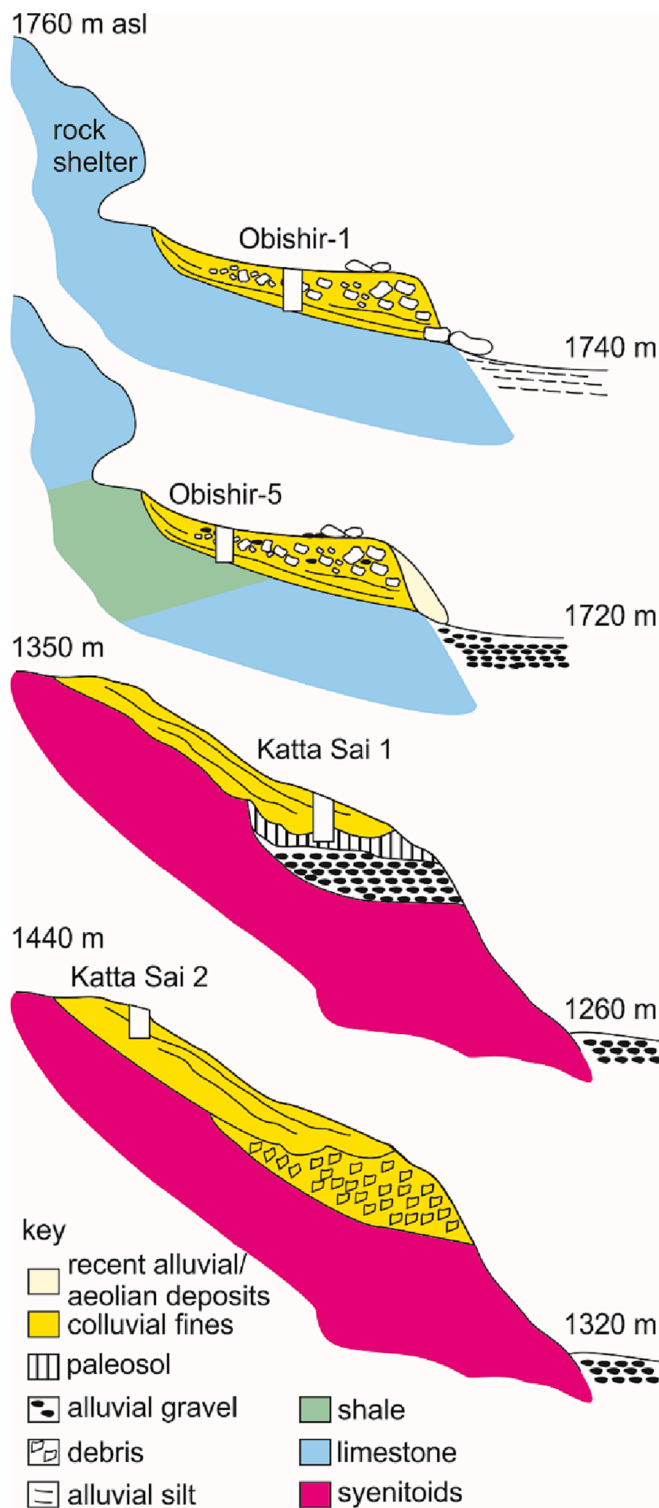


Fig. 1. Map with the location of the archaeological complexes. The Obishir complex is situated on the northern slopes of the Alay range, south of the Fergana Valley in Kyrgyzstan. The Katta Sai is along the Chatkal Range slopes, which is to the northwest of the Fergana Valley in Uzbekistan. Physical and cultural vector map data from Natural Earth ([www.naturalearthdata.com](http://www.naturalearthdata.com)).



**Fig. 2.** Schematic cross-sections at the selected sites. Katta Sai is located along a steep slope, whereas Obishir is at the cliff's toe in front of a rock shelter. The two complexes have differing Quaternary sequences, different morphology of deposits and different lithology of bedrock. What is in common is the presence at both complexes of coarse-grained material of colluvial origin and fine material of differing genesis.

gravelly, and boulderly diamictons with massive structure (Table 2). The clastic sequence spans from 13 ka BP to the Middle Ages, and sediments onlap a limestone and shale bedrock (Devonian). The Obishir-5 site contains cultural layers related to early pastoralism (Taylor et al.,

**Table 1**

Obishir-1 stratigraphy after Brancaleoni et al., (2022). The age of sediments was estimated through optical stimulated luminescence dating (OSL) (Brancaleoni et al., 2022).

Layer	Age (Lab code) (ky BP)	Max thickness (cm)	Matrix color Munsell dry; moist	Description	Interpretation
1		10	5YR 4/1; 5YR 3/1	Topsoil (O and A soil horizons) of a Mollisol, with moss and thin vegetation, sandy silt material, organic matter. Angular and sub-angular clasts of different sizes. Irregular parallel the sloping ground, gradual lower boundary	Weak soil formation, stability phase
2		50	10YR 6/3; 10YR 5/3	Matrix-supported, massive, clast moderate, gravelly diamicton (Islamov's dump). Angular gravel-and-cobble-sized limestone clasts, extremely poorly sorted. Fairly visible and erosional lower boundary	Modern anthropogenic deposit
3		5	10YR 5/2; 10YR 4/2	Paleosol (A soil horizon) below the pre-1970 ground surface, darker than the surrounding material, characterized by small aligned angular pebble-sized clasts and cobbles, the thickness is irregular. Angular and sub rounded gravel-sized limestone clasts from 2 mm to 2 cm. Gradual lower boundary	Weak soil formation, stability phase
4	9.3 ± 0.7 (188254); 8.8 ± 0.5 (188253);	100	10YR 7/3; 10YR 5/4	From clast supported to matrix-supported,	Talus, early Neolithic (Obishirian)

(continued on next page)

Table 1 (continued)

Layer	Age (Lab code) (ky BP)	Max thickness (cm)	Matrix color Munsell dry; moist	Description	Interpretation
	9.5 ± 0.8 (188296)			massive, clast rich, gravelly diamicton. In the middle, rock fragments were poorly aligned. Angular gravel-sized limestone clasts, extremely poorly sorted, chaotic structure. Dmin 2 mm, Dmax 30 cm. Fairly visible, inclined, and gradual lower boundary	
5	14.9 ± 0.8 (188255)	80	10YR 6/4; 10YR 5/4	Matrix-supported very close to grain-supported, massive, gravelly diamicton with 76 % of clast amount, poorly sorted material. Angular gravel-and-cobble-sized limestone clasts. Dmin 2 mm, Dmax 19 cm. Fairly visible, inclined, and erosional lower boundary	Talus, redeposited material, Upper Paleolithic
6	18.9 ± 1.0 (188256); 19.2 ± 1.3 (188297);	200	10YR 7/3; 10YR 5/4	Matrix-supported, massive, gravelly diamicton. Clast amount increases from bottom to top, poorly sorted material; lenses of silty material, and weakly visible lamination in the lowermost part. Angular gravel-and-cobble-sized limestone clasts, chaotic distribution. Bottom: Minimum diameter (Dmin) 2 mm, Maximum	Talus interfingering with aeolian silt lenses, Upper Paleolithic

Table 1 (continued)

Layer	Age (Lab code) (ky BP)	Max thickness (cm)	Matrix color Munsell dry; moist	Description	Interpretation
					diameter (Dmax) 8 cm. Top: from 2 mm to 14 cm. Bedrock

2021), where animal excrements were observed (from unpublished micromorphological analysis). Nowadays, the Obishir sites, particularly the Obishir-5, are used for grazing domestic animals (sheep and horses mainly). The vegetation cover is composed of broad-leaved trees and shrubs. The ground surface at the Obishir-5 is scattered with domestic animal excrements; guano was not noted.

Katta Site complex is located in Dukent Sai valley, near Yongiobod village in the Angren district of Tashkent province, eastern Uzbekistan. The region (the Chatkal Range and mid-belt of the southwestern slopes of the Fergana Valley) is known for its high levels of precipitation, which are the highest in the territories surrounding the Fergana Valley (Aki-maliev, Zaurov and Eisenman, 2013). Katta Sai complex consists of two key sites: Katta Sai 1 and Katta Sai 2, located 1.3 km apart. The sites are located in the upper part of a steep slope (Fig. 2).

The sedimentary sequence in Katta Sai 1 is composed of six stratigraphic units (Fig. 3). The sedimentary material is poorly sorted with a silty matrix and carbonate concretions (Table 3). The sequence was described as bioturbated and disturbed (Table 3).

The sedimentary sequence at Katta Sai 2 is made of four main stratigraphic units and several subunits (Table 4), with the sedimentary material described as silty loams that vary in the amount of carbonate concretions and aggregates (Table 4). The skeleton is mainly composed of igneous rock fragments and carbonate concretions (Table 4).

The Katta Sai complex is regarded as late Middle Paleolithic (Krajcarz et al., 2016b; Kot et al., 2022), and Katta Sai 2 has been attributed to the Initial Upper Paleolithic (Kot et al., 2022). The chronology of Katta Sai 1 spans from MIS3 to Late Holocene (Bronze Age) (Krajcarz et al., 2016b; Pavlenok et al., 2021); Katta Sai 2 approximately spans from 80 ka BP to 3 ka BP, i.e., Upper Pleistocene – Upper Holocene (Kot et al., 2022).

The sites have common characteristics, including loess-like (silty matrix) sediments situated on a slope, Upper Pleistocene – Holocene chronology, an admixture of coarse clasts of non-aeolian origins, and bimodal grain size distribution: silty groundmass and gravel-sized rock fragments. As described in previous studies, Table 5 summarizes the main depositional processes for each site.

### 3. Material and methods

#### 3.1. Grain size analysis

During geoarchaeological investigations at the Obishir sites, bulk samples were collected for grain size analyses. Obishir-1 results have already been published in Brancaleoni et al., (2022), but the results for Obishir-5 have not yet been reported. Samples at the Obishir sites were dry-sieved with non-standard sieves (2, 5, 10, 20 and 50 mm). We weighed each fraction, and a portion of the fraction <2 mm was sent for laser diffraction analysis.

For the Obishir-1, laser diffraction analysis (range 0.01–2000 µm) was conducted at the certified Laboratory Jars S.A. (Poland). Mean values (%) were calculated for each layers for the three main fractions: clay (<5 µm), silt (5–63 µm), and sand (63–2000 µm). For the Obishir 5 site, laser diffraction analysis was performed at the Institute of Geography RAS using a Malvern Mastersizer 3000 laser analyzer (range



**Table 2**

Obishir-5 stratigraphy after Osipova et al. (2020) and Taylor et al. (2021). The age of layers was established through radiocarbon (14C) and thermoluminescence dating (TL) (Osipova, 2020; Shnaider et al., 2017; Taylor et al., 2021). Both non-calibrated and calibrated radiocarbon dates are given. For calibrated age, we give the probability information (e.g., 95.4%). The ages were calibrated using OxCal v4.4.4 (Bronk Ramsey, 1995; 2001), and atmospheric data from Reimer et al. (2020).

Layer	Sub-layers	Age (Lab code) (y BP)	Max thickness (cm)	Matrix color Munsell dry; moist	Description	Interpretation
0			30		Recent topsoil, matrix supported, clast moderate diamicton, massive, matrix is dark gray silt with plant roots and litter. Lower boundary gradual	Weak soil formation, stability phase
1		1591 ± 26 (OxA-37833, 14C), 1530-1406 (95.4%) cal; 1650 ± 20 (PLD-31751, 14C), 1589-1515 (80.4%) cal	60	10YR 7/1; 2.5Y 5/2	Matrix-supported, clast poor, fine diamicton with light gray to grayish brown silt with pottery sherds, bones charcoals and reddened lenses. Mid- to coarse-grained limestone clasts (chaotic pattern). Lower boundary clear, marked with change in color and texture	Bronze Age and Middle Ages cultural layer
2	2.1	7324 ± 105 (GV-2118, 14C), 8359-7963 (95.4%) cal	5	10YR 7/2; 10YR 6/3	Matrix-supported, clast moderate weakly laminated diamicton with light gray to pale brown thin-laminated silty matrix. Lower boundary clear, inclined, sedimentary	Reworked cultural layers bearing an Obishirian assemblage (early Neolithic)
	2.2	6989 ± 45 (AA-114469, 14C), 7876-7700 (77.6%) cal	40	7.5YR 7/2; 10YR 5/4	Matrix-supported, from clast moderate to clast rich, gravelly diamicton with pinkish gray to yellowish brown loose silty matrix. Sparse fine-grained limestone clasts. Lower boundary sharp, discordant	
	2.3	6950 ± 40 (Poz-145006, 14C), 7862-7683 (91.2%) cal; 7405 ± 25 (PLD-31752, 14C), 8328-8174 (94.5%) cal; 7499 ± 95 (GV-2119, 14C), 8455-8161 (88.5%) cal	60	10YR 6/2; 10YR 3/3	Matrix-supported, clast rich, gravelly diamicton with light brownish-gray to dark brown silty loamy matrix with abundant lithic artifacts. Very abundant fine- to mid-grained limestone clasts (planar texture) and fine pebble-sized clasts (0.5–10 cm). Lower boundary inclined, erosional, marked with mid- and coarse-grained limestone clasts	
	2.4	9410 ± 30 (PLD-31753, 14C), 10735-10565 (94.8%) cal	40	10YR 7/2; 10YR 4/3	Matrix-supported, clast rich, gravelly diamicton with light gray to brown silty loamy matrix. Very abundant fine- to mid-grained limestone clasts (planar texture) and fine pebble-sized clasts (0.5–1 cm). Lower boundary inclined, discordant, marked with mid- and coarse-grained limestone clasts	
3		7257 ± 19 (GrM-11929, 14C), 8170-8011 (95.4%) cal	90	10YR 7/3; 10YR 5/4	Matrix-supported, from clast moderate to clast rich, bouldery diamicton with very pale brown to yellowish-brown silty matrix, massive structure. Small amount of fine- to mid-grained limestone clasts (chaotic pattern). Lower boundary inclined, discordant, marked by accumulation of coarse-grained limestone clasts	Colluvial-aeolian Obishirian (early Neolithic)
4		8842 ± 18 (GrM-11871, 14C), 9964-9769 (53.2%) cal	110	10YR 7/3; 10YR 5/4	Matrix-supported, clast moderate, gravelly diamicton with very pale brown to yellowish-brown silty matrix, massive structure. Small amount of fine- to mid-grained limestone clasts (chaotic texture). Lower boundary unclear, gradually passing into layer 5	Colluvial-aeolian, Upper Paleolithic-Epipaleolithic
5		12.2 ± 1.9 (UG-7089, TL) ky BP; 12.4 ± 1.9 (UG-7090, TL) ky BP	70	10YR 6/3; 10YR 5/5	Matrix-supported, clast moderate, gravelly diamicton with pale brown to yellowish-brown hard silty matrix, massive structure, preserved only in depressions of the bedrock. Bedrock	Colluvial-aeolian, Upper Paleolithic-Epipaleolithic

0.01–3160 µm), following the procedure described in Timireva et al. (2022). Mean values (%) were calculated for each layer for the three main fractions: clay (<5.01 µm), silt (5.01–63.1 µm), and sand (63.1–3160 µm).

Regarding the Katta Sai complex, during fieldworks, separated bulk samples were collected for dry-sieving and for clay, silt and sand fraction estimation. The dry sieving was carried out with non-standard sieves (2, 5, 10, 20 and 50 mm) directly at the sites. The sampling location is shown in Supplementary material in Figs. S8 and S11. For estimating the clay, silt and sand fractions at Katta Sai 1 site, we considered 29 samples collected in 2013 (samples numbered 22–51; Supplementary material, Figs. S6 and S7), which were already analyzed and published in Krajcarz et al. (2016b). The procedure is described in the same paper.

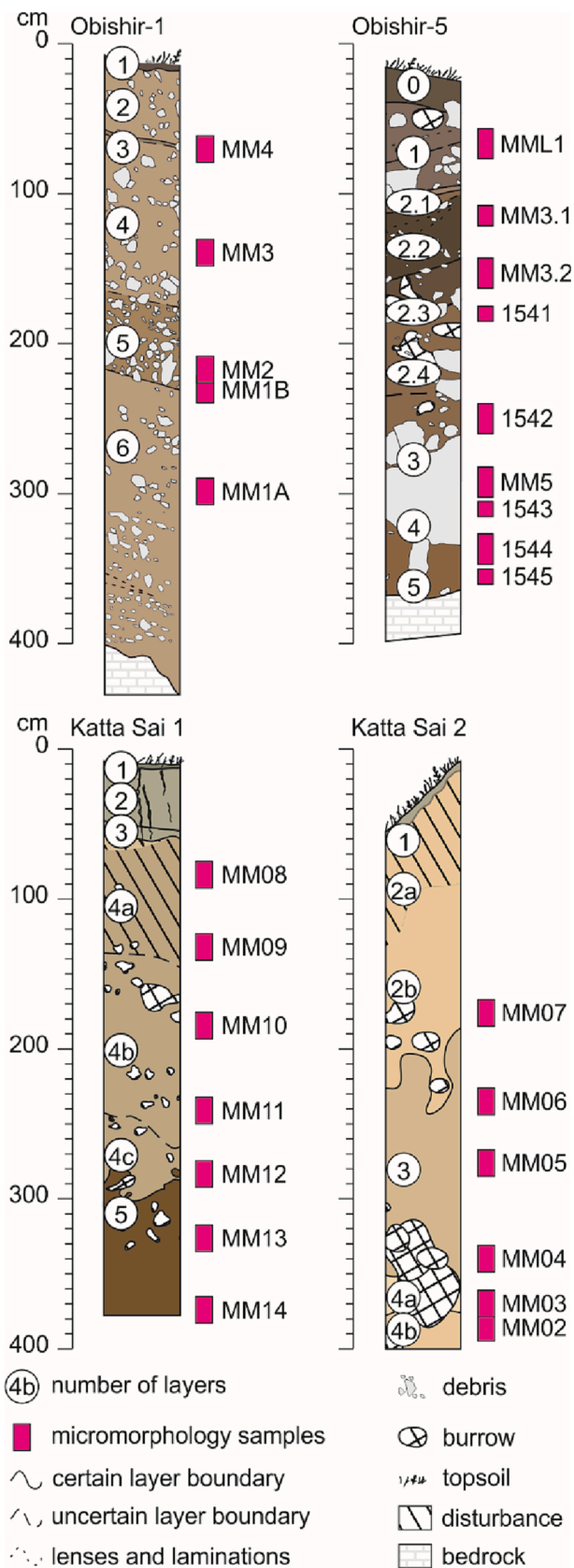
For the Katta Sai 2 site, new particle size measurements for the estimation of clay, silt and sand fractions were performed on 36 samples collected in 2015 along the profile S21/S-R21/S (Fig. S11 in Supplementary material). The sediment samples were dried, crushed, gently grated in a mortar, and sieved through a 2 mm mesh. The sediments were then homogenized. Particle size measurements were taken three

times for each sample using a Malvern Mastersizer 2000 Hydro G apparatus with stirring for 5 min under ultrasounds. Mean values (%) from the three measurements were compiled for the three main fractions: clay (<5.5 µm), silt (5.6–63 µm), and sand (>63 µm). For all sites, we defined the coarse fraction (C) as all the fractions above 2 mm, and as fine fraction (f) as all fractions below 2 mm.

### 3.2. Micromorphology

We sampled the stratigraphic sequences for micromorphology. Overall, 28 blocks were collected from which 42 thin sections were produced. Thin sections were made according to the procedure described in Brancaleoni et al. (2022). At the Institute of Geological Sciences, Polish Academy of Sciences, thin sections were observed under a polarizing microscope (ECLIPSE LV100POL, magnification range 2.5–50).

During micromorphological analysis, we adopted the concept of partial fabrics (Stoops, 2021). We determined two partial fabrics (PFs). The first PF comprises the coarse mineral components. The second PF is



**Table 3**

Katta Sai 1 stratigraphy after [Krajcarz et al. \(2016b\)](#), thickness and boundary information was estimated from the same paper (i.e., Fig. 1 and from the text). Age of layers was estimated through U-series and radiocarbon dating ([Krajcarz et al., 2016b](#); [Pavlenok et al., 2021](#)). Radiocarbon dates were calibrated using OxCal v4.3.2 ([Bronk Ramsey, 1995; 2001](#)) and IntCal13 atmospheric curve ([Reimer et al., 2013](#)).

Layer	Age (Lab code) (ky BP)	Thickness (min and max in cm)	Matrix color Munsell dry; moist	Description	Interpretation
1		5–10	10YR 7/2; 10YR 4/3	Topsoil	Soil formation
2		10–50	10YR 7/3; 10YR 4/3	Artificially disturbed sediments. Upper boundary distinct	Artificial deposit Andronovo culture
3/3a		10–20	10YR 7/3; 10YR 4/3	Artificially disturbed sediments. Upper boundary distinct	
4a	26.3 ± 3.4 (UG -7030, TL)	70–100	10YR 7/3; 10YR 4/4	Similar to below but strongly bioturbated. Upper boundary distinct	Colluvial-aeolian bioturbated
4b		100–120	10YR 7/2; 10YR 5/4	Similar to 4c, carbonate concretions and the sediment consists of numerous aggregates of 1–5 cm size and irregular shape. Upper boundary gradual	Colluvial-aeolian with Middle Paleolithic
4c	38.1 ± 1.0 (W -3250, U-series); 35.3 ± 0.7 (Poz-82,152, 14C), 41,399 - 38,559 cal BP (95.4%); 35.4 ± 0.8 (Poz -82,153, 14C), 41,651 - 38,511 cal BP (95.4%)	20–70	10YR 7/2; 10YR 5/4	Silty sediment, rich in Paleolithic artifacts and subfossil snail shells. Upper boundary gradual	Colluvial-aeolian with Middle Paleolithic
5		150	10YR 6/3 10YR 7/2; 10YR 4/4	Brownish, weakly laminated silty sediment with sand intercalation in the bottom part. Upper boundary	Colluvial-aeolian

**Fig. 3.** Stratigraphic profiles at the selected sites with location of micromorphology samples. A thorough stratigraphic description for each site is given in [Table 1](#) (Obishir-1), [Table 2](#) (Obishir-5), [Table 3](#) (Katta Sai 1), and [Table 4](#) (Katta Sai 2). Section drawings and extensive location of sampling is given in Supplementary material.

(continued on next page)

Table 3 (continued)

Layer	Age (Lab code) (ky BP)	Thickness (min and max in cm)	Matrix color Munsell dry; moist	Description	Interpretation
6		Not given	Not given	sharp and erosional? Sand and gravel	Alluvial terrace

the groundmass, which includes voids, grains, pedofeatures, and micromass. We paid special attention to the relationship between the two PFs and micro-features developed at the boundary between them, with a particular focus on the silt fraction. To describe the samples, we followed the guidelines proposed by Stoops (2021), with the exception of calcium carbonate accumulations. For these, we used the terminology and classification suggested by Blank and Fosberg (1990).

## 4. Results

### 4.1. Field observations

The Obishir-1 and -5 sites are located at the toe of a very steep rocky cliff (as shown in Fig. 2), where the slope is gently sloping at approximately 10 degrees. Debris was detached from the cliff, and accumulated ending its run down the slope due to changes in slope angle. In contrast, the Katta Sai 1 and 2 are situated along a steep slope with an inclination of about 30 degrees (as shown in Fig. 2), but there is no rocky cliff present as a source of debris material.

Table 4

Katta Sai 2 stratigraphy after Krajcarz et al. (2016b) and Kot et al. (2022). Thickness and skeleton information was estimated from Kot et al. (2022) and unpublished data respectively. Age of layers is reported as in Krajcarz et al. (2016b) and Kot et al. (2022). The age was estimated through radiocarbon (14C), TL and OSL. Radiocarbon dates were calibrated with IntCal20 (Reimer et al., 2020) using OxCal v4.4.2 (Bronk Ramsey, 1995; 2001).

Layer	Sublayer	Age (Lab code) (ky BP)	Thickness (min and max in cm)	Matrix color Munsell dry; moist	Description	Interpretation
1			2–20	10YR 7/2; 10YR 4/2	Modern topsoil, silty loam, strongly bioturbated by insect/worm burrowing and plant roots. Skeleton made of igneous rocks fragments and carbonate concretions. Gradual lower boundary	Soil formation
2	2 (dark)	2.71 ± 21 (MAMS- 48231, 14C), 2851–2761 cal y BP	40	10YR 7/2; 10YR 4/3	Silty loam, porous, slightly bioturbated by insect/worm burrowing	Anthropogenic feature (grave)
	2a		30–70	10YR 8/3; 10YR 6/4 variable	Bioturbated by insect/worm burrowing, with mollusk shells and lithics. Skeleton as in layer 1. Gradual upper boundary	Colluvial-aeolian
	2b	26.3 ± 3.4 (UG-7030, TL); 48.6 ± 7.0 (UG-7069, TL)	10–90	10YR 8/3; 10YR 6/4 variable	Silt/silty loam, soft in dry state, with dispersed fine aggregates visible in close view. Skeleton made of igneous rock fragments. Gradual upper boundary	Colluvial-aeolian Middle and Upper Paleolithic assemblage
	2c	12.3 ± 8.3 (GdTL- 3354, OSL)	20–40	10YR 8/3; 10YR 6/4 variable	Silt/silty loam, soft in dry state, porous, strongly bioturbated by insect/worm burrowing. Skeleton as in layer 2b. Upper boundary possibly man made	Colluvial-aeolian bioturbated
3	3a	27.0 ± 3.5 (UG-7068, TL); 39.0 ± 1.5 (Poz-98409, 14C), 45840–41200 (95.4%) cal y BP;	20–40	10YR 8/2; 10YR 7/3	Silt/silty loam, soft in dry state, more porous than Sublayer 2b, with dispersed fine aggregates visible in close view, with mollusk shells and lithics. Skeleton as in layer 2b. Weakly marked upper boundary	Colluvial-aeolian with Middle and Upper Paleolithic assemblage
	3b	43.0 ± 2.0 (Poz-98408, 14C), 52330–42840 (95.4%) cal y BP	variable	10YR 6/3; 10YR 5/4	Silt/silty loam, soft in dry state, brownish sediment, with abundant fine whitish carbonate clasts. Skeleton made of igneous rock fragments	Colluvial-aeolian with Middle and Upper Paleolithic assemblage
	3c	63.8 ± 4.4 (GdTL- 3355, OSL); 70.4 ± 10.0 (UG-7070, TL)	variable	10YR 8/2; 10YR 7/3	Silty loam, hard and compacted when dry, with coarse aggregates. Skeleton made of igneous rock fragments and carbonate concretions	Colluvial-aeolian
4	4a	42.1 ± 6.3 (UG-7071, TL)	20–40		Similar to 4b. Skeleton made of igneous rock fragments and carbonate concretions. Weakly marked upper boundary	Colluvial-aeolian
	4b		20	10YR 8/2; 10YR 7/3	Massive yellowish silt/silty loam, soft when dry. Weakly marked upper boundary	Aeolian deposit

### 4.2. Grain size analysis

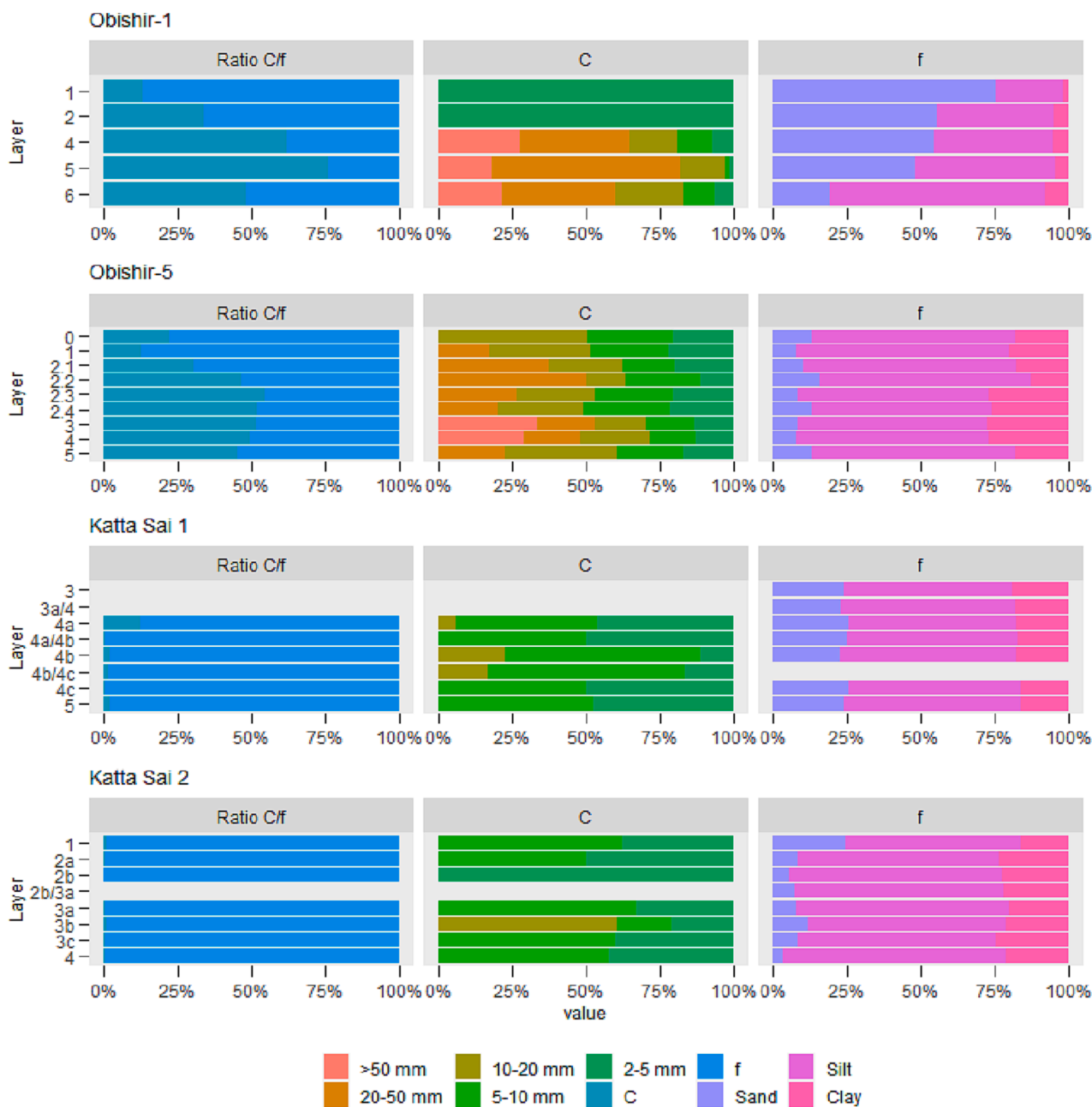
The sediments found at the sites are predominantly silts with varying amounts of coarser material, as shown in Fig. 4. Specifically, Obishir-1 and -5 contain matrix-supported diamictons as described in Table 1, Table 2, and shown in Fig. 4. Meanwhile, the Katta Sai sites consist mainly of silts, as indicated in Table 3, Table 4, and shown in Fig. 4.

In Fig. 4, it is evident that the amount of coarse fraction is more abundant at the Obishir sites, with a few layers exceeding 50% coarse fraction (Fig. 4, C/f ratio). Conversely, the Katta Sai complex has significantly less coarse fraction (Fig. 4, C/f ratio). However, pebble-sized clasts were observed in thin sections, particularly in layers identified as colluvium (see Tables 3 and 4).

Table 5

Depositional processes at the selected sites already assessed by previous studies (Krajcarz et al., 2016b; Osipova et al., 2020; Taylor et al., 2021; Brancaleoni et al., 2022; Kot et al., 2022).

	Obishir-1	Obishir-5	Katta Sai 1	Katta Sai 2
Aeolian accumulation	✓	✓	✓	✓
Colluvial/alluvial accumulation	✓	✓	✓	✓
Alluvial erosion and re-deposition (e.g., run-off)		✓	✓	✓
Colluvial redeposition (gravity-induced translocation down the slope)	✓			✓
Post-depositional processes induced by bioturbation and pedogenesis	✓	✓	✓	✓



**Fig. 4.** Grain size results for each site. Ratio C/f – ratio between coarse fractions (>2 mm, indicated as C) and fine fractions (<2 mm, indicated as f). C – coarse fraction data from dry sieving (2, 5, 10, 20, 50 mm). f – fine fraction data from laser diffraction method (Clay, Silt and Sand). Here we show the average value for each layer. The Obishir sites represent a coarser facies than the Katta Sai ones.

### 4.3. Lithological and sedimentary analysis

The lithology of the debris varies among sites. At the Obishir-1, the coarse mineral components are primarily limestone rock fragments, while at the Obishir-5, limestone, shale, and igneous rock fragments are present. At the Katta Sai, the mineral grains are mainly igneous rock fragments and carbonate nodules. The matrix at the Obishir consists of silt and fine sand grains, primarily composed of dominant calcite, common quartz, micas, clay minerals, Fe/Mn nodules, and feldspar grains. The micromass is characterized by calcite, Fe/Mn nodules, limpic clay fragments, and amorphous organic matter. The fine material at Katta Sai is loamy, with dispersed common silt-sized quartz, feldspar, micas, Fe/Mn nodules, and fewer calcite grains.

The groundmass surrounding the clasts is typically loamy, with a color varying from yellowish-grayish brown at the Obishir sites to

yellowish reddish-brown at the Katta Sai sites. The microstructure is mostly massive, with randomly distributed silt-and-sand-sized components. Locally, the groundmass was more complex, characterized by vughy microstructure, or weak granostriated b-fabric. The pebble-sized mineral grains are mainly characterized by clasts of three lithologies (limestone, shale, and igneous), with clasts randomly distributed and in an open porphyric relationship with the groundmass.

### 4.4. Micro-features at the skeleton-matrix contact

This section presents micro-features observed under the microscope that characterize the clast-matrix contacts. The micro-features identified at the contact between the two PFs are: loamy cappings, ferruginous cappings, loamy coatings, dusty coatings, phosphatic coating, CaCO<sub>3</sub> secondary accumulations, and cracks. Table 6 provides a synthetic

**Table 6**  
Micro-features surrounding coarse material at the selected sites.

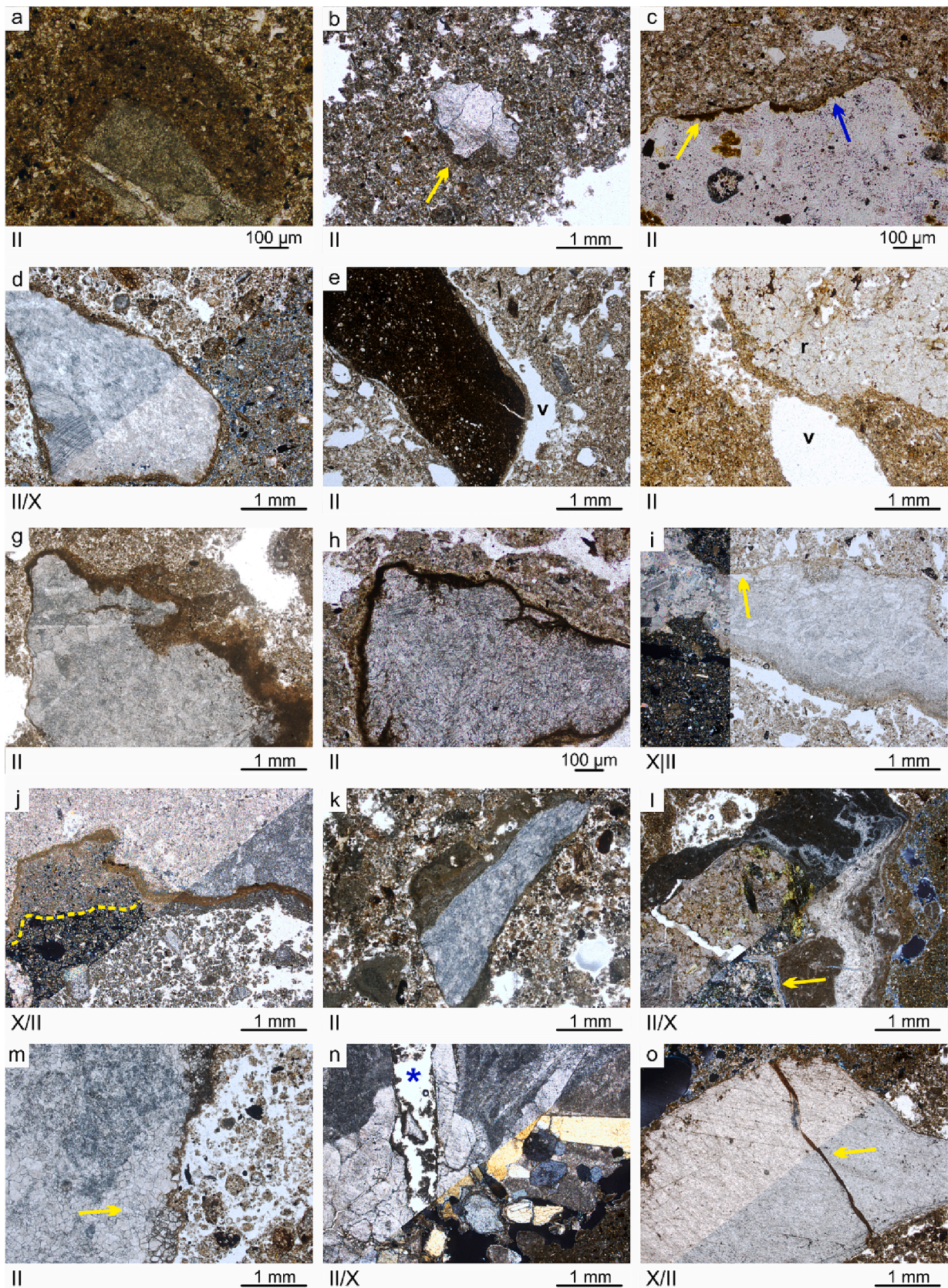
Features	Obishir-1	Obishir-5	Katta Sai 1	Katta Sai 2	Interpretation	Micro- photograph
<b>Loamy cappings</b>	On top of rock fragments and often only partially preserved. Overall poorly organized internal fabric with very weak laminations and infiltration of fine mineral grains (calcite) and organic matter nodules. Few were relatively well developed (300 µm thick) and showed a crescentic shape. Few cappings on undersides of clasts	Weakly developed and associated with coating surrounding the clast not only on the top surface	Thin and not well-developed compacted capping on top of a few igneous fragments, associated with fine weathering products	Observed on top of a few igneous fragments associated with bioturbated groundmass	If not associated with biovoids and/or bioturbated groundmass: High energy water inflow after melting snow, and later erosion and redeposition (?). If associated with biovoids and/or bioturbation: Bioturbation feature	<a href="#">Fig. 5abc</a>
<b>Ferruginous cappings</b>	Well-developed crescentic shape with irregular boundaries	Not observed	Not observed	Not observed	Water dripping	
<b>Loamy coatings</b>	Loamy matrix coatings surrounding free mineral grains, especially sub-rounded, with low birefringence	Loamy/clayish material attached at surfaces of clasts and bones, birefringence higher than surrounding micromass, leading to a granostriated b-fabric. Common in the central part of the sequence, associated with biogenic and anthropogenic components (e.g. charcoals, ashes, bones, organic matter)	Loamy coatings surrounding rock fragments usually associated with voids and channels	Same as Katta Sai 1	Down-slope redeposition/ Paleosol with archaeological material characterizing colluvium in case of Obishir-5/ Bioturbation	<a href="#">Fig. 5def</a>
<b>Dusty fine silt/ coarse clay coatings</b>	Irregularly laminated flame-like shaped, characterizing only limestone fragments, and slightly more birefringent than surrounding matrix; internal fabric different, finer than surroundings.	Orange, dark brown and opaque, surrounding only limestone clasts, very thin, non-laminated, usually penetrating the internal part of clasts	Not observed	Not observed	Clay infiltration. Associated with paleosol and rapid infiltration of water.	<a href="#">Fig. 5g</a>
<b>Phosphatic coatings on mineral grains</b>	Thin rim around limestone fragments. Associated with <i>ex-situ</i> paleosol, and younger paleosol	Rim around coarse limestone fragments	Not observed	Not observed	Leaching water rich in phosphorous	<a href="#">Fig. 5i</a>
<b>Calcium carbonate rind, coat and pendant</b>	Common rinds and coats, much fewer pendants. In some case, associated with voids and often damaged. Many grains bearing these features were in secondary position	Common rinds and coats; pendants were not observed. Coats can be found on the top and at the bottom surface of rock fragments. In some cases, weathered or damaged.	Rarely observed coat on sides of igneous rock fragments	Rarely observed coarse igneous rock fragments with well-developed coat/ pendant.	CaCO <sub>3</sub> accumulation followed by down-slope redeposition or rotation of clasts	<a href="#">Fig. 5kl</a>
<b>Other precipitations</b>	Ferruginous material commonly attached to and attacking the mineral grains	Same as Obishir-1	Opaque material within rock fragments	Same as Katta Sai 1	Chemical weathering	<a href="#">Fig. 5h</a>
<b>Cracks</b>	Rock fragments generally presenting smooth cracks; cracks were empty, filled with loamy material or with reprecipitation of mainly calcite and gypsum. Secondary mineral precipitation often observed within cracks, in some cases detached from the main fragment. Few <i>in-situ</i> shattered clasts occurred	Same as Obishir-1, found mineralized calcite veins in shale fragments	Rock fragments with filled cracks were observed, filling fine and opaque material, such as clay and oxides. Chlorite replacement often observed	Same as Katta Sai 1	Secondary mineralization/ Weathering	<a href="#">Fig. 5no</a>
		Not observed	Not observed	Rarely observed	Cryoturbation	<a href="#">Fig. 5no</a>

description and a tentative interpretation for each selected site, while [Fig. 5](#) showcases the most informative micro-photographs. Additionally, [Table 7](#) presents the distribution of features for each site along the vertical profiles.

## 5. Discussion

### 5.1. Loamy cappings

Loamy or silty cappings are textural characteristics occurring on top of large, coarse mineral grains or the up-sides of aggregates or other coarse elements (Courty et al., 1989; Stoops, 2021). Cappings are



(caption on next page)

**Fig. 5.** Microphotographs. II: plane-polarized light. X: cross-polarized light. **(a)** Well-developed crescent-shaped dark brown loamy capping with darker laminae, the surrounding micromass is massive, loamy and lighter in color. The capping is made of compacted material with incorporated organic matter, thus resulting in a darker color. The groundmass-capping contact is sharp (Obishir-1 – Unit 6 MM1A). **(b)** Crescent-shaped capping or coating (?) (arrow) on the underside of a rock fragment made of solely calcite crystals; being on the underside, this might suggest reorientation or redeposition of the clast. Contact between micromass and capping is sharp (Obishir-1 – Unit 6 MM1A). **(c)** Igneous rock fragment with thin capping made of opaque fine material (pellicular alteration, yellow arrow), and loamy material (blue arrow); contact with micromass is sharp (Katta Sai 2 – Unit 4b MM1). **(d)** Limestone rock fragment with loamy coating all around the clast, the coating is slightly more birefringent than the surrounding groundmass, for the presence of clayey material; to note is that the groundmass has a granostriated b-fabric, and micromass a crystallitic b-fabric. Contact with groundmass is not sharp everywhere; in some cases, smaller grains are attached to the coating (Obishir-5 – Unit 2.3 MM3.2). **(e)** Dark opaque shale fragment coated with loamy material, to note is the void (v) between the clast and the micromass; the void shape is similar to that characterizing the clast, indicating a downward rotation of the shale clast, possibly due to thin section preparation (?). Surrounding groundmass with vesicles and channels (Obishir-5 – Unit 3 MM5). **(f)** Igneous rock fragment (r) heavily altered with voids and opaque material within (dotted alteration), worth noting is the coating at the bottom surface associated with a bio-gallery (v), the coating material has been probably pushed toward the fragment walls. Groundmass is massive (Katta Sai 1 – Unit 4b MM11). **(g)** Irregularly banded dusty coating, locally “cemented” with low birefringence, if seen at X, to note the flame-like shape. Groundmass is massively disrupted by large voids, contact is either sharp and gradual with dusty clayey material impregnating the micromass (Obishir-1 – Unit 6 top part MM1B). **(h)** Pellicular opaque coating penetrating and attacking the clast, indicating alteration. Vuggy groundmass, micromass-coating contact is sharp (Obishir-5 – Unit 2.3 MM3.2). **(i)** Phosphatic coating (arrow) around coarse limestone fragment, at X the coating shows undifferentiated b-fabric, gradual contact with micromass; micromass is impregnated (Obishir-5 – Unit 3 MM1542). **(j)** Banded (aggradative) coating, clayey birefringent material directly at the contact with clast followed by micritic calcite forming a second band and impregnating the micromass (dashed line), especially where the clast shows an indentation. The groundmass is characterized by complex packing voids with a medium–high degree of separation (Obishir-1 – Unit 6 MM1A). **(k)** Secondary calcium carbonate accumulation (coat), developed and altered on top of the clast, weakly developed on the underside, contact with micromass is sharp (Obishir-5 – Unit 1 MM1). **(l)** Very well-developed and complex CaCO<sub>3</sub> accumulation (>1-mm thick) on top and side of an igneous rock fragment, the accumulation detached from the clast leading to new pedogenic carbonate precipitation filling the void at the clast-pendant contact (arrow), contact with micromass is sharp, voids are present (Katta Sai 2 – Unit 3b/3c MM46). **(m)** Disintegration of a coarse limestone clast most probably by plant roots or some other form of weathering; Granoblastic internal fabric favored the process; fine sand crystals of calcite are coated by clayey material, possibly a product of alteration (Obishir-5 – Unit 3 MM1542). **(n)** Recrystallisation of euhedral crystals of gypsum within fairly opened cracks (asterisk) in a limestone fragment; also here, crystals are coated with loamy material (Obishir-1 – Unit 6 MM1A). **(o)** Smooth crack (arrow) characterizing a large calcite crystal-filled fine material, typical calcite cleavage visible especially in X (Obishir-1 – Unit 6 MM1A).

**Table 7**

Feature-types charted against the different layers in each site. Key: ● few; ●● common; ●●● dominant.

Site	Chronology	Unit	Loamy cappings	Ferruginous capping	Loamy coating	Dusty fine silt/coarse clay coatings	Phosphatic coatings on mineral grains	CaCO <sub>3</sub> rind, coat and pendant	Other precipitations	Cracks	Gypsum crystals	
Obishir-1	Holocene	1; 2	No samples									
		3		●●	●●	●	●	●●●	●●		●	
		4			●●	●		●●	●●	●●		
		5			●	●		●●	●	●●	●	
		6 top				●●	●●	●	●●	●●	●●	dissolution
		6 bottom		●●		●			●●	●	●●	●
Obishir-5	Holocene	0; 2.1	No samples									
		1			●		●	●●●	●● (opaque)			
		2.2	●	●	●●	●		●●	●	●●		
		2.3		●	●●●	●		●●	●●	●●	●●	
		2.4			●●			●●	●●	●●	●●	
		3			●●			●●	●	●●	●●	
		4			●		●	●●	●●	●●	●●	
5			●●		●		●●		●●			
Katta Sai 1	Holocene/ Pleistocene	1–3	No samples									
		3/4a	●		●					●●●		
		4a			●●			●	●			
		4b	●	●	●				●			
		4c	No clasts in thin sections									
		4c/5				●						
5		●	●				●●					
Katta Sai 2	Holocene	1	No sample									
		2	No features, very few clasts in thin sections									
		3		●	●			●●	●	●		
		3b/3c	●					●				
		3c	No features									
		4a/4b	No clasts in thin sections									

commonly associated with turbulent water rapidly flowing through sediments (Courty et al., 1989). They have been observed in conditions where the vegetation is sparse, thus not protecting from a rapid water

inflow. Cappings have also been found in cold, arid settings with permafrost (e.g., Meier et al., 2019); and in mountainous periglacial slopes where snow cover is seasonal (e.g., Texier and Meireles, 2003;

Pawelec and Ludwikowska-Kędzia, 2016); in Pleistocene deposits (e.g., Macphail and Goldberg, 2003); and related to solifluction lobe (Bertran and Texier, 1999). More generally, cappings indicate the action of cryogenic processes (Van Vliet-Lanoë, Fox and Gubin, 2004).

We observed a few, well-developed, crescent-shaped, loamy cappings only within layer 6 (Upper Pleistocene) at the bottom part of the sequence at the Obishir-1 (Table 6; Fig. 5a; Table 7). We interpreted them as a result of cold conditions during the Last Glacial Maximum (LGM), together with *in-situ*-shattered clasts and vertically oriented clasts (Brancaleoni et al., 2022). Concerning cappings that were partially preserved (Table 6; Fig. 6), we can assume that they were affected by later erosion and redeposition, which whether or not

involved the coarse fraction depending on the energy of the erosional process. In a few cases, cappings were found at the bottom surface of clasts (Fig. 5b; Fig. 6), thus supporting rotation and/or redeposition. At the Obishir-5, Katta Sai 1, and 2, well-developed crescent-shaped cappings were not observed (Table 6; Fig. 5c). In these sites, only weakly developed cappings were observed with sporadic frequency (Table 7).

## 5.2. Coatings

Coatings are similar to cappings, but they can surround the clast instead of being found only on top of the coarse material (e.g., Fig. 5d; Stoops, 2021). Coatings can be of different material and morphology
















Micro feature		Archaeological importance							Notes	
		Reorientation of clasts	Redeposition, transport	Relocation of fine material	Frost action (cold climate proxy)	Unidentified physical disturbances	Chemical weathering (humid climate proxy)	Bioturbation		Human/animal activity
No specific features										Clast not affected by post-sedimentary processes
Voids around the clast						yes		yes?		Relative movement between clast and groundmass
Loamy capping		no	no		yes					Frost action after deposition, no transport after
Loamy capping in non-upside position		yes	yes?		yes					Clast reoriented after development of capping
Loamy coating			yes							Possibly rotation
Fragmentary loamy capping or coating			yes					yes?		Erosion after development of capping or coating
Dusty coating							yes			Chemical alteration of limestone
Loamy coating and bio-gallery		no	no	no				yes		Bioturbation contributing to formation of coating
Loamy phosphatic coating		no	no	no					yes	Leaching of P-rich waters
CaCO <sub>3</sub> coat on the under-side		no	no	no						Accumulation of calcium carbonate
CaCO <sub>3</sub> coat on top		yes?	yes?	no						Transport? after accumulation of calcium carbonate
In situ shattering		no	no		yes					Frost action after deposition, no transport after
Shattering cracks filled with groundmass		no	no	yes	yes					Relocation of fines after frost action, no transport after
Shattering cracks empty		no	no	no	yes					Frost action after deposition, no transport after
Shattering cracks with recrystallization		no	no	no	yes		yes			Frost action after deposition, no transport after

Fig. 6. Typical micro-features at the contact zone between clasts and silty groundmass in colluvial-aeolian sediments at the selected sites.



(Stoops, 2021) and therefore, classified and interpreted accordingly. Because they have been attributed to a wide range of processes, it is essential to distinguish the material they are made of (Stoops, 2021).

Loamy coatings were observed in all selected sites (Tables 6 and 7). Overall, they are attached to clasts, and in some case, the material is more compacted than the surrounding matrix. In the case of sediments affected by soil formation, the coating is also made of clayish material (Fig. 5d), which gives a higher birefringence to the coating. In many cases, they can be eroded by post-depositional processes and only partially preserved and attached to the clast (Fig. 6), making them difficult to interpret.

At the Obishir-1, brownish loamy coatings surrounding clasts were observed, and they have been interpreted as a result of transportation and redeposition down the slope (Brancaleoni et al., 2022). At the Obishir-5, loamy coatings were essentially made of the matrix attached to clasts' surfaces. They were commonly found in the cultural layers characterizing the sequence around 1 m below the ground surface. The cultural layers were characterized by localized granostriated b-fabric due to loamy coatings around coarse components (Fig. 5d).

Loamy coatings can also be a result of bioturbation. Clasts with compacted coatings attached to the surfaces were observed in association with faunal or plant activity features, such as bio-galleries or bioturbated groundmass (Fig. 5f). Bioturbation-related coatings were expressed in all deposits affected by bioturbation at the selected sites. Moreover, in Fig. 5e, we showed that some void could be created between the clast and groundmass when the clast rotates, leading perhaps to a coating that would not form otherwise. This feature might be a result of thin section preparation and/or transport of blocks.

Dusty coatings mostly occurred at the Obishir sites (Table 6; Fig. 5g; Table 7). Yellowish orange dusty fine-silt and coarse-clay coatings produced flame-like textural pedofeatures with irregular laminations (Fig. 5g). These features result from rapid water infiltration (Table 6, Fig. 5g), and they were associated with an *ex-situ* paleosol at the top of layer 6 (Brancaleoni et al., 2022). Clayish pellicular coatings (Fig. 5h) were generally the effect of illuviation or a result of chemical alteration attacking the clast. Given the pellicular thickness, we expect a low rate of the aforementioned processes. Phosphatic coatings were observed at the Obishir-5 (Fig. 5i; Table 7), and not elsewhere. We interpreted these features as a result of leaching of phosphorus-rich solutions percolating from an upper portion of the sequence connected with the Obishirian cultural layers (Table 2).

### 5.3. CaCO<sub>3</sub> accumulations

Calcium carbonate accumulations are usually found all around the clast (rinds) and/or on the undersides of clasts (coats and pendants), and they are mainly composed of calcium carbonate and impurities (Gile, Peterson and Grossman, 1966; Blank and Fosberg, 1990; Brock and Buck, 2005; Durand et al., 2018). They result from pedogenic processes in which hydraulic conditions, clast size, and lithology are the main factors controlling the morphology and thickness of the coatings (Courty et al., 1994; Treadwell-Steitz and McFadden, 2000; Khormali, Abtahi and Stoops, 2006). Moreover, these carbonate coatings might reflect climate changes (Blank and Fosberg, 1990; Courty et al., 1994; Khormali, Abtahi and Stoops, 2006; Durand et al., 2018). Interestingly, we observed CaCO<sub>3</sub> accumulation in the selected sites (Fig. 5j-l), even though the lithology of the coarse fractions at the Obishir and Katta Sai sites differed.

At the Obishir sites, these accumulations were in some cases very complex, showing the typical lamina-aggradation pattern, and were expressed in sediments with a frequency that is relatively consistent throughout the profiles (Table 7). The thickness varied from pellicular to 0.5 mm. The consistency in frequency and the differing thickness might be a further indication of the mixing of the material comprising the sequences. In calcic horizon, usually carbonate nodules and accumulations might develop in the central portion of the profile (Retallack,

2019), whereas here we found these features all along the profiles. Moreover, because the lithology is mainly limestone and particular preferences for clast size were not noted, the co-existence of thin and thick coatings in sediments might be further evidence of mixing. Carbonate calcium accumulation can also be an effect of the porosity of the sediments (Courty et al., 1994).

Coats and pendants can also be used as a proxy for assessing a reorientation of clasts (Fig. 5k). Usually, coatings are found on the undersides of clasts (Gile, Peterson and Grossman, 1966; Retallack, 2019). We might deduce a rotation or redeposition of the clast when the coating did not occur at the bottom surface. Overall, this interpretation should be taken with caution when dealing with cave deposits or other karst environments, where the coating could have originated when the clast was still attached to the cave wall (Miller, 2015). At the Obishir sites, these accumulations were often damaged, being the source for calcitic nodules, sand- and fine-pebble-sized calcitic material found in the groundmass.

Regarding the Katta Sai, we noted common CaCO<sub>3</sub> accumulations in Katta Sai 2 (Table 6; Fig. 5l; layer 3 Table 7). As shown in Fig. 5l, the well-developed and pendant-like accumulation was detached from the clast, leading to new calcite precipitation in the void formed between the clast and the accumulation itself. This is in line with the observations made by Brock and Buck (2005), thus confirming that pendants do not always form stalactite-like, where the innermost layers are the oldest and the outermost the youngest ones. This might have implications when dating these features for archeological purposes, we recommend to sample the accumulation along its entire thickness to check for inversions.

### 5.4. Cracks

Cracks usually form along the weakest planes within clasts. They are mostly a result of physical weathering, which may further lead to chemical weathering. Rock fragments at the sites showed smooth cracks, which were either empty, or recrystallized. Cracks were also filled with loamy material from the groundmass or opaque finer material (Fig. 5n, o; Fig. 6). Filled cracks might be evidence of finer particles relocation and could serve as a proxy for establishing *in-situ* processes and their chronology. For instance, in Fig. 5n, a clast showed gypsum recrystallisation that was eventually disrupted *in-situ* by the formation of a crack.

Gypsum (CaSO<sub>4</sub>·H<sub>2</sub>O) crystals are usually associated with strong evaporation in arid environments (Khormali et al., 2003; Miller, Goldberg and Berna, 2013) and related to changes of the underground water table in soils (Poch, Artieda and Lebedeva, 2018). Dissolution of gypsum features is related to relatively wetter conditions. We found intergrowth features at the bottom of layer 6 (Table 6; Fig. 5m; Table 7) and dissolution features at the top of layer 6 at the Obishir-1 (Table 7). This might give us a paleoclimatic signal in which bottom of layer 6 accumulated during a drier period (formation of gypsum crystals) followed by slightly wetter conditions (dissolution features). This is in line with the paleo-environmental interpretation given in Brancaleoni et al. (2022) where the bottom of layer 6 accumulated during drier conditions whereas layer 5 during slightly wetter ones.

Disintegration of coarse clasts was also observed (Fig. 5m). We concluded that it contributed to the *in-situ* production of the sand and silt fraction and its incorporation into the groundmass, especially when the clasts are coarse-crystalline or show a granoblastic fabric (Fig. 5m). Moreover, the disintegrated products (single crystals) were coated with fine material such as clayey material (Fig. 5m), possibly derived from the alteration of the clast itself and matrix material (Fig. 5n).

### 5.5. The groundmass

At the contact between the two PFs, we must distinguish two cases: the first is when the clast is free from micro-features attached to its surfaces, hence at direct contact with the groundmass; and the second is

when the clast shows secondary features attached to its surfaces. Moreover, we need to distinguish the micro-feature characterizing the clast in the first place.

In the first case, when the contact was just direct and the groundmass intact, we can assume that the primary character between the silty-gravel components was preserved because we have no evidence to the contrary. Furthermore, in this case, we can suggest that the material that surrounded the debris was not affected by post-depositional disturbance, and if so, only by the vertical relocation of particles. If a void or multiple voids occurred between the two PFs, we can assume that the contact was somehow disrupted or the finer material was not abundant enough to completely fill the debris' open-work structure.

In the second case, when a micro-feature occurs, the contact between the two PFs has been somehow altered. Loamy coatings have been interpreted as an indicator of redeposition, implying that the primary contact between the two fabrics has been altered. This is very difficult to assess only by looking at the very contact, especially for these sites where commonly, the coated material and the groundmass have similar characteristics. Only in the cases of loamy coatings or cappings characterized by a portion of clay, the contact between the coating and the groundmass was locally very sharp. It was also observed that some particles were attached to the coating by bridges created by the micro-mass, due to cohesive properties of the finer particles.

Regarding CaCO<sub>3</sub> accumulations and phosphatic features formed *in-situ*, in many cases, the groundmass, and better the micromass, was impregnated by these secondary products (e.g., Fig. 5j). If these micro-features were relict, meaning they formed *ex-situ*, the groundmass is simply not affected by them, and the contacts tend to be sharp. We also observed that some secondary features and processes affecting clasts are a source material for groundmass components (Fig. 5m, n). Thus, distinguishing the source between loess and secondary products is a complicated matter in these particular deposits, an issue that micromorphology alone struggles to solve, especially in bioturbated or disturbed sediments such as the ones encountered in the Obishir and Katta Sai complexes where lamination, usually indicating aeolian activity, could have been disrupted.

### 5.6. Micro-features rate, relative chronology and history of the sites

We can assume that well-developed carbonate accumulations, such as coats and pendants, have formed over an extended period, possibly with varying rates over time. As a matter of fact, these carbonate features are in many cases altered, well-developed, and exhibit different laminas. Previous studies have suggested that carbonate accumulation primarily occurred before the Late Pleistocene, as they are associated with less arid environments (Blank and Fosberg, 1990; Khormali, Abtahi and Stoops, 2006). In this regard, we might expect more developed features during wetter conditions and less developed features during more dry conditions. In some cases, the accumulation were eroded and coated with matrix material, indicating later reworking, where erosion and coating postdate the carbonate accumulation. It should be noted that some of these features are still forming *in-situ* at present, as shown in Fig. 5j where the micromass is impregnated, and in Fig. 5l where new calcitic precipitation is observed.

Regarding the frequency of carbonate accumulations (Table 7), a clear difference is evident between the Obishir and Katta Sai complexes. The Obishir sites, being rock shelters, exhibit a higher abundance of carbonate accumulations, due to the presence of abundant carbonate coarse debris, providing a more available source of calcium (Ca).

Disintegration and cracks always postdate the disrupted feature. For example, in Fig. 5n, the cracks postdated the *in-situ* formation of euhedral gypsum crystals. Furthermore, features related to chemical alteration pose challenges in terms of establishing their timing and may exhibit a different temporal pattern. They may be contemporary to carbonate accumulations since they are also associated with wetter environments. Features associated with frost action may be linked to the

LGM (Brancaleoni et al., 2022) (Table 1), particularly the well-developed ones, such as those found in layer 6 of the Obishir-1 (Table 7). However, they can also result from seasonal frost heave or some other type of reworking processes (e.g., bioturbation, solifluction or human activities such as dumping) if found in Holocene layers. For instance, loamy coatings are associated with cultural layer 2 at the Obishir-5. These coatings may also be related to geomorphological instability, which likely occurred more intensively in the Obishir area since the Late Glacial (Brancaleoni et al., 2022) (Table 1). Phosphatic coatings at the Obishir-5 might be a result of anthropogenic and domestic animal activities at the site, which was dated to around 6000 BCE (Taylor et al., 2021; Table 2).

At the Obishir-1, loamy cappings were found exclusively at the bottom of layer 6, together with euhedral gypsum crystals (Table 7). Cappings have been attributed to cold conditions, while gypsum crystals suggest dry conditions. Layer 6 is dated to the LGM (Table 1), which supports this hypothesis. The top of layer 6 exhibits gypsum dissolution features (Table 7), along with loamy and dusty coating. This might indicate slightly improved climatic conditions around 15 ky BP (Brancaleoni et al., 2022). Layer 5 consists of redeposited material (Brancaleoni et al., 2022), without any distinct features (Table 7). From layer 4 onwards, micro-features associated with wetter environments and pedogenesis (loamy coatings, ferruginous cappings and precipitations) are relatively more abundant. Gypsum-related features provide evidence of oscillating dry and wet conditions throughout the profile. CaCO<sub>3</sub> accumulations at the Obishir-1 are consistently present throughout the profile, possibly indicating redeposition. Cracks themselves do not appear to be proxies for any specific climatic signal, and they are quite common at the Obishir sites (Table 7).

At the Obishir-5, layers 5 and 4 are characterized by loamy, dusty, and phosphatic coatings, indicating wetter conditions and infiltration of phosphatic-contaminated waters. Layer 3 also was affected by phosphatic rich waters (Table 7). Features associated with wetter conditions are common in cultural layers, in some cases being dominant (e.g., layer 2.3; Table 7). Loamy cappings might be linked to seasonal frost heave or other reworking processes. CaCO<sub>3</sub> accumulations dominate in layer 5, 3 and 1, and are common elsewhere.

The Katta Sai sites exhibit fewer features, making it challenging to reconstruct their history based on the two PFs (Table 7). However, observations suggest possible intra-site differences in terms of calcium carbonate accumulations. At the Katta Sai sites, we observed carbonate accumulations at specific stratigraphic positions: layer 4a (Katta Sai 1); and layer 3 and 3b/3c at the Katta Sai 2 (Table 7). Layer 4a and 3 are both dated to around 26 ky BP, whereas layer 3b/3c was dated to around 67 ky BP (Table 3 and Table 4), indicating individual chronologies of these features associated with Marine Isotope Stages (MIS) 2 and 4, during which cold conditions prevailed (Rasmussen et al., 2014).

### 5.7. General remarks and implications for archaeological sites

Our study addresses the issue of equifinality in interpreting site formation and site-specific conditions, as highlighted in previous researches (e.g., Kielhofer et al., 2020). By analyzing micro-features related to the contact between the coarser mineral components and finer groundmass around, we observed a wide range of processes at this contact. However, we found that the same features were often attributed to different processes, demonstrating the complexity of the formation processes. The main difference among the sites we considered was the geomorphological setting, which affected the granulometric characteristics (Fig. 4). Rock fragments were more abundant at the Obishir sites, resulting in more features observed at their contacts (Table 7). Additionally, local conditions affected granulometric and micromorphological characteristics, as seen at the Obishir sites.

Our study emphasizes the importance of recognizing formation processes and post-depositional disturbances at archaeological sites. By examining features and processes occurring at the contact between silty

and gravelly material, we can support more general interpretations. The most common features at the selected sites were loamy coatings, calcium carbonate accumulations, and alteration of clasts. However, the most difficult features to distinguish and classify were loamy cappings and coatings, which had often been re-modeled by later processes (Fig. 6). As a result, the primary processes were difficult to assess. Nevertheless, the fact that the features are partially preserved implies post-depositional disturbance, which can result from a wide range of processes, including erosion, faunal and plant activity. Therefore, it is recommended to analyze the context in which the sediments accumulated and the overall groundmass in which these features are observed. For example, if the clast with a coating or a capping is associated with a biogallery or a groundmass showing traces of bioturbation (Fig. 6), it is likely that the coating is a result of bioturbation activity (faunal or phytogenic, depending on the type of bioturbation features), which tends to push the groundmass material toward the surfaces of clasts resulting in a compaction of the groundmass (Fig. 5f; Fig. 6). Regarding other types of coating observed, such as dusty, clayey, and phosphatic, we attributed the first two to rapid infiltration of water and the latter to later dripping of phosphorus-rich waters from cultural layers.

A parallel can be drawn with the gravel-sized artifacts, particularly regarding secondary calcium carbonate accumulation. Interestingly, at the selected archaeological sites, artifacts are often found covered by a  $\text{CaCO}_3$  crust (Fig. 7). For example, as shown in Fig. 7, a Bronze Age stone slab (panel d) in Katta Sai 1 is characterized by a carbonate crust in the very same way as the Paleolithic core (panel e). This supports the hypothesis of multiple phases of carbonate accumulation.

At the Obishir sites, calcium carbonate accumulations were commonly observed throughout the profile, including cultural layers. These features were mostly altered and eroded at those sites. At the Katta Sai, these secondary accumulations were found in single stratigraphic positions with indications of ongoing processes, such as in Fig. 5l. Additionally, as shown in Fig. 5k and l, a carbonate accumulation can be found on top and on the side and partially damaged in cultural layer 1 at the Obishir-5 (Table 2), and 3b/3c at the Katta Sai 2 (Table 4). This suggests that the carbonate crusts were formed before the transport and final deposition of clasts (and by extension, artifacts) within these layers. Therefore, the artifacts were already transported with the crust, and the position of the crust if on the upper side should indicate redeposition of an individual artifact.

We did not observe a sharp distinction between Pleistocene and Holocene sediments solely by looking at contacts between silty and gravelly material at the selected sites (Table 7). This could be due to weak climatic differences in the region, similar depositional processes or equifinality problems, mixing of material, different sampling resolutions, and different textures characterizing the sites. We could also conclude that clasts in sediments dated to LGM recorded certain traces of frost action, which were not observed in Holocene sediments, such as crescentic cappings, *in-situ* shattered clasts, and vertical-oriented clasts (Brancaleoni et al., 2022). Additionally, Holocene sediments at these sites were more affected by pedogenesis, bioturbation, and human activity processes than Pleistocene sediments. For instance, at the Obishir-5, loamy coatings were mainly present in initial Holocene sediments that also contained archaeological components, such as charcoal, ash, dung



Fig. 7. Carbonate crust usually characterizes artifacts at selected sites. a) Lithic material from Obishir-5 (layer 4 - excavations 2021). b) Microbladelet core from Obishir-5 (layer 2 - excavations 2016). c) Flake from Obishir-5 (layer 2 - excavations 2016). d) Grinding stone dated to the Bronze Age collected at Katta Sai 1, layer 4a. e) Paleolithic core retrieved from Katta Sai 1, layer 4b, affected by carbonate crust (blue arrow) and cracked (yellow arrow).

material, and bone fragments (Table 6).

## 6. Conclusions

Four sites in Central Asia were chosen for their distinctive modes of sediment accumulation: aeolian and colluvial. The methodology used included grain size analysis and, more importantly, micromorphology, which enabled the examination of the silt-gravel contact in these sediments. Micro-features on the surfaces of clasts were identified and classified into four main types: loamy cappings and coatings, secondary calcium carbonate accumulations, cracks. The contact between the coarse and fine material was frequently altered and marked by features related to mineral grain alteration, frost action, redeposition, pedogenetic processes, and anthropogenic activity. The processes affecting gravelly geogenic components and their micro-features may also reflect those impacting gravelly archaeological artifacts, such as secondary calcium carbonate accumulations. A tentative relative chronology and history based on the identified micro-features was proposed.

## 7. Formatting of funding resources

This study was supported by the National Science Centre, Poland (grant number 2018/29/B/ST10/00906). Fieldworks in Kyrgyzstan were supported by RSF (grant number 19-78-10053) and the National Science Centre, Poland (grant number 2018/29/B/ST10/00906). Fieldworks in Uzbekistan were financed by the National Science Centre, Poland (grant number 2017/25/B/HS3/00520 for the Polish expedition) and the RSF (grants number 20-09-00440a and 22-18-00568).

## 8. Declaration of generative AI and AI-assisted technologies in the writing process

During the preparation of this work the corresponding author used ChatGPT in order to proofread the text and improve language clarity. After using this tool/service, the author reviewed and edited the content as needed and takes full responsibility for the content of the publication.

## Author contribution

**GB:** conceptualization, data collection, data analysis and interpretation, drafting, revision. **MTK:** supervision, conceptualization, data collection, revision. **MKo, SvS:** excavation, data collection, revision. **PM** and **RK:** grain size data analysis, revision. **AA, KP, MKh, SAK:** excavation, data collection.

## Declaration of Competing Interest

The authors declare that they have no known competing financial interests or personal relationships that could have appeared to influence the work reported in this paper.

## Data availability

Data will be made available on request.

## Acknowledgements

We thank Ewa Deput for producing beautiful thin sections. We thank Nadav Nir (Freie Universität Berlin) for comments on a previous version of the manuscript. We would like to acknowledge students and volunteers involved in the excavations. We thank the anonymous referees who knowledgeably reviewed the manuscript.

## Appendix A. Supplementary material

Supplementary data to this article can be found online at <https://doi.org/10.1016/j.jasrep.2023.104118>.

## References

- Akimaliev, D.A., Zaurov, D.E., Eisenman, S.W., 2013. The geography, climate and vegetation of Kyrgyzstan. In: Eisenman, S.W., Zaurov, D.E., Struwe, L. (Eds.), *Medicinal Plants of Uzbekistan and Kyrgyzstan*. Springer, Central Asia, p. 340.
- Bertran, P., Texier, J.P., 1999. Facies and microfacies of slope deposits. *Catena* 35 (2–4), 99–121. [https://doi.org/10.1016/S0341-8162\(98\)00096-4](https://doi.org/10.1016/S0341-8162(98)00096-4).
- Blank, R.R., Fosberg, M.A., 1990. Micromorphology and classification of secondary calcium carbonate accumulations that surround or occur on the undersides of coarse fragments in Idaho (U.S.A.). *Dev. Soil Sci.* 19 (C), 341–346. [https://doi.org/10.1016/S0166-2481\(08\)70345-3](https://doi.org/10.1016/S0166-2481(08)70345-3).
- Brancaleoni, G., Shnaider, S., Osipova, E., Danukalova, G., Kurbanov, R., Deput, E., Alisher kyzy, S., Abdykanova, A., Krajcarz, M.T., 2022. Depositional history of a talus cone in an arid intermontane basin in Central Asia: an interdisciplinary study at the Late Pleistocene-Late Holocene Obishir-I site, Kyrgyzstan. *Geoarchaeology*. John Wiley and Sons Inc 37 (2), 350–373.
- Brock, A.L., Buck, B.J., 2005. A new formation process for calcic pendants from Pahrangat Valley, Nevada, USA, and implication for dating Quaternary landforms. *Quat. Res.* 63 (3), 359–367. <https://doi.org/10.1016/j.yqres.2005.01.007>.
- Bronk Ramsey, C., 1995. Radiocarbon calibration and analysis of stratigraphy: the OxCal program. *Radiocarbon* 37 (2), 425–430.
- Bronk Ramsey, C., 2001. Development of the radiocarbon program OxCal. *Radiocarbon* 43 (2A), 355–363.
- Brunet, M.F., Sobel, E.R., Mccann, T., 2017. Geological evolution of central Asian basins and the western Tien Shan range. *Geol. Soc. Special Publ.* 427 (1), 1–17. <https://doi.org/10.1144/SP427.17>.
- Courty, M.-A., Goldberg, P., Macphail, R., 1990. Soils and micromorphology in archaeology. *Soil Sci.* 150 (6), 904.
- Courty, M.-A., Marlin, C., Dever, L., Tremblay, P., Vachier, P., 1994. The properties, genesis and environmental significance of calcitic pendants from the High Arctic (Spitsbergen). *Geoderma*. Elsevier 61 (1–2), 71–102.
- Dlussky, K.G., 2009. Loess deposits. In: *Encyclopedia of Earth Sciences Series*. Springer, Dordrecht, pp. 522–524.
- Dodonov, A.E., 2002. Quaternary of Middle Asia: Stratigraphy, Correlation, Paleogeography. GEOS, Moscow.
- Durand, N., et al., 2018. Calcium carbonate features. In: Stoops, G., Marcellino, V., Mees, F. (Eds.), *Interpretation of Micromorphological Features of Soils and Regoliths*, second ed. Elsevier, Amsterdam, pp. 206–258.
- Gile, L.H., Peterson, F.F., Grossman, R.B., 1966. Morphological and genetic sequences of carbonate accumulation in desert soils. *Soil Sci.* 101 (5), 347–360. <https://doi.org/10.1097/00010694-196605000-00001>.
- Khormali, F., Abtahi, A., Mahmoodi, S., Stoops, G., 2003. Argillic horizon development in calcareous soils of arid and semiarid regions of southern Iran. *Catena* 53 (3), 273–301.
- Khormali, F., Abtahi, A., Stoops, G., 2006. Micromorphology of calcitic features in highly calcareous soils of Fars Province, Southern Iran. *Geoderma* 132 (1–2), 31–46. <https://doi.org/10.1016/j.geoderma.2005.04.024>.
- Kielhofer, J., et al., 2020. The micromorphology of loess-paleosol sequences in central Alaska: a new perspective on soil formation and landscape evolution since the Late Glacial period (c. 16,000 cal yr BP to present). *Geoarchaeology* 35 (5), 701–728. <https://doi.org/10.1002/geo.21807>.
- Kot, M., Pavlenok, G., Krajcarz, M.T., Szymanek, M., Fedorowicz, S., Moska, P., Khudjanazarov, M., Szymczak, K., Leloch, M., Kogai, S., Talamo, S., Fewlass, H., Pavlenok, K., 2022. Is there Initial Upper Palaeolithic in Western Tien Shan? Example of an open-air site Katta Sai 2 (Uzbekistan). *J. Anthropol. Archaeol. Academic Press* 65, 101391.
- Krajcarz, M.T., Cyrek, K., Krajcarz, M., Mroczek, P., Sudoł, M., Szymanek, M., Tomek, T., Madeyska, T., 2016a. Loess in a cave: Lithostratigraphic and correlative value of loess and loess-like layers in caves from the Kraków-Częstochowa Upland (Poland). *Quat. Int. Pergamon* 399, 13–30.
- Krajcarz, M.T., Kot, M., Pavlenok, K., Fedorowicz, S., Krajcarz, M., Lazarev, S.Y., Mroczek, P., Radzhabov, A., Shnaider, S., Szymanek, M., Szymczak, K., 2016b. Middle Paleolithic sites of Katta Sai in western Tien Shan piedmont, Central Asiatic loess zone: Geoarchaeological investigation of the site formation and the integrity of the lithic assemblages. *Quat. Int.* 399, 136–150.
- Krajcarz, M.T., Szymanek, M., Krajcarz, M., Pereswiet-Soltan, A., Alexandrowicz, W.P., Sudoł-Procyk, M., Louys, J., 2020. Shelter in Smoleń III - A unique example of stratified Holocene clastic cave sediments in Central Europe, a lithostratigraphic stratotype and a record of regional paleoecology. *PLoS ONE* 15 (2), e0228546.
- Kroh, P., Dolnicki, P. and Łajczak, A. (2021) 'Subnival Processes and Subnival Sedimentation Mechanisms, the Pamir-Alay Mts., Tajikistan', *Land* 2021. Multidisciplinary Digital Publishing Institute, 10(2), p. 104. doi: 10.3390/LAND10020104.
- Lancaster, N., 2020. On the formation of desert loess. *Quat. Res. Cambridge University Press* 96, 105–122. <https://doi.org/10.1017/QUA.2020.33>.
- Macphail, R.I., Goldberg, PAUL, 2003. Gough's Cave, Cheddar, Somerset: Microstratigraphy of the Late Pleistocene/earliest Holocene sediments. *BGE* 58 (S1).
- Meier, L.A., Krauze, P., Prater, I., Horn, F., Schaefer, C.E.G.R., Scholten, T., Wagner, D., Mueller, C.W., Kühn, P., 2019. Pedogenic and microbial interrelation in initial soils under semiarid climate on James Ross Island, Antarctic Peninsula region. *Biogeosciences* 16 (12), 2481–2499.
- Miller, C.E., 2015. A Tale of Two Swabian Caves: Geoarchaeological Investigations at Hohle Fels an Geissenklosterle. Kerns Verlag, Tübingen.

- Miller, C.E., Goldberg, P., Berna, F., 2013. Geoarchaeological investigations at Diepkloof Rock Shelter, Western Cape, South Africa. *J. Archaeol. Sci.* Academic Press 40 (9), 3432–3452. <https://doi.org/10.1016/j.jas.2013.02.014>.
- Nishiaki, Y., Aripdjanov, O., Arai, S., Akashi, C., Nakata, H., Sayfullayev, B., Ergashev, O., Suleimanov, R., 2022. Neolithization during the 6th millennium BCE in western Central Asia: New evidence from Kaynar Kamar Rockshelter, Hissar Mountains, Southeast Uzbekistan. *Archaeol. Res. Asia*. Elsevier 30, 100352.
- Ospova, E., et al., 2020. Palaeoenvironmental conditions of the Palaeolithic-Neolithic transition in the Fergana Valley (Central Asia) – New data inferred from fossil molluscs in Obishir-V rockshelter (Kyrgyzstan). In: *Quaternary International*. Elsevier Ltd, (November). <https://doi.org/10.1016/j.quaint.2020.11.009>.
- Pavlenok, K., Kot, M., Pavlenok, G., Krajcarz, M.T., Khudjanazarov, M., Leloch, M., Szymczak, K., 2021. Middle Paleolithic technological diversity during MIS 3 in the Western Tian Shan piedmonts: example of the Katta Sai 1 open-air loess site. *Archaeol. Res. Asia* 25, 100262.
- Pawelec, H., Ludwikowska-Kędzia, M., 2016. Macro- and micromorphologic interpretation of relict periglacial slope deposits from the holy cross mountains, Poland. *Permafrost Perigl. Process.* 27 (2), 229–247. <https://doi.org/10.1002/ppp.1864>.
- Poch, R.M., Artieda, O., Lebedeva, M., 2018. Chapter 10 Gypsic features. In: *Interpretation of Micromorphological Features of Soils and Regoliths*. Elsevier, pp. 259–287.
- Rasmussen, S.O., Bigler, M., Blockley, S.P., Blunier, T., Buchardt, S.L., Clausen, H.B., Cvijanovic, I., Dahl-Jensen, D., Johnsen, S.J., Fischer, H., Gkinis, V., Guillevic, M., Hoek, W.Z., Lowe, J.J., Pedro, J.B., Popp, T., Seierstad, I.K., Steffensen, J.P., Svensson, A.M., Vallenga, P., Vinther, B.M., Walker, M.J.C., Wheatley, J.J., Winstrup, M., 2014. A stratigraphic framework for abrupt climatic changes during the Last Glacial period based on three synchronized Greenland ice-core records: refining and extending the INTIMATE event stratigraphy. *Quat. Sci. Rev.* Elsevier Ltd 106, 14–28.
- Reimer, P.J., Austin, W.E.N., Bard, E., Bayliss, A., Blackwell, P.G., Bronk Ramsey, C., Butzin, M., Cheng, H., Edwards, R.L., Friedrich, M., Grootes, P.M., Guilderson, T.P., Hajdas, I., Heaton, T.J., Hogg, A.G., Hughen, K.A., Kromer, B., Manning, S.W., Muscheler, R., Palmer, J.G., Pearson, C., van der Plicht, J., Reimer, R.W., Richards, D.A., Scott, E.M., Southon, J.R., Turney, C.S.M., Wacker, L., Adolphi, F., Büntgen, U., Capano, M., Fahrni, S.M., Fogtmann-Schulz, A., Friedrich, R., Köhler, P., Kudsk, S., Miyake, F., Olsen, J., Reinig, F., Sakamoto, M., Sookdeo, A., Talamo, S., 2020. The IntCal20 Northern Hemisphere radiocarbon age calibration curve (0–55 cal kBP). *Radiocarbon* 62 (4), 725–757.
- Reimer, P.J., Bard, E., Bayliss, A., Beck, J.W., Blackwell, P.G., Ramsey, C.B., Buck, C.E., Cheng, H., Edwards, R.L., Friedrich, M., Grootes, P.M., Guilderson, T.P., Hafflidason, H., Hajdas, I., Hatté, C., Heaton, T.J., Hoffmann, D.L., Hogg, A.G., Hughen, K.A., Kaiser, K.F., Kromer, B., Manning, S.W., Niu, M., Reimer, R.W., Richards, D.A., Scott, E.M., Southon, J.R., Staff, R.A., Turney, C.S.M., van der Plicht, J., 2013. IntCal13 and Marine13 radiocarbon age calibration curves 0–50,000 years cal BP, 55. *Radiocarbon*, Cambridge University Press, pp. 1869–1887.
- Retallack, G.J., 2019. *Soils of the Past: An Introduction to Paleopedology*. Third Edit. Wiley-Blackwell, Hoboken, NJ.
- Sanders, D., 2010. Sedimentary facies and progradational style of a Pleistocene talus-slope succession, Northern Calcareous Alps, Austria. *Sediment. Geol.* Elsevier B.V. 228 (3–4), 271–283. <https://doi.org/10.1016/j.sedgeo.2010.05.002>.
- Sanders, D., Ostermann, M., Kramers, J., 2009. Quaternary carbonate-rocky talus slope successions (Eastern Alps, Austria): Sedimentary facies and facies architecture. *Facies* 55 (3), 345–373. <https://doi.org/10.1007/s10347-008-0175-z>.
- Shnaider, S.V., Krajcarz, M.T., Viola, T.B., Abdykanova, A., Kolobova, K.A., Fedorchenko, A.Y., Alisher-kyzy, S., Krivoschapkin, A.I., 2017. New investigations of the Epipalaeolithic in western Central Asia: Obishir-5. *Antiquity* 91 (360), 6–12. <https://doi.org/10.15184/aqy.2017.213>.
- Spinapolic, E.E., Zerboni, A., Meyer, M.C., Talamo, S., Mariani, G.S., Gliganic, L.A., Buti, L., Fusco, M., Maiorano, M.P., Silvestrini, S., Sorrentino, R., Vazzana, A., Romandini, M., Fiorini, A., Curci, A., Benazzi, S., 2022. Back to Uluzzo – archaeological, palaeoenvironmental and chronological context of the Mid-Upper Palaeolithic sequence at Uluzzo C Rock Shelter (Apulia, southern Italy). *J. Quat. Sci.* 37 (2), 217–234.
- Stoops, G., 2021. *Guidelines for Analysis and Description of Soil and Regolith Thin Sections*. Second Edi. Wiley.
- Taylor, W.T.T., Pruvost, M., Posth, C., Rendu, W., Krajcarz, M.T., Abdykanova, A., Brancaleoni, G., Spengler, R., Hermes, T., Schiavinato, S., Hodgins, G., Stahl, R., Min, J., Alisher kyzy, S., Fedorowicz, S., Orlando, L., Douka, K., Krivoschapkin, A., Jeong, C., Warinner, C., Shnaider, S., 2021. Evidence for early dispersal of domestic sheep into Central Asia. *Nat. Human Behav.* 5 (9), 1169–1179.
- Texier, J.P., Meireles, J., 2003. Relict mountain slope deposits of northern Portugal: Facies, sedimentogenesis and environmental implications. *J. Quat. Sci.* 18 (2), 133–150. <https://doi.org/10.1002/jqs.752>.
- Timireva, S.N., Kononov, Y.M., Sycheva, S.A., Taratunina, N.A., Kalinin, P.I., Filippova, K.G., Zakharov, A.L., Konstantinov, E.A., Murray, A.S., Kurbanov, R.N., 2022. Revisiting the Taman peninsula loess-paleosol sequence: Middle and Late Pleistocene record of Cape Pekla. *Quat. Int. Pergamon* 620, 36–45.
- Treadwell-Steitz, C., McFadden, L.D., 2000. Influence of parent material and grain size on carbonate coatings in gravelly soils, Palo Duro Wash, New Mexico. *Geoderma*. Elsevier 94 (1), 1–22. [https://doi.org/10.1016/S0016-7061\(99\)00075-0](https://doi.org/10.1016/S0016-7061(99)00075-0).
- Van Vliet-Lanoë, B., Fox, C.A., Gubin, S.V., 2004. In: *Cryosols*. Springer Berlin Heidelberg, Berlin, Heidelberg, pp. 365–390.
- Waroszewski, J., Sprafke, T., Kabala, C., Muszyfaga, E., Łabaz, B., Woźniczka, P., 2018. Aeolian silt contribution to soils on mountain slopes (Mt. Ślęża, southwest Poland). *Quat. Res.* Cambridge University Press 89 (3), 702–717.

## ***Appendix C – Scientific paper 3***

Brancaleoni, G., Shnaider, S., Lempart, G., Deput, E., Abdykanova, A., Krajcarz, M. T. Geoarchaeological approach for tackling the function and preservation state of the Obishir-5 site, the earliest Neolithic site in the Fergana Valley, submitted on 23<sup>rd</sup> October 2023 at the *Journal of Archaeological and Anthropological Science*

1       **Geoarchaeological approach for tackling the function and**  
2 **preservation state of the Obishir-5 site, the earliest Neolithic**  
3 **site in the Fergana Valley**

4       **Authors**

5       **Greta Brancaleoni\***, Institute of Geological Sciences, Polish Academy of Sciences, 51/55  
6 Twarda st, 00-818 Warsaw, Poland (ORCID 0000-0002-5563-3729;  
7 [greta.brancaleoni@twarda.pan.pl](mailto:greta.brancaleoni@twarda.pan.pl))

8       **Svetlana Shnaider** APSACA Laboratory, National Center of Archaeology, Uzbek Academy  
9 of Sciences, 81 Mirzo Ulugbek Street, Tashkent, Uzbekistan (ORCID 0000-0003-2230-4286;  
10 [sveta.shnayder@gmail.com](mailto:sveta.shnayder@gmail.com))

11       **Malgorzata Lempart-Drozd**, Institute of Geological Sciences, Polish Academy of Sciences,  
12 1 Senacka st, 31-002 Cracow, Poland (ORCID 0000-0001-7394-5951; [ndlempar@cyf-kr.edu.pl](mailto:ndlempar@cyf-kr.edu.pl))

13       **Jan Goleń**, Institute of Geological Sciences, Polish Academy of Sciences, 1 Senacka st, 31-  
14 002 Cracow, Poland (ORCID 0000-0002-0107-0647; [ndgolen@cyf-kr.edu.pl](mailto:ndgolen@cyf-kr.edu.pl))

15       **Ewa Deput**, Institute of Geological Sciences, Polish Academy of Sciences, 51/55 Twarda st,  
16 00-818 Warsaw, Poland

17       **Aida Abdykanova**, American University of Central Asia, 7/6 Aaly Tokombaev st, Bishkek  
18 720060, Kyrgyzstan (ORCID 0000-0002-7238-9065; [abdykanova\\_a@auca.kg](mailto:abdykanova_a@auca.kg))

19       **Maciej T. Krajcarz**, Institute of Geological Sciences, Polish Academy of Sciences, 51/55  
20 Twarda st, 00-818 Warsaw, Poland (ORCID 0000-0002-1240-0664; [mkrajcarz@twarda.pan.pl](mailto:mkrajcarz@twarda.pan.pl))

21       *\*corresponding author*

22        **Abstract**

23        Obishir-5 is the eponymous and pivotal site of the Obishirian archaeological unit. The Obishirian  
24        is an early Neolithic culture that spread in the Fergana Valley and neighboring territories  
25        including the Pamirs between 9.5 and 6.5 ka BP. The importance of the Obsihir-5 site lies in its  
26        provision of some of the earliest evidence for the utilization of livestock in the mountainous  
27        regions of interior Central Asia. Geoarchaeological investigations, including the application of  
28        textural, geochemical, mineralogical and micromorphological methods at Obishir-5 focused on  
29        the reconstruction of geogenic and anthropogenic formation processes and disturbances  
30        responsible for the alteration of the sedimentary and the archaeological record. The geogenic  
31        material present at the site comprises an unconsolidated, poorly sorted mixture of angular rock  
32        fragments, which have accumulated through gravity-induced processes, alongside fine-grained  
33        sediment resulting from aeolian processes and in situ weathering. The archaeological material,  
34        including bones, charcoals and herbivore dung is intermixed with geogenic sediments and shows  
35        evidence of reworking. This archaeological material likely originated from anthropogenic  
36        activities, such as herding and firing, and subsequently subjected to post-depositional disturbance,  
37        including bioturbation, trampling, and organic matter degradation. The sediments at Obishir-5  
38        retain characteristics mainly associated with the following occupational phases: (1) Bronze Age  
39        and Middle Ages, (2) Obishirian, and (3) the Epipaleolithic. Through the study of the sedimentary  
40        record, we have been able to infer that the Obishirian culture relied on domestication of animals,  
41        especially ruminant. However, it is worth noting that the unit at this site has been affected by  
42        reworking processes, leading to fragmentation and poor preservation. While the methodologies  
43        employed have been successful in discerning the main formation history at the site, several aspects  
44        remain in needs of further clarification. Moreover, bulk sample analysis has failed to detect  
45        important aspects within the sedimentary record, which can only be unveiled through  
46        micromorphology.

47        *Keywords:* micromorphology, site formation, Obishirian culture, Kyrgyzstan, Central Asia

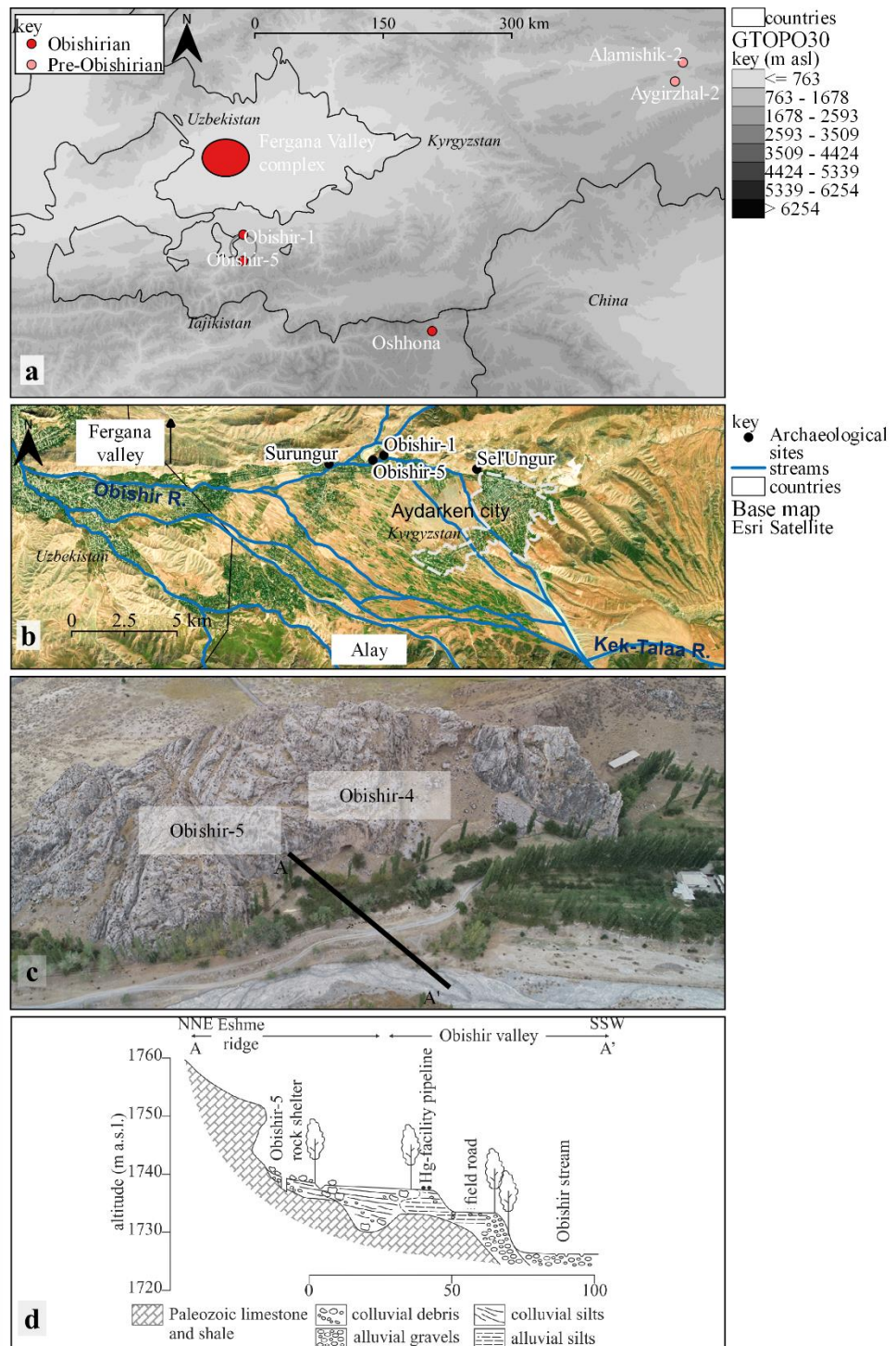
48

49



## 50 **1 Introduction**

51 Obishir-5, also referred to as Obishir-V (39°57'23.3" N, 71°16'52.4" E; 1710 m a.s.l.), is an  
52 archaeological site located in Kyrgyzstan, situated at the southern margin of the Fergana Valley  
53 (**Fig. 1a**). This site holds significant importance, as it serves as the eponymous and pivotal site of  
54 the Obishirian archaeological unit. Notably, the Obishirian culture is characterized by its  
55 distinctive microblade technology, boasting an industry primarily dominated by bladelets and  
56 microblades featuring alternating and ventral retouch, end-scrapers, single trapezoids, bone awls  
57 (Islamov, 1980; Fedorchenko *et al.*, 2018; Shnaider *et al.*, 2020).



58

59 **Fig. 1** The Obishir-5 site is located in a intermontane valley at the toe of the Alay range **a**)  
 60 Location of Obishir sites, as a base map we used a digital elevation model products GTOPO30  
 61 (DEM; gt30e060n90 and n40; source USGS EROS Archive), the geographical coordinates give  
 62 the location of the sites (for a list of coordinates refer to Supplementary Material Table S1); **b**)  
 63 close-up on the Aydarken basin; **c**) drone imagery of the Obishir-5 site area; and **d**) a schematic  
 64 cross-section of the Obishir-5 site area

65 This cultural unit is closely associated with the surge in the number of archaeological sites  
 66 throughout the Fergana Valley and its surrounding territories during the Early Holocene (Shnaider  
 67 *et al.*, 2020; Osipova *et al.*, 2021). Its influence extends from the southern reaches of the Tien

68 Shan, with archaeological sites in Fergana Valley, such as the Obishir complex site to the southern  
69 expanse of the Pamir Mountains (Brancaleoni *et al.*, 2022). The Obishirian assemblages are dated  
70 between 9.5 and 6.5 thousand years before present (ka BP) (Osipova *et al.*, 2021; W. T. T. Taylor  
71 *et al.*, 2021; Brancaleoni *et al.*, 2022). The site not only exhibits the Obishirian culture but also  
72 feature an Epipaleolithic assemblage dating back to between 11 and 8 ka BP (Osipova *et al.*, 2021;  
73 W. T. T. Taylor *et al.*, 2021; Brancaleoni *et al.*, 2022).

74 The term ‘Obishirian’ was first introduced by U. Islamov (Islamov, 1980), who initially  
75 attributed the culture to the Mesolithic period. However, a recent groundbreaking study on faunal  
76 remains at Obishir-5 conducted by W. T. T. Taylor *et al.* (2021) has yielded crucial findings that  
77 indicate a connection between the Obishirian culture and early domestic animals (i.e. *Ovis* and  
78 *Capra*). These remains were found in stratigraphic unit 2, dating to around 8 ka BP. This  
79 discovery not only sheds light on the early utilization of domestic animals in the Fergana Valley  
80 mountains but also prompts a reclassification of the Obishirian culture to the early Neolithic  
81 period. Consequently, the Obishirian culture could likely revolve around a domestication-based  
82 economy, however to date evidence of herding are lacking.

83 In addition, current literature (Osipova *et al.*, 2021; W. T. T. Taylor *et al.*, 2021; Serdyuk *et*  
84 *al.*, 2023) concerning Obishir-5 raises certain concerns regarding site integrity. These concerns  
85 encompass a range of issues, including:

- 86 a. inconsistent radiocarbon dating results along the profile (W. T. T. Taylor *et al.*, 2021);
- 87 b. *Ovis* and *Capra* remains’ presence within stratigraphic units 1-3, and to some extent  
88 in unit 4 (W. T. T. Taylor *et al.*, 2021);
- 89 c. variation in the preservation status of bone collagen and DNA amongst specimens  
90 (W. T. T. Taylor *et al.*, 2021), indicative of poor preservation for some bones;
- 91 d. limited variability of malacofauna (Osipova *et al.*, 2021) and small mammal  
92 assemblages (Serdyuk *et al.*, 2023) within the stratigraphic sequence, possibly  
93 suggesting climatic stability over extended periods.

94 This climatic stability seems to diverge from the broader climatic changes documented across  
95 the region, particularly within the mountainous interior of central and western Tian-Shan and the  
96 Pamirs. While the complex climatic patterns lack clear long-term trends (Spate, Leipe and  
97 Motuzaite Matuzeviciute, 2022), they reflect fluctuating moisture levels and precipitation  
98 availability from the final Pleistocene through the Late Holocene (Mathis *et al.*, 2014; Heinecke  
99 *et al.*, 2018; Jiang *et al.*, 2020; Li *et al.*, 2020; Spate, Leipe and Motuzaite Matuzeviciute, 2022).

100 The afore-mentioned observations have led to the assumption that Obishir-5’s sedimentary  
101 material have undergone reworking. This reinterpretation underscores the likelihood that distinct  
102 signals stemming from diverse proxies (such as chronology and faunal remains) could be

103 influenced by similar reworking processes. Given that Obishir-5 occupies a pivotal role in  
104 comprehending various herding patterns, diverse subsistence strategies, and stands as a key  
105 Obishirian site within the region, delving into the site's formation and accounting for post-  
106 depositional disturbances becomes paramount.

107 Moreover, a crucial goal is to search for evidence of herding recorded at the site. Following  
108 the findings of (W. T. T. Taylor *et al.*, 2021), we have preliminary evidence that the culture  
109 exploited domestic animals. The question that arises is whether these domestic animals were  
110 hunted or taken at the site. Answering this question would validate the hypothesis of a pastoral  
111 economy. Alternatively, the Obishirian economy might have been based on hunting feralized  
112 domestic animals rather than herding livestock. To address these concerns, a geoarchaeological  
113 investigation was devised, incorporating several methods that are independent from faunal  
114 remains: grain size distribution analysis, geochemistry and mineralogy assessments, and the  
115 microscopic analysis of sediments (micromorphology).

## 116 **2 The site**

117 Obishir-5 is located at the foothills of an ENE-WSW-oriented Eshme ridge also indicated as  
118 Eshme Too in Soviet topographic maps at a 1:100k scale. To the south, this ridge faces the  
119 Aydarken basin drained by several streams, including Obishir (**Fig. 1b**). These streams are  
120 relatively small, braided, and periodically recharged by meltwaters from winter snow and  
121 mountain glaciers in the Alay mountains to the S, primarily resulting in outflows during the winter  
122 and spring seasons. The drainage pattern follows an ESE-WNW direction within the valley (**Fig.**  
123 **1b**), where artificial drainage is also present. The basin stretches approximately 18 km from E to  
124 W and is about 6 km wide. The surrounding landscape is predominantly mountainous,  
125 characterized by a series of E-W oriented ridges to the north and south, enclosing the Aydarken  
126 basin, essentially a small intermountain basin filled with Quaternary deposits, predominantly of  
127 alluvial, aeolian, and colluvial origin. The western end of the valley is sealed off as the streams  
128 converge into the Sokh river (Brancaleoni *et al.*, 2022).

129 Several small urban areas are located within the basin, with Aydarken (known as Khaydarkan  
130 in Russian) being one of the largest and most urbanized cities, second only to Sokh. Apart from  
131 urban centers, there are isolated rural houses and farming structures scattered throughout the  
132 basin. Agriculture and pastoralism are the predominant land use types, with fruit orchards  
133 commonly cultivated for local commercial purposes. It is worth mentioning that the Eshme ridge  
134 has been extensively exploited for its mineral resources since the 1940s (UNEP, UNITAR, and  
135 Zoï E. Network, 2009) resulting in a landscape dominated by tailings piles, mines, and shafts  
136 (Brancaleoni *et al.*, 2022).

137 As per the current Köppen-Geiger climate classification map (Beck *et al.*, 2018), the climate  
138 in the study area is characterized as arid (B), steppe (S), and cold (k), with a mean annual air  
139 temperature (MAT) below 18 °C and mean annual precipitation (MAP) estimated to be below  
140 250 mm per year. Given its arid nature, the terrain experiences limited and sparse surface  
141 vegetation (Cooke, Warren and Goudie, 1993) and is susceptible to mass movement erosive  
142 events downslope (French, 2019). Moreover, in arid and semi-arid environments, rock outcrops  
143 and surface debris often undergo flaking, spalling, splitting, and granular disintegration (Cooke,  
144 Warren and Goudie, 1993).

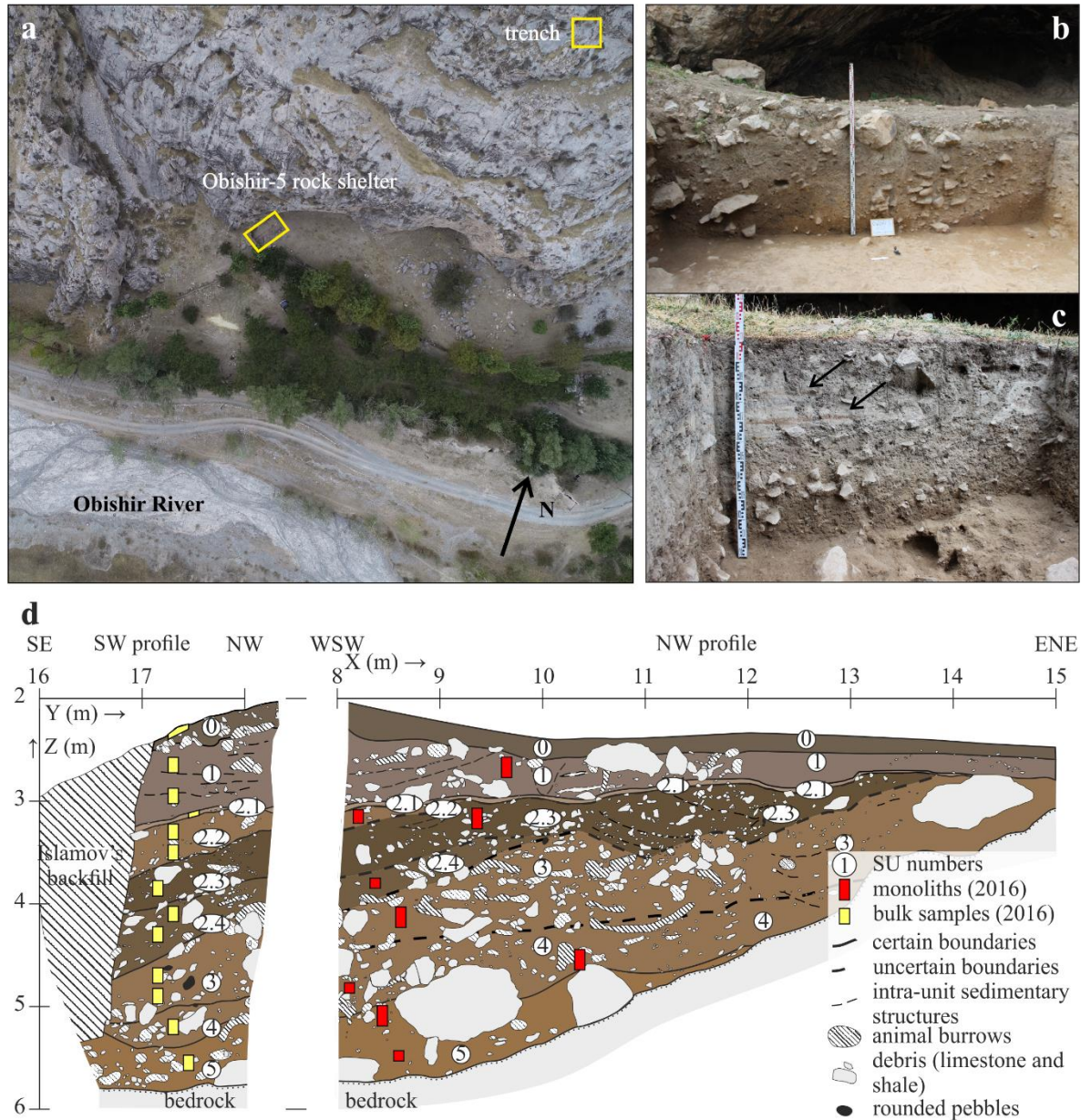
145 Rock shelters and small caves are ubiquitous in the Eshme Ridge. Significantly, several  
146 archaeological sites, such as Obishir-1, Sel'Ungur Cave, and Surungur are on the southern flank  
147 of the Eshme ridge (**Fig. 1b**), all sharing a geomorphological setting akin to that observed at  
148 Obishir-5 (**Fig. 1cd**). These sites are typically found at the base of a steep cliff, positioned in front  
149 of a rock shelter niche or a cave entrance, with associated talus deposits overlaying the bedrock  
150 or a flat alluvial terrace (Brancaleoni *et al.*, 2022). These steep cliffs mainly face south, and range  
151 in height from 20 to 30 m. The Obishir stream flows just in front of Obishir-5, approximately  
152 150 m away to the south (**Fig. 1cd**). Its flat terraces are used for agriculture and pastoral activities.

153 At Obishir-5, the talus cone spans approximately 60 m in width and extends around 50 m  
154 downslope from the cliff's base to the south, where it likely interfingers with the alluvial terrace  
155 (**Fig. 1cd**). The bedrock surface at Obishir-5 is irregular (**Fig. 1d**), as evidenced by geophysical  
156 surveys conducted at the site (Olenchenko *et al.*, 2017), revealing depressions of approximately  
157 10 meters in depth filled with loose sediments of anthropogenic origin. This uneven bedrock  
158 surface is likely a result of karstic processes. The talus' maximum thickness therefore up to *circa*  
159 10 m (**Fig. 1d**). It is plausible that the cone initially had larger dimensions in terms of length and  
160 height, which may have been reduced over time due to subsequent erosional processes.

## 161 **2.1 Sedimentary sequence: macroscopic stratigraphy and chronology**

162 The Quaternary sequence at the site was originally characterized by U. Islamov (Islamov,  
163 1980), who identified nine stratigraphic units. However, during the 2016 field campaign, thanks  
164 to a trench opened in front of the rockshelter (**Fig. 2a**) a reevaluation of the stratigraphy led to the  
165 recognition of six stratigraphic units (Fedorchenko *et al.*, 2018; Osipova *et al.*, 2021; W. T. T.  
166 Taylor *et al.*, 2021). In this study, we adhere to the same stratigraphic scheme (see Table S2 in  
167 Supplementary Information (SI)), consisting of stratigraphic units (SU) from SU0 to SU5 (from  
168 top to bottom), with SU2 being further divided into four subunits (Sub2.1, Sub2.2, Sub2.3 and  
169 Sub2.4). It is important to note that identifying units was challenging due to their limited visibility.  
170 Recognition was based on subtle changes in physical properties such as texture, color variation,  
171 gravel and boulder content (**Fig. 2bcd**), as well as the presence or absence of anthropogenic

172 elements (see Table S2 in SI). The boundaries between units were not consistently continuous  
 173 and were often disrupted by larger clasts and animal burrowing (**Fig. 2d**, Table S2 and Figure S1  
 174 in SI). The only distinct boundaries were observed between SU1 and Sub2.1, while the others  
 175 were discerned through faint sub-linear arrangements of larger boulders.



176

177 **Fig. 2** The Obishir-5 site. **a**) Drone imagery of the site, the main trench is in front of a rock-  
 178 shelter; **b**) NW profile photograph after the 2021 campaign; **c**) NW profile photograph after 2016  
 179 campaign, arrows point to reddened substrate; **d**) Drawing of the two profiles SW and NW of the  
 180 main trench (2016-2019) with location of micromorphology (monoliths) and bulk samples (after  
 181 W. T. T. Taylor *et al.*, 2021). Please note that the inclination of the boundary between SU3 and  
 182 SU4 has been revisited, as for now the boundary is less inclined. Z is in m below the site datum.

183 The sedimentary material falls into the category of matrix supported, fine, bouldery and  
 184 gravelly diamictos (Miall, 1978; Zieliński and Pisarska-Jamrozy, 2012; Osipova *et al.*, 2021)  
 185 (refer to Tables S2 in SI). The sequence initiates with SU5, which represents the terminal

186 Pleistocene and directly overlies the bedrock. This unit is characterized by compaction and a  
187 lighter matrix color in comparison to the overlying units. SU4 closely resembles SU5 but with  
188 occasional lithic components. The lower part of the profile (from SU5 to the base of SU3) exhibits  
189 similarities with mixed loess-debris deposits found in neighboring sites like Sel'Ungur Cave and  
190 Obishir-1 (Krivoshapkin *et al.*, 2020; Brancaleoni *et al.*, 2022). SU3 displays a softer texture and  
191 contains large charcoal fragments. SU2 is darker in color, ranging from pinkish gray (Sub2.2) to  
192 dark brown (Sub2.3). It features a lenticular shape with lateral variations, especially toward the  
193 ENE direction. SU2 presents a disturbed internal structure and is further divided into various  
194 subunits. The pinkish gray color often indicates the presence of ash material, whereas dark brown  
195 hue suggests organic matter. SU2 is characterized by its soft texture chaotic distribution of large  
196 charcoal and bone fragments. Radiocarbon dates for SU3 and SU2 tend to cluster around 8 ka BP  
197 (Table S1 in SI; Early Holocene)(W. T. T. Taylor *et al.*, 2021), although some inconsistencies are  
198 observed within these ages. The boundary between SU1 and SU2 is marked by a thin laminated  
199 and fairly compacted stratum (Sub2.1). SU1 exhibits a lighter coloration and a distinct sharp lower  
200 boundary. Notably, pottery shards and reddened lenses (similar to intact *in-situ* fireplaces; **Fig.**  
201 **2c**) were observed. Both SU1 and SU2 contain archaeological materials, such as bones and large  
202 charcoal fragments, with pottery found in SU1 and personal ornaments in SU2 (Fedorchenko *et*  
203 *al.*, 2018; Shnaider *et al.*, 2019). Previously published chronological data (Table S2 in SI)  
204 (Shnaider *et al.*, 2017; Taylor *et al.*, 2020; Osipova *et al.*, 2021) are presented in Table S2 (SI)  
205 and highlight inconsistencies in the dates, with a few outliers among them (Ramsey, 2009; W. T.  
206 T. Taylor *et al.*, 2021). However, the dates from the lowest unit, SU5, indicate that the entire  
207 sequence spans approximately the last 12000 years (Table S2 in SI).

## 208 **3 Methods**

### 209 **3.1 Field studies**

210 Field excavations were conducted following established methods and standards, as previously  
211 detailed (W. T. T. Taylor *et al.*, 2021). Photographic documentation was taken using a Canon  
212 D600 camera and a DJI Phantom 4 Pro quadcopter. Geoarchaeological sampling was carried out  
213 over different campaigns (2016, 2019, 2021), culminating in the collection of 13 bulk samples  
214 and seven monoliths. The investigation of the site employed a conventional geological approach,  
215 drawing from previously proposed methodologies (e.g., Goldberg and Macphail, 2013; Macphail  
216 and Goldberg, 2017; Karkanis and Goldberg, 2019; Krajcarz *et al.*, 2020; Brancaleoni *et al.*,  
217 2022).

218 To identify the stratigraphic units, a combination of lithostratigraphic characteristics  
219 (including distinctions in texture, color, and subtle sedimentary structures) and an

220 allostratigraphic approach (recognizing the presence of discontinuities and unconformities) was  
221 employed. This approach adhered to recommendations given by Hughes (2010) and Räsänen et  
222 al. (2009).

### 223 **3.2 Grain size analysis**

224 Grain size analysis serves as a tool for classifying sedimentary environments (Blott and Pye,  
225 2001). In this context, our grain size analyses were undertaken with the aim of characterizing  
226 sediment texture and sorting, in order to find differences or similarities with other deposit types  
227 or akin sediments within the Obishir-5 sequence.

228 Initiating the process, preliminary dry sieving employing a 2-mm sieve was executed on site  
229 to separate the coarse fraction from the fine fraction. Subsequently, the coarse fraction underwent  
230 further dry-sieved using 2, 5, 10, 20, and 50 mm sieves at the site. During the sieving procedure,  
231 notations were made regarding the petrographic composition and the archaeological materials,  
232 with corresponding weight recorded. In some case, the archaeological material was handpicked.  
233 The fine fraction (< 2 mm) was subjected to a laboratory drying process at 105 °C. This dried fine  
234 fraction was then subdivided into multiple representative subsamples intended for grain size  
235 analysis, chemical and later mineralogical analyses.

236 For the subsamples designated for grain size analysis, laser diffraction was employed and  
237 carried out by Redzhep Kurbanov. The procedure is detailed in Timireva et al. (2022) and  
238 Brancaloni et al. (2023). The ensuing analysis encompassed the distribution and statistical  
239 evaluation of the sediments' fine fraction. This analysis was conducted utilizing GRADISTAT  
240 v9.1 (Blott and Pye, 2001).

### 241 **3.3 Micromorphology of sediments**

242 Micromorphological studies represent a common approach for evaluating site formation  
243 processes and post-depositional disturbances. This method offers the ability to observe the  
244 original spatial arrangement of soil components and their interrelationships. To this end,  
245 undisturbed and properly oriented monoliths were meticulously collected from the principal  
246 excavation trench at the Obishir 5 site. The specifics of block sampling and thin section  
247 preparation are elaborated in the SI (Section S7).

248 Thin sections, prepared according to these procedures, were subjected to analysis under  
249 various lighting conditions, including plane-polarized light (ppl), cross-polarized light (xpl),  
250 oblique incident light (oil), and epifluorescence. Additionally, we employed a Scanning Electron  
251 Microscope (SEM) in conjunction with Energy Dispersive Spectroscopy (EDS) for elemental



252 analysis of select components and minerals within chosen thin sections. In compliance with  
253 guidelines set forth by Stoops (2021), the thin sections were described.

254 The process involved the creation of high-quality digitized images of thin sections directly  
255 from the microscope with a mechanical stage, utilizing both ppl and xpl illumination. These  
256 images are available in Zenodo.org. Our workflow comprised a two-fold approach. Initially, we  
257 described the principal elements of the thin section fabric in accordance with Stoops' guidelines  
258 (Stoops, 2021). We conducted a qualitative assessment of their frequency, and a semi-quantitative  
259 evaluation of their dimensions. The latter was achieved by measuring the maximum length of a  
260 minimum of three instances of the same component type during microscopic examination, with  
261 the aid of software NIS-Elements.

262 Subsequently, our analysis delved into micro-components (SI Table S9) and their  
263 interrelationships, ultimately leading to a comprehensive description of the entire thin section (SI  
264 Table S10). This methodology contributes to a thorough comprehension of the sedimentary  
265 makeup and the intricate processes that shaped the site's development over time.

### 266 **3.4 Geochemistry**

267 We performed chemical analyses, including carbonate content determination (refer to  
268 Brancaleoni *et al.*, 2022), as well as CHNS elemental analyses performed using a Vario  
269 MicroCUBE CHNS analyzer at the Institute of Geological Sciences (PAS, Warsaw, Poland). In  
270 addition, we employed coupled plasma mass spectrometry (ICP-MS) at the Bureau Veritas  
271 Minerals Laboratory in Vancouver, Canada, to estimate the concentrations of an extensive array  
272 of elements (refer to Krajcarz, 2019; Brancaleoni *et al.*, 2022)). To unveil relationships within  
273 our data, we computed a correlation matrix for the concentrations of these elements.

274 Given that our dataset displayed a lack of normal distribution, we opted for the Spearman  
275 method, a non-parametric correlation approach. These computations were conducted within the  
276 RStudio v3 environment. The resulting correlation matrix allowed us to identify patterns and  
277 potential causal connections between various variables. It also enabled the identification of  
278 pertinent geochemical indices that warrant consideration.

279 In assessing geochemical indices, we focused on the most prevalent elements, as ascertained  
280 through ICP-MS analysis (SI Section S4). Our approach involved the use of concentration ratios  
281 between two elements: one more soluble and mobile, and another that is comparatively less  
282 soluble and less mobile. This method serves to assess mineral weathering and alteration. Notably,  
283 this approach aligns with methodologies established in prior research (Buggle *et al.*, 2011;  
284 Krajcarz *et al.*, 2016).

285 It is important to note that while these geochemical proxies provide valuable insights, caution  
286 is advised due to their formulation for specific sediment types (such as loess), which may differ  
287 from the composition at the Obishir-5 site. In our case, these proxies are adopted to provide  
288 qualitative observations, contributing to a broader understanding of the site's geochemical  
289 characteristics.

### 290 **3.5 Infra-Red spectroscopy and Powder X-ray diffraction**

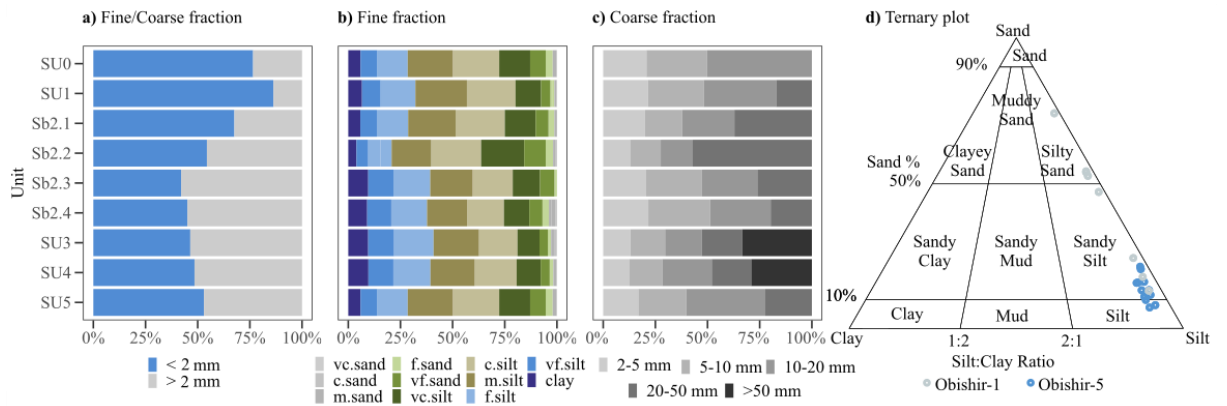
291 To gain a comprehensive understanding of the mineral phases within the deposit, we employed  
292 both Fourier-Transform infrared spectroscopy (FTIR) and Powder X-ray diffraction (PXRD).  
293 FTIR was initially utilized to conduct preliminary examinations of samples, serving to identify  
294 both inorganic and organic components, and assess the samples' purity. PXRD analysis, on the  
295 other hand, facilitated both qualitative and quantitative assessments of the minerals present in the  
296 samples. This technique enabled the tracking of mineralogical changes throughout the profile.

297 Thirteen samples, originating from six distinct stratigraphic units and four subunits (SU0, SU1,  
298 SU2, Sub2.1, Sub2.2, Sub2.3, Sub2.4, SU3, SU4, and SU5, see **Fig. 2d** for their location), were  
299 selected for analysis. The analytical process began by drying the samples at 105°C, followed by  
300 milling using a cylinder mill with agate balls. Subsequently, a pretreatment involving HCl (30%)  
301 was applied to eliminate a substantial portion of carbonates. Additional specifics concerning the  
302 methodologies employed are elaborated in the SI (Sections S4 and S5).

## 303 **4 Results**

### 304 **4.1 Textural analysis**

305 The sediments under investigation exhibited characteristics consistent with diamicton  
306 (Table S2 in SI) (Zieliński and Pisarska-Jamrozy, 2012; Pawelec and Ludwikowska-Kędzia,  
307 2016; Osipova *et al.*, 2021), displaying poor sorting, i.e., displaying a wide range of grain sizes  
308 spanning from clay to gravel and boulder (**Fig. 3**). A significant proportion of coarse (> 2 mm)  
309 material was detected, with the coarse material accounting for around 50% in Sub2.3 and lower  
310 units and < 50% in the upper units (**Fig. 3a**).



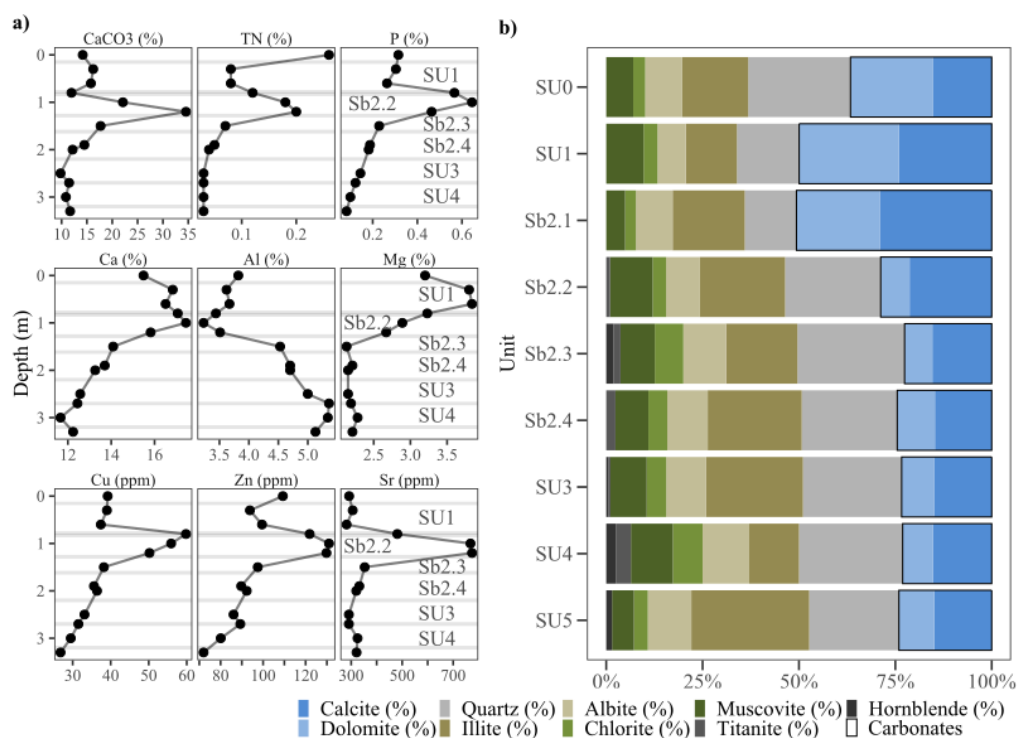
311

312 **Fig. 3** Textural properties of sediments at Obishir-5. **A)** Fine and coarse ratio; **b)** fine fraction  
 313 < 2 mm, clay  $\leq 2 \mu\text{m}$ , vf silt  $\leq 3.98$ , f silt  $\leq 7.94$ , m silt  $\leq 15.8$ , c silt  $\leq 31.6$ ,  
 314 vc silt  $\leq 63.1$ , vf sand  $\leq 126$ , f sand  $\leq 251$ , m sand  $\leq 501$ , c sand  $\leq 1000$ , vc sand  $\leq$   
 315 2000, vf pebbles  $\leq 3160 \mu\text{m}$  size scale adopted in the GRADISTAT program, modified from  
 316 UDDEN (1914) after Wentworth (1922); and **c)** Coarse fractions > 2 mm; **d)** Ternary plot (after  
 317 Blott and Pye, 2001) showing Obishir-1 and Obishir-5 grain size results. Obishir-1 is a site in  
 318 the vicinity located in a similar geomorphological setting (**Fig. 1b** and refer to Brancaleoni et al.,  
 319 (2022), data show a coarsening upward tendency typical for talus deposits at Obishir-1, whereas  
 320 Obishir-5 data are all clustered together and they are rather homogeneous, possibly indicating  
 321 reworking

322 The primary composition of fine fraction was coarse silt, with dimensions ranging from 0.01  
 323 to 0.05 mm (**Fig. 3bd**). Concurrently, the coarse grains primarily fell within the range of 5-20 mm  
 324 (**Fig. 3c**), constituting the prevailing component within the coarse fraction. Upon analyzing the  
 325 fine/coarse ratio across the sequence, a pattern emerged. Upper units (SU0, SU1, Sub2.1, Sub2.2;  
 326 **Fig. 3a**) exhibited a heightened concentration of fines (< 2 mm), with the most notable peak in  
 327 SU1 (**Fig. 3a**). In contrast, Sub2.3, Sub2.4 and lower units displayed a near-balanced ratio close  
 328 to 1 (**Fig. 3ad**).

## 329 4.2 Geochemical and mineralogical analyses

330 The sediments under examination in this study exhibit a calcareous nature, coupled with  
 331 relatively low levels of organic matter (as illustrated in **Fig. 4a**). In investigating the interplay  
 332 between element contents, our analysis revealed two prominent clusters: the Al-group  
 333 (comprising Al, Na, Fe, Ni, Rb, and Ti), and the Ca-group (encompassing Ca, Mg, P, Cu, Zn, Sr)  
 334 (**Fig. 4a**, Supplementary Material section S3). The upper portion of the profile (SU0, SU1, Sub2.1,  
 335 and Sub2.2) prominently showcased Ca-group elements, while the lower segment featured the  
 336 Al-group constituents (Sub2.3, Sub2.4, SU3, SU4, and SU5).



337

338 **Fig. 4** Geochemical and mineralogical results. **a)** Selected geochemical profiles. **b)** PXRD  
 339 results, refer to Table S3 in SI

340 For an in-depth understanding of the sediment composition, mineralogical analysis was  
 341 performed, utilizing Fourier Transform Infrared Spectroscopy (FTIR) and powder X-ray  
 342 diffraction (PXRD). FTIR spectra across all examined samples demonstrated minimal variation  
 343 among each other (Figure S7 in SI). Notably, the absence of IR bands within the range of 3000  
 344  $\text{cm}^{-1}$  to 2800  $\text{cm}^{-1}$  indicated the lack of organic matter. High frequency numbers, coupled with  
 345 OH stretching bands at 3620  $\text{cm}^{-1}$  and 3380  $\text{cm}^{-1}$ , provided evidence for the presence of structural  
 346 and adsorbed water, as well as the existence of dioctahedral (-Al,  $\text{Fe}^{3+}$ ) phyllosilicates. Carbonate  
 347 content was readily identifiable through sharp bands at 1430  $\text{cm}^{-1}$  (calcite), 1440  $\text{cm}^{-1}$  (dolomite),  
 348  $\sim 880 \text{ cm}^{-1}$  (calcite and dolomite), 730  $\text{cm}^{-1}$  (dolomite), and 713  $\text{cm}^{-1}$  (calcite).

349 Notable observations emerged in samples from units SU2.2, SU2.3, SU2.4, SU3, SU4, and  
 350 SU5, showcasing a depletion in dolomite content (refer to Figure S7 in SI). A distinct hump  
 351 centered around 1640  $\text{cm}^{-1}$  indicated the involvement of water in the structure of clay minerals.  
 352 Furthermore, the presence of two bands at 800 and 781  $\text{cm}^{-1}$  indicated the presence of quartz.  
 353 Within the FTIR spectra, no discernible bands characteristic of phosphates were identified,  
 354 remaining within the detection limit of the technique, 0.5-1% (Figure S7 in SI).

355 Incorporating PXRD analysis, no significant disparities were apparent among the analyzed  
 356 samples. Quantitative examination of PXRD scans is in Table S5 in SI and illustrated in **Fig. 4b**,  
 357 with the corresponding PXRD patterns detailed in Figure S8 in SI. Our analysis indicated a

358 consistent presence of quartz, calcite, dolomite, illite, muscovite, albite, and chlorite across all  
359 sediment samples (**Fig. 4b**). Some deeper units showcased traces of hornblende and titanite (as  
360 listed in Table S5 in SI and illustrated in **Fig. 4b**). The sediment composition was primarily  
361 composed of carbonates (~20-50%) and quartz (~25%) (**Fig. 4b**). Notably, the concentration of  
362 carbonates exhibited a downward trend with increasing depth in the sequence, juxtaposed with a  
363 slight rise in silicate/phyllosilicate concentration (**Fig. 4b**). Sediments within units SU0, SU1, and  
364 SU2.1 displayed an enrichment in dolomite and a corresponding decrease in quartz content (**Fig.**  
365 **4b**).

### 366 **4.3 Micromorphological analysis**

367 A detailed description and distribution of micromorphological features along the profile can  
368 be found in SI, specifically in Tables S7-S9, with a summary provided here and in **Table 1**. Coarse  
369 geogenic components within the sediments were primarily composed of carbonate, shale, and  
370 igneous rock fragments (refer to Table S8-S10). These components were interspersed within a  
371 finer groundmass, exhibiting a double open porphyric related distribution. Both shale and  
372 limestone fragments were consistently present throughout the samples, with shale being more  
373 prevalent in the lower section of the sequence. This could potentially be attributed to their  
374 proximity to the shale bedrock or loose shale debris. In contrast, igneous rock fragments exhibited  
375 higher frequency in the upper part of the sequence (Table S8 in SI).

376

377

**Table 1** Summary of selected micromorphological features and components characterizing the sediments at the Obishir-5 (Key: 1 single occurrence; ● few; ●● common; ●●● dominant; Papules – redeposited clay cutans; LMC - authigenic low-magnesium carbonates; P – Phosphatic)

Unit	b-fabric	Micro-structure	Ground-mass	Trampling lamination lenses	Aggregate	Biogenic and anthropogenic components						Redeposited and illuviated clay			Secondary phosphates and carbonates			
						Dung	Phytolith	Charcoal	Ash	Bone	Suspected burnt bone	Papules	Coating	Dusty infill	Apatite nodule	P Coating	LMC	Calcified root
1	Crystallitic; stipple speckled	Microlaminated horizon	Calcitic compacted	●●	●●●	●●●	●●●	●●●	●	●		●					●	
2.1	not studied																	
2.2	Brownish stipple speckled	Granular	Calcitic, organic matter, fecal spherulites		●●●	●●●	●	●●●		●●	●		●		●●			
2.3	Yellowish Stipple speckled; spherulitic	Granular	Calcitic, organic matter, fecal spherulites		●●●	●●●	●	●●●	●	●●	1		●●			●		
2.4	Grayish stipple speckled	Granular and intergrain, loose granular	Calcitic, organic matter		●●●	●●	●●	1	●	●		●	●					
3	Grayish stipple speckled; Brown stipple speckled	Granular, intergrain	Calcitic, organic matter		●●		1	●●●	●●	●●	●	●●	●●				●●	

Unit	b-fabric	Micro-structure	Ground-mass	Trampling lamination lenses	Aggregate	Biogenic and anthropogenic components						Redeposited and illuviated clay			Secondary phosphates and carbonates			
						Dung	Phytolith	Charcoal	Ash	Bone	Suspected burnt bone	Papules	Coating	Dusty infill	Apatite nodule	P Coating	LMC	Calcified root
4	Brown stipple speckled	Compact micro-granular, locally vughy	Clayey		•			1		•		•	•			•	•	•
5	Locally undifferentiated micromass and brown stipple speckled	Compact micro-granular, locally vesicular, massive, vughy	Clayey		•					1?		•		•	•	•	1	••

378

379

380 Fine sand-and-silt fabric encompassed common minerals like quartz, calcite, mica, feldspar,  
 381 and clay minerals, consistently identified in all collected samples. The relationship with the clayey  
 382 micromass was also porphyric, generally chaotic, except for a distinct sorted and laminated  
 383 horizon evident in SU1. At the microscopic level, rock fragments (shale, limestone and igneous  
 384 rocks) displayed signs of disintegration and alteration (refer to Brancaleoni *et al.*, 2023).

385 The key archaeological components identified included fragments of dung, bones (including  
 386 suspected burnt specimens), and charcoals, char, ash, and phytoliths (**Table 1**). Rare fragments  
 387 of lithic debitage and suspected pottery fragments were also noted (Table S8 in SI).  
 388 Archaeological components were commonly present in the upper part of the sequence (in SU1,  
 389 SU2 and SU3 upper part; **Table 1**), but were notably scarce in the lower segment (in SU4 and  
 390 SU5), limited to tiny charcoal and suspected bone fragments.

391 Among the coarse archaeological components, charcoal and dung pellets predominated,  
 392 accompanied by a few specimens of bone fragments. Fine sand-and-silt components encompassed  
 393 low-magnesium carbonate spherules and anthropogenic debris. This debris featured charred and  
 394 organic material, small bone fragments, and dung pellets as described in **Table 1**, **Table 2**, and  
 395 Table S8 in SI.

396 In SU3 and SU2, the archaeological components were randomly dispersed and intermixed with  
 397 the geogenic components, occasionally found matrix-coated. In contrast, a more structured  
 398 arrangement was observed in SU1, where archaeological components were horizontally aligned  
 399 within a microlaminated horizon (**Table 1**).

400 Dung pellets were observed in SU1, Sub2.2, Sub2.3 and 2.4 (**Table 2**), each exhibiting varying  
 401 degrees of preservation. Of note, dung pellets featured internal fecal spherulites. A sole calcined  
 402 specimen was found in Sub2.3. The bones displayed signs of weathering, including cracking,  
 403 dissolution, recrystallization, and suspected heat-induced transformation.

404 **Table 2** *Dung material charted against each unit where it was observed (ppl – plain polarized*  
 405 *light; xpl – crossed polarized light)*

Unit/Subunit	Size	Description	Interpretation
SU1	1 mm	Yellow rounded or elongated orange aggregates in ppl with detrital grains, bluish b-fabric and partially isotropic in xpl. Tiny fecal spherulites sometimes not noted. Horizontally aligned, associated with laminated microstructure, elongated phytoliths and charcoals in the groundmass.	Unknown producers, possibly juvenile herbivores



Sub2.2	0.5 mm	Yellow in ppl, from rounded to oval shape, edges from well visible with a weak rim to blending with the groundmass. Convoluted and fibrous internal structure, internal porosity, internal phytolith debris, yellow limpic clay, organic matter, fecal spherulites and calcitic pseudomorphs. In xpl, few specimens isotropic.	Herbivore producers, possibly sheep, dung partially phosphatized and disrupted
Sub2.3	2 – 0.5 mm	Yellow, light brown and orange pellets (in ppl). From rounded to irregular shape and blending with the groundmass, some with rim. Convoluted and fibrous internal structure, internal porosity, internal phytolith debris, yellow limpic organic matter, fecal spherulites. In xpl, bluish b-fabric and some isotropic. A specimen was observed partially calcined.	Herbivore producers, dung partially phosphatized and disrupted
Sub2.4	0.5 mm	In ppl, orange and yellow with sub-rounded shape, some specimens are disrupted. Fairly laminated structure, limpic yellow organic matter, internal fecal spherulites and detrital grains. In xpl, partially isotropic and bluish b-fabric.	Herbivore producers, dung partially phosphatized and disrupted

406

407 The micromass was more clayey in lower units (**Table 1**). It appeared more calcitic in SU3  
408 than SU4 and SU5 and was characterized by dung and dung spherulites in Sub2.3 and Sub2.2  
409 (**Table 1**). In SU1, it appeared calcitic and locally well cemented (**Table 1**).

## 410 **5 Discussion**

### 411 **5.1 Sedimentological and micromorphological markers of deposition**

412 We sought for markers of differing deposition modes in the sediments through textural and  
413 micromorphological analyses. Textural analyses showed minimal variations between units (SI,  
414 **Fig. 3**). This suggests either a limited variability in depositional processes or the influence of post-  
415 depositional reworking. The analysis demonstrates a bi-modal distribution of grain sizes  
416 (domination of silt and pebble-sized fractions). This pattern likely points toward two distinct

417 depositional modes. The coarse fraction's association with colluvial processes, often influenced  
418 by gravity induced mechanisms, is evident. Simultaneously or alternately, the fine fraction  
419 appears influenced by aeolian forces and physical disintegration.

420 Moreover, it is worth noting that talus deposits typically display a general coarsening upward  
421 tendency as shown in Obishir-1 a neighboring site (Brancaleoni *et al.*, 2022). However, this  
422 anticipated trend is not mirrored at Obishir-5 (**Fig. 3d**). This departure from the expected pattern  
423 suggests the presence of erosion, reworking, and homogenization processes. These factors  
424 collectively point towards the likelihood of a truncated talus interpretation.

425 Micromorphological analysis provides further support for the findings from textural  
426 examination. The observed porphyric *c/f* related distribution of the coarse geogenic fabric aligns  
427 with the characteristics indicative of colluvial deposition, with the main source likely originating  
428 from the overhanging cliff. The consistent nature of coarse geogenic fabric throughout the profile  
429 supports constant colluviation at the site. This continuous colluviation may have contributed to  
430 syn-depositional changes within the sedimentary material. And further points to a limited care of  
431 the site by its users. Among the coarse geogenic fabric, igneous fragments are of particular  
432 interest. They are largely considered allochthonous components that have likely been introduced  
433 to the site through human-related activities.

434 Distinguishing between material accrued via aeolian inputs and the result of in-situ  
435 disintegration of coarse geogenic elements poses a challenge. Lenses and lamination within the  
436 sediments were not observed. While it is complex to definitively delineate their individual  
437 contributions to the fine fraction accumulation, it is plausible that both processes played a role.  
438 Furthermore, an hypothesis emerges suggesting that the principal source of fine aeolian material  
439 could be the overhanging cliff itself, which again challenges the recognition of aeolian inputs.  
440 The fine material, nestled within crevices of the rocky cliff, might have experienced transport  
441 down the slope due to a combination of gravitational forces and aeolian activity. This hypothesis  
442 provides additional support for the colluvial deposition model. Moreover, the presence of  
443 redeposited laminated papules adds to the evidence for colluvial deposition and the recycling of  
444 material within this dynamic landscape. Collectively, the micromorphological and textural  
445 analyses underscore the intricate interplay of processes that have shaped the sedimentary profile,  
446 highlighting the multifaceted nature of sediment deposition and transformation at the site.

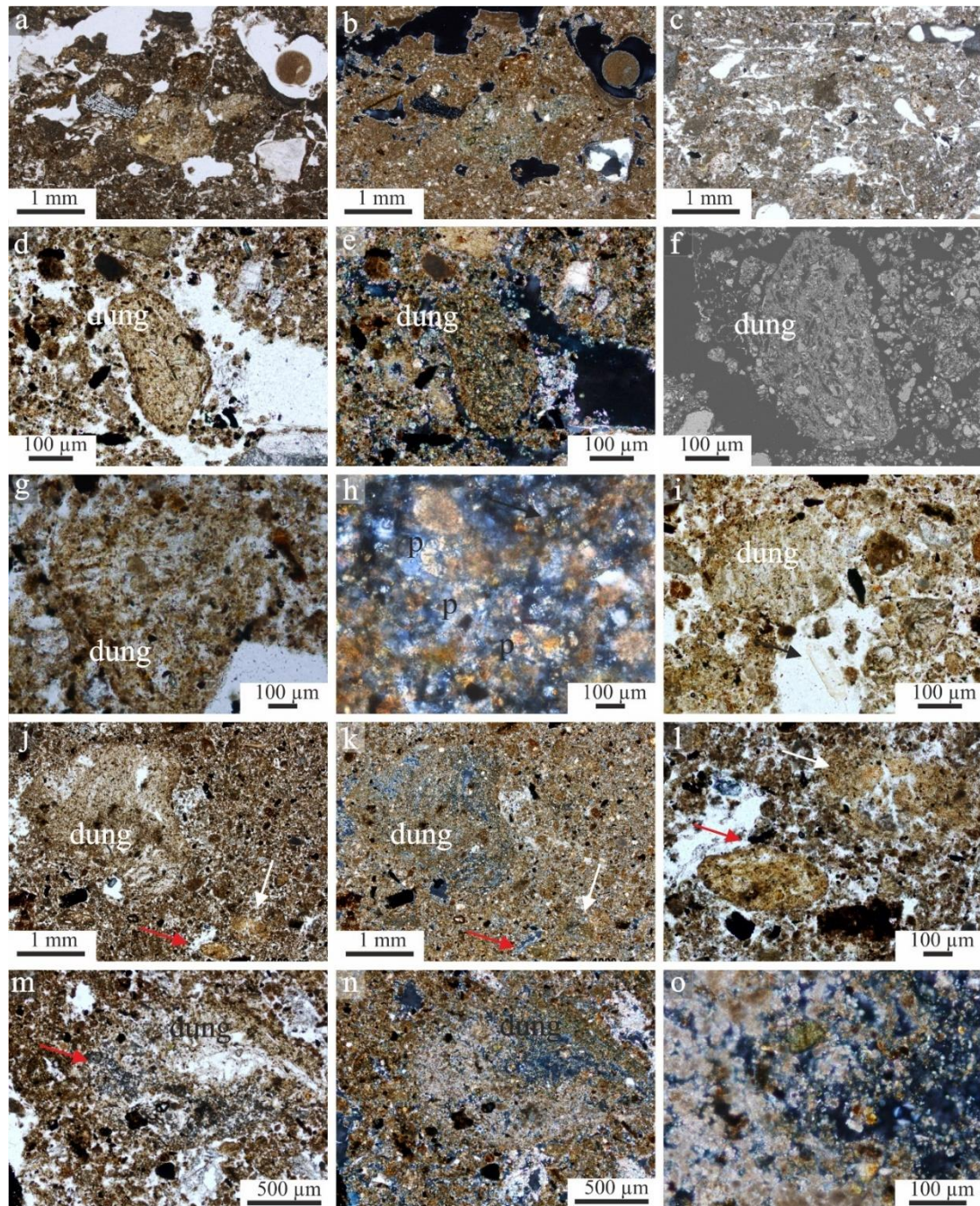
## 447 **5.2 Micromorphological markers of human-related activities**

448 Obishir-5 holds one of the earliest evidence for the use of livestock in the mountains of interior  
449 Central Asia (W. T. T. Taylor *et al.*, 2021). This is in line with evidence of herding in the  
450 mountains of eastern Uzbekistan together with evidence of human and herbivore dung material

451 in Chatyr Kol lake sediments in central Kyrgyzstan (Schroeter *et al.*, 2020; Nishiaki *et al.*, 2022;  
452 Spate, Leipe and Motuzaitė Matuzeviciute, 2022).

453 Stone artefacts (Shnaider *et al.*, 2017; Fedorchenko *et al.*, 2018) and faunal remains (Osipova  
454 *et al.*, 2021; W. T. T. Taylor *et al.*, 2021; Serdyuk *et al.*, 2023) have been recovered from the  
455 sediments at the site. Among these remains, those attributed to domestic livestock showed traces  
456 of human modifications, as highlighted by (W. T. T. Taylor *et al.*, 2021). The micromorphological  
457 investigation sought for markers related to human activities associated with herding practices.

458 The presence of dung material in the sediments of the Obishir-5 site corresponds with the  
459 evidence provided by the faunal assemblage analysis (W. T. T. Taylor *et al.*, 2021). Specifically,  
460 in SU2 (Sub2.2, Sub2.3 and 2.4), the analysis of dung such as its morphology and features such  
461 as fecal spherulites, calcium carbonate pseudomorphs, fibrous internal structure and presence of  
462 phytoliths (**Table 2**), suggested a connection with herbivores producers in most instances (**Table**  
463 **2; Fig. 5**). It is reasonable to suspect that herbivore dung can be attributed to sheep and goat, based  
464 on the findings of zooarchaeological studies (W. T. T. Taylor *et al.*, 2021) and comparisons with  
465 other published results (Brönnimann *et al.*, 2017; Karkanas and Goldberg, 2018).



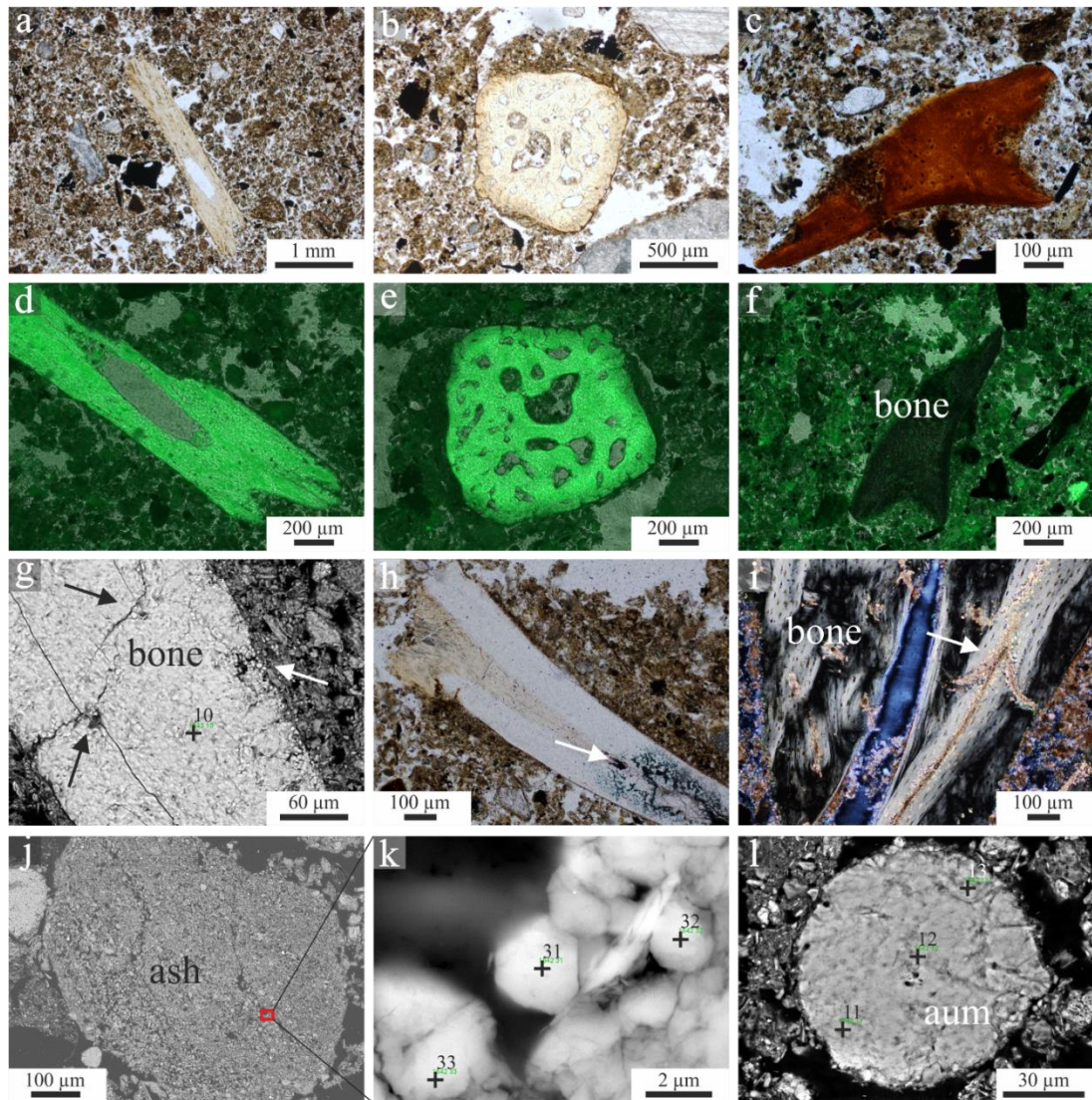
466

467 **Fig. 5** Examples of dung pellets at the Obishir-5 site (ppl – plane polarized light; xpl – crossed  
 468 polarized light); **a**) yellowish dung pellets (thin section L1; SU1) in ppl and **b**) in xpl showing  
 469 bluish b-fabric; **c**) planar empty voids once filled with plant material standing as an evidence for  
 470 foddering (thin section L1; SU1) **d**) and **e**) dung pellet in ppl and xpl with internal phytoliths and  
 471 fecal spherulites, **f**) same specimen showing internal fibrous structure under SEM (thin section  
 472 3.1; Sub2.2); **g**) dung pellet with blending in edges (thin section 3.1; Sub2.2) and **h**) close-up on  
 473 the internal composition of the pellet in **g**, visible are carbonate pseudomorphs (p) and fecal  
 474 spherulites (arrow); **i**) dung pellet associated with invertebrate (arrow)(thin section 3.2; Sub2.3);  
 475 **j**) and **k**) dung pellet in ppl and xpl, convoluted structure and internal porosity, arrows point to  
 476 oval yellowish pellets (thin section 3.2; Sub2.3); **l**) close-up on oval and fine-grained dung pellets,  
 477 yellow limpic organic matter with convoluted structure; **m**) and **n**) partially calcined (red arrow  
 478 points at micritic crystals) dung fragment in ppl and xpl (thin section 3.2, Sub2.3); **o**) close up to  
 479 boundary between calcined and non-burned material showing fecal spherulites

480 In SU1 (examples in **Fig. 5ab**), dung fragments showed very tiny fecal spherules, and in some  
481 instances, these spherules were absent. This may point toward different producers  
482 (non-herbivores) or be evidence of juvenile producers (W. Matthews, pers. comm.). However,  
483 SU1 sediments showcased a relatively high content of in situ horizontally aligned, elongated and  
484 tubular phytoliths (**Table 1**) and voids where plant remains once were (**Fig. 5c**). The presence of  
485 phytoliths within trampled sediments of SU1 could be taken as an indicator of foddering activities  
486 at the site (Macphail *et al.*, 1997). Consequently, this indirectly indicates the presence of  
487 ruminants at the site.

488 The association between dung material and residues from burning processes (Mentzer, 2014)  
489 is commonly interpreted as an effect of pastoral activities (Angelucci *et al.*, 2009). Microscopic  
490 examination unveiled a close association between dung material and burn-related features  
491 (Sub2.3, **Fig. 5g–h**). Fire by-products such as charcoal, charred material, bones, dung and  
492 occasionally ash and rubified aggregates are indicative of activities linked with fire (Mentzer,  
493 2014) (**Table 1**, Table S9 in SI).

494 Coarse bones, positioned in Sub2.2, Sub2.3 and SU3, exhibit indications of potential burning  
495 (**Fig. 6cf**). This conclusion is evidenced by observable color alteration (Stiner *et al.*, 1995; Estévez  
496 *et al.*, 2014; Rubio *et al.*, 2020; Marcazzan, Miller and Conard, 2022) (**Fig. 6cf**, **Table 1**; Sub2.2,  
497 Sub2.3 and SU3). In Sub2.2 and 2.3, according to bones' aspect (as red or orange, when observed  
498 under ppl) and their non-autofluorescence under epifluorescence (**Fig. 6cf**), we may deduce that  
499 the transformation was caused by heat exposure, likely reaching temperatures between 100°C and  
500 400°C—a comparison drawn from (Villagran *et al.*, 2017). Tests in epifluorescence light further  
501 corroborated varying degrees of burning. In particular, bone specimens displaying a yellow hue  
502 under ppl (**Fig. 6ab**), showed autofluorescence under epifluorescence (**Fig. 6de**), in contrast to the  
503 orange and reddish bones (**Fig. 6cf**). Adding to this, faunal macro remains from SU2 also  
504 displayed burn marks, an observation documented by (W. T. T. Taylor *et al.*, 2021). This  
505 combined evidence underscores the presence of fire-related activities and their intimate  
506 association with the deposition and transformation processes within the archaeological context.



507

508 **Fig. 6** A collection of microphotographs taken under polarizing microscope (a-c; ih),  
 509 epifluorescent light (d-f), and SEM (g; i-d); ppl – plane polarized light and xpl – crossed  
 510 polarized light; a–c) examples of bones, a) and b) are non-burned respectively cortical and  
 511 spongy immersed in a granulated groundmass and associated with char (observed in thin section  
 512 3.2; Sub 2.3); whereas c) is possibly burned (thin section 3.1, Sub2.2); d–e) specimens in a–c)  
 513 under epifluorescent light, d) and e) are both autofluorescent (channels C1+C5, see SI), in  
 514 polarized light they appear light yellow (ab); panel f) non-fluorescent bone fragment, possibly  
 515 due to heat-induced transformations or other taphonomic processes such as humification and  
 516 oxidation, this is the same specimen as in c) but rotated. g) in-situ cracked bone (black arrows),  
 517 the left edge is corroded and being disintegrated (white arrow)(thin section 3.2; Sub2.3); h) bone  
 518 specimen, its left extremity is corroded (arrow) in ppl (thin section 1542; SU3); i) cortical bone  
 519 cracked and recrystallized along the cracks (arrow) in xpl (this is a close-up of the same specimen  
 520 in Fig. 7f) (thin section 3.2; Sub2.3); j) ash nodule consisting of k) rhombohedral crystal of low-  
 521 magnesium carbonates (SI) and clay minerals (1542; SU3); l) spherulitic authigenic mineral  
 522 (aum), for its spectra the reader is referred to SI (1542; SU3).

523 A burnt dung pellet was found in Sub2.3, exemplified by the illustration in Fig. 5g–h (Table  
 524 2), where a dung fragment displayed partial transformation into ash (calcined), a phenomenon  
 525 commonly associated with fire. In samples representing SU3, Sub2.4, Sub2.3, and SU1 we  
 526 observed ash. Aggregates with rhombohedral calcite crystals were found in SU3 (Fig. 6jk).

527 In SU1, single rhombohedral calcite crystals were dispersed in the groundmass. Their  
528 composition is primarily calcareous (Figure S13-15 in SI). Ash composition can exhibit  
529 variability (Mallol, Mentzer and Miller, 2017), with ashes from plants and dung often being  
530 mainly calcareous (Mallol, Mentzer and Miller, 2017). This leads us to the conclusion that the  
531 calcined ash in unit SU3, might likely originate from plants and/or dung. Moreover, well-  
532 rounded reddened clay aggregates were also observed in SU1 and Sub2.2 (Table S8 in SI).  
533 Reddening of soil is generally taken to be linked with heat effects (Mentzer, 2014; Mallol,  
534 Mentzer and Miller, 2017; Röpke and Dietl, 2017).

535 Examining combustion features, we found that their arrangement and fabric indicated their  
536 disassembled nature, resembling features that they were not intact (where samples were taken at  
537 least; however, no macroscopic combustion features were directly observed during the  
538 excavations, excluding those in SU1 illustrated in **Fig. 2c**). Additionally, the fabric of the  
539 identified combustion remnants is akin to dumped features described by (Miller *et al.*, 2010). Our  
540 hypothesis is that intentional burning of plant and dung might have occurred in SU2 (Sub2.2, 2.3  
541 and 2.4) and SU3, given their higher prevalence compared to burnt bone fragments (refer to **Table**  
542 **1**), which were likely accidentally burnt. Moreover, the predominance of cortical bone specimens,  
543 with spongy bones less common, suggests that the observed bones were likely waste material that  
544 could have been inadvertently or deliberately discarded into the fire.

545 Furthermore, in SU1, SU2 (Sub2.2, 2.3 and 2.4) and SU3 (where they were sampled),  
546 charcoals were mostly coarse, some appearing humidified, and their ratio to ash was relatively  
547 high, indicating potential low oxygen availability or incomplete combustion (Mentzer, 2014).  
548 However, this inference should be approached with caution due to relative higher chemical  
549 stability of wood charcoal compared to ashes (Mentzer, 2014). The presence of a few laminated  
550 ash aggregates could suggest incomplete combustion possibly caused by extinction by water, for  
551 laminated burned material has been linked with secondary reworking by water (Araujo *et al.*,  
552 2008; Mentzer, 2014). Unfortunately, due to the few features found, this interpretation requires  
553 further investigation at the site. The use of fire for cleansing purposes, a common practice in  
554 stabling, might also have been employed at the site. The varying degrees of burning observed in  
555 different components (charcoals, dung, and bones) could potentially indicate reworking processes  
556 at the site and instances of incomplete combustion.

### 557 **5.3 Geochemical and mineralogical markers of deposition**

558 The different geochemical signals can provide insights into the sources of fine material  
559 accumulation, especially regarding i) geogenic inputs, involving physical disintegration of parent  
560 material and aeolian contributions, and ii) archaeological inputs. The concentration of Ca-group  
561 elements, which includes Ca, Mg, P, Cu, Zn, and Sr, predominantly occurs in the upper part of

562 the profile. This trend aligns with the increase in carbonates (calcite and dolomite, **Fig. 4b**). Ca is  
563 the main component of carbonate rocks and minerals, therefore is taken to be mostly linked with  
564 the physical disintegration of the coarse limestone pieces, presence of calcareous components  
565 such as nodules, authigenic minerals and ash. CaCO<sub>3</sub> calculated after HCl pre-treatment and Ca  
566 measured with ICP-MS are not in a strict relationship (Table S4 in SI), indicating that Ca does  
567 not come exclusively from the carbonate bedrock.

568 Interestingly, Ca is positively correlated with P, a correlation that holds statistical significance  
569 ( $\rho < 0.005$ , Table S4 in SI). This signal is relatively pronounced in SU1, SU2.2, SU2.3, potentially  
570 tied to the presence of bones, dung and ash. Although phosphates were not detected by the PXRD  
571 method, which has limitations in detecting phosphates (PXRD detection limit for qualitative  
572 analysis ~3%), the close correlation between P and Cu indicates a likely shared source. This  
573 source could be bat guano or other mammal feces (Kehl *et al.*, 2014). For Cu and Zn are usually  
574 found in mammal feces (Miko, Kuhta and Kapelj, 2016; Linder, 2020; Adesso *et al.*, 2022; Sokol  
575 *et al.*, 2022). Bat guano was not recognized in thin sections. Fecal pellets containing spherulites  
576 and phytoliths, associated primarily with herbivores and ungulates, were observed in thin sections  
577 of Sub2.2, Sub2.3, and Sub2.4. This observation aligns with the micromorphological,  
578 zooarchaeological, and proteomic analyses presented by W. T. T. Taylor *et al.* (2021) at the site.

579 The relationship between P and Sr might indicate a shared source in bone fragments. It is worth  
580 considering that phosphates are more stable in an alkaline soil environment, potentially explaining  
581 the positive correlation between Ca and P, given Ca's abundance. The high Mg signal in SU1  
582 (**Fig. 3c**) is related to the presence of dolomite and low-magnesium authigenic carbonates as  
583 confirmed by PXRD (**Fig. 4b**) and SEM-EDS (Figure S10-12 in SI).

584 The Al-group elements (Al, Na, Fe, Ni, Rb, and Ti) are linked with siliceous minerals like  
585 feldspars and phyllosilicates (Chen *et al.*, 2013). The mineralogical analysis revealed the presence  
586 of albite, illite, muscovite and traces of chlorite, as well as an increase of silicates and  
587 phyllosilicates with depth (**Fig. 4b**). The downward trend in the concentration of these elements  
588 (from Sub2.4 downward) may be associated with bedrock alteration (mostly shale), aeolian  
589 contribution, and limited vertical clay relocation as indicated by the relative more clayey  
590 groundmass, coating and occasional dusty infilling (**Table 1**).

## 591 **5.4 Disturbances of the sedimentary record**

### 592 **5.4.1 Trampling**

593 The sedimentary arrangement observed under the microscope at the Obishir-5 site was  
594 influenced by a variety of post-depositional processes. Notably, trampling, bioturbation, and  
595 organic matter degradation played significant roles in shaping the final sediment structure.



596 Trampling, a well-known process, results from the repeated movement of humans or animals over  
597 the ground (Nir *et al.*, 2022). In SU1, evidence suggests that trampling likely occurred due to the  
598 presence of grazing livestock at the site. Additionally, the sediment could have been impacted by  
599 the introduction of detrital grains through animal movement or by their incorporation into fodder.  
600 Further signs of animal interaction can be observed through the presence of residual elongated  
601 phytoliths, which are indicative of foddering practices.

#### 602 **5.4.2 Bioturbation**

603 Bioturbation, stemming from the activities of soil fauna and plant interactions, plays a pivotal  
604 role in soil dynamics. This phenomenon, however, complicates the identification of original  
605 sedimentary processes, as it entails the mixing, reworking, homogenizing, and rearranging of  
606 sedimentary material (Goldberg *et al.*, 2009; Goldberg, Miller and Mentzer, 2017; Miller and  
607 Juilleret, 2020). Moreover, bioturbation has implications for chronometric dating, often rendering  
608 results less reliable (Fitzsimmons *et al.*, 2020). Archaeological sediments, particularly those rich  
609 in organic matter like dung and charcoal fragments as found at the Obishir 5 site, are susceptible  
610 to bioturbation due to the activities of soil fauna. This process has the potential to disturb the  
611 integrity of the sedimentary and archaeological record at Obishir-5.

612 The influence of bioturbation is particularly evident in sediments with a higher concentration  
613 of dung material, as seen in SU2 (Table S8 in SI). In Sub2.3, we actually captured evidence of  
614 invertebrate activity within the sediment (**Fig. 5i**). Moreover, in SU3, we identified a rodent molar  
615 within sample MM2101 (Table S8). Along with that, we observed extensive earthworm activity  
616 throughout the sequence (Table S8).

617 The peculiar fabric of SU2 and SU3, characterized by a granular structure and a chaotic pattern  
618 involving various components, along with the mixing of geogenic and archaeological inputs,  
619 suggests the possibility of reworking. This fabric is reminiscent of what has been documented in  
620 other arid regions characterized by significant bioturbation, often associated with anthropogenic  
621 activities like herding (Shahack-Gross and Finkelstein, 2008). Furthermore, the presence of fecal  
622 spherulites, distributed both within the dung material and throughout the sediment's groundmass,  
623 underscores the extent of mixing and reworking attributed to processes like bioturbation.

#### 624 **5.4.3 Other taphonomic processes**

625 The decomposition of organic matter is an additional taphonomic process that influences the  
626 sedimentary material at the Obishir-5 site. The occurrence of phosphatic impregnations and  
627 nodules (Table S8 in SI) is commonly associated with the decomposition of organic matter,  
628 particularly that originating from mammal feces (Shahack-Gross, 2011; Sokol *et al.*, 2022).

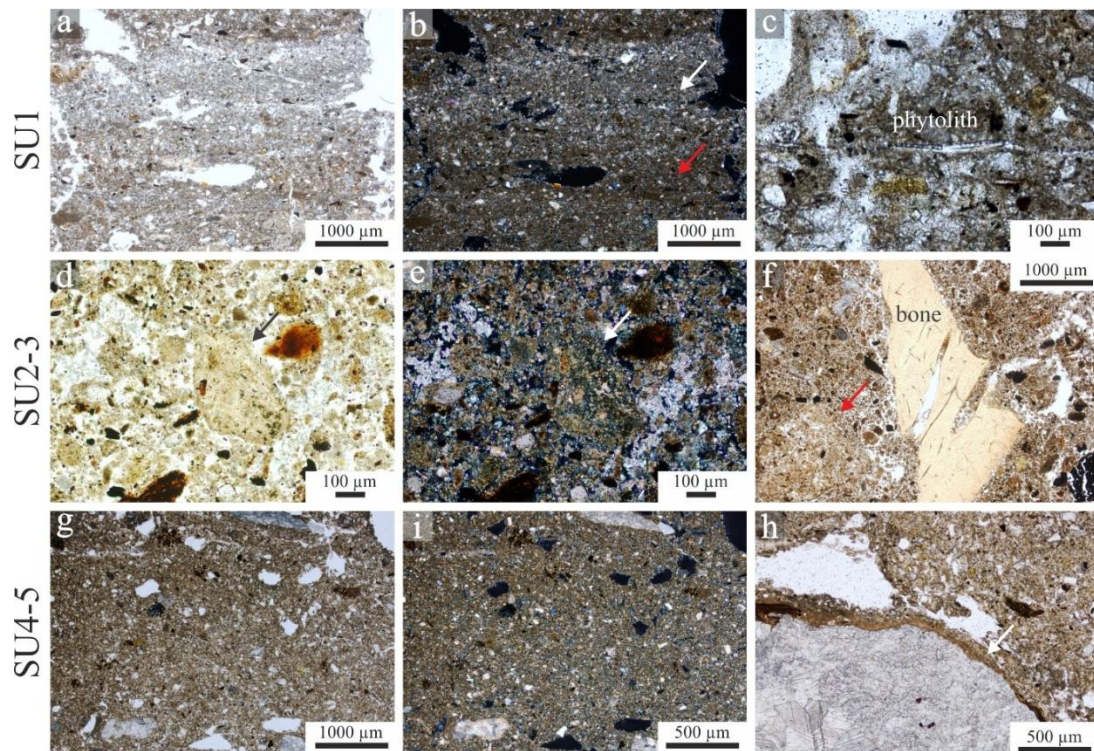
629 Within SU1, the presence of voids stemming from plant material decomposition (**Fig. 5c**) is likely  
630 an in-situ phenomenon.

631 Moreover, bones' preservation state was qualitatively assessed during micromorphological  
632 analysis. In SU2 and SU3, a significant portion of specimens displayed signs of weathering,  
633 corroded edges, early stages of dissolution, recrystallization, and cracking (**Fig. 6a–i**). This  
634 degradation aligns with findings reported by (W. T. T. Taylor *et al.*, 2021), who highlighted  
635 varying states of bone collagen and DNA preservation among specimens, indicating compromised  
636 preservation for certain bones. In Sub2.2, the presence of apatite nodules (Table S8 in SI) signifies  
637 alterations within the sedimentary and archaeological materials. Additionally, the appearance of  
638 authigenic minerals offers evidence for pedogenetic processes impacting the sedimentary record  
639 (Verrecchia *et al.*, 1995).

640 It is important to consider that the site is located at the base of a limestone cliff and is situated  
641 on a slope. Therefore, the arrangement of elements and the granular microstructure could also  
642 result from colluvial processes, such as solifluction. A fabric similar to that observed in SU2 and  
643 SU3 has also been noted in dumped deposits (Miller *et al.*, 2010; Marcazzan, Miller and Conard,  
644 2022).

## 645 **5.5 Model of site formation**

646 The site is characterized by stratified different cultural assemblages, that are: Epipaleolithic,  
647 Obishirian, Bronze Age and Middle Ages assemblages. The sediments retained characteristics  
648 mainly connected with the differing occupational phases (**Fig. 7**). In particular, we divided the  
649 sequence into 3 facies: SU5 and SU4, SU3 and SU2, SU1 and SU0.



650

651 **Fig. 7** Microphotographs illustrating differences in the sedimentary record likely connected  
 652 with differing occupational facies; **a-c**) Bronze and Middle Ages (SU1) facies is characterized by  
 653 an horizon with **(ab)** micro laminated structure with differing b-fabric, white arrow is indicating  
 654 a whitish gray crystallitic b-fabric due to sorted mineral grains (mainly quartz and calcite), red  
 655 arrow is indicating steeple speckled due to loamy brown material; and **(c)** broken elongated  
 656 phytolith, evidence of post-depositional modifications due to trampling; **d-f**) Obishirian (SU2 and  
 657 SU3), total reworking reflects the chaotic arrangement and typical granular microstructure of  
 658 the fabric, **(de)** groundmass made of biological droppings, black and white arrows point a dung  
 659 aggregate in ppl and xpl respectively, fecal spherulites occur within the aggregate and in the  
 660 surrounding groundmass, **(e)** b-fabric is dotted due to fecal spherulites, except for voids which  
 661 are partially filled by micritic calcite; **(f)** this facies is featured by typical association of  
 662 components, that are dung aggregates (red arrow), bone (white arrow) and charcoal fragments,  
 663 note that the bone is in situ cracked (a close-up on the cracks is given in **Fig. 6f**); **g-h**)  
 664 Paleolithic's typical compacted micro-granular structure (SU4 and SU5) and rare amount of  
 665 archaeological components and the presence of phosphatic features led to a suspected  
 666 decomposition of elements, as shown in **h** the white arrow points a phosphatic rim characterizing  
 667 a sub-rounded limestone pebble.

### 668 5.5.1 SU5 and SU4

669 SU5 and SU4, both representing the Epipaleolithic cultural horizon, share geological  
 670 similarities at both macro and microscopic scales, encompassing texture, lithological  
 671 composition, and fabric (**Fig. 3**, **Fig. 4**, and **Table 1**). The sediments in these units are coarse silts  
 672 (Table S3 in SI). They contain a higher proportion of coarse clasts (ratio  $\approx 1$ , **Fig. 3a**), mostly  
 673 resulting from the physical disintegration of the shale bedrock. Mineralogically, there is a slight  
 674 enrichment in silicates and phyllosilicates (**Fig. 4b**). From a geochemical perspective, SU5 and  
 675 SU4 exhibit slightly higher concentration of Al-group elements compared to the units situated  
 676 above them.

677 Micromorphologically, both units are represented by a low frequency of archaeologically  
678 important materials and a slightly more compacted, clayey fabric (**Table 1; Fig. 7gi**). Bioturbation  
679 (both faunal and phytogenic) is evident in the form of rounded voids, with certain features  
680 indicative of arid climate (xeric conditions) such as calcified roots (**Table 1**). The matrix and  
681 coarse clasts display irregularly impregnation of calcite and phosphatic solutions (**Table 1; Fig.**  
682 **7h**), suggesting the possibility of secondary disturbances within these deposits. Taphonomic  
683 evidence, such as apatite nodules and P coating (Table S8 in SI), are weak and not very well  
684 developed. This suggests that the low frequency of archaeological material might be a result low-  
685 intensity human occupation. Additionally, the development of rims around rock fragments (**Fig.**  
686 **7h**) and bioturbation features might point toward a very low sedimentation rate. The accumulation  
687 of debris mainly originating from colluvial processes, and fine particles as a result of weathering  
688 and aeolian processes.

### 689 **5.5.2 SU3 and SU2**

690 *SU3* exhibits similar textural, geochemical, and mineralogical characteristics to *SU4* and *SU5*  
691 (**Fig. 3** and **Fig. 4**). These sediments consists mainly of medium silts (Table S3 in SI), and show  
692 enrichment in silicates and phyllosilicates (**Fig. 4b**), reflected in a slight enrichment in Al-group  
693 elements (**Fig. 4a**). However, when examined microscopically, *SU3* reveals a more developed  
694 granular structure, and a more calcitic groundmass, distinguishing it from the more brownish  
695 character of *SU5* and *SU4* (details in **Table 1**). Moreover, *SU3* exhibits an increase in size and  
696 frequency of coarse charcoal fragments, presence of bones, and suspected ash, features absent in  
697 the units below (**Table 1**). Moreover, a cluster of low-magnesium carbonate authigenic minerals  
698 is observed (**Table 1**). Despite the microscopic surge in charcoal and presence of bone,  
699 geochemically, *SU3* does not indicate a higher content of organic matter or P and other  
700 archaeologically important elements (**Fig. 3c**).

701 At the microscopic scale, elements like randomly distributed charcoals, occasional bones, and  
702 ash nodules might suggest reworking (**Table 1**). The presence of carbonate authigenic minerals  
703 remains a topic of debate, as they could potentially originate from pedogenetic processes under  
704 extremely arid conditions where Ca is particularly abundant (Durand *et al.*, 2018). Similar  
705 features have been described by (Verrecchia *et al.*, 1995) in laminar crust and were interpreted as  
706 a result of bacterial activity reflecting dry and wet spells. In the sediments of Obishir-5, these  
707 authigenic minerals were found in association with ash. Supporting pedogenetic processes  
708 interpretation though, indices such as such as Ti/Zr, CPA, Al<sub>2</sub>O<sub>3</sub>/TiO<sub>2</sub> ratios, which assess  
709 alteration and pedogenesis, indicate higher alteration in this portion of the profile (Figure S6 in  
710 SI). The accumulation of debris mainly originating from colluvial processes, and fine particles as  
711 a result of weathering, aeolian processes and anthropogenic activity.

712 Macroscopically, *SU2* appears darker in color with shades of pink, indicating the presence of  
713 organic matter and ash material respectively. This points towards the possibility of syn- or post-  
714 depositional accumulation of anthropogenic material within the talus. *SU2* is further divided into  
715 several subunits (Sub2.1–Sub2.4) at the macroscopic scale. However, differences between sub-  
716 units were very subtle and not really discernable at the microscale (**Table 1**, Table S8 in SI),  
717 partially due to limited and distant sampling. Furthermore, there are subtle texture differences  
718 between subunits, with the sediments being very fine sandy coarse silts for all subunits except  
719 Sub4.2, which is classified as very fine sandy medium silt (Table S3).

720 Geochemically, Sub2.4 and Sub2.3 show similarities, with a steady increase of Ca-group  
721 elements and constant decrease of Al-group elements upward (**Fig. 4a**). Mineralogically, Sub2.4  
722 and Sub2.3 resemble the units below (**Fig. 4b**). Conversely, Sub2.2 and 2.1 revealed concentration  
723 peaks in Ca-group (P, Cu, Zn and Ca) elements and an increase in carbonates (**Fig. 4**). This  
724 suggests a relatively higher concentration of these elements corresponding to the deposition of  
725 zoogenic inputs, particularly due to the accumulation of bones and herbivore dung droppings.

726 At the microscopic scale, Sub2.4, 2.3 and 2.2 reveal a granular microstructure and the presence  
727 of herbivore dung and fire-related features, indicating that, along with geogenic processes,  
728 herding and firing activities contributed to anthropogenic inputs. Dung pellets unequivocally  
729 appear from Sub2.4 upward (**Table 1**, **Table 2**). Moreover, we assessed the use of wood and dung  
730 material as fuel during firing, and accidentally, the use of bones (**Fig. 6**). The sediments are  
731 typified by chaotic arrangement of geogenic material mixed with archaeological important  
732 components such as bone, dung and charcoal fragments. The fabric was taken to be the result of  
733 post-depositional disturbances, especially bioturbation carried out by soil earthworms,  
734 invertebrates, and small rodents (**Table 1**).

735 Following the deposition of *SU2*, a potential gap in sedimentation occurred, possibly  
736 connected to abandonment or erosional processes at the site, as supported by texture analyses  
737 (**Fig. 3a**). This gap in the sedimentation might have favored soil formation and, consequently, the  
738 reworking of these deposits. Soil formation is further evidenced by the trends in various  
739 geochemical elements (**Fig. 4a**). Approximately 1 meter below the surface, corresponding to  
740 Sub2.1 and Sub2.2, several element peaks (such as N, P, Ca, Al) indicate the presence of a  
741 paleosol's topsoil. Gradual changes (either increases or decreases) of some element  
742 concentrations below that depth point toward eluviation from a former surface and illuviation at  
743 deeper parts of the sequence. Such a pattern additionally supports the presence of a paleosol  
744 (Weihrauch, Söder and Stoddart, 2022). This is supported by weathering and alteration ratios,  
745 such as Na/Al, Ti/Zr, K<sub>2</sub>O/Na<sub>2</sub>O, and CPA (Figure S6 in SI).

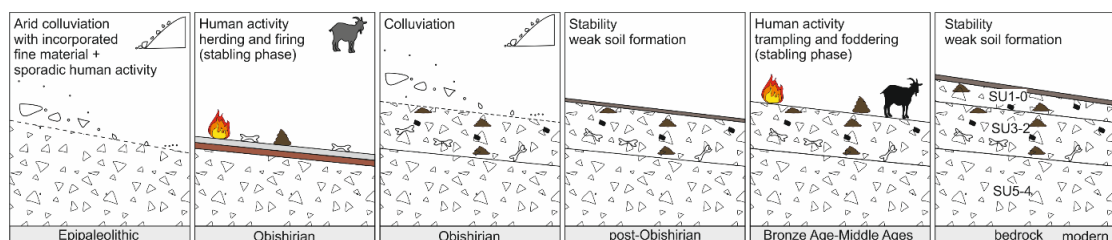
746 Due to the high level of disturbances in SU2 and SU3, it is challenging to assess the original  
 747 site formation processes. Nevertheless, it is clear that these units contain an Obishirian cultural  
 748 assemblage with evidence of herding practices.

### 749 5.5.3 SU1 and SU0

750 *SU1*, deposited between the Bronze Age and Middle Ages (Osipova *et al.*, 2021), presents  
 751 finer sediment texture (**Fig. 3a**; characterized as coarse silt, Table S3 in SI) compared to the  
 752 underlying units (**Fig. 3**). In the field, *SU1* appeared noticeably lighter in color. This finer texture  
 753 could suggest better land management practices, possibly involving the removal of coarser  
 754 materials to optimize land use.

755 Geochemical and mineralogical data revealed an increase in Mg and decrease in Ca in  
 756 comparison to the layers beneath (**Fig. 4**). This might indicate pedogenesis (Ca illuviation as  
 757 supported by geochemical ratios Ca/Al, Ca/Na and Ca/Ti in Figure S8 in SI) and/or alteration of  
 758 the bedrock. At the micromorphological level, the archaeological material, especially dung  
 759 pellets, exhibited horizontal alignment, and the fabric displayed evidence of trampling (e.g.,  
 760 subparallel micro laminated and platy microstructure, alignment of components), as well as  
 761 bioturbation by soil fauna (**Table 1**, Table S8 in SI). The presence of low-magnesium authigenic  
 762 carbonates and a compacted and occasionally cemented micromass might indicate pedogenesis  
 763 and the formation of a crust, a common process in arid environments. Trampling could have been  
 764 caused by both humans and animals. The presence of dung droppings, along with elongated  
 765 phytoliths, suggests animal presence and foddering. Therefore, *SU1* likely served as living floors  
 766 where livestock congregated and grazed.

767 *SU0* represents the current topsoil developed on top of *SU1*. With *SU1*, it shares similar texture  
 768 (Table S3 in SI). What distinguishes this unit is the relatively higher concentration of total  
 769 nitrogen (TN) compared to units below (**Fig. 4a**). This is indicative of a stability phase, suggesting  
 770 a cessation in accumulation processes favoring soil development. In **Fig. 8**, we illustrate a  
 771 schematic formation model for Obishir-5.



772

773

**Fig. 8** Schematic formation model of the Obishir-5 site

## 774 **5.6 Archaeological implications**

775 The mountains of Central Asia are home to several archaeological sites that likely developed  
776 a mixed pastoral-hunting economy (W. Taylor *et al.*, 2021; Yin, Zhang and Yu, 2023). Among  
777 these sites, Obishir-5 is a unique example of the use of livestock since the Early Holocene to the  
778 early Middle Ages. In this discussion, we delve into the evidence found in the sedimentary record  
779 to explore the use of the site.

780 The Epipaleolithic record at Obishir-5, mainly found in SU5 and SU4, is quite sparse. From a  
781 sedimentary perspective, these units retain very few markers, making it challenging to interpret  
782 the site's use during this period. It's possible that the site was only sporadically visited or used,  
783 given the limited evidence in the sediments.

784 The Obishirian assemblage comes into focus in the upper part of SU3 and the entirety of SU2.  
785 SU2, in particular, yields a faunal assemblage with the earliest evidence of domestic animals in  
786 the region, namely sheep and goats (*Ovis* and *Capra*). This is supported by the sedimentary  
787 record, which reveals the presence and relatively high frequency of herbivore dung material,  
788 although often disrupted.

789 SU2 represents a period of relatively intense occupation. We identified an accumulation of  
790 charcoals, charred material, ash, bones and herbivore dung (**Table 1**, **Table 2**, **Fig. 5**, and **Fig. 6**).  
791 Herbivore dung pellets suggest that the herds were kept at the site alive; it might also point to the  
792 use of the site as a sheep/goat pen, perhaps fenced. Animal enclosures usually show trampling  
793 features, but trampling was not observed in the sedimentary record. Analogies of the site used as  
794 a pen are still visible in modern times at the site, especially in Obishir-4 (**Fig. 2c**). The herding  
795 practices might have included practices of cleansing by firing, as supported by the presence of  
796 charcoal, ash and charred material. Moreover, the burnt dung might support the practice of  
797 burning dung as fuel, but also be evidence of fumier-style firing of the stable floor.

798 From W. T. T. Taylor *et al.* (2021) we know that the bones belong to domestic animals and  
799 were processed, revealing cut marks. This might indicate that the site or its vicinity was used as  
800 a butchery. Therefore, it's likely that both humans and livestock were present at the site  
801 simultaneously. This is also purported by personal ornaments made of soft stones found in SU2  
802 and SU3 (Fedorchenko *et al.*, 2018). What's also clear is that the sediments contain numerous  
803 signs of reworking, although it remains unclear whether anthropogenic, such as cleaning, racking  
804 and/or dumping, common stable management practices; or geogenic processes, such as  
805 gravity-induced events or bioturbation, were the dominant agents of this reworking. In sum, the  
806 Obishirian assemblage at the site is poorly preserved and has been subjected to various reworking  
807 processes.

808 Moving to the Bronze Age and Middle Ages facies, we find evidence of stock grazing at the  
809 site as well as firing activities. However, there are fewer bones, which may indicate better  
810 management and cleanliness of the site. This is further supported by textural analyses, which  
811 show a reduced coarse fraction in SU1, along with signs of trampling. Moreover, trampling is a  
812 common feature observed in animal enclosures.

813 Both macroscopic and microscopic observations reveal that firing activities were concentrated  
814 in the westernmost part of the excavation trench. These observations align with field evidence  
815 and features observed in a micromorphological sample (MM2101, see Table S9 and Figure S16  
816 in SI). These microscopic features imply the presence of burnt materials in the vicinity of the site  
817 and point toward reworking of the sedimentary material. Moreover, different agents of reworking  
818 played a role in shaping the fabric of the sediment, as discussed earlier.

819 The evidence of disturbances in the sedimentary material should be considered when analyzing  
820 the archaeological record. Mixing of different assemblages due to bioturbation, human-related  
821 activities and colluvial processes must be taken into account in the final interpretation.  
822 Furthermore, the sedimentation at Obishir-5 was likely influenced by erosion or gaps in  
823 sedimentation, as recorded between SU2 and SU1.

824 In addition, certain characteristics found at the site in SU1 and SU2, and partially SU3,  
825 resemble fumier sequences known from the Mediterranean area (e.g., Macphail *et al.*, 1997;  
826 Boschian and Montagnari-Kokelj, 2000; Angelucci *et al.*, 2009; Fernández-Palacios *et al.*, 2023).  
827 These characteristics include: presence of burnt animal dung and vegetal remains, presence of  
828 fecal spherulites and phytoliths, a granular structure of sediments with mixing of geogenic and  
829 anthropogenic material, a relatively modest artifact assemblage. The key difference is that, unlike  
830 Mediterranean fumiers, we do not macroscopically observe the well-bedded layer-cake structure.  
831 Instead, the sediments exhibit chaotic color changes. Therefore, we may surmise that SU3 and  
832 SU2 represent a heavily reworked succession of burned and unburned units mixed together by  
833 syn- and post-depositional processes (**Fig. 6**), likely the result of seasonal stabling of livestock.

## 834 **6 Conclusions**

835 The main geogenic processes responsible for the accumulation of sedimentary sequences at  
836 Obishir-5 are colluvial, aeolian and in situ weathering in nature. In addition to these natural  
837 processes, anthropogenic activities have played a significant role in depositing and organizing  
838 fine materials, particularly those associated with fires and pastoral activities, such as the presence  
839 of livestock at the site. Bioturbation has left tangible evidence of mixing and disruption within  
840 the sedimentary record, which may also extend to the archaeological record. The site has also  
841 undergone degradation and soil formation processes over time. These sediment characteristics are



842 primarily linked to three occupational phases: (1) the Bronze Age and Middle Ages, (2) the  
843 Obishirian culture, and (3) the Epipaleolithic period. Various geochemical signals have helped us  
844 differentiate between different sources of fine material accumulation, including physical  
845 disintegration of parent materials, aeolian inputs, and archaeological contributions.

846 This study provides additional evidence of the significance of Obishir-5 in understanding early  
847 pastoralism in the region. The presence of herbivore dung within the sediments of SU2 strongly  
848 suggests the past presence of ruminants at the site. This finding aligns with the conclusions of the  
849 study by W. T. T. Taylor et al., (2021) and supports the idea of an economy centered around  
850 various forms of herding. However, the investigation into site formation processes reveals  
851 significant sedimentary reworking, indicating that the Obishirian cultural record at the site is  
852 fragmented. Therefore, caution must be exercised when making archaeological interpretations  
853 based on these findings.

854 It's important to note that while geochemical and mineralogical analyses have their merits,  
855 they failed to detect certain critical aspects captured by the microscopic method  
856 (micromorphology). Micromorphology has unveiled hidden facets of the sedimentary records that  
857 other applied methodologies could not reveal. Future work at the site should strive for a  
858 comprehensive integration of micromorphology, mineralogy, and chronological analyses.  
859 Regarding micromorphology, higher-resolution sampling is recommended to better identify  
860 differences between subunits and sedimentological features such as boundaries and lateral  
861 variations. Additionally, micro-analytical methods should be considered for the study of these  
862 sediments, as bulk sample analyses failed to detect the presence of phosphates, which were  
863 revealed in the microscopic record.

864 To gain a deeper understanding of the reworking processes, it is advisable to measure the  
865 inclination of coarse rock fragments to determine the extent and manner of colluvial processes at  
866 the site. Furthermore, a more extensive geo-ethnoarchaeological study is essential for a better  
867 comprehension of pastoral activities at the site, including the application of stable isotope analysis  
868 and biomarkers on sediments. The chronology of the sequence exhibits several discrepancies  
869 between measurement and deposition of deposits, warranting further radiocarbon and optical  
870 dating measurements to clarify these offsets and sedimentary gaps throughout the sequence. It is  
871 recommended that optical dating covers the entire sequence, with efforts made to avoid sampling  
872 burrows where possible.

## 873 **7 Acknowledgments**

874 We extend our thanks to all the people involved in the excavation, especially Saltanat Alisher  
875 Kyzy and Temerlan ('Tima') Chargynov from the National Kyrgyz University. Tima also

876 collected one micromorphological sample in 2021 when the fieldworks to Kyrgyzstan were not  
877 possible due to COVID pandemic. We acknowledge Redzhep Kurbanov for performing grain size  
878 analysis at Lomonosov Moscow State University, Oleh Hnylko from the Institute of Geology and  
879 Geochemistry of Combustible Minerals at the National Academy of Science of Ukraine in Lviv  
880 for his valuable explanation about the complex geology of the Aydarken basin, and Jarosław  
881 Tyszką for providing us with access to the fluorescence microscope.

882 This study was supported by the National Science Centre, Poland (grant number  
883 2018/29/B/ST10/00906). Fieldworks in Kyrgyzstan were supported by Russian Science Fund  
884 (grant number 19-78-10053) and the National Science Centre, Poland (grant number  
885 2018/29/B/ST10/00906).

## 886 **8 Author contributions**

- 887 – GB designed the study, drafted and revised the manuscript, and analyzed and interpreted  
888 micromorphological, geochemical, and textural data.
- 889 – SS provided access to the site, supervised the excavations and revised the manuscript.
- 890 – ML contributed to the manuscript by analyzing and interpreting PXRD and FTIR data  
891 and by drafting and revising the manuscript.
- 892 – JG assisted in acquiring fluorescence microphotographs and revised the manuscript.
- 893 – EW produced the thin sections for micromorphology studies.
- 894 – AA provided site access and excavation permits, as well as revised the manuscript.
- 895 – MK designed the study, supervised the work, and provided critical revisions to the  
896 manuscript, while also acquiring micromorphological, geochemical, and textural data.

## 897 **9 Statements and Declarations**

898 The authors have no relevant financial or non-financial interests to disclose.

## 899 **10 References**

- 900 Adesso, R. *et al.* (2022) ‘Geochemical characterization of clastic sediments sheds light on  
901 energy sources and on alleged anthropogenic impacts in cave ecosystems’, *International Journal*  
902 *of Earth Sciences*, 111(3), pp. 919–927. doi: 10.1007/s00531-021-02158-x.
- 903 Angelucci, D. E. *et al.* (2009) ‘Shepherds and karst: The use of caves and rock-shelters in the  
904 Mediterranean region during the Neolithic’, *World Archaeology*, 41(2), pp. 191–214. doi:  
905 10.1080/00438240902843659.
- 906 Araujo, A. G. M. *et al.* (2008) ‘Lapa das boleiras rockshelter: stratigraphy and formation  
907 processes at a paleoamerican site in Central Brazil’, *Journal of Archaeological Science*. Academic  
908 Press, 35(12), pp. 3186–3202. doi: 10.1016/J.JAS.2008.07.007.

- 909 Beck, H. E. *et al.* (2018) ‘Present and future köppen-geiger climate classification maps at 1-  
910 km resolution’, *Scientific Data*. The Author(s), 5, pp. 1–12. doi: 10.1038/sdata.2018.214.
- 911 Blott, S. J. and Pye, K. (2001) ‘GRADISTAT: A GRAIN SIZE DISTRIBUTION AND  
912 STATISTICS PACKAGE FOR THE ANALYSIS OF UNCONSOLIDATED SEDIMENTS’, 26,  
913 pp. 1237–1248. doi: 10.1002/esp.261.
- 914 Boschian, G. and Montagnari-Kokelj, E. (2000) ‘Prehistoric Shepherds and Caves in the  
915 Trieste Karst (Northeastern Italy)’, *Geoarchaeology - An International Journal*, 15(4), pp. 331–  
916 371. doi: 10.1002/(SICI)1520-6548(200004)15:4<331::AID-GEA3>3.0.CO;2-H.
- 917 Brancaloni, G. *et al.* (2022) ‘Depositional history of a talus cone in an arid intermontane basin  
918 in Central Asia: An interdisciplinary study at the Late Pleistocene–Late Holocene Obishir-I site,  
919 Kyrgyzstan’, *Geoarchaeology*. John Wiley and Sons Inc, 37(2), pp. 350–373. doi:  
920 10.1002/gea.21892.
- 921 Brancaloni, G. *et al.* (2023) ‘A closer look at clasts and groundmass: Micromorphological  
922 features in sediments with archaeological significance in Obishir and Katta Sai complexes  
923 (Central Asia)’, *Journal of Archaeological Science: Reports*. Elsevier, 51, p. 104118. doi:  
924 10.1016/j.jasrep.2023.104118.
- 925 Brönnimann, D. *et al.* (2017) ‘Excrements of Herbivores’, *Archaeological Soil and Sediment  
926 Micromorphology*. John Wiley & Sons, Ltd, pp. 55–65. doi: 10.1002/9781118941065.CH6.
- 927 Buggle, B. *et al.* (2011) ‘An evaluation of geochemical weathering indices in loess-paleosol  
928 studies’, *Quaternary International*, 240(1–2), pp. 12–21. doi: 10.1016/j.quaint.2010.07.019.
- 929 Chen, H. F. *et al.* (2013) ‘The Ti/Al molar ratio as a new proxy for tracing sediment  
930 transportation processes and its application in aeolian events and sea level change in East Asia’,  
931 *Journal of Asian Earth Sciences*. Pergamon, 73, pp. 31–38. doi: 10.1016/J.JSEAES.2013.04.017.
- 932 Cooke, R., Warren, A. and Goudie, A. (1993) *Desert Geomorphology*. London: UCL Press.
- 933 Durand, N. *et al.* (2018) ‘Calcium Carbonate Features’, in Stoops, G., Marcellino, V., and  
934 Mees, F. (eds) *Interpretation of Micromorphological Features of Soils and Regoliths*. 2nd edn.  
935 Amsterdam: Elsevier, pp. 206–258.
- 936 Estévez, J. *et al.* (2014) ‘Microtaphonomy in archaeological sites: The use of soil  
937 micromorphology to better understand bone taphonomy in archaeological contexts’, *Quaternary  
938 International*. Elsevier Ltd, 330(1), pp. 3–9. doi: 10.1016/J.QUAINT.2013.08.007.
- 939 Fedorchenko, A. Y. *et al.* (2018) ‘Personal ornament production technology in the early  
940 holocene complexes of western central Asia: Insights from Obishir-5’, *Archaeology, Ethnology  
941 and Anthropology of Eurasia*, 46(1), pp. 3–15. doi: 10.17746/1563-0110.2018.46.1.003-015.
- 942 Fernández-Palacios, E. *et al.* (2023) ‘Reconstructing formation processes at the Canary Islands  
943 indigenous site of Belmaco Cave (La Palma, Spain) through a multiproxy geoarchaeological  
944 approach’, *Geoarchaeology*. doi: 10.1002/gea.21972.
- 945 Fitzsimmons, K. E. *et al.* (2020) ‘Thinking Outside the Box at Open-Air Archeological  
946 Contexts: Examples From Loess Landscapes in Southeast Romania’, *Frontiers in Earth Science*,  
947 8. doi: 10.3389/feart.2020.561207.
- 948 French, C. (2019) *A Handbook of Geoarchaeological Approaches to Settlement Sites and  
949 Landscapes, A Handbook of Geoarchaeological Approaches to Settlement Sites and Landscapes*.  
950 Oxford: Oxbow Books. doi: 10.2307/j.ctvh1dthr.
- 951 Goldberg, P. *et al.* (2009) ‘Bedding, hearths, and site maintenance in the Middle Stone Age of  
952 Sibudu Cave, KwaZulu-Natal, South Africa’, *Archaeological and Anthropological Sciences*,  
953 1(2), pp. 95–122. doi: 10.1007/s12520-009-0008-1.

- 954 Goldberg, P. and Macphail, R. I. (2006) *Practical and Theoretical Geoarchaeology*. Malden,  
955 MA USA: Blackwell Publishing Ltd. doi: 10.1002/9781118688182.
- 956 Goldberg, P., Miller, C. E. and Mentzer, S. M. (2017) ‘Recognizing fire in the paleolithic  
957 archaeological record’, *Current Anthropology*, 58, pp. S175–S190. doi: 10.1086/692729.
- 958 Heinecke, L. *et al.* (2018) ‘Vegetation change in the eastern Pamir Mountains, Tajikistan,  
959 inferred from Lake Karakul pollen spectra of the last 28 kyr’, *Palaeogeography,*  
960 *Palaeoclimatology, Palaeoecology*, 511, pp. 232–242. doi: 10.1016/j.palaeo.2018.08.010.
- 961 Hughes, P. D. (2010) ‘Geomorphology and Quaternary stratigraphy: The roles of morpho-  
962 litho-, and allostratigraphy’, *Geomorphology*. Elsevier, pp. 189–199. doi:  
963 10.1016/j.geomorph.2010.07.025.
- 964 Islamov, U. I. (1980) *Obishirskaya kultura (Obishir culture)*. Tashkent: Tashkent: Phan.
- 965 Jiang, Q. *et al.* (2020) ‘A Persistently Increasing Precipitation Trend Through the Holocene in  
966 Northwest China Recorded by Black Carbon  $\delta^{13}\text{C}$  From Sayram Lake’, *Frontiers in Earth*  
967 *Science*. Frontiers Media S.A., 8, p. 228. doi: 10.3389/feart.2020.00228.
- 968 Karkanas, P. (Takis) and Goldberg, P. (2019) *Reconstructing Archaeological Sites*  
969 *Understanding the Geoarchaeological Matrix*.
- 970 Karkanas, P. and Goldberg, P. (2018) *Reconstructing Archaeological Sites, Reconstructing*  
971 *Archaeological Sites*. Wiley-Blackwell. doi: 10.1002/9781119016427.
- 972 Krajcarz, M. T. *et al.* (2016) ‘Middle Paleolithic sites of Katta Sai in western Tian Shan  
973 piedmont, Central Asiatic loess zone: Geoarchaeological investigation of the site formation and  
974 the integrity of the lithic assemblages’, *Quaternary International*, 399, pp. 136–150. doi:  
975 10.1016/j.quaint.2015.07.051.
- 976 Krajcarz, M. T. (2019) ‘Alteration of the metal content in animal bones after 2.5-year  
977 experimental exposure to sediments’, *Archaeological and Anthropological Sciences*. Springer  
978 Verlag, 11(1), pp. 361–372. doi: 10.1007/s12520-017-0533-2.
- 979 Krajcarz, M. T. *et al.* (2020) *Shelter in Smoleń III - A unique example of stratified Holocene*  
980 *clastic cave sediments in Central Europe, a lithostratigraphic stratotype and a record of regional*  
981 *paleoecology, PLoS ONE*. doi: 10.1371/journal.pone.0228546.
- 982 Krivoschapkin, A. *et al.* (2020) ‘Middle Paleolithic variability in Central Asia: Lithic  
983 assemblage of Sel’Ungur cave’, *Quaternary International*. Elsevier, 535(August), pp. 88–103.  
984 doi: 10.1016/j.quaint.2018.09.051.
- 985 Li, Y. *et al.* (2020) ‘Moisture evolution in Central Asia since 26 ka: Insights from a Kyrgyz  
986 loess section, Western Tian Shan’, *Quaternary Science Reviews*. Elsevier Ltd, 249, p. 106604.  
987 doi: 10.1016/j.quascirev.2020.106604.
- 988 Linder, M. C. (2020) ‘Copper homeostasis in mammals, with emphasis on secretion and  
989 excretion. A review’, *International Journal of Molecular Sciences*, 21(14), pp. 1–22. doi:  
990 10.3390/ijms21144932.
- 991 Macphail, R. I. *et al.* (1997) ‘The soil micromorphological evidence of domestic occupation  
992 and stabling activities’, *Memorie dell’Istituto Italiano di Paleontologia Umana*, V, pp. 53–88.
- 993 Macphail, R. I. and Goldberg, P. (2017) *Applied soils and micromorphology in archaeology,*  
994 *Applied Soils and Micromorphology in Archaeology*. Cambridge University Press. doi:  
995 10.1017/9780511895562.
- 996 Mallol, C., Mentzer, S. M. and Miller, C. E. (2017) ‘Combustion Features’, in Nicosia, C. and  
997 Stoops, G. (eds) *Archaeological Soil and Sediment Micromorphology*. Hoboken, NJ: John Wiley  
998 & Sons, Ltd, pp. 299–330.

- 999 Marcazzan, D., Miller, C. E. and Conard, N. J. (2022) ‘Burning, dumping, and site use during  
1000 the Middle and Upper Palaeolithic at Hohle Fels Cave, SW Germany’, *Archaeological and*  
1001 *Anthropological Sciences*, 14(9), p. 3. doi: 10.1007/s12520-022-01647-7.
- 1002 Mathis, M. *et al.* (2014) ‘Regional vegetation patterns at lake Son Kul reveal Holocene  
1003 climatic variability in central Tien Shan (Kyrgyzstan, Central Asia)’, *Quaternary Science*  
1004 *Reviews*, 89, pp. 169–185. doi: 10.1016/j.quascirev.2014.01.023.
- 1005 Mentzer, S. M. (2014) ‘Microarchaeological Approaches to the Identification and  
1006 Interpretation of Combustion Features in Prehistoric Archaeological Sites’, *Journal of*  
1007 *Archaeological Method and Theory*, 21(3), pp. 616–668. doi: 10.1007/s10816-012-9163-2.
- 1008 Miall, A. D. (1978) ‘Lithofacies types and vertical profile models in braided river deposits: a  
1009 summary’, *Fluvial Sedimentology*, 5, pp. 597–600.
- 1010 Miko, S., Kuhta, M. and Kapelj, S. (2016) ‘Environmental Baseline Geochemistry of  
1011 Sediments and Percolating Waters in the Modrić Cave, Croatia’, *Acta Carsologica*, 31(1), pp.  
1012 135–149. doi: 10.3986/ac.v31i1.409.
- 1013 Miller, B. A. and Juilleret, J. (2020) ‘The colluvium and alluvium problem: Historical review  
1014 and current state of definitions’, *Earth-Science Reviews*. Elsevier, 209(July), p. 103316. doi:  
1015 10.1016/j.earscirev.2020.103316.
- 1016 Miller, C. E. *et al.* (2010) ‘Dumping, Sweeping and Trampling: Experimental  
1017 Micromorphological Analysis of Anthropogenically Modified Combustion Features’,  
1018 *Paleoethnologie*, (2), pp. 25–37. doi: 10.4000/paleoethnologie.8197.
- 1019 Nir, N. *et al.* (2022) ‘Footpaths: Pedogenic and geomorphological long-term effects of human  
1020 trampling’, *Catena*. Elsevier B.V., 215. doi: 10.1016/J.CATENA.2022.106312.
- 1021 Nishiaki, Y. *et al.* (2022) ‘Neolithization during the 6th millennium BCE in western Central  
1022 Asia: New evidence from Kaynar Kamar Rockshelter, Hissar Mountains, Southeast Uzbekistan’,  
1023 *Archaeological Research in Asia*. Elsevier, 30, p. 100352. doi: 10.1016/j.ara.2022.100352.
- 1024 Olenchenko, V. *et al.* (2017) ‘Geoelectric Structure of the Obishir-5 Archaeological Site  
1025 (Kyrgyzstan) Based on Electrotomography Data’, *Teoriya i praktika arkheologicheskikh*  
1026 *issledovaniy*, 4(4), pp. 150–157. doi: 10.14258/tpai(2017)4(20).-11.
- 1027 Osipova, E. *et al.* (2021) ‘Palaeoenvironmental conditions of the Palaeolithic–Neolithic  
1028 transition in the Fergana Valley (Central Asia) – New data inferred from fossil molluscs in  
1029 Obishir-V rockshelter (Kyrgyzstan)’, *Quaternary International*. Pergamon, 605–606, pp. 287–  
1030 299. doi: 10.1016/J.QUAINT.2020.11.009.
- 1031 Pawelec, H. and Ludwikowska-Kędzia, M. (2016) ‘Macro- and Micromorphologic  
1032 Interpretation of Relict Periglacial Slope Deposits from the Holy Cross Mountains, Poland’,  
1033 *Permafrost and Periglacial Processes*, 27(2), pp. 229–247. doi: 10.1002/ppp.1864.
- 1034 Ramsey, C. B. (2009) ‘Dealing with outliers and offsets in radiocarbon dating’, *Radiocarbon*,  
1035 51(3), pp. 1023–1045. doi: 10.1017/s0033822200034093.
- 1036 Räsänen, M. E. *et al.* (2009) ‘A shift from lithostratigraphic to allostratigraphic classification  
1037 of Quaternary glacial deposits’, *GSA Today*, 19(2), pp. 4–11. doi: 10.1130/GSATG20A.1.
- 1038 Röpke, A. and Dietl, C. (2017) ‘Burnt Soils and Sediments’, in Nicosia, C. and Stoops, G.  
1039 (eds) *Archaeological Soil and Sediment Micromorphology*. John Wiley & Sons, Ltd, pp. 173–  
1040 180. doi: 10.1002/9781118941065.ch21.
- 1041 Rubio, L. *et al.* (2020) ‘Spectrophotometric color measurement to assess temperature of  
1042 exposure in cortical and medullar heated human bones: A preliminary study’, *Diagnostics*,  
1043 10(11). doi: 10.3390/diagnostics10110979.

- 1044 Schroeter, N. *et al.* (2020) ‘How to Deal With Multi-Proxy Data for Paleoenvironmental  
1045 Reconstructions: Applications to a Holocene Lake Sediment Record From the Tian Shan, Central  
1046 Asia’, *Frontiers in Earth Science*, 8(September), pp. 1–18. doi: 10.3389/feart.2020.00353.
- 1047 Serdyuk, N. V. *et al.* (2023) ‘Holocene vertebrate fauna in Fergana Valley, Kyrgyzstan, based  
1048 on fossils from the Obishir-5 rock shelter’, *Geobios*. Elsevier Masson. doi:  
1049 10.1016/J.GEOBIOS.2023.01.002.
- 1050 Shahack-Gross, R. (2011) ‘Herbivorous livestock dung: Formation, taphonomy, methods for  
1051 identification, and archaeological significance’, *Journal of Archaeological Science*. Academic  
1052 Press, 38(2), pp. 205–218. doi: 10.1016/J.JAS.2010.09.019.
- 1053 Shahack-Gross, R. and Finkelstein, I. (2008) ‘Subsistence practices in an arid environment: a  
1054 geoarchaeological investigation in an Iron Age site, the Negev Highlands, Israel’, *Journal of*  
1055 *Archaeological Science*. Academic Press, 35(4), pp. 965–982. doi: 10.1016/J.JAS.2007.06.019.
- 1056 Shnaider, S. V. *et al.* (2017) ‘New investigations of the Epipalaeolithic in western Central  
1057 Asia: Obishir-5’, *Antiquity*. Antiquity Publications, 91(360). doi: 10.15184/aqy.2017.213.
- 1058 Shnaider, S. V. *et al.* (2019) ‘Results of Field Studies at the Obishir-5 Site in 2018–2019’,  
1059 *Problems of Archaeology, Ethnography, Anthropology of Siberia and Neighboring Territories*,  
1060 XXV, pp. 286–292.
- 1061 Shnaider, S. V. *et al.* (2020) ‘New insights into the Epipalaeolithic of western Central Asia:  
1062 The Tutkaulian complex’, *Quaternary International*. Elsevier Ltd, 535, pp. 139–154. doi:  
1063 10.1016/j.quaint.2018.10.001.
- 1064 Sokol, E. V. *et al.* (2022) ‘Phosphate Record in Pleistocene-Holocene Sediments from  
1065 Denisova Cave: Formation Mechanisms and Archaeological Implications’, *Minerals*, 12(5). doi:  
1066 10.3390/min12050553.
- 1067 Spate, M., Leipe, C. and Motuzaite Matuzeviciute, G. (2022) ‘Reviewing the  
1068 Palaeoenvironmental Record to Better Understand Long-Term Human-Environment Interaction  
1069 in Inner Asia During the Late Holocene’, *Frontiers in Ecology and Evolution*, 10(July). doi:  
1070 10.3389/fevo.2022.939374.
- 1071 Stiner, M. C. *et al.* (1995) ‘Differential Burning, Recrystallization, and Fragmentation of  
1072 Archaeological Bone’, *Journal of Archaeological Science*, 22(2), pp. 223–237. doi:  
1073 10.1006/jasc.1995.0024.
- 1074 Stoops, G. (2021) *Guidelines for Analysis and Description of Soil and Regolith Thin Sections*.  
1075 Second Edi. Wiley.
- 1076 Taylor, W. *et al.* (2021) ‘High altitude hunting, climate change, and pastoral resilience in  
1077 eastern Eurasia’, *Scientific Reports*. Nature Research, 11(1). doi: 10.1038/S41598-021-93765-W.
- 1078 Taylor, W. T. T. *et al.* (2020) ‘Early Pastoral Economies and Herding Transitions in Eastern  
1079 Eurasia’, *Scientific Reports*, 10(1), p. 60516. doi: 10.1038/s41598-020-57735-y.
- 1080 Taylor, W. T. T. *et al.* (2021) ‘Evidence for early dispersal of domestic sheep into Central  
1081 Asia’, *Nature Human Behaviour*. doi: 10.1038/s41562-021-01083-y.
- 1082 Timireva, S. N. *et al.* (2022) ‘Revisiting the Taman peninsula loess-paleosol sequence: Middle  
1083 and Late Pleistocene record of Cape Pekla’, *Quaternary International*. Pergamon, 620, pp. 36–  
1084 45. doi: 10.1016/J.QUAINT.2021.06.010.
- 1085 UDDEN, J. A. (1914) ‘Mechanical composition of clastic sediments’, *Geological Society of*  
1086 *America Bulletin*, 25(1), pp. 655–744. doi: 10.1130/gsab-25-655.
- 1087 UNEP, UNITAR and Zoï E. Network (2009) *Khaidarkan Mercury: Addressing Primary*  
1088 *Mercury Mining in Kyrgyzstan*.

- 1089 Verrecchia, E. P. *et al.* (1995) 'Spherulites in Quaternary Laminar Crusts', *Journal of*  
1090 *Sedimentary Research*, A65(4), pp. 690–700.
- 1091 Villagran, X. S. *et al.* (2017) 'Bone and Other Skeletal Tissues', in Nicosia, C. and Stoops, G.  
1092 (eds) *Archaeological Soil and Sediment Micromorphology*. First. John Wiley & Sons Ltd., pp.  
1093 11–38.
- 1094 Weihrauch, C., Söder, U. and Stoddart, S. (2022) 'The identification of archaeologically  
1095 interesting depths from vertical soil phosphorus prospections in geoarchaeology', *Geoderma*.  
1096 Elsevier, 418, p. 115850. doi: 10.1016/j.geoderma.2022.115850.
- 1097 Wentworth, C. K. (1922) 'A Scale of Grade and Class Terms for Clastic Sediments', *The*  
1098 *Journal of Geology*, 30(5), pp. 377–392. doi: 10.1086/622910.
- 1099 Yin, C., Zhang, J. and Yu, X. (2023) 'Mountain valleys, alluvial fans and oases:  
1100 Geomorphologic perspectives of the mixed agropastoral economy in Xinjiang (3000–200 BC)',  
1101 *Frontiers in Earth Science*, 11(February). doi: 10.3389/feart.2023.1109905.
- 1102 Zieliński, T. and Pisarska-Jamrozy, M. (2012) 'Jakie cechy litologiczne osadów warto  
1103 kodować, a jakie nie?', *Przegląd Geologiczny*, 60(7), pp. 387–397.
- 1104

---

## **Supplementary Information**

### Geoarchaeological approach for tackling the function and preservation state of the Obishir-5 site, the earliest Neolithic site in the Fergana Valley

**Greta Brancaleoni\***, Institute of Geological Sciences, Polish Academy of Sciences, 51/55 Twarda st, 00-818 Warsaw, Poland (ORCID 0000-0002-5563-3729; [greta.brancaleoni@twarda.pan.pl](mailto:greta.brancaleoni@twarda.pan.pl))

**Svetlana Shnaider** APSACA Laboratory, National Center of Archaeology, Uzbek Academy of Sciences, 81 Mirzo Ulugbek Street, Tashkent, Uzbekistan (ORCID 0000-0003-2230-4286; [sveta.shnayder@gmail.com](mailto:sveta.shnayder@gmail.com))

**Malgorzata Lempart-Drozd**, Institute of Geological Sciences, Polish Academy of Sciences, 1 Senacka st, 31-002 Cracow, Poland (ORCID 0000-0001-7394-5951; [ndlempar@cyf-kr.edu.pl](mailto:ndlempar@cyf-kr.edu.pl))

**Jan Goleń**, Institute of Geological Sciences, Polish Academy of Sciences, 1 Senacka st, 31-002 Cracow, Poland (ORCID 0000-0002-0107-0647; [ndgolen@cyf-kr.edu.pl](mailto:ndgolen@cyf-kr.edu.pl))

**Ewa Deput**, Institute of Geological Sciences, Polish Academy of Sciences, 51/55 Twarda st, 00-818 Warsaw, Poland

**Aida Abdykanova**, American University of Central Asia, 7/6 Aaly Tokombaev st, Bishkek 720060, Kyrgyzstan (ORCID 0000-0002-7238-9065; [abdykanova\\_a@auca.kg](mailto:abdykanova_a@auca.kg))

**Maciej T. Krajcarz**, Institute of Geological Sciences, Polish Academy of Sciences, 51/55 Twarda st, 00-818 Warsaw, Poland (ORCID 0000-0002-1240-0664; [mkrajcarz@twarda.pan.pl](mailto:mkrajcarz@twarda.pan.pl))

*\*corresponding author*



## S1. List of archaeological sites mentioned in the main text

*Table S 1 List of coordinates for the sites mentioned in the main text*

Region	Site	N	E	H	Source
Fergana	Obishir-5	39°57'23.3"	71°16'52.4"	1710	GPS
Fergana	Obishir-1	39°57'28.6"	71°17'08.9"	1752	GPS
Fergana	Sel'Ungur Cave	39° 57' 12" N	71° 19' 31" E		(Krivoshapkin <i>et al.</i> , 2020)
Fergana	Surungur rockshelter	39°57'24.41"N	71°15'29.03"E		Dropped pin on Google Earth
Pamir	Oshhona	39°16'2.08" N	73°18' 20.33" E	3976	GPS
Naryn	Aygirzhal-2	41°17'	75°49'		Dropped pin on Google Earth
Naryn	Alamishik-2	41°26'	75°54'		Dropped pin on Google Earth

## S2. Macroscopic observation

### S2.1 Macro-stratigraphic observations at the site

Six stratigraphic units (SUs) were identified in the field, and the description of these units is provided in **Table S 2**. They were numbered in ascending order from SU0 to SU5 within the main trench. SU2 was further divided into four subunits: Sub2.1, Sub2.2, Sub2.3, and Sub2.4. The distinction between these SUs is not very clear, and distinct changes were not identified. SUs were mainly distinguished based on differences in colors, macro-archaeological features (such as the presence or absence of charcoals, bones, and pottery sherds), and gravel content. The boundaries between SUs are still a subject of debate, with the exception of the boundary between SU1 and SU2, which was very clear in the field.

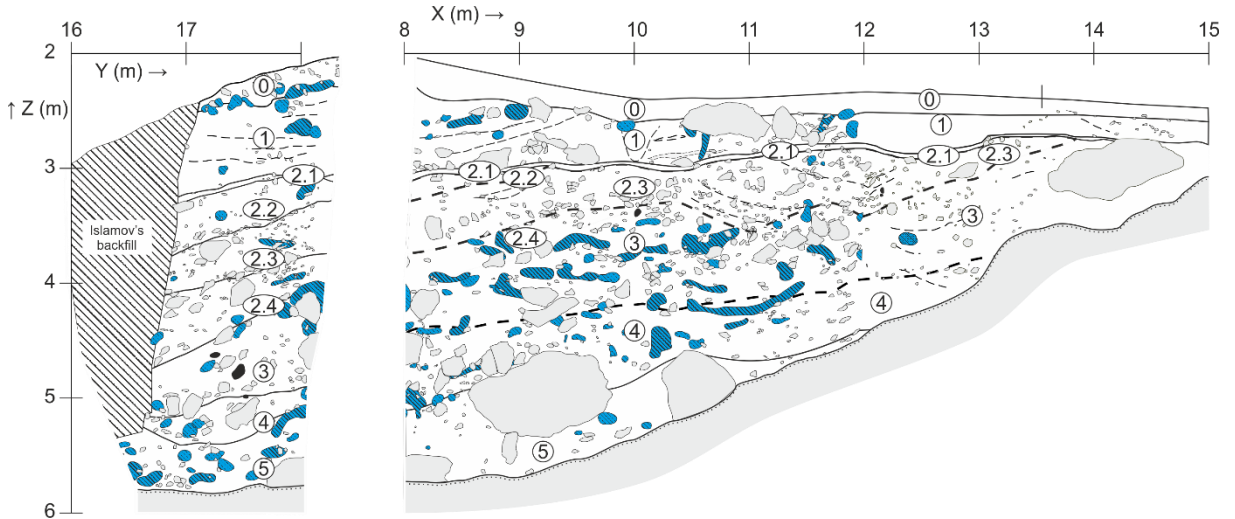
*Table S 2 Obishir-5 stratigraphy after Osipova et al., (2020) and Taylor et al., (2021) in (Brancaloni et al., 2023). The age of layers was established through radiocarbon and thermoluminescence dating (Osipova et al., 2020; Taylor et al., 2021), here we give non calibrated results. Layer 5 age was determined through thermoluminescence dating.*

Layer	Sub-layers	Age (BP)	Max thickness (cm)	Matrix color Munsell dry; moist	Description	Interpretation
0			30		Recent topsoil, matrix supported, clast moderate diamicton, massive, matrix is dark gray silt with plant roots and litter. Lower boundary gradual	Soil formation, stability phase
1		1591±26; 1650±20	60	10YR 7/1; 2.5Y 5/2	Matrix-supported, clast poor, fine diamicton with light gray to grayish brown silt with pottery sherds, bones and charcoals; with reddened lenses and anthropogenic pits. Mid- to coarse-grained limestone clasts (chaotic pattern). Lower boundary clear, marked with change in color and texture	Bronze Age and Middle Ages cultural layer

2	2.1	7324±105	5	10YR 7/2; 10YR 6/3	Matrix-supported, clast moderate weakly laminated diamicton with light gray to pale brown thin-laminated silty matrix. Lower boundary clear, inclined, sedimentary	Reworked cultural layers bearing an Obishirian assemblage
	2.2	6989±45	40	7.5YR 7/2; 10YR 5/4	Matrix-supported, from clast moderate to clast rich, gravelly diamicton with pinkish gray to yellowish brown loose silty matrix. Sparse fine-grained limestone clasts. Lower boundary sharp, discordant	
	2.3	7405±25; 7499±95	60	10YR 6/2; 10YR 3/3	Matrix-supported, clast rich, gravelly diamicton with light brownish-gray to dark brown silty loamy matrix with abundant lithic artifacts. Very abundant fine- to mid-grained limestone clasts (planar texture) and fine pebble-sized clasts (0.5-10 cm). Lower boundary inclined, erosional, marked with mid- and coarse-grained limestone clasts	
	2.4	9410±30	40	10YR 7/2; 10YR 4/3	Matrix-supported, clast rich, gravelly diamicton with light gray to brown silty loamy matrix. very abundant fine- to mid-grained limestone clasts (planar texture) and fine pebble-sized clasts (0.5-1 cm). Lower boundary inclined, discordant, marked with mid- and coarse-grained limestone clasts	
3		7257±19	90	10YR 7/3; 10YR 5/4	Matrix-supported, from clast moderate to clast rich, bouldery diamicton with very pale brown to yellowish-brown silty matrix, massive structure. Small amount of fine- to mid-grained limestone clasts (chaotic pattern). Lower boundary inclined, discordant, marked by accumulation of coarse-grained limestone clasts	Colluvial-aeolian with anthropogenic inputs and Obishirian assemblage
4		8842±18	110	10YR 7/3; 10YR 5/4	Matrix-supported, clast moderate, gravelly diamicton with very pale brown to yellowish-brown silty matrix, massive structure. Small amount of fine- to mid-grained limestone clasts (chaotic texture). Lower boundary unclear, gradual passing into layer 5	Colluvial-aeolian, Upper Paleolithic-Epipaleolithic
5		12.2±1.9 ky BP; 12.4±1.9 ky BP	70	10YR 6/3; 10YR 5/5	Matrix-supported, clast moderate, gravelly diamicton with pale brown to yellowish-brown hard silty matrix, massive structure, preserved only in depressions of the bedrock. Bedrock	Colluvial-aeolian, Upper Paleolithic-Epipaleolithic

## S2.2 Animal burrowing

Animal burrows are very common throughout the sequence and affect all SUs (**Figure S 1**). At Obishir-5, animal burrowing is both a macro- and micro-scale phenomenon. At the macro-scale, it is possible to observe tubular morphologies filled with dark gray material and with clear boundaries (aka krotovinas, (Pietsch, 2013)). These morphologies represent the action of small mammals, for instance rodents, e.g., mole voles as suggested by (Serdyuk *et al.*, 2023).



**Figure S 1** Animal burrowing mapping within the NW Obishir-5 profile. Burrows are represented by objects filled with blue shade.

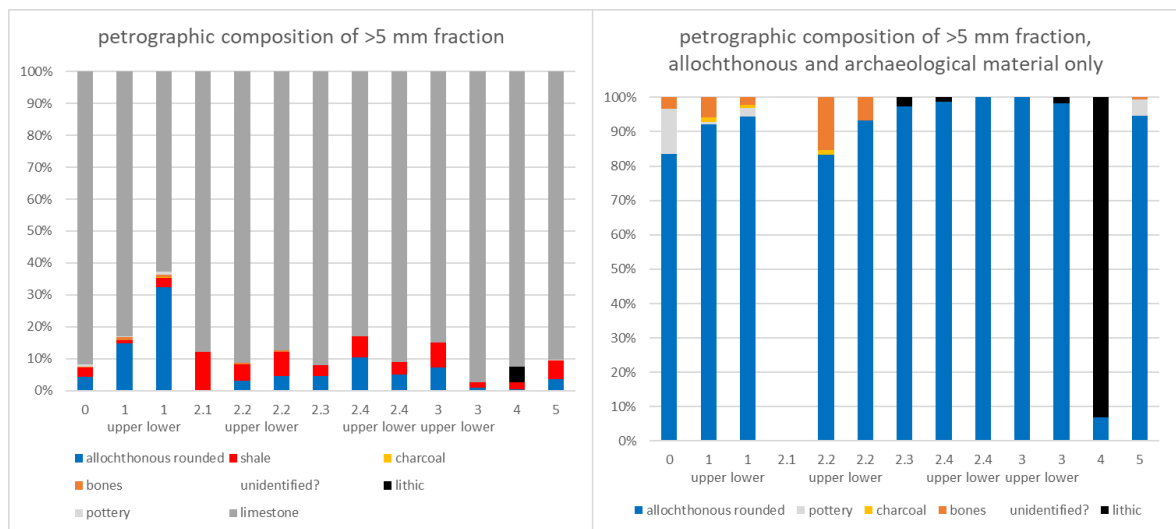
## S3. Grain size and petrographic data

In **Table S 3**, we report the statistical summary obtained using GRADISTAT v9.1. In **Figure S 2**, we illustrate the petrographic composition. The petrographic composition is dominated by limestone (in each unit is > 50%) and shale clasts. Rounded limestone pebbles occurred in each unit, except for SU2.1. Lithic, pottery sherds and charcoals are minor components.

**Table S 3** Sample statistics for the fine fraction at Obishir-5

Sample ID	Depth (m)	Unit	Sample type	Sediment Name	MODE 1 MODE 2 MODE 3 ( $\mu\text{m}$ )	MEDIAN or $D_{50}$
1	0.00	SU0	Unimodal, Poorly Sorted	Very Sandy Fine Coarse Silt	22.55	19.97
2	0.30	SU1	Unimodal, Poorly Sorted	Very Sandy Fine Coarse Silt	22.55	17.83
3	0.60	SU1	Bimodal, Poorly Sorted	Coarse Silt	14.20 22.55	15.49
4	0.80	Sub2.1	Unimodal, Poorly Sorted	Very Sandy Fine Coarse Silt	22.55	19.18
5	1.00	Sub2.2	Unimodal, Poorly Sorted	Very Sandy Fine Coarse Silt	28.35	25.52
6	1.20	Sub2.2	Unimodal, Poorly Sorted	Very Sandy Fine Very Coarse Silt	35.70	28.49

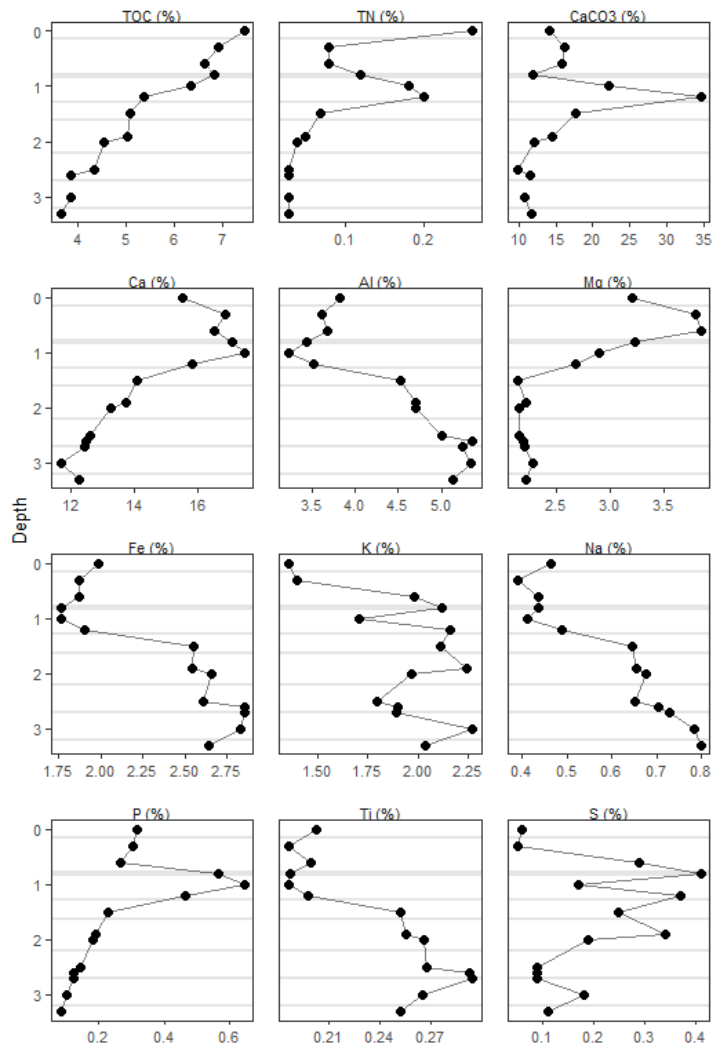
7	1.50	Sub2.3	Bimodal, Poorly Sorted	Very Sandy Silt	Fine Coarse	14.20 22.55	14.43
8	1.90	Sub2.4	Bimodal, Very Poorly Sorted	Very Sandy Silt	Fine Medium	14.20 22.55	15.86
9	2.00	Sub2.4	Trimodal, Very Poorly Sorted	Very Sandy Silt	Fine Medium	14.20 22.55 449.5	15.09
10	2.50	SU3	Unimodal, Poorly Sorted	Medium Silt		14.20	12.47
11	2.70	SU3	Trimodal, Very Poorly Sorted	Very Sandy Silt	Fine Medium	14.20 22.55 712.5	14.34
12	3.00	SU4	Bimodal, Poorly Sorted	Very Sandy Silt	Fine Coarse	22.55 14.20	14.20
13	3.30	SU5	Unimodal, Poorly Sorted	Very Sandy Silt	Fine Coarse	22.55	19.97



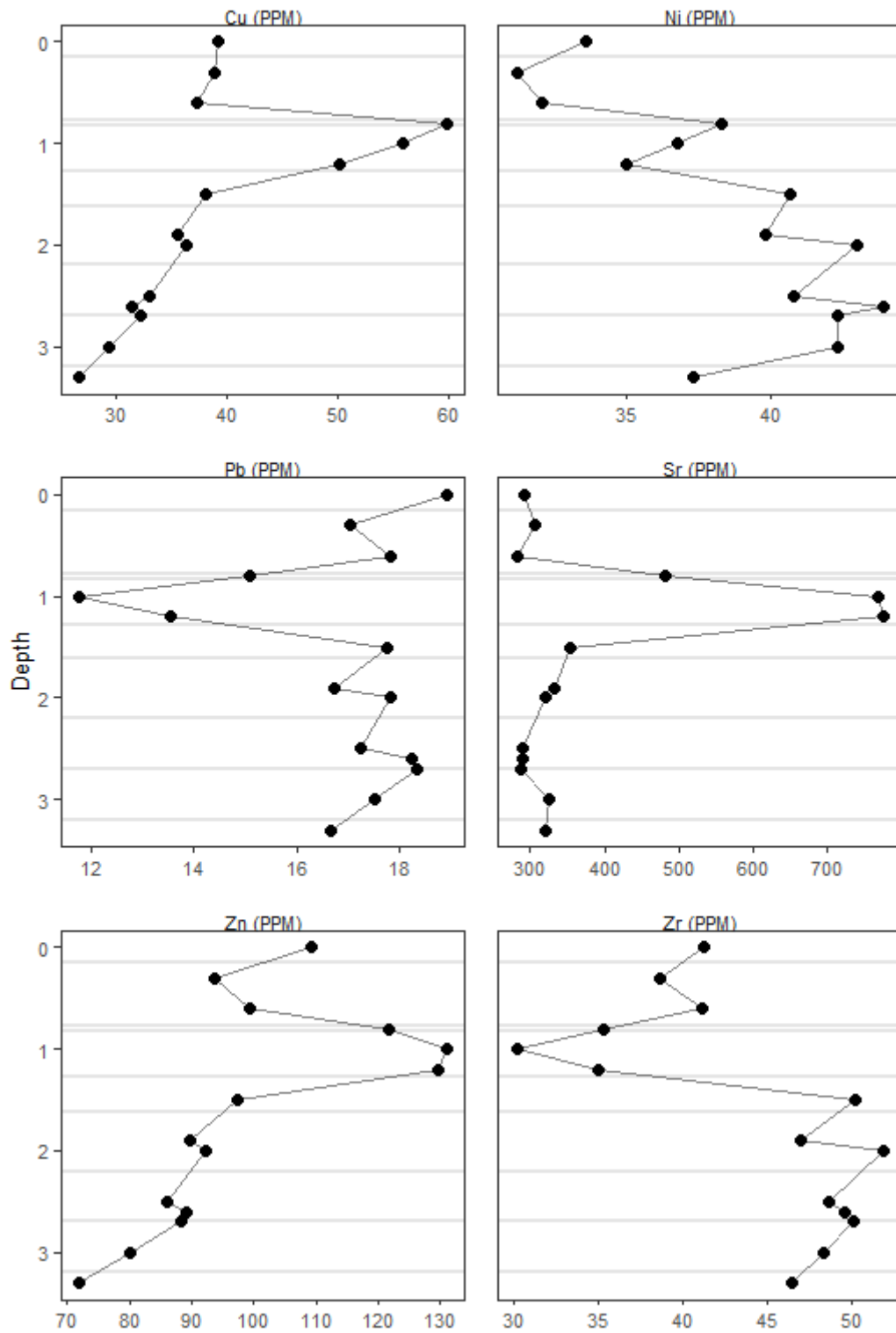
**Figure S 2** Petrographic composition of sediments at Obishir-5

## S4. Geochemical profiles, indices and analyses

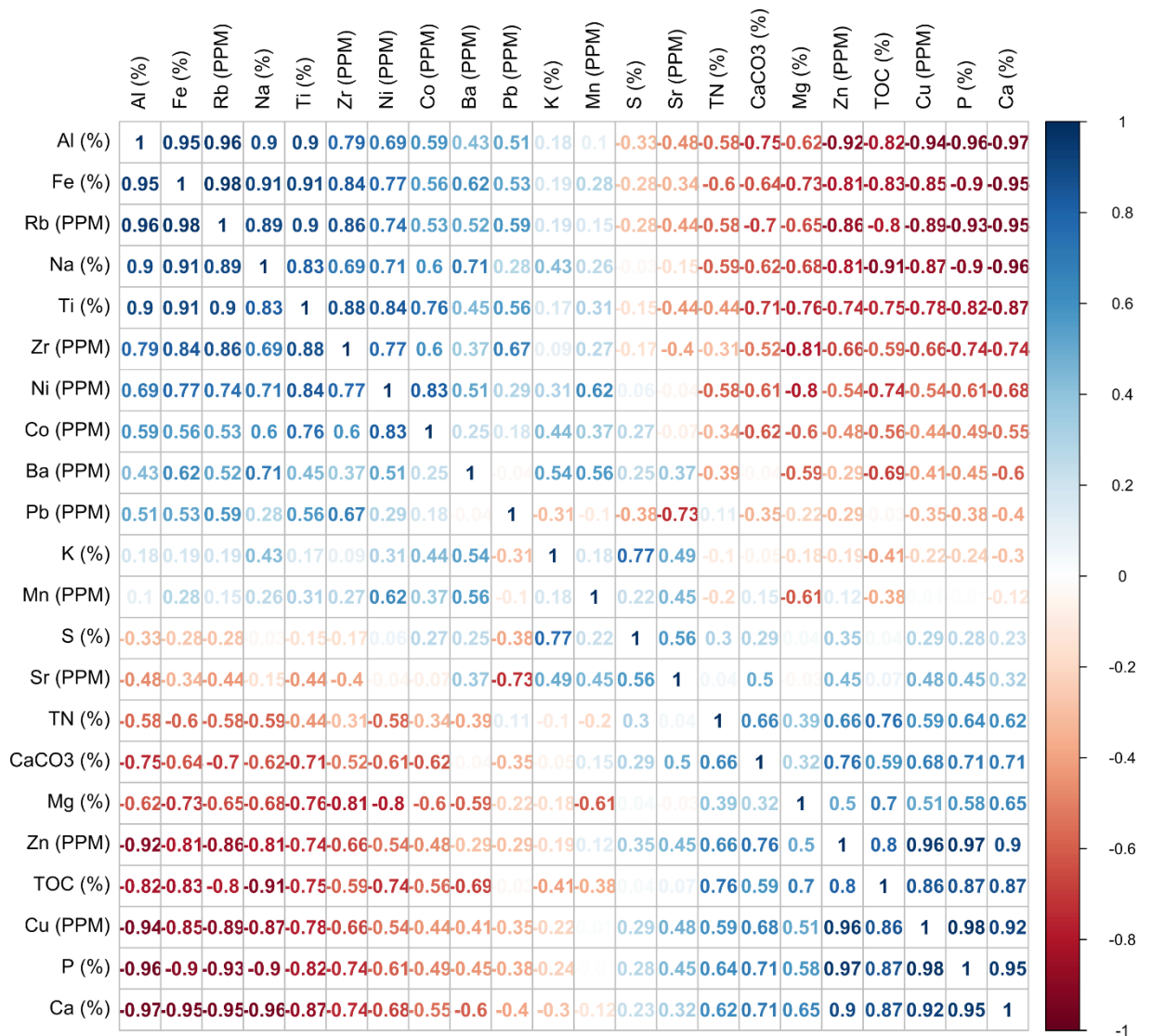
CaCO<sub>3</sub> content ranged between 10 and 35% (**Figure S 3**). Organic matter content is expressed as TOC (Irb. %) and TN (Irb. %). TOC (Irb. %) content was between 3.66 and 7.43, whereas TN (Irb. %) is 0.03 and 0.26 (**Figure S 3**). ICP-MS analyses reported major elements including Ca, Al, Mg, Fe, K, Na, P and Ti (see **Figure S 3**). Trace elements are illustrated in **Figure S 4**. In summary, two main groups of elements with similar trends are identified: the Al-group (Al, Na, Fe, Ni, Rb, and Ti) and Ca-group (Ca, Mg, P, Cu, Zn, Sr). The Spearman correlation matrix confirmed this pattern (see **Figure S 5**). Regarding the indices (see **Figure S 6**), we calculated them based on the Spearman correlation matrix. Correlation matrix statistical significance is given in **Table S 4** Correlation matrix p-values. To test different deposition modes associated with distinct geochemical groups, we utilized the following ratios: Ca/Al, Ca/Na, Ca/Ti and Ca-related group to Al-related group (Ca+Mg+P+Cu+Zn+Sr/Al+Na+Fe+Ni+Rb+Ti). For assessing silicate weathering, we used the Na/Al, Al<sub>2</sub>O<sub>3</sub>/TiO<sub>2</sub>, K<sub>2</sub>O/Na<sub>2</sub>O, and Chemical Proxy Alteration (CPA) indices. CPA is a molar ratio  $Al_2O_3/(Al_2O_3 + Na_2O) \times 100$ . Al<sub>2</sub>O<sub>3</sub>/TiO<sub>2</sub>, K<sub>2</sub>O/Na<sub>2</sub>O and CPA were considered more reliable in our case, as they are less influenced by the dynamics of CaCO<sub>3</sub> within the profile (Buggle *et al.*, 2011; Krajcarz *et al.*, 2016; Brancaloni *et al.*, 2022). To assess weathering within the Ca-related group, we used the Ca/Mg.



**Figure S 3** Major elements measured with IC-PMS. TOC, TN and major elements from elemental analyses. CaCO<sub>3</sub> from HCl pre-treatment. Other elements' concentrations were retrieved with ICPMS (< 1mm). Depth is in m below the ground surface.



*Figure S 4 Trace elements measured with ICP-MS analysis. Depth is in m below the ground surface.*

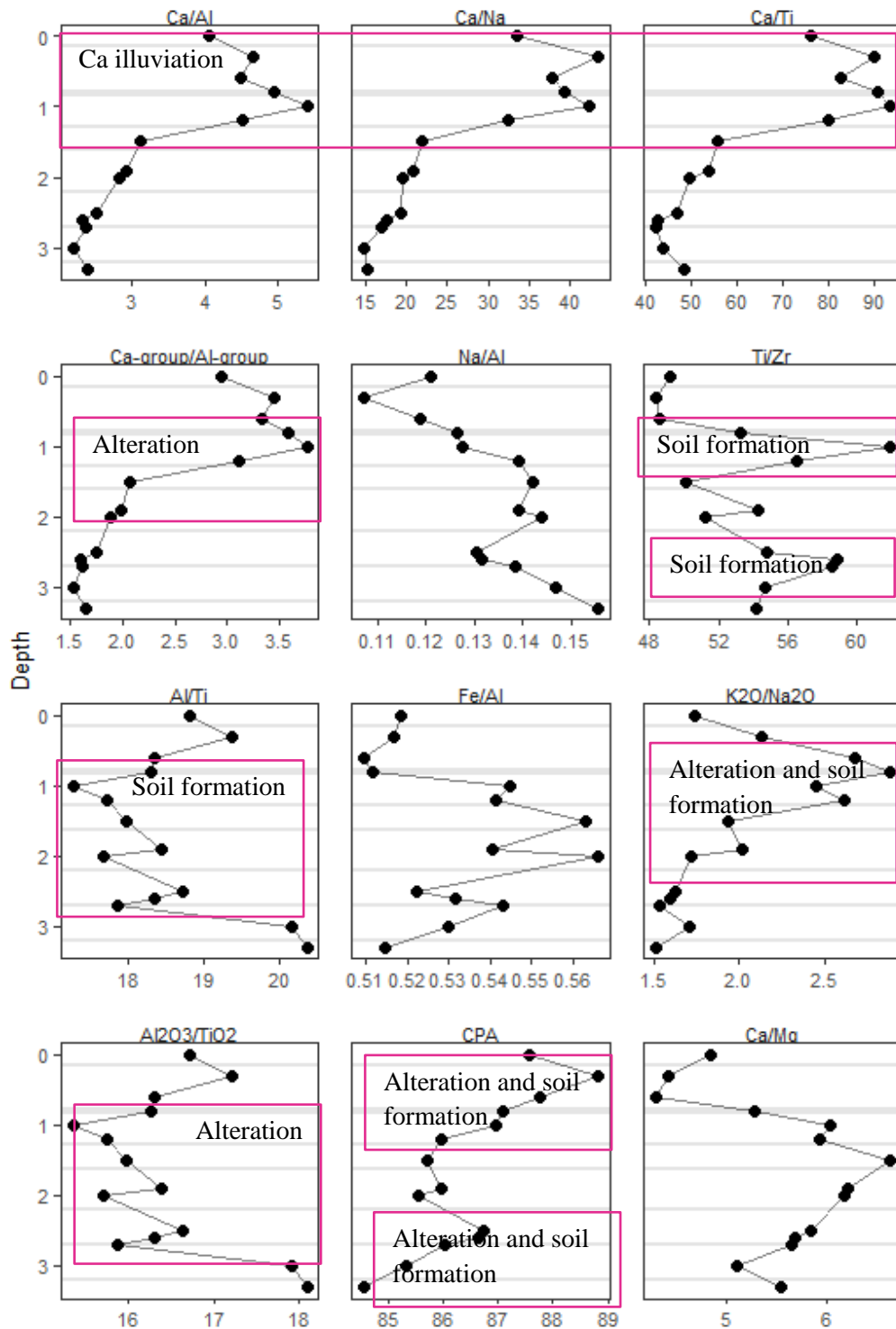


**Figure S 5** Correlation matrix. Correlation matrix of elements with the Spearman method (Friendly, 2002). The table shows correlation coefficients between variables. Each cell in the table shows the correlation between two variables. The correlation can be positive or negative, there is perfect positive correlation when the value is 1 and perfect negative correlation when the value in the cell is -1. Here we ranked the data using "FPC" for the first principal component order.



Table S 4 Correlation matrix p-values

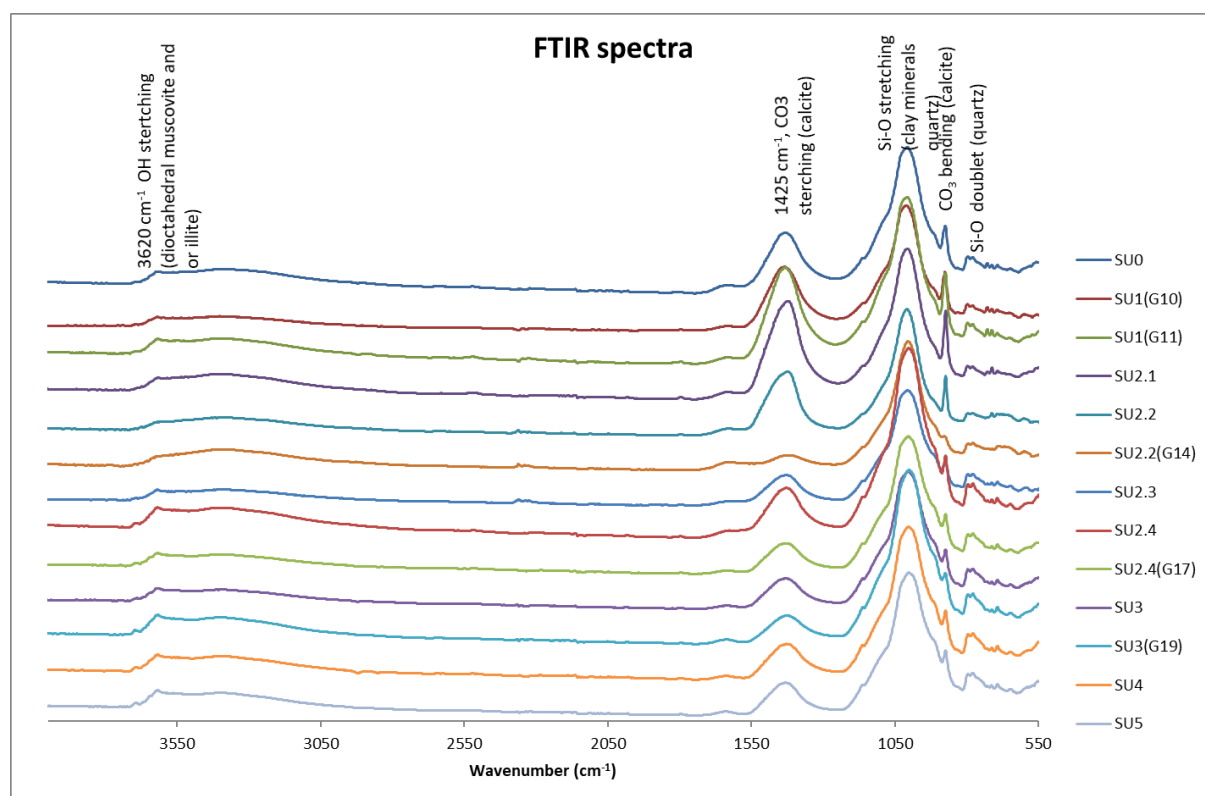
	Cu (PPM)	Pb (PPM)	Zn (PPM)	Ni (PPM)	Co (PPM)	Mn (PPM)	Fe (%)	Sr (PPM)	Ca (%)	P (%)	Mg (%)	Ba (PPM)	Ti (%)	Al (%)	Na (%)	K (%)	Zr (PPM)	S (%)	Rb (PPM)	CaCO3 (%)	TOC (%)	TN (%)
Cu (PPM)	NA	<b>0.0018</b>	<b>0.0000</b>	0.2270	0.2230	0.7089	<b>0.0006</b>	<b>0.0013</b>	<b>0.0003</b>	<b>0.0000</b>	0.1048	0.4167	<b>0.0021</b>	<b>0.0002</b>	<b>0.0015</b>	0.8488	<b>0.0002</b>	0.0374	<b>0.0001</b>	0.0655	0.0173	0.7184
Pb (PPM)	<b>0.0018</b>	NA	<b>0.0040</b>	0.4121	0.1762	0.2527	0.0359	<b>0.0000</b>	0.0419	<b>0.0007</b>	0.6184	0.5967	0.0378	0.0249	0.1149	0.6390	<b>0.0009</b>	0.1200	0.0073	0.0168	0.5439	0.4270
Zn (PPM)	<b>0.0000</b>	<b>0.0040</b>	NA	0.1554	0.0873	0.5986	<b>0.0007</b>	<b>0.0003</b>	<b>0.0005</b>	<b>0.0000</b>	0.1165	0.7864	<b>0.0030</b>	<b>0.0001</b>	<b>0.0011</b>	0.6350	<b>0.0002</b>	0.0830	<b>0.0001</b>	0.0073	0.0155	0.3857
Ni (PPM)	0.2270	0.4121	0.1554	NA	<b>0.0000</b>	<b>0.0019</b>	<b>0.0003</b>	0.4521	<b>0.0018</b>	0.0922	<b>0.0001</b>	0.0637	<b>0.0001</b>	<b>0.0013</b>	<b>0.0011</b>	0.0771	0.0061	0.8428	<b>0.0014</b>	0.1596	<b>0.0023</b>	0.0851
Co (PPM)	0.2230	0.1762	0.0873	<b>0.0000</b>	NA	0.0613	<b>0.0015</b>	0.1457	<b>0.0046</b>	0.0587	<b>0.0027</b>	0.3286	<b>0.0006</b>	<b>0.0023</b>	<b>0.0039</b>	0.0399	<b>0.0040</b>	0.7142	<b>0.0026</b>	0.0504	0.0164	0.2605
Mn (PPM)	0.7089	0.2527	0.5986	<b>0.0019</b>	0.0613	NA	0.1260	0.1534	0.1929	0.8567	<b>0.0018</b>	0.0076	0.0829	0.2379	0.1165	0.1140	0.5447	0.6222	0.3249	0.6228	0.0756	0.2584
Fe (%)	<b>0.0006</b>	0.0359	<b>0.0007</b>	<b>0.0003</b>	<b>0.0015</b>	0.1260	NA	0.0409	<b>0.0000</b>	<b>0.0001</b>	<b>0.0002</b>	0.0603	<b>0.0000</b>	<b>0.0000</b>	<b>0.0000</b>	0.2003	<b>0.0000</b>	0.2177	<b>0.0000</b>	0.0680	<b>0.0000</b>	0.1780
Sr (PPM)	<b>0.0013</b>	<b>0.0000</b>	<b>0.0003</b>	0.4521	0.1457	0.1534	0.0409	NA	0.0485	<b>0.0005</b>	0.7182	0.2611	0.0485	0.0208	0.1087	0.6599	<b>0.0017</b>	0.1053	0.0074	<b>0.0007</b>	0.4835	0.7054
Ca (%)	<b>0.0003</b>	0.0419	<b>0.0005</b>	<b>0.0018</b>	<b>0.0046</b>	0.1929	<b>0.0000</b>	0.0485	NA	<b>0.0000</b>	<b>0.0003</b>	0.0453	<b>0.0000</b>	<b>0.0000</b>	<b>0.0000</b>	0.1969	<b>0.0000</b>	0.2072	<b>0.0000</b>	0.0823	<b>0.0000</b>	0.1665
P (%)	<b>0.0000</b>	<b>0.0007</b>	<b>0.0000</b>	0.0922	0.0587	0.8567	<b>0.0001</b>	<b>0.0005</b>	<b>0.0000</b>	NA	0.0519	0.3664	<b>0.0003</b>	<b>0.0000</b>	<b>0.0003</b>	0.5465	<b>0.0000</b>	0.1064	<b>0.0000</b>	0.0398	0.0080	0.6383
Mg (%)	0.1048	0.6184	0.1165	<b>0.0001</b>	<b>0.0027</b>	<b>0.0018</b>	<b>0.0002</b>	0.7182	<b>0.0003</b>	0.0519	NA	<b>0.0022</b>	<b>0.0002</b>	<b>0.0009</b>	<b>0.0001</b>	0.0739	0.0073	0.7427	<b>0.0019</b>	0.5457	<b>0.0002</b>	0.1499
Ba (PPM)	0.4167	0.5967	0.7864	0.0637	0.3286	0.0076	0.0603	0.2611	0.0453	0.3664	<b>0.0022</b>	NA	0.0719	0.1167	0.0249	0.0393	0.2660	0.6628	0.1605	0.1520	0.0080	0.3664
Ti (%)	<b>0.0021</b>	0.0378	<b>0.0030</b>	<b>0.0001</b>	<b>0.0006</b>	0.0829	<b>0.0000</b>	0.0485	<b>0.0000</b>	<b>0.0003</b>	<b>0.0002</b>	0.0719	NA	<b>0.0000</b>	<b>0.0000</b>	0.2379	<b>0.0000</b>	0.2427	<b>0.0000</b>	0.0715	<b>0.0001</b>	0.2212
Al (%)	<b>0.0002</b>	0.0249	<b>0.0001</b>	<b>0.0013</b>	<b>0.0023</b>	0.2379	<b>0.0000</b>	0.0208	<b>0.0000</b>	<b>0.0000</b>	<b>0.0009</b>	0.1167	<b>0.0000</b>	NA	<b>0.0000</b>	0.2440	<b>0.0000</b>	0.1629	<b>0.0000</b>	0.0337	<b>0.0000</b>	0.1569
Na (%)	<b>0.0015</b>	0.1149	<b>0.0011</b>	<b>0.0011</b>	<b>0.0039</b>	0.1165	<b>0.0000</b>	0.1087	<b>0.0000</b>	<b>0.0003</b>	<b>0.0001</b>	0.0249	<b>0.0000</b>	<b>0.0000</b>	NA	0.0727	<b>0.0002</b>	0.3976	<b>0.0000</b>	0.1158	<b>0.0000</b>	0.1330
K (%)	0.8488	0.6390	0.6350	0.0771	0.0399	0.1140	0.2003	0.6599	0.1969	0.5465	0.0739	0.0393	0.2379	0.2440	0.0727	NA	0.3621	0.0059	0.2747	0.8384	0.0465	0.6074
Zr (PPM)	<b>0.0002</b>	<b>0.0009</b>	<b>0.0002</b>	0.0061	<b>0.0040</b>	0.5447	<b>0.0000</b>	<b>0.0017</b>	<b>0.0000</b>	<b>0.0000</b>	0.0073	0.2660	<b>0.0000</b>	<b>0.0000</b>	<b>0.0002</b>	0.3621	NA	0.2596	<b>0.0000</b>	0.0318	0.0074	0.6789
S (%)	0.0374	0.1200	0.0830	0.8428	0.7142	0.6222	0.2177	0.1053	0.2072	0.1064	0.7427	0.6628	0.2427	0.1629	0.3976	0.0059	0.2596	NA	0.1796	0.1715	0.6320	0.3740
Rb (PPM)	<b>0.0001</b>	0.0073	<b>0.0001</b>	<b>0.0014</b>	<b>0.0026</b>	0.3249	<b>0.0000</b>	0.0074	<b>0.0000</b>	<b>0.0000</b>	<b>0.0019</b>	0.1605	<b>0.0000</b>	<b>0.0000</b>	<b>0.0000</b>	0.2747	<b>0.0000</b>	0.1796	NA	0.0260	<b>0.0004</b>	0.2842
CaCO3 (%)	0.0655	0.0168	0.0073	0.1596	0.0504	0.6228	0.0680	<b>0.0007</b>	0.0823	0.0398	0.5457	0.1520	0.0715	0.0337	0.1158	0.8384	0.0318	0.1715	0.0260	NA	0.3736	0.4836
TOC (%)	0.0173	0.5439	0.0155	<b>0.0023</b>	0.0164	0.0756	<b>0.0000</b>	0.4835	<b>0.0000</b>	0.0080	<b>0.0002</b>	0.0080	<b>0.0001</b>	<b>0.0000</b>	<b>0.0000</b>	0.0465	0.0074	0.6320	<b>0.0004</b>	0.3736	NA	0.0305
TN (%)	0.7184	0.4270	0.3857	0.0851	0.2605	0.2584	0.1780	0.7054	0.1665	0.6383	0.1499	0.3664	0.2212	0.1569	0.1330	0.6074	0.6789	0.3740	0.2842	0.4836	0.0305	NA



**Figure S 6** Ratios and indices. *Ti/Zr*, *Al/Ti* and *Fe/Al* were estimated to test changes in fine source, *Ti* is more abundant in clays and less in aeolian dust, therefore connected with soil formation. *Ca/Ti* should reflect carbonate leaching. *Na/Al* increases with increasing alteration. *Al<sub>2</sub>O<sub>3</sub>/TiO<sub>2</sub>* ratio decreases with increasing alteration, whereas *K<sub>2</sub>O/Na<sub>2</sub>O* and *CPA* increase with increasing alteration and pedogenesis.

## S5. Fourier Infrared spectroscopy

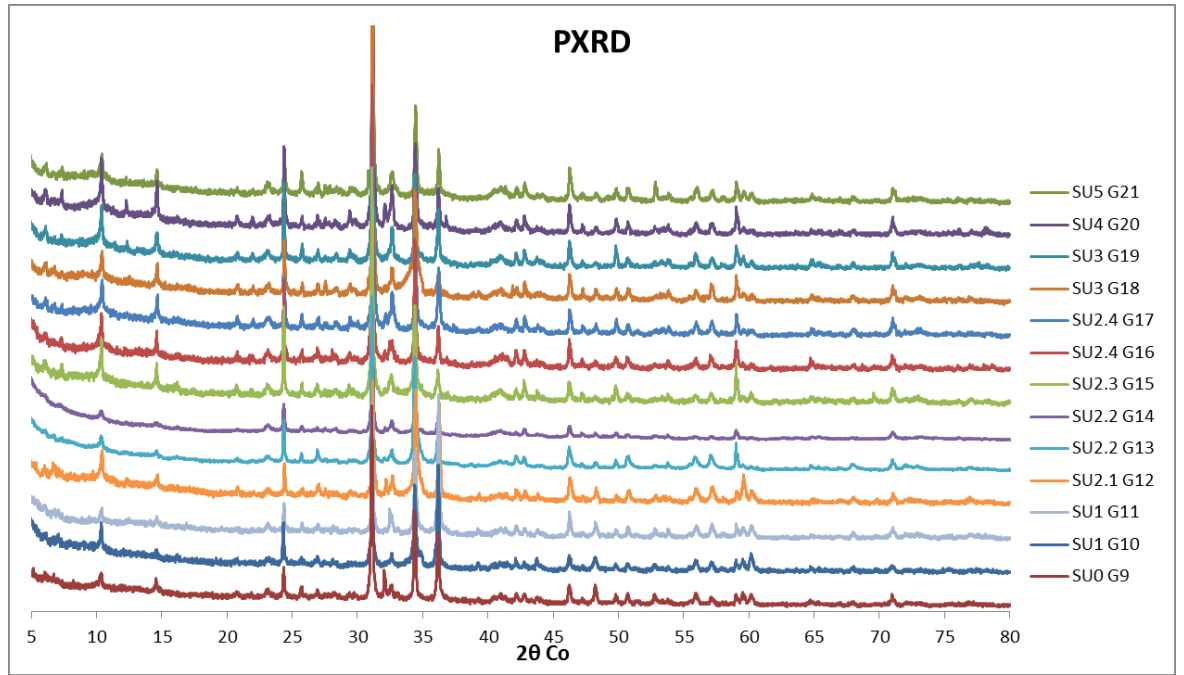
FTIR measurements were performed using a Nicolet 6700 spectrometer with a DTGS KBr detector (Thermo Scientific, USA). The measurements were performed using an attenuated total reflectance (ATR) technique. FTIR spectra were collected in 4000 – 550  $\text{cm}^{-1}$  range at a resolution of 6  $\text{cm}^{-1}$  as 100-scan averages. The samples were gently ground in agate mortar. For ATR technique about 5 mg of powdered sample was placed on diamond crystal mold and pressed to create a thin film. Results are illustrated in **Figure S 7**. Raw data are stored with the corresponding author.



*Figure S 7 FTIR spectra for chemical compounds analysis obtained for sediments collected along profile after HCl pretreatment, sampling location is given in the main text Fig.2d*

## S6. Powder X-ray diffraction

The samples were analyzed using powder X-ray diffraction (PXRD). All specimens were dispersed and gently pressed on a silicon low-background holder using a random preparation. A Bruker D8 advanced series II diffractometer (Bruker, Karlsruhe, Germany) equipped with LPSD VANTEC-1 detector operating in the Bragg-Brentano geometry with a CoK $\alpha$  X-ray tube (35 kV, 40 mA) was used. PXRD patterns were collected in the 0-80  $^{\circ}2\theta$  range with counting step 0.014 $^{\circ}$  and counting time 5 s/step. For qualitative analysis EVA software (ver. 4.2.0.31), the Crystallography Open Database (COD), the ICDD's Powder Diffraction File (PDF) were used. Spectra are given in **Figure S 8**. For quantitative analysis PXRD data was analyzed with Profex/BGMN 3.14.2 software package with structural models based on ICSD database. This program allows to estimate the weight fractions of crystalline phases based Rietveld refinement procedure (Doebelin and Kleeberg, 2015). Detection limit for quantitative analysis is  $\sim 2\%$ . Results are given in **Table S 5**. Raw data are stored with the corresponding author.



**Figure S 8** PXRD patterns for mineralogical analysis performed for sediments collected along profile, sampling location is given in the main text in Fig.2d.

**Table S 5** Quantitative analysis based on PXRD results

Depth (m)	Unit	Label	Quartz (%)	Calcite (%)	Dolomite (%)	Illite (%)	Albite (%)	Chlorite (%)	Muscovite (%)	Titanite (%)	Hornblende (%)
0	SU0	G9	26.5	15.3	21.3	17.1	9.6	3.1 <sup>a</sup>	7		
0.3	SU1	G10	19	19.5	24.9	20.2	6.9	3.1 <sup>a</sup>	6.3		
0.6	SU1	G11	13.3	28.7	26.8	6.3	7.8	4.1 <sup>a</sup>	13.1		
0.8	SU2.1	G12	13.4	28.9	21.7	18.7	9.5	2.8 <sup>a</sup>	4.9		
1	SU2.2	G13	22.9	31.2	8.9	14.2	7.3	3.4 <sup>a</sup>	10.2	2.0 <sup>a</sup>	
1.2	SU2.2	G14	26.7	11.4	6.1	30	10.2	3.6 <sup>a</sup>	11.9		
1.5	SU2.3	G15	27.8	15.4	7.2	18.5	11.1	7.4	8.9	1.8 <sup>b</sup>	1.9 <sup>b</sup>
1.9	SU2.4	G16	24.6	14.1	7.1	31.3	8.7	5.2	6.7	2.5 <sup>a</sup>	
2	SU2.4	G17	25	15.4	12.45	17.5	12.3	4.6	10.4	2.3 <sup>a</sup>	
2.5	SU3	G18	24.3	16.6	7.45	28.3	9.1	4.8	8.5	1.0 <sup>b</sup>	
2.6	SU3	G19	26.9	13.35	9.3	21.9	11.6	5.3	10.3		1.2 <sup>b</sup>
3	SU4	G20	26.9	15.2	7.9	12.9	12.1	7.7	10.9	3.9 <sup>a</sup>	2.5 <sup>a</sup>
3.3	SU5	G21	23.3	14.9	9.2	30.6	11.3	3.6	5.7		1.5 <sup>b</sup>

Notes: <sup>a</sup> – close to the limit of quantification (LOQ), <sup>b</sup> – close to the limit of detection (LOD).

## S7. Micromorphology

## S7.1 Sampling

The samples were collected with plastic boxes (Kubiena boxes), or carved with a knife and secure with plaster. All samples were collected orthogonally oriented to the ground surface.

## S7.2 Thin section production

The thin sections were prepared by Ewa Deput in the sample preparation laboratory at the Institute of Geological Sciences (Polish Academy of Sciences – Warsaw). In the laboratory, the monoliths were air-dried for two weeks, carefully rinsed with ethanol, air-dried once more, and then impregnated with Araldite 2020, a two-component epoxy resin. The impregnation process was applied twice: first from one selected flat side, and once cured, from the opposite side. To allow the epoxy to slowly infiltrate the sediment, the samples were left at room temperature and under normal air pressure for 48 hours for each impregnation. Vacuum setting was avoided as it had a tendency to cause cracking during testing. To assess the quality of impregnation, several millimeter-thick slabs were trimmed from both sides of the monolith. If the inner part had not fully impregnated visually, the impregnation procedure was repeated. Once properly impregnated, the monoliths were cut into approximately 45x80 mm slabs with a thickness of 5 mm, using a circular saw equipped with diamond-coated blades. The selected slabs were then polished, affixed onto 45x80 mm basal glass slides using Araldite 2020, and further polished with progressively finer polishing pastes to create 30 µm thin sections..

## S7.3 Microscopy acquisition details

*Plain and crossed polarized light:* Observations were carried out at Institute of Geological Sciences in Warsaw–Polish Academy of Sciences–utilizing a Microscope Nikon ECLIPSELV100, objectives 2.5-100, camera Nikon, image acquisition and processing software NIS-Elements.

*Automated scans:* Scans were acquired at University of Warsaw – Department of Geology utilizing a Microscope Nikon ECLIPSELV100, automated scan “ProScanIII Prior”, camera Nikon DS-Fi1, the acquisition software was NIS-Elements BR v4.20.01, with acquisition parameters as follows: Objective 2x, Overlap 5%, Focus surface mode, acquisition time ≈ 10min.

Name file: year\_site\_objective\_Exposure\_gain\_sample\_plain/cross polarized light\_author

*Epifluorescence light:* Observations were carried out at the Institute of Geological Sciences in Cracow–Polish Academy of Sciences–utilizing Zeiss Axio Observer Z.1 fluorescence microscope with four different filter sets for fluorescent imaging as reported in [Table S 6](#)

*Table S 6 Fluorescence microscope acquisition information*

Channel	Illumination Method	Filter set	Filter Ex. Wavelength	Beam Splitter	Filter Em. Wavelength	Light Source	Exposure Time	Camera
C1	Epifluorescence	65 (HE)	BP 475/30 (HE)	FT 495 (HE)	BP 550/100 (HE)	HXP 120 V	850 ms/400 ms*	Axiocam 503
C2	Epifluorescence	50	BP 640/30	FT 660	BP 690/50	HXP 120 V	9000 ms	Axiocam 503
C3	Epifluorescence	63 (HE)	BP 572/25 (HE)	FT 590 (HE)	BP 629/62 (HE)	HXP 120 V	1350 ms	Axiocam 503
C4	Epifluorescence	43	BP 545/25	FT 570	BP 605/70	HXP 120 V	600 ms	Axiocam 503
C5	Transmitted light	NA	NA	NA	NA	TL Halogen Lamp	variable	Axiocam 503

*SEM-EDS*: Observations were carried out at the Faculty of Geology of the University of Warsaw. Specifics are detailed in **Table S 7** SEM-EDS specifics.

*Table S 7 SEM-EDS specifics*

<b>Features</b>	<b>Zeiss Sigma VP</b>	<b>Zeiss Auriga</b>
EDS	<b>Brucker model XFlash 6I10</b> XFlash 6I10 detector type is silicon drift detector with internal FET (iFet SDD), active area 5 mm <sup>2</sup> , Max count rate 10 <sup>6</sup> cps, energy resolution >= 123 eV	
Resolution	1.3 nm at 20 kV	1.2 nm at 15 kV
Accelerated voltage	0.1 to 30kV	0.1 to 30kV
Magnification	12x to 1000000x	12x to 1000000x
Motorized stage	5 Axis X=125 mm, Y=125 mm	6 Axis X=100 mm, Y=100 mm
Detectors	SE, InLens (annular SE detector), VPSE (variable pressure secondary electron detector), BSE	SE, InLens (annular SE detector), BSE, STEM (scanning transmission electron microscope detector), EBSD detector
FIB (Focused ion beam imaging) column	resolution 5 nm at 30 kV, accelerated voltage: 1 to 30kV, magnification: 30x to 500000x	
Mode	Low vacuum mode	SEM-Cryo mode for observations of the 'wet' specimens, for example biological materials
Types of sample	Any type of dry and conductive sample; also in thin sections	
Sample preparation	carbon or metal coated in high vacuum mode; non-conductive sample in Zeiss Sigma low vacuum mode; 'Wet' samples prepared in cryo mode and metal coated	

## S7.4 Micromorphological features and General description of main micro-components

Table S 8 Summary of micromorphological features and components characterizing the sediments at the Obishir-5

			Sediments' fabric descriptive features						Selected Components												
Samples	SU	MF	Ground-mass	Texture	b-fabric	Porosity	Micro-structure (from optical microscope observation)	Pedality	Igneous rock fragment	Chert	Pottery	Aggregates	Dungy aggregates	Herbivore dung with fecal spherulites	Fecal spherulites in groundmass	Phytoliths	Red rounded aggregates	Charcoals and charred material	Ashy nodules	Bones	Burnt bones
MML1	1	1	Grayish brown and dark brown	Loamy fine sand with pebbles		Planar voids, Vughs, Vesicles, Channels, Chambers	Microlaminated horizon, rest of thin section very complex due to bioturbation	Very complex, very difficult to classify (see main text for some examples)	++	NA	+	+++	+++	NA	NA	+++ elongated, horiz. aligned	++	+++	NA	+	NA
MML3.1	2.2	2	Yellowish brown	Loam and fine sand with pebbles		Packing Vughs, Channels, Vesicles, Chambers	Granular	Crumbs and granules commonly fine but also coarse, more or less rounded, weakly developed and separated	+	NA	1 suspected	+++	+++	++	++	+ inside dung fragments	++	+++	NA	++	+
MML3.2	2.3	2	Yellowish brown	Loam and fine sand with pebbles		Packing, Vesicles, Channels, Planes	Granular	Crumbs and granules commonly fine but also few coarse, more or less rounded, developed and separated	NA	1	NA	+++	+++	+++ calcined	++	+ inside dung fragments	++	+++	+	++	1
MM1541	2.4	2	Yellowish grayish brown	Loam with pebbles		Packing, Vughs, Channels	Granular and intergrain, loose granular	Crumbs and granules, mainly coarse, developed and highly separated	NA	NA; 1	NA	+++	++	+	NA	++ inside and outside dung fragments	NA	1	+	+	NA
MM1542; MM2101	3	2	Yellowish grayish brown	Silty fine sand with pebbles		Packing, Vesicles, Channels, Few chambers	Granular*, intergrain	Crumbs and granules, Granules are developed and weakly separated	NA	NA	NA	+++; ++	++; NA	NA	NA	1 rounded; NA	+	+++; +	++; NA	++; 1 rodent molar	+
MM1543	4	3	Yellowish orange brown	Silt and sand with pebbles		Vughs and rounded chambers	Compact micro-granular**, locally vughy	Crumbs and granules, Weakly developed and weakly separated	NA	NA	NA	+	NA	NA	NA	NA	NA	1	NA	+	NA
MML5	4	3	Yellowish light brown	Clayey silt and fine sand with pebbles		Channels, Planes, Vesicles, Vughs	Compact micro-granular, locally vesicular, micro-granular, vughy	Crumbs and granules, and locally subangular blocky peds; Weakly separated	NA	NA	NA	+	NA	NA	NA	NA	NA	1	NA	1 assoc. with void	NA

			Sediments' fabric descriptive features						Selected Components													
Samples	SU	MF	Ground-mass	Texture	b-fabric	Porosity	Micro-structure (from optical microscope observation)	Pedality	Igneous rock fragment	Chert	Pottery	Aggregates	Dungy aggregates	Herbivore dung with fecal spherulites	Fecal spherulites in groundmass	Phytoliths	Red rounded aggregates	Charcoals and charred material	Ashy nodules	Bones	Burnt bones	
MM1544	5	3	Yellowish light brown towards grey	Clayey silt and fine sand with randomly dispersed coarse grains		Channels, Vesicles, Vughs	Compact micro-granular, locally vesicular, massive, vughy	Granules and crumbs, Weakly separated, weakly developed pedality	NA	NA	NA	+	NA	NA	NA	NA	NA	NA	NA	NA	NA	NA
MM1545	5	3	Yellowish light brown	Clayey silt with randomly dispersed coarse grains		Channels, Vesicles, Vughs	Compact micro-granular, locally vesicular, vughy	Granules and crumbs, Weakly separated, weakly developed pedality	NA	NA	NA	+	NA	NA	NA	NA	NA	NA	NA	1?	NA	NA

Key: NA not noted; 1 single occurrence; + few; ++ common; +++ dominant

Samples	SU	Microfacies	Selected post-depositional features and components													
			Authigenic minerals (low-magnesium carbonates)	Apatite nodules	Phosphatic impregnation	Shell fragments	Rodent molar	Invertebrate	Earthworm biospheroid	Earthworm organo-mineral excrement	Calcitic impregnation	Compacted micritic calcite impregnating the groundmass	Calcitic nodules and concretions	Calcified root cells and micritic granular aggregates	Dusty infillings	Redeposited clay nodules limpic and laminated
MML1	1	1	+	NA	NA	+	NA	NA	NA	++	+	+++	+++	NA	NA	+
MML3.1	2.2	2	NA	++	NA	++	NA	NA	NA	++	++	NA	+++	NA	NA	NA
MML3.2	2.3	2	NA	NA	NA	+	NA	<b>1</b>	NA	++	++	NA	+++	NA	NA	NA
MM1541	2.4	2	NA	NA	NA	1	NA	NA	NA	++		NA	+++	NA	NA	+
MM1542; MM2101	3	2	++; NA	NA	NA	++	NA; <b>1</b>	NA	NA	++	++;	NA	+++	NA	NA	++ laminated
MM1543	4	3	+	NA	NA	+	NA	NA	<b>1</b>	++	+	NA	+++	NA	NA	++
MML5	4	3	NA	NA	++	NA	NA	NA	suspected	++	+	NA	+++	+	NA	+
MM1544	5	3	1	NA	++	NA	NA	NA	NA	++	+	NA	+++	++	+	1 laminated
MM1545	5	3	NA	NA	+	NA	NA	NA	NA	++	+	NA	+++		NA	+

Key: NA not noted; 1 single occurrence; + few; ++ common; +++ dominant



**Table S 9 Description of main components**

<b>Mineral components</b>	<b>Description</b>	
Carbonate rock fragments	From si to fp, randomly distributed, mostly angular and occasionally rounded, colour is gray, fossiliferous, crystalline, micro-crystalline. Travertine is present. When fossiliferous, grainstone and/or packstone with poorly sorted skeletal grains such as echinoderms and foraminifera (fusulinids, beresella), sponges (stromatoporoids) which are typical for shelf and reef carbonates (Ordovician to Late Devonian limestones). Affected by 2 <sup>nd</sup> CaCO <sub>3</sub> coatings	
Shale fragments	From si to fp, randomly distributed, platy, splinters elongated fragments. At PPL, it appeared dark brown, foliated with mineralization, striated fabric. Affected by 2 <sup>nd</sup> CaCO <sub>3</sub> coatings	
Igneous rock fragments	Ms to cs, angular and subangular, weathered with chlorite replacement, made of quartz and feldspar	
Fine sand and silt	Common calcite, quartz, k-feld grains, also clay minerals (most common chlorite), Fe and Mn oxides, mica splinters. Calcite, quartz and k-feld were observed in strict association. Clay minerals were mainly randomly distributed, columnar or rod-like, orange or yellow in ppl and high interference colors in xpl. Fine-sand-sized charred material and organic matter components were also observed (MM1541, MML3.2, MML3.1, and MML1).	
Authigenic minerals	Fs, associated with ash, spherulitic, they occur alone of clustered, yellowish or light gray, radial pattern, high relief at ppl. At xpl, extinction crosses. They occurred locally in cluster or isolated in samples 1543, 1542, and L1.	
<b>Clay and Mn/Fe components</b>		
Coatings	Mainly in the form of pedorelict, such as fragments of si and ms limpid non laminated but also well laminated clay papules. In the lowermost part of the section, clayey dense incomplete infilling such as dusty coating in channel. Common Mn/Fe cappings on top of limestone grains.	
Nodules	Few typic and dendritic Fe/Mn nodules and limpic clayey nodules, more common angular oxides	
<b>Calcitic components</b>		
Coatings	External and internal hypocoatings associated with compacted walls. Infillings are dense and incomplete as calcified root cells and micritic granular aggregates Common pendent and rinds which are fluorescent under epifluorescence light	Pendent and rinds found in all samples
Nodules	Fp to ms typic (?) and/or concentric nodules made of micrite and sparite, autofluorescent	nice example in 3.2
<b>Other components</b>		
Bone fragments	Mostly angular, and splinter-like representing cortical bones, but rounded spongy specimens also occurred, from fine-sand- to coarse-sand-sized. The color varied from white, passing through yellowish to reddish orange at PPL. Bones were black and/or represented by light gray interference colors of the apatite fibers at XPL. The haversian channel were still visible in some specimens. A rodent molar was observed. Bones were commonly cracked, with corroded and/or disintegrated edges, some specimen with internal vesicles, and signs of weathering and recrystallization. Both rounded and broken bones were found together. Macrofaunal remains recovered were mainly attributed to domesticated sheep and goats (Taylor <i>et al.</i> , 2021).	Nice examples in sample 3.2
Woody charcoal fragments	Mostly woody, elongated, prismatic and, sub-rounded. Some of them resulted chunked, reduced in smaller particles or in-situ cracked or with altered edges. In some specimens the cell structure was visible. Charcoals were also characterized by vesicles and some were reddened. They possibly represented broad leave trees and shrub (Moskal pers. comm.). Opaque in PPL and XPL.	Representative examples in 1542, 3.1 and L1
Shell fragments	Associated with charcoals and bones, the identification followed (Canti, 2017), and for a detailed taxonomic description see (Osipova <i>et al.</i> , 2020). Lack of intact shells.	
Char	Charred material was opaque in PPL and XPL, its color varied from black to red, mainly amorphous characterized by as well as cracks and internal vesicles sometimes filled with oxalate. In a few cases the internal structure could be seen which allowed to attribute the material to wood.	
Chert	Coarse piece of debitage made of flint, surface was altered.	

Pottery	Red compacted clayey material, one suspected specimen was characterized by a single small phytolith
Phytoliths	Few observed throughout the sequence, more abundant in SU1. In SU2 were found in voids, cluster of 4-5 elements of non-articulated dendritic, rounded with oval cells and bluish pinkish walls. In SU1 very elongated specimens also were observed. Observed inside dung pellets.
Biospheroids	Rarely observed, associated with compacted soil and biovoids, autofluorescent, calcite minerals radially oriented
Dung material	Dung pellets are detailed in the main text. The specimens that carried fecal spherulites they were attributed to herbivores, especially to ungulates such as sheep and goats.
Ash	In sub-rounded rounded aggregates with rhombohedral calcite, autofluorescent. One example fairly laminated. In SU1 also single rhombohedral crystals were observed
Aggregates	Loamy aggregates and reddened clay aggregates with detrital grains

Key: si – silt; fs – fine sand; ms – medium sand; cs – coarse sand; fp – fine pebble

**Table S 10** General micromorphological description of samples collected at the Obishir-5

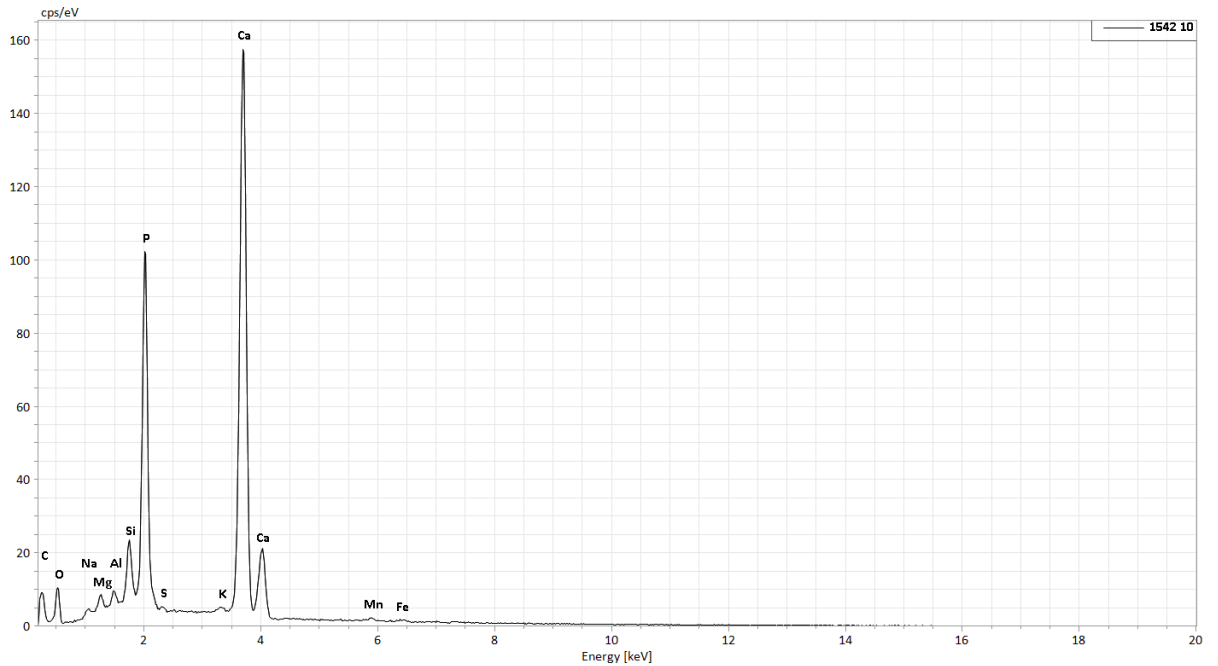
Unit	Sample	Micromorphological description	Interpretation
SU0	-	Not studied	Current top soil
SU1	MML1	Horizon with microlaminated microstructure, the surrounding is bioturbated presenting granular structure. Yellowish gray micritic calcite groundmass, occasionally well compacted. Coarse-silt-and-fine-sand-sized calcite, quartz, mica and clay mineral grains and occasional authigenic minerals (low-magnesium carbonate spherulites). Horizontally aligned, in lenses and forming microlamination. Occasionally well compacted. Fine pebbles igneous and limestone rock fragments occasionally appeared randomly distributed. Varying-sized vughs, vesicles, channels and chambers and very narrow and elongated voids. Coarse dung aggregates with bluish b-fabric were horizontal-aligned and subrounded, elliptical and compacted. Elongated and subhorizontal-aligned phytoliths with signs of breakage. Very coarse charcoals, charred and partially charred plant remains occurred. Pottery suspected. Compacted and cemented calcitic hypocoatings and impregnations. Common coarse carbonate nodules present.	Reworked unit with anthropogenic inputs affected by stock trampling with traces of foddering
Sub2.1	-	Not studied	Laminated unit due to trampling or colluvial processes (needs further investigation)
Sub2.2	MML3.1	Brown gray loamy groundmass with randomly distributed coarse-silt-and-fine-sand-sized calcite, quartz, clay mineral and Fe/Mn oxide grains. Debris of charred black material. Microstructure is granular with unsorted and sub-rounded crumbs and granules weakly developed and separated. Common and randomly distributed coarse rock fragments (limestone, shale and igneous). Weakly developed packing voids between granules, and vughs, channels, vesicles and chambers are common. Coarse woody charcoals randomly distributed, some chunked specimens. Common rounded yellowish dung fragments with fecal spherulites, randomly distributed. Some specimens are intact, others disrupted. Fecal spherulites also dispersed in the groundmass. Common bone fragments, varying colors (from dark orange to yellow), randomly distributed and corroded, with sign of recrystallization. Occasionally shell fragments were observed. Suspected pottery. Carbonate and apatite nodules were commonly observed.	Reworked unit with herbivore dung pellets and disassembled burnt features

Sub2.3	MML3.2	Similar to above but with coarser and more abundant bone fragments and dung material with fecal spherulites. One piece of weathered debitage was observed. Dung material was found calcined and some specimens were observed with phytoliths. Carbonate concentric nodules were observed which were fluorescent under epifluorescent light, characterized by higher and lower auto fluorescent bands. Bioturbation forms carried out by invertebrates.	Reworked colluvial unit with dung material and disassembled firing features
Sub2.4	MM1541	Thin section is small and possibly disturbed during transport and/or preparation. Similar to Sub2.2 but with a very loose granular microstructure. To note is the presence of dungy aggregates with fecal spherulites and phytoliths. Few rounded fine charcoal and chars are present as well as very altered bones.	Reworked unit with herbivore dung and rare burnt features
SU3	MM1542	Yellowish light brown groundmass with clayey silt and fine sand (calcite, quartz, feldspar, mica and clay minerals) with pebbles (limestone and shale fragments). Microstructure is granular and intergrain made of crumbs and granules with different degree of pedality but generally weak. Porosity is dominated by weakly developed packing voids, vesicles, channels and few chambers. Coarse woody charcoal fragments represent the common archeological-related component associated with char debris, char material was also found attached to void walls. Suspected dung fragments were observed without spherulites. Finer bone fragments commonly observed, cracked, dissolved and clayey of varying colors (yellow and orange). This material included clusters of fine silty spherulites of low-magnesium carbonates ( <i>authigenic minerals</i> ). Ashy nodules and a rounded phytolith occurred. Occasional shell fragments were observed. Bioturbation forms were recognized as earthworm made	Reworked unit with firing features
SU3 NNE part	MM2101	Sedimentary structures were absent. Yellowish brown groundmass with similar geogenic components to samples above. Vermicular microstructure. Fewer charcoals and bones. Highly bioturbated. A rodent molar was observed and occasional shell fragments.	Reworked unit with few burnt features
SU4 top	MM1543	Small sample with more compacted material due to sampling. Sedimentary structures were absent. Yellowish brown groundmass with compact micro-granular microstructure. Fine sand and silt components similar to samples above, as well as the coarse rock fragments. One single authigenic mineral was observed. Few and tiny bone and shell fragments found as well as one specimen of phytolith. A earthworm biospheroids was observed. Calcitic nodules were present. Porosity was made of vughs and rounded chambers.	Colluvial-aeolian unit with low archaeological components and traces of phosphatization
SU4 bottom	MML5	Sedimentary structures were not observed. Yellowish light brown groundmass with similar geogenic components as above. Microstructure was compact micro-granular, locally vesicular, massive and vughy. Single occurrence of bone and charcoal fragments. Porosity made of channels, planes, vesicles and vughs. Phosphatic rinds around limestone fragments and partially impregnated groundmass. Calcitic nodules were present. Microlaminated clay papule.	Unit with low archaeological components and traces of phosphatization and recycled material
SU5 top	MM1544	Similar to above. Highly bioturbated material. No sedimentary structures were present. Locally phosphatic impregnated groundmass and phosphatic rinds on limestone pebbles. Calcitic hypocoating surrounding voids. Presence of calcified root cells and micritic granular aggregates associated with voids. Dusty infilling partially closing biogalleries. Large concave bioturbation structure in the top left corner.	Unit with low archaeological components and traces of phosphatization and

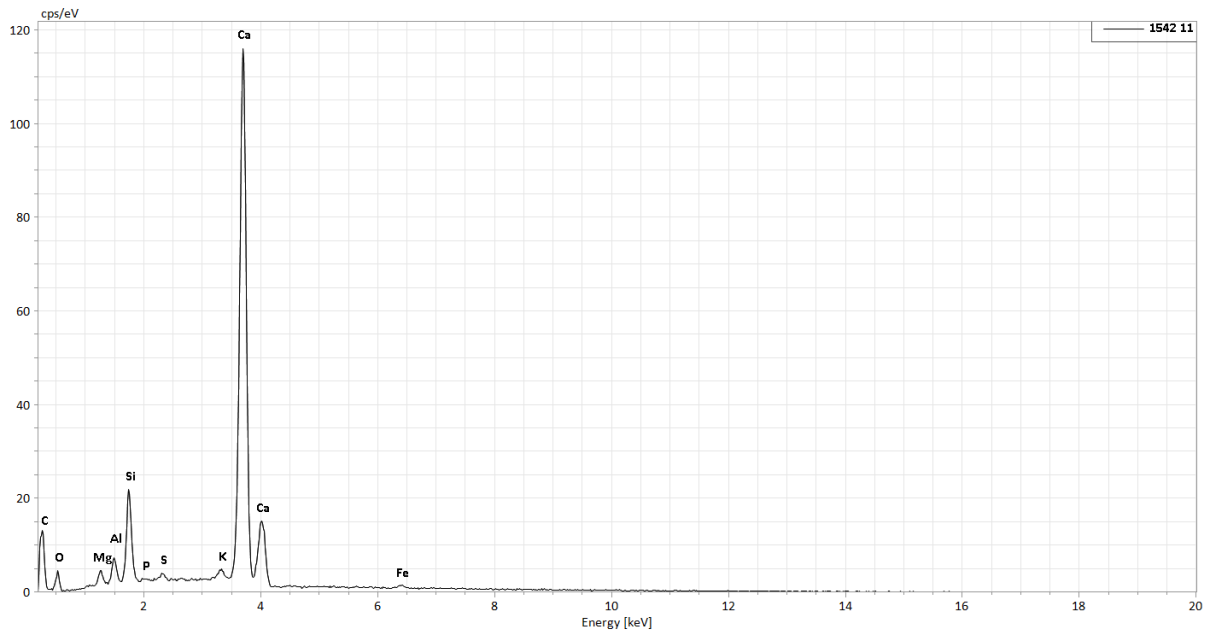
		One single occurrence of authigenic mineral. Voids are commonly loosely filled with organo-mineral excrements of rounded shape.	sporadic clay illuviation
SU5 bottom	MM1545	Similar to above but authigenic minerals were not noted.	As above

### S7.5 SEM-EDS SPECTRA

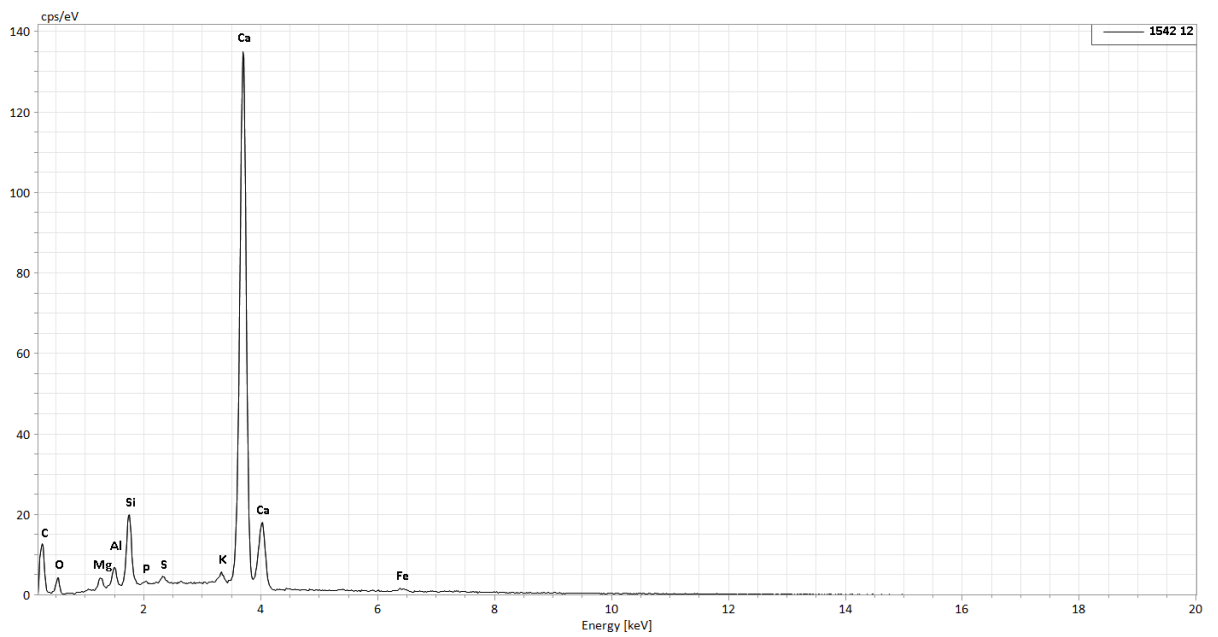
SEM-EDS spectra of points 10 in Fig.6d; 11, 12 and 13 in Fig.6c; and 31, 32, 33 in Fig.6b. The point number is in each spectrum on the top left.



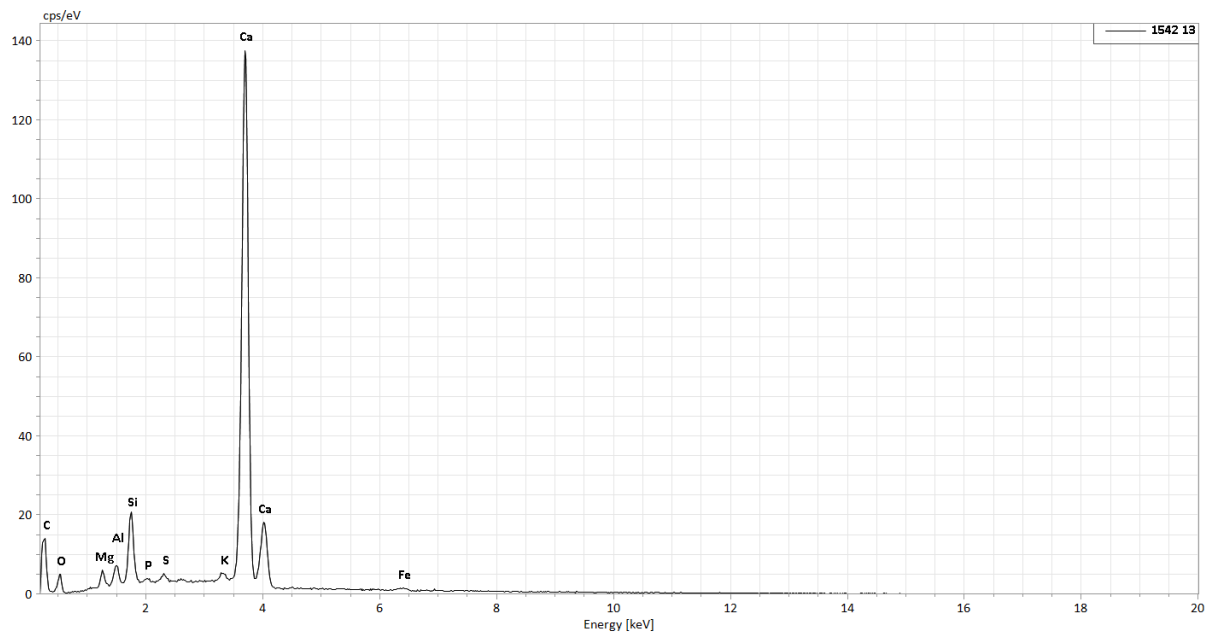
*Figure S 9 Spectrum n 10 of a bone specimen (Fig.6g in the main text) made of apatite*



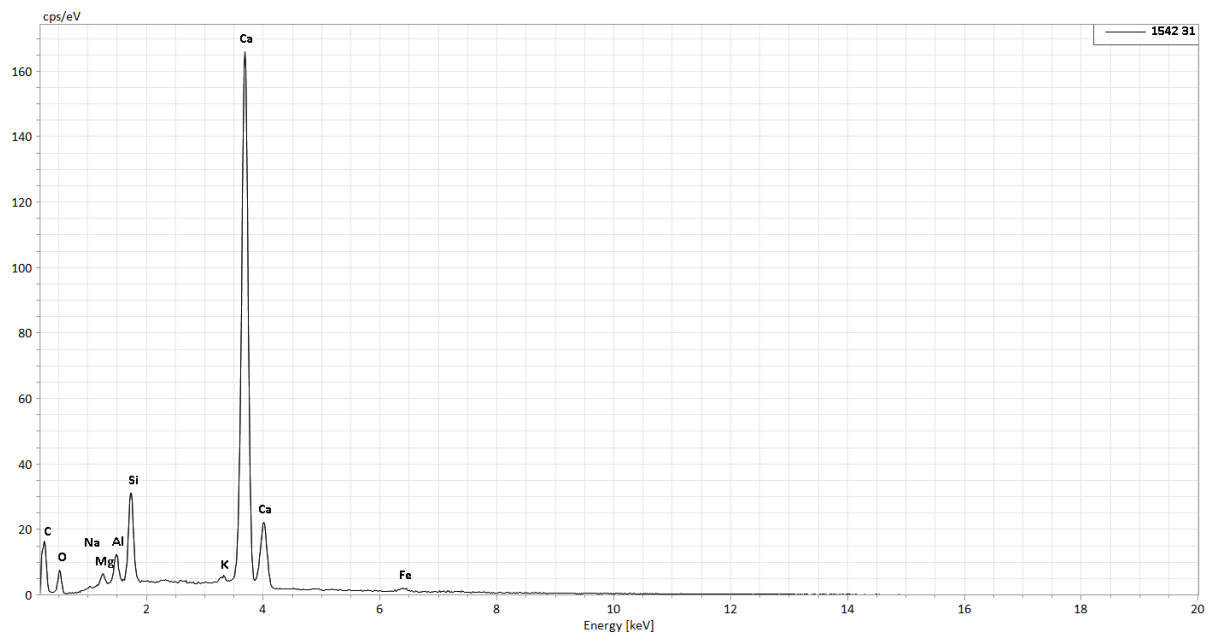
**Figure S 10** Spectrum of point n 11 (Fig.6l in the main text) taken within a authigenic mineral mainly composed of carbonate and traces of Mg, S, K. Elements such as Si, Al and Fe are probably deriving from the background.



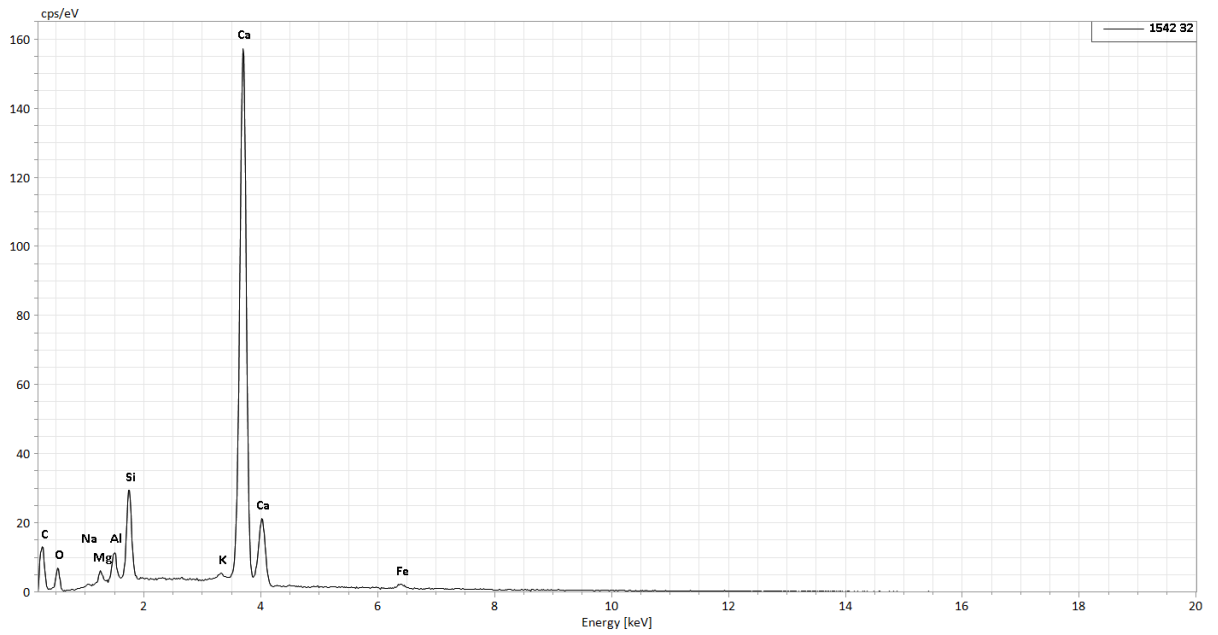
**Figure S 11** Spectrum of point n 12 (Fig.6l in the main text) taken within a authigenic mineral mainly composed of carbonate and traces of Mg, S, K.



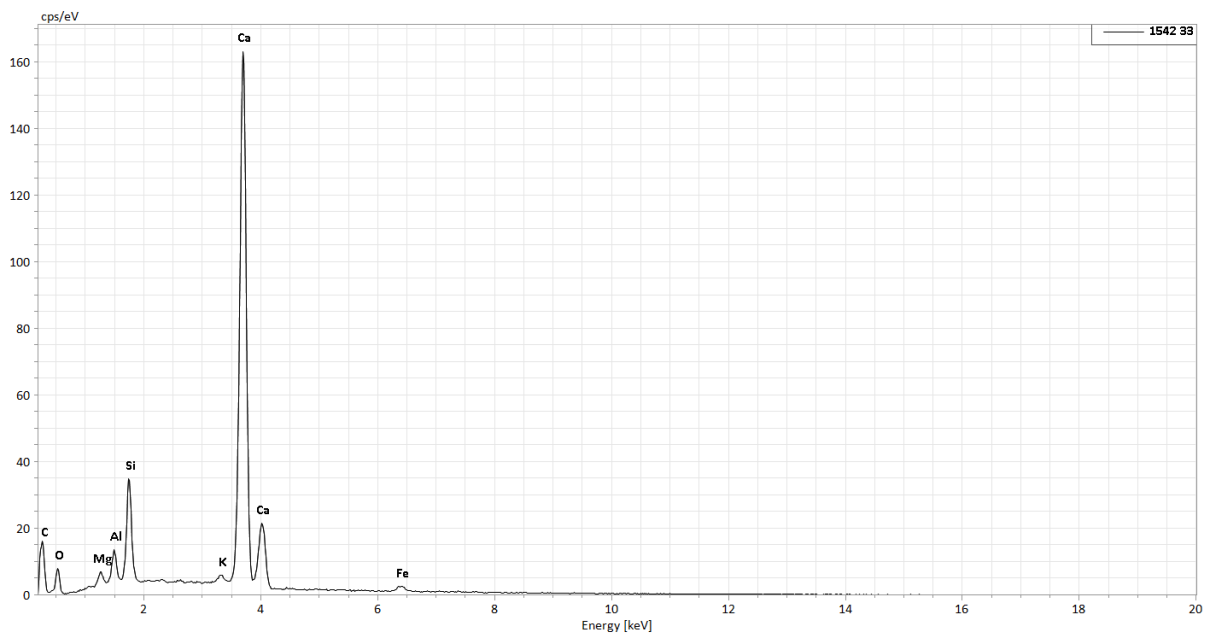
**Figure S 12** Spectrum of point n 13 (Fig.6l in the main text) taken within a authigenic mineral mainly composed of carbonate and traces of Mg, S, K



**Figure S 13** Spectrum of point n 31 (Fig.6k in the main text) taken within a rhombohedral crystal within an ashy nodule, mainly composed of carbonate and traces of Mg and K

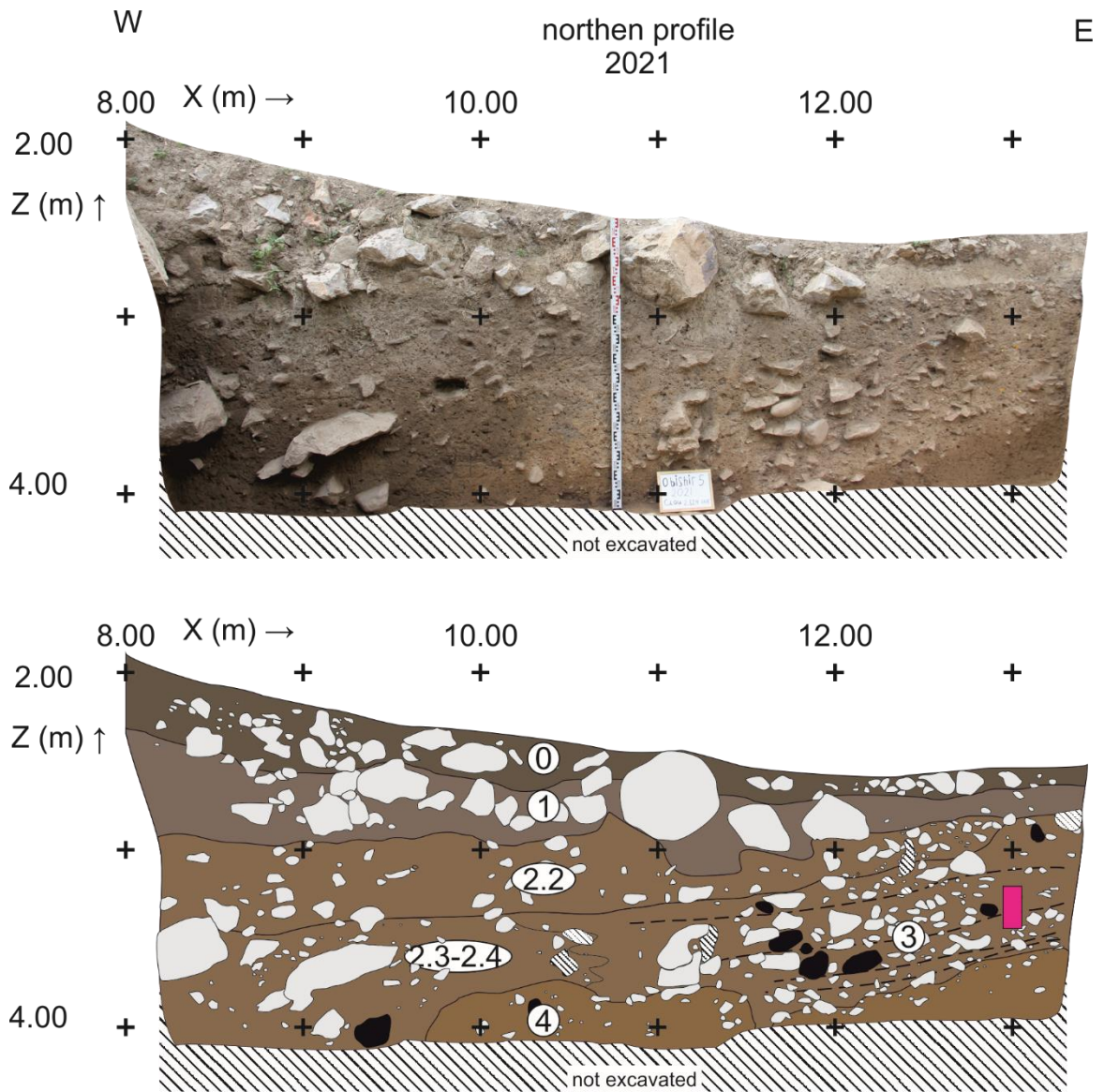


**Figure S 14** Spectrum of point n 32 (Fig.6k in the main text) taken within a rhombohedral crystal within an ashy nodule, mainly composed of carbonate and traces of Mg



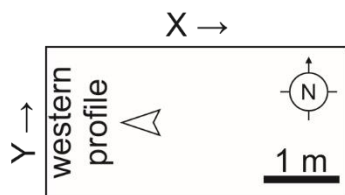
**Figure S 15** Spectrum of point n 31 (Fig.6k in the main text) taken within a rhombohedral crystal within an ashy nodule, mainly composed of carbonate and traces of Mg and K

## S8. 2021 campaign stratigraphic drawing



Plan of excavation area:

■ MM samples



## S9. References

Brancaleoni, G. *et al.* (2022) 'Depositional history of a talus cone in an arid intermontane basin in Central Asia: An interdisciplinary study at the Late Pleistocene–Late Holocene Obishir-I site, Kyrgyzstan', *Geoarchaeology*. John Wiley and Sons Inc, 37(2), pp. 350–373. doi: 10.1002/gea.21892.

Brancaleoni, G. *et al.* (2023) 'A closer look at clasts and groundmass: Micromorphological features in sediments with archaeological significance in Obishir and Katta Sai complexes



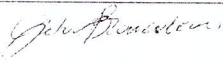

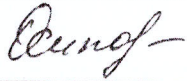
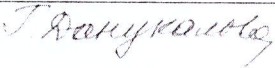
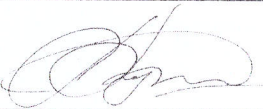


- (Central Asia)', *Journal of Archaeological Science: Reports*. Elsevier, 51, p. 104118. doi: 10.1016/j.jasrep.2023.104118.
- Buggle, B. *et al.* (2011) 'An evaluation of geochemical weathering indices in loess-paleosol studies', *Quaternary International*, 240(1–2), pp. 12–21. doi: 10.1016/j.quaint.2010.07.019.
- Doebelin, N. and Kleeberg, R. (2015) 'Profex: A graphical user interface for the Rietveld refinement program BGMN', *Journal of Applied Crystallography*. International Union of Crystallography, 48, pp. 1573–1580. doi: 10.1107/S1600576715014685.
- Friendly, M. (2002) 'Corrgrams: Exploratory displays for correlation matrices', *The American Statistician*, 56, pp. 316–324.
- Krajcarz, M. T. *et al.* (2016) 'Middle Paleolithic sites of Katta Sai in western Tian Shan piedmont, Central Asiatic loess zone: Geoarchaeological investigation of the site formation and the integrity of the lithic assemblages', *Quaternary International*, 399, pp. 136–150. doi: 10.1016/j.quaint.2015.07.051.
- Krivoshapkin, A. *et al.* (2020) 'Middle Paleolithic variability in Central Asia: Lithic assemblage of Sel'Ungur cave', *Quaternary International*. Elsevier, 535(August), pp. 88–103. doi: 10.1016/j.quaint.2018.09.051.
- Osipova, E. *et al.* (2020) 'Palaeoenvironmental conditions of the Palaeolithic–Neolithic transition in the Fergana Valley (Central Asia) – New data inferred from fossil molluscs in Obishir-V rockshelter (Kyrgyzstan)', *Quaternary International*. Elsevier Ltd, (November). doi: 10.1016/j.quaint.2020.11.009.
- Pietsch, D. (2013) 'Krotovinas - soil archives of steppe landscape history', *Catena*. Elsevier B.V., 104(October), pp. 257–264. doi: 10.1016/j.catena.2012.12.003.
- Serdyuk, N. V. *et al.* (2023) 'Holocene vertebrate fauna in Fergana Valley, Kyrgyzstan, based on fossils from the Obishir-5 rock shelter', *Geobios*. Elsevier Masson. doi: 10.1016/J.GEOBIOS.2023.01.002.
- Taylor, W. T. T. *et al.* (2021) 'Evidence for early dispersal of domestic sheep into Central Asia', *Nature Human Behaviour*. doi: 10.1038/s41562-021-01083-y.



***Appendix D – Author contribution  
statement***

## Statement of Contribution of Co-Authors for Thesis by Published Papers

The authors listed below have certified that:

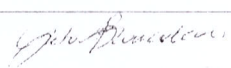
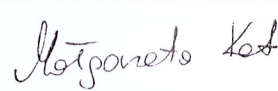
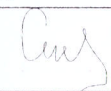
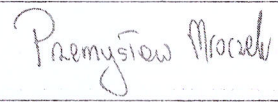
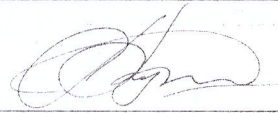
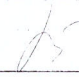

1. They agree to the use of the publication in the student's thesis and its publication on the BIP site consistent with any limitations set by publisher requirements.

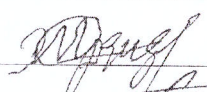
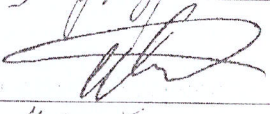
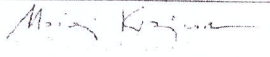
Article I				
Title	Depositional history of a talus cone in an arid intermontane basin in Central Asia: An interdisciplinary study at the Late Pleistocene–Late Holocene Obishir-I site, Kyrgyzstan			
Journal	Geoarchaeology			
Publishing date	First published: 08 November 2021			
Impact Factor	1.7			
DOI	<a href="https://doi.org/10.1002/gea.21892">https://doi.org/10.1002/gea.21892</a>			
Authors				
	Name and surname	Percentage share	Contribution	Signature
1.	Greta Brancaleoni	50	Design, drafting, data acquisition, analysis, interpretation, revision	
2.	Svetlana Shnaider	8	Drafting, data acquisition, archaeological assemblage analysis, interpretation, revision	
3.	Evgeniya Osipova	1	Mollusk analysis	
4.	Guzel Danukalova	5	Drafting, mollusk analysis, interpretation, revision	
5.	Redzhap Kurbanov	6	Drafting, dating analysis, interpretation	
6.	Ewa Deput	2	Data acquisition	
7.	Saltanat Alisher kyzy	1	Data acquisition	

8.	Aida Abdykanova	2	Data acquisition, revising	
9.	Maciej T. Krajcarz	25	Design, drafting, data acquisition, analysis, revision, supervision	

The authors listed below have certified that:

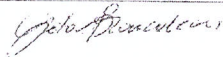
1. They agree to the use of the publication in the student's thesis and its publication on the BIP site consistent with any limitations set by publisher requirements.

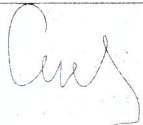
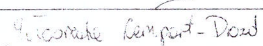
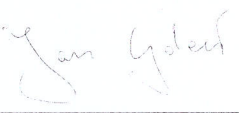
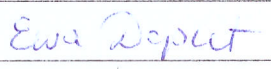

Article II				
Title	A closer look at clasts and groundmass: Micromorphological features in sediments with archaeological significance in Obishir and Katta Sai complexes (Central Asia)			
Journal	Journal of Archaeological Science: Reports			
Publishing date	First published: 5 August 2023			
Impact Factor	1.6			
DOI	<a href="https://doi.org/10.1016/j.jasrep.2023.104118">https://doi.org/10.1016/j.jasrep.2023.104118</a>			
Authors				
	Name and surname	Percentage share	Contribution	Signature
1.	Greta Brancaleoni	68	Design, drafting, data acquisition, analysis, interpretation, revision	
2.	Małgorzata Kot	3	Data acquisition	
3.	Svetlana Shnaider	3	Data acquisition	
4.	Przemysław Mroczek	3	Grain size analysis	
5.	Redzhep Kurbanov	3	Grain size analysis	
6.	Aida Abdykanova	1	Data acquisition	
7.	Saltanat Alisher kyzy	1	Data acquisition	

8.	Mhukkidin Khudjanazarov	1	Data acquisition	
9.	Konstantin Pavlenok	1	Data acquisition	
10.	Maciej T. Krajcarz	26	Design, data acquisition, revision, supervision	

The authors listed below have certified that:

1. they meet the criteria for authorship in that they have participated in the conception, execution, or interpretation, of at least that part of the publication in their field of expertise;
2. they take public responsibility for their part of the publication, except for the responsible author who accepts overall responsibility for the publication;
3. there are no other authors of the publication according to these criteria;
4. potential conflicts of interest have been disclosed to (a) granting bodies, (b) the editor or publisher of journals or other publications, and (c) the head of the responsible academic unit, and
5. they agree to the use of the publication in the student's thesis and its publication on the BIP site consistent with any limitations set by publisher requirements.

Article III				
Title	Geoarchaeological approach for tackling the function and preservation state of the Obishir-5 site, the earliest Neolithic site in the Fergana Valley			
Journal	Archaeological and Anthropological Sciences			
Status	submitted			
Impact Factor	2.2			
DOI				
Authors				
	Name and surname	Percentage share	Contribution	Signature
1.	Greta Brancaleoni	70	Design, drafting, data acquisition, analysis, interpretation, revision	

2.	Svetlana Shnaider	3	Data acquisition, revision	
3.	Małgorzata Lempart-Drozd	10	Mineralogical analysis, interpretation, drafting, revision	
4.	Jan Goleń	2	Fluorescence microscope analysis	
5.	Ewa Deput	2	Data acquisition	
6.	Aida Abdykanova	2	Data acquisition, revision	
7.	Maciej T. Krajcarz	11	Design, drafting, data acquisition, revision, supervision	